VIBRATION REDUCTION OF FLEXIBLE ROTORS

by

Irvin Redmond, BSc, CEng, MIMechE

A Thesis submitted to the University of Strathclyde
for the
Degree of Doctor of Philosophy
in Mechanical Engineering

Department of Dynamics and Control
University of Strathclyde
Glasgow, Scotland

October 1985

I dedicate this thesis to the memory of my brother Matthew

ACKNOWLEDGEMENTS

I should like to thank Professor C.R. Burrows and Dr. R.F. McLean for their valuable guidance and encouragement throughout the work.

I am grateful also to Dr. M.N. Sahinkaya who provided so much inspiration and assistance in many ways during the project.

I should like to acknowledge the contribution made by Lim Tau Meng who constructed the electronic control circuitry for use with the electromagnetic controller.

To my fellow research students within the Department, I express my gratitude for their latent contribution in a number of forms.

Thanks are also due to all technicians who assisted in the construction of the experimental rig.

To my wife Maureen, for preparing the initial thesis draft and without whose continual understanding and support this work could never have been presented, I owe a debt of gratitude.

To my parents whose contribution through the years has been immense, I am forever indebted and express my sincere gratitude.

I am also grateful to Mrs. Ann McNaught for her excellent typing of the final thesis.

I express my thanks to the SERC and the Institution of Mechanical Engineers for the financial assistance provided.

To all others who helped in some way I extend my appreciation.

ABSTRACT

A novel method of flexible-rotor vibration control, using an active contactless angular electromagnetic actuator is presented.

A theoretical comparison of radial and angular damping is performed. Three different performance indices are defined and used to determine controller optimum damping/location data for different shaft systems. The controller settings are determined for two main cases:

i) such that only one damping value is allowed throughout the entire shaft speed range (passive or fixed-gain active control),

ii) the damping value is controlled as a function of rotor speed (adaptive control).

The parameter optimisation, made possible by the creation of a simple but efficient numerical technique employed in conjunction with the transfer matrix method, is restricted to considering a speed range covering the first three rigid-bearing critical speeds for a uniform shaft supported by a variety of bearings. However, the approach is sufficiently general to allow the study of any required speed range.

It is shown that for both the radial and angular dampers when mounted at the bearings, there is a definite support stiffness value above which the angular damper is the more efficient, but below which the opposite is true. When the conditions for 'fixed-points' are satisfied, then a simple on-off control strategy can be used effectively employing either type of controller. Angular damping is shown also to be an effective means of suppressing 'oil-whirl' type instability.

The theoretical work is supported by experimental investigations on a laboratory rig which is representative of a general flexible rotor system. An electromagnetic controller is mounted at one bearing and the reduction of shaft unbalance response and bearing forces recorded for various conditions.

Significant reductions in system synchronous response are observed at running speeds close to the first critical speed when electromagnetic stiffness and/or damping is employed. When electromagnetic damping is introduced, non-synchronous vibration components, resulting from shaft asymmetries, are also eliminated.

The combined theoretical and experimental studies show angular control to be a viable alternative means of reducing flexible rotor vibrations.

CONTENTS

NOMENCLATURE

A	Shaft cross-sectional area (m^2); magnet pole face area (m^2)
Av	Amplitude of shaft displacement in the direction of the y axis
Aw	Amplitude of shaft displacement in the direction of the z axis
a	Whirl orbit major axis (m); distance of controller from LH support (m)
a_c, a_k	Coefficients relating measured shaft slope to estimated electromagnetic damping and stiffness moments respectively
B	Magnetic flux density (TESLA)
b	Whirl orbit minor axis (m); non-dimensional controller location
b_c, b_k	Coefficients relating measured shaft slope to estimated electromagnetic damping and stiffness moments respectively
b'	Shaft support damping coefficient (Ns/m)
b"	Shaft internal damping coefficient (Ns/m)
C	Control damping coefficient (radial: Ns/m; angular: Nms/rad); excitation couple (Nm)
C_2	Jeffcott-Rotor system damping (Ns/m)
C_F	System effective angular feedback damping coefficient
C_L	Angular damping coefficient resulting from undesirable control circuit phase lags (Nms/rad)
C_{LA}	Linearised axial damping coefficient acting at radius r (Ns/m)

$C_{L\phi}$, $C_{L\theta}$ Linearised angular damping coefficients (Nms/rad)

C_N Nominal angular feedback damping coefficient (Nms/rad)

C_{opt} Optimum passive control damping value

C_{REF} Microcomputer digital setting corresponding to a physical control-damping value

C_S Equivalent system damping rate (Nms/rad)

C_ϕ, C_θ Non-linear angular damping coefficients (Nms^2/rad^2)

$\underline{C}$ System damping matrix

C_{xx}, C_{xy}, C_{yx}, C_{yy} Oil-film damping coefficients where the first subscript represents the direction of force and the second the direction of displacement (Ns/m)

C_{nzz}, C_{nzy}, C_{nyz}, C_{nyy} Support radial damping coefficients where the second subscript represents the direction of force and the third the direction of displacement. The first subscript denotes the sub-level being considered (Ns/m)

$C_{n\phi\phi}$, $C_{n\phi\theta}$, $C_{n\theta\phi}$, $C_{n\theta\theta}$ Support angular damping coefficients. All definitions as above (Nms/rad)

D Shaft diameter (m)

E Young's Modulus (N/m^2)

$\overline{E}$ Young's Modulus (complex) (N/m^2)

e Jeffcott-Rotor mass eccentricity (m)

F Electromagnetic force (N); external force (N)

F_c Radial control force (N)

$F_{e\phi}$, F_{er} Effective central angular and radial control forces respectively (Nm and N)

F_u	External force due to mass unbalance (N)
F_v	Dimensionless frequency ratio in x-y plane ($=\omega/\omega_{nv}$)
F_w	Dimensionless frequency ratio in x - z plane ($=\omega/\omega_{nw}$)
F_x	Component of bearing oil-film force in x direction (N)
F_y	Component of bearing oil-film force in y direction (N)
$\underline{F}$	System flexibility matrix; field transfer matrix
$\overline{\underline{F}}_c$	General control force vector
$\overline{\underline{F}}_{cy}$	Vector containing radial control forces acting in y direction
$\overline{\underline{F}}_{cz}$	Vector containing radial control forces acting in z direction
f	Dimensionless frequency ratio (ω/ω_{NAT})
G	Shear modulus (N/m^2); magnetic air-gap length (m)
G_1, G_2	Angular control proportional and derivative feedback gains
G_3, G_4	Radial control proportional and derivative feedback gains
GF	Gauge-factor
$\overline{G}$	Complex shear modulus (N/m^2)
g	Dimensionless material loss-factor
H	Magnetic field strength (ampere-turns/metre)
$\underline{H}$	Coefficient matrix
h_{f1}	Dimensionless angular proportional feedback gain

h_{f2}	Dimensionless radial proportional feedback gain
I	Shaft second moment of area (m^4); electromagnet coil current (amps)
I_{FY}, I_{FZ}	Transverse moment of inertia of sub-level element about y and z axes respectively (kgm^2)
I_P	Point polar moment of inertia (kgm^2)
I_S	Equivalent system inertia (kgm^2)
I_T	Point transverse moment of inertia (kgm^2)
$\underline{I}$	Identity matrix
i	Magnet current (amps); $i^2 = -1$
K, K_a, K_b	State vector correction factors
K_2	Jeffcott-Rotor system stiffness (N/m)
K_B	Shaft support stiffness (N/m)
K_F	System effective angular feedback stiffness coefficient (Nm/rad)
K_L	Angular stiffness coefficient resulting from undesirable control-circuit phase-lags (Nm/rad)
K_{LA}	Linearised axial stiffness coefficient acting at radius r (N/m)
$K_{L\phi}$, $K_{L\theta}$	Linearised angular stiffness coefficients (Nm/rad)
K_N	Nominal angular feedback stiffness coefficient (Nm/rad)
K_P	Angular stiffness coefficient resulting from pre-magnetising current (Nm/rad)
K_{REF}	Microcomputer digital-setting corresponding to a physical control-stiffness value
K_S	Equivalent system stiffness (Nm/rad); shaft stiffness (N/m)

K_{ϕ}, K_{θ} Non-linear angular stiffness coefficients (Nm/rad^2)

$\underline{K}$ System stiffness matrix

K_{xx}, K_{xy}, K_{yx}, K_{yy} Oil-film stiffness coefficients where the first subscript represents the direction of force and the second the direction of displacement (N/m)

K_{nzz}, K_{nzy}, K_{nyz}, K_{nyy} Support radial stiffness coefficients where the second subscript represents the direction of force and the third the direction of displacement. The first subscript denotes the sub-level being considered (N/m)

$K_{n\phi\phi}$, $K_{n\phi\theta}$, $K_{n\theta\phi}$, $K_{n\theta\theta}$ Support angular stiffness coefficients. All definitions as above (Nm/rad)

k Electromagnet constant (Nm^2/amp^2); shaft slope measurement system gain (volts/rad); current feedback gain (volts/amp)

L Beam element length (m); shaft length (m)

l Number of shaft stations used for computation of response

M Bending moment (Nm)

M_c Control couple (Nm)

M_e External excitation moment (Nm)

M_f Feedback control moment (Nm)

M_F Mass of sub-level element (kg)

M_y, M_z Bending moments about shaft y and z axes respectively (Nm)

$\underline{M}$ System mass matrix

$\underline{\bar{M}}_{cy}$ Vector containing angular control moments acting about y axis

$\underline{\bar{M}}_{cz}$	Vector containing angular control moments acting about z axis
m	Point mass (kg); Jeffcott-Rotor system mass (kg); number of shaft stations
m_u	Unbalance mass (kg)
N	Number of magnet coil turns
N_e	Number of linear equations resulting from shaft end conditions
N_i	Number of linear equations resulting from shaft intermediate conditions
N_L	Number of support levels
N_t	Total number of linear equations resulting from shaft boundary conditions
n	Order of system state vector; number of external control forces
P	Reaction force at rigid shaft-support (N)
PI	System performance index
$\underline{P}$	System external force vector; point transfer matrix
p	Exponential growth/decay factor; magnet control moment phase angle (degrees)
p_c, p_L, p_m	Magnet control moment phase angles (degrees)
Q	Change in beam slope at a hinged-joint (rads)
$\underline{Q}_r$	Vector of real parts of rotor response phasors
$\underline{Q}_i$	Vector of imaginary parts of rotor response phasors
q_{mc}	Controlled rotor response at location m
q_{mu}	Uncontrolled rotor response at location m

q_{ua}	Uncontrolled shaft response at angular controller - controller mounted at support (m)
q_{ur}	Uncontrolled shaft response at radial controller - controller mounted at shaft centre (m)
$\underline{q}_c$	Vector containing controlled rotor response values
$\underline{q}_u$	Vector containing uncontrolled rotor response values
$\underline{\overline{Q}}_{ce}$	Vector of controlled response phasors at controller locations
$\underline{\overline{Q}}_{ue}$	Vector of uncontrolled response phasors at controller locations
$\overline{Q}_{mc}$	Controlled response phasor at shaft location m
$\overline{Q}_{mu}$	Uncontrolled response phasor at shaft location m
$\overline{Q}_{dc}$	Controlled response phasor at controller location
$\overline{Q}_{du}$	Uncontrolled response phasor at controller location
R	Residual function (= $K_a - K_b$); dimensionless angular controller radius (r/L)
$\underline{\overline{R}}$	System receptance matrix
r	Receptance (m/N); radius of mass unbalance (m); effective radius of angular controller (m); shaft orbital radius (m)
$\underline{\overline{r}}$	System receptance matrix
S	Jeffcott-Rotor system eigenvalues (rad/sec)
TR	Transmissibility
t	Time (seconds)
$\underline{U}$	Element transfer matrix; control force vector

$\underline{U}'$, $\underline{U}''$	Partial system transfer matrices
$\underline{u}$	System modal matrix
$\underline{u}^T$	Transposed system modal matrix
V	Shear force (N)
V_i, V_o	Strain gauge bridge input and output volts respectively
V_y, V_z	Shear force in y and z directions respectively (N)
v	Shaft displacement along y axis (m)
$\underline{v}$	Vector of system principle co-ordinates
$\underline{v}_c$	Vector of real components of shaft displacements v (m)
$\underline{v}_s$	Vector of imaginary components of shaft displacements v (m)
v_c	Real component of shaft displacement v (m)
v_s	Imaginary component of shaft displacement v (m)
W_i	Instability onset speed (rad/sec)
W_c	Shaft first critical speed (rad/sec)
w	Shaft displacement along z axis (m)
$\underline{w}_c$	Vector of real components of shaft displacements w (m)
$\underline{w}_s$	Vector of imaginary components of shaft displacements w (m)
w_c	Real component of shaft displacement w (m)
w_s	Imaginary component of shaft displacement w (m)
$\underline{\overline{X}}$	Vector of shaft displacement phasors
x	Shaft journal displacement in x direction (m)
$\underline{x}$	Vector of system generalised displacements
y	Shaft journal displacement in y direction (m)

$\underline{Z}$	State vector
$\underline{Z}^{I}, \underline{Z}^{II}, \underline{Z}^{NL}$	State vectors at system levels I, II and NL respectively
$\underline{\overline{Z}}$	Controller dynamic-stiffness matrix
α	Real part of eigenvalue (rad/sec); real influence coefficient (m/N); phase angle defining orientation of mass unbalance (rad)
$\alpha_{1,2,3,4}$	Jeffcott-Rotor real receptances
$\overline{\alpha}$	Complex receptance
β	Dimensionless frequency ratio (ω/ω_c)
β_v, β_w	Phase angles of shaft displacements along the y and z axes respectively (rad)
γ	Phase angle denoting orientation of shaft initial-bend (rad)
δ	Initial estimate of state vector coefficient; logarithmic decrement
ε	Mechanical strain; shaft initial-bend magnitude (m)
$\overline{\varepsilon S}_{\emptyset n}$	Shaft slope at station n, in x-z plane, due to initial-bend (rad)
$\overline{\varepsilon S}_{\theta n}$	Shaft slope at station n, in x-y plane, due to initial-bend (rad)
$\overline{\varepsilon}_{vn}$	Shaft component of initial-bend, at station n, in y direction (m)
$\overline{\varepsilon}_{wn}$	Shaft component of initial-bend, at station n, in z direction (m)
ζ	System damping factor

Θ	Shaft slope in x-y plane (rad); shaft angular displacement at controller location - Jeffcott-Rotor (rad); shaft slope feedback signal (rads)
Φ	Shaft slope in x-z plane (rad); receptance phase angle (rads); shaft slope feedback signal (rad)
Φ_L	Undesirable control circuit phase lag (rad)
λ	System complex eigenvalue/frequency (rad/sec)
$\underline{\lambda}$	Matrix containing system eigenvalues (natural frequencies)
ρ	Material density (kg/m^3); controlled system damping factor (Jeffcott-Rotor)
ρ_2	Uncontrolled system damping factor (Jeffcott-Rotor)
ρ_{f1}	Dimensionless angular derivative feedback gain
ρ_{f2}	Dimensionless radial derivative feedback gain
μ	Receptance magnitude (m/N)
μ_o	Permeability of free space ($4\pi \times 10^{-7}$ Henry/metre)
μ_r	Relative permeability
Ψ_a	Phase angle defining occurrence of shaft maximum displacement (rad)
Ω	Shaft rotational frequency (rad/sec)
ω	Shaft precession rate (rad/sec)
ω_{CR}	Undamped critical speed - Jeffcott-Rotor (rad/sec)
ω_d	Damped critical speed - Jeffcott-Rotor (rad/sec)
ω_n	Beam nth natural frequency (rad/sec)
ω_{nv}	Shaft natural frequency in x-y plane (rad/sec)
ω_{nw}	Shaft natural frequency in x-z plane (rad/sec)

CHAPTER 1

INTRODUCTION

The continual demand on modern-day machinery to transmit increasing power levels at higher rotational speeds has resulted in the employment, in many practical installations, of long slender shafts with running speeds above their first and second, and in some instances even higher order, critical speeds.

This has led to the development of more stringent design criteria, but cases still arise where vibrations in rotating machinery cause machine breakdown or a need to operate away from the design speed. In other cases problems have arisen due to a change in operational requirements after a machine has been installed.

The impossibility of avoiding all vibration problems by action taken at the design stage has encouraged the study of methods for altering system parameters 'in-situ' using passive or active control devices.

Investigations to date have mainly been restricted to the study of rotor systems, in which vibration control is achieved through incorporation of an external radial damper mounted at some location along the shaft between the bearings. Whilst this means of control may be acceptable on a laboratory rig, in practice many situations occur where access to this shaft portion may be extremely limited or even impossible.

Consequently, in such circumstances an alternative effective control strategy would be desirable. The work

described within this thesis is of a combined theoretical and experimental nature and demonstrates how the introduction of external control forces in an angular, as opposed to radial, sense can lead to an efficient means of system vibration attenuation. Access problems are eliminated since the angular control forces may be applied effectively at the rotor supports. In addition, the control function is implemented, without the need for physical contact with the rotating shaft, by utilising electromagnets as the control actuators.

1.1 Thesis Format

In Chapter 2 a literature review is presented covering historical and recent works in the field of shaft whirling. Current methods of vibration control are also discussed with special emphasis on the application of electromagnets. A summary of the limitations of previous work leads to an outline of the main aims of this work.

Current rotordynamic methods of analysis are reviewed in Chapter 3 where the transfer matrix method is proposed as the most suitable for the application.

Chapter 4 gives a detailed description of the transfer matrix method when employed for the free and forced vibration analysis of rotor systems. The modified method is employed in order to minimise the possibility of numerical instability which normally occurs because of the small difference of large numbers. The fundamental system transfer matrices are developed and include effects such as mass unbalance, shaft initial-bend, gyroscopic moments and support sub-level characteristics. Application of

the method, in the form of a computer program, to various rotor models, confirms the accuracy and effectiveness in employing this technique for vibration analysis.

In Chapter 5 the concept of angular control is introduced and applied to the case of a simple Jeffcott-rotor where comparison is made with conventional radial control. The controller performance comparison is subsequently extended to multi-mode systems where three representative performance indices are investigated. A new efficient control optimisation procedure is created and employed to allow determination of optimum control locations and control forces for both controller types.

Chapters 6 and 7 describe the experimental portion of the work.

In Chapter 6 the laboratory rotor, designed and constructed specifically for the experimental investigations, is described fully along with all other equipment employed throughout the project. Details of all relevent component calibrations are included.

Chapter 7 gives details of all experimental tests performed. The test results, consisting mainly of test rotor response measurements for various levels and types of angular electromagnetic control force, are presented and analysed in detail. Predicted responses are provided for comparison and give an indication of the degree of accuracy of the numerical techniques employed.

In Chapter 8 the conclusions resulting from the theoretical and experimental investigations are summarised and suggestions for further work given.

CHAPTER 2

LITERATURE REVIEW

2.1 Introduction

Vibrating/rotating flexible-shaft systems have received much attention by many researchers; as a result the amount of literature available today is vast. Any attempt to compile a complete literature survey on this topic would be a mammoth task and its value questionable.

In the field of rotating machinery, a variety of topics are inexorably coupled and discussion of one in isolation may not be possible or even prudent. Consequently, the review is fairly extensive even though the material chosen is limited to that thought to most suitably represent the main links in the historical chain of research in this field. The review is in two sections:

a) Whirling of Shafts

b) Vibration Control

2.2 Whirling of Shafts

2.2.1 Synchronous Whirl

It is a well known fact that if the speed of a rotating shaft is gradually increased, a certain speed is attained at which the shaft radial deflection increases dramatically and the shaft is said to whirl or whip. If insufficient damping is present, shaft failure may finally occur.

Although the problem of shaft whirling has been known

to exist for some time, it is only just over one hundred years since one of the first papers on the subject was published by Rankine [1]. In 1869, in an article published in The Engineer, Rankine attempted to explain theoretically, the behaviour of an unloaded, frictionless, uniform shaft. He wrongly concluded that the shaft motion would be stable below and unstable above the first critical speed.

Twenty-five years later, in 1894, Dunkerly [2] presented the results of experiments which he performed on a number of shaft/pulley arrangements. His experimental results were compared to theory developed by Professor Osborne Reynolds and an empirical formula was derived for calculating the critical speeds of a variety of shaft arrangements, viz:

$$1/\omega_c^2 = 1/\omega_1^2 + 1/\omega_2^2 + 1/\omega_r^2 + \ldots 1/\omega_n^2$$

where ω_c is the natural frequency of the complete system and ω_r is the natural frequency of the beam with the r^{TH} mass alone on the beam.

The next major contribution to the subject was made by Chree [3] in 1904 who completely re-assessed the situation making use of Dunkerly's experimental results. Chree initially did not fully understand the nature of shaft whirl since he stated that it could not be considered as a form of forced vibration.

Chree considered Dunkerly's methods to be analogous to Lord Rayleigh's technique [4] for obtaining approximate frequencies of beam vibrations. Rayleigh showed how, at

least, an upper bound on the natural frequency could be estimated by assuming a mode shape for the vibrating system. Any discrepancy between assumed and actual mode would effectively result in additional system constraints leading to a raising of the predicted frequency.

Although this early work was very useful in helping to establish guidelines for the prediction of critical speeds for simple shaft systems, the fundamental theory of shaft whirling was still not fully understood at this stage.

It was not until 1919 that a full rational explanation of shaft whirling appeared in a paper by H.H. Jeffcott [5]. Jeffcott concluded that when a shaft was rotated, its geometrical axis would rotate around its original deflected form in a bent fashion, the amount of bend depending mainly on the relationship between the rotational speed and the critical speed. Thus, Jeffcott explained for the first time the behaviour of a simple rotating shaft/rotor system at any speed and showed that the shaft whirling problem could be considered as that of a system subjected to forced vibrations.

Six years later Kimball and Hull [6] performed experiments on a loaded unbalanced shaft passing through its critical speed, the results confirming Jeffcott's theory.

Stodola [7] proved experimentally the now well known fact, that as a shaft runs through its critical speed, the centre of gravity of the rotor moves from outside the shaft centre and geometric centre to between the two. He

also performed an interesting experiment on an unloaded shaft, first running the shaft in water, then in free air. He found the critical speeds in both cases were almost identical, but the amplitude substantially reduced in the former case due to the much increased external damping.

The effect of shaft initial-bend can be shown to cause a shaft whirling motion similar to that due to unbalance. Bishop [8] demonstrated how Jeffcott's theory could be modified to allow for this additional effect. Parkinson et al [9] confirmed experimentally that the exciting force resulting from shaft initial-bend cannot be removed for all speeds through shaft balancing, but that the balance correction mass could be chosen so that the shaft does not whirl at its first critical speed. In fact, the only way to ensure 'Perfect Balance' of such a shaft is to somehow completely remove the initial shaft bend [8]. Of course this is impossible to achieve in practice.

Over the years, numerous researchers have contributed to the field of rotor-dynamics, none more so than Stodola [7]. He showed that the inclusion of large diameter discs on a uniform rotating shaft resulted in the introduction of gyroscopic effects which tended to stiffen the shaft and thus raise the critical speeds. Gyroscopic couples tend to stiffen the shaft only when the shaft precesses in a direction corresponding to that of shaft rotation (see Section 7.5.8). If the shaft is vibrating as opposed to rotating, the converse is true and the natural frequencies are, in fact, decreased. In many

cases the effect of the above may be so small that it could be neglected. However, in a number of modern-day machines, for instance gas/steam turbine applications, exlusion of gyroscopic effects may lead to serious discrepancies between actual and predicted response.

Stodola [7] also presented an iterative procedure for calculating higher order natural frequencies of multi-mass systems. As with Rayleigh's method, it is first necessary to guess the mode-shapes for the relevant frequencies. However, Stodola's method is more accurate since the initially guessed mode-shapes are refined through subsequent iteration.

Myklestad [10] in 1944 and Prohl [11] in 1945, developed a tabular method for predicting the natural frequencies and normal modes of transversely vibrating beams and shafts respectively. The techniques employed were basically an extension of the procedures adopted by Holzer [12] in the analysis of torsional systems. The methods allow for determination of the natural frequencies when all system boundary conditions are satisfied.

In 1951, Linn and Prohl [13], analysing first a Jeffcott-rotor model then a shaft with distributed mass, demonstrated how the incorporation of support flexibility could greatly alter (reduce) the shaft critical speeds, a phenomenon first recognised by Stodola in 1927 [7].

At this point in time, most rotor analyses assumed either rigid-supports or, at most, support resilience independent of rotational frequency.

With the knowledge that the introduction of support-

flexibility could significantly reduce the critical speeds of a flexible-shaft system, early attempts were made to incorporate this effect empirically. Initially, a simple approach was adopted [14] where, from observations in the field, a variety of bearing configurations could be classified according to their static deflections. The method was fairly successful for prediction of the first critical speed, but as equipment rated-speeds increased so also did the requirement for more refined procedures.

Caruso [15] showed how a high-speed rotor system could be analysed, allowing for frequency-dependent support characteristics, using the Dynamic Stiffness Method. He described how the method, basically a mechanical-impedance method, allowed for the calculation of the shaft and bearing dynamic-stiffnesses as separate units. The two components could then be combined to provide details of the dynamic response of the complete system. Although early vibration analyses of large rotor systems consisted mainly of the calculation of undamped critical-speeds and normal modes, it is now common to incorporate prediction of the system dynamic response resulting from external forcing due to, for example, shaft mass unbalance.

The fundamental theory of whirling, established earlier by Jeffcott for a simple single-degree-of-freedom system, was extended by a number of workers and applied to complex multi-degree-of-freedom systems by utilising a number of system sub-elements which, when combined in some fashion, would allow assessment of the dynamic response of

large real rotor systems. In the last few decades such advances were made possible due, mainly, to the advent of the large electronic digital computer.

Such numerical methods normally necessitate the modelling of the real shaft as a set of rigid masses connected by massless, flexible beam elements. Modelling error is thus unavoidable in the analysis. However, with proper choice of the number of elements, this error may be reduced to a minimum. Gladwell [16] showed that for transversely vibrating beams modelled as described above, the modelling error was proportional to $1/N^2$ for one or two free-ends and $1/N^4$ for other end conditions, where N is the total number of discrete masses employed. Care must be taken with some analysis methods [63], since the use of too many elements may lead to inaccuracy due to truncation errors.

Most present-day analysis programs make use of matrix methods which are ideally suited for programming on a digital computer. The Transfer-Matrix Method [17], basically the Myklestad-Prohl Method in matrix form, and Finite-Element Method [18], are excellent examples (see Chapter 3 for a full explanation of these and other methods).

Koenig [19] developed a procedure which could be employed for the analysis of a rotor system supported on a maximum of 15 supports and included effects such as bearing/foundation damping, stiffness and mass, rotor unbalance and gyroscopic moments. System undamped critical speeds and unbalance response data could be

calculated, with the limitation that only axi-symmetric bearing supports could be considered. Koenig's program was applied to various rotor systems [20] with the calculated critical speeds found to be in good agreement with those estimated using other analysis methods. Useful information regarding shaft/bearing displacements and bearing forces was obtained.

It has been recognised for some time now [21] that journal (oil-film) bearings of the type normally employed on turbine installations, exhibit stiffness and damping qualities. The introduction of bearing flexibility has the effect of lowering the critical speeds, whilst the rotor response is normally reduced when system damping is present. Shaft internal damping in most cases is extremely small and may be ignored, at least in the forced response analysis. However, if external damping is small, then the shaft internal damping can greatly affect the system stability [21]. In fact, unless the shaft supports exhibit anisotropic properties (e.g. oil-film bearings) this form of damping will have no influence whatsoever on the shaft synchronous response. As a consequence, in most practical cases, the only contribution to system damping will be from the bearing oil-film. The position of the bearings on the shaft is thus of critical importance if their energy-dissipating function is to be fully utilised.

Kirk and Gunter [22] investigated the effect of various values of support damping and stiffness on the synchronous and transient response of a single-mass

flexible (Jeffcott)-rotor. They found that in order to reduce rotor amplitude, the support mass ratio (support-mass/disc-mass) should be kept as small as possible. If this can be achieved, then an optimum support damping value may be chosen so that the rotor steady-state response may be limited to the rotor unbalance eccentricity.

Much effort has been expended in attempting to ensure realistic modelling of the bearing-support dynamics. The oil-film in plain journal bearings may be idealised as a linearised combination of four damping and four stiffness coefficients which vary according to the shaft rotational speed [23]. In reality, oil-film bearings behave in a non-linear fashion and the assumptions for linearisation are reasonably accurate only when the movement of the shaft journal is restricted to small perturbations about the steady operating position. However, Lund [24] indicates that even for amplitudes as large as 40% of the bearing clearance, the linear coefficients still provide sufficient accuracy in most cases.

Analytical expressions for the linearised oil-film coefficients of a short journal bearing were obtained by Holmes [23].

In oil-film bearings the shaft journal not only moves radially, but also in an angular sense. It is therefore possible to introduce another eight coefficients to account for angular damping and stiffness effects [25]. However, in most cases these angular coefficients, along with oil-film inertia effects, may be excluded from the general analysis without any discernable loss of accuracy.

Bannister [26] showed that cases may exist where accurate modelling of the bearing oil-film can only be achieved when non-linear effects are considered. He employed twenty-eight bearing coefficients and achieved good agreement between predicted and measured journal response for a range of operating conditions. It was suggested that it may be possible to use even fewer coefficients without incurring significant loss of modelling accuracy.

Good agreement was also obtained by Lund and Orcutt [27] when they employed the transfer-matrix technique to predict the unbalance response of a rotor-bearing system where each bearing oil-film was represented by 4 stiffness and 4 damping coefficients.

In recent years, an attempt has been made to include the mass, stiffness and damping characteristics of the support structure/foundation. This is of great importance in the field of power generation where nowadays large steam turbo-alternator sets are normally mounted on a tall concrete or steel frame.

The Finite-Element method is well-suited to the analysis of complex vibrating systems and has recently been employed [28] to analyse the dynamic response of some large turbo-rotor-foundation systems. It has been shown [29] that considerable detail is normally required in the idealisation of the system model before accurate results may be obtained. Consequently, more accurate data pertaining to the bearing-support/foundation dynamics is required to ensure good agreement between theory and practice.

Alternatively, in many instances [30] a fully comprehensive rotor-bearing-foundation model need not be required to represent the practical situation, as long as the designer has the capability to predict the alteration in the dynamic response of the overall system when certain system parameters are allowed to vary.

One way of achieving this is to adopt a method of the type suggested by Wang and Lund [31]. Here the rotor and foundation characteristics can be organised individually and combined to provide the complete system dynamics. The foundation parameters could thus be altered easily without the need for complete rotor system analysis, or vice-versa.

Although a number of efficient linear rotor-dynamic analysis methods are available, many phenomena such as sub-harmonic resonance and instability limit cycles cannot be investigated using the linear approach. As a result, more effort is being applied to the analysis of non-linear rotor-dynamics. Adams [32] recently presented a procedure for the non-linear analysis of the response of flexible-rotors with many bearings. He studied steady-state and transient vibrations in a steam turbine, including such effects as seal forces, gyroscopic moments and hydraulic/aerodynamic forces and found sub-harmonic resonance resulting from large mass unbalance.

2.2.2 Self-Excited Whirl

One of the major problems found to occur in various high-speed shaft applications, particularly those

employing oil-film bearings, is that of instability.

One of the earliest researchers to investigate shaft instability was Newkirk [33]. In 1924 he showed experimentally that a shaft running above its first critical speed, may whirl at a frequency approximately equal to its fundamental natural frequency. The whirling amplitude was found to be increased by the fitting of hubs or sleeves on the shaft. Additionally, he demonstrated that the introduction of bearing pedestal flexibility helped reduce the shaft instability.

Smith [21] confirmed the latter finding theoretically with the proviso that stiffness asymmetry would have to be present in the bearing housings.

Newkirk [33] and Kimball [34] made major contributions to the understanding of this problem and suggested that a predominant contributory factor was the friction emanating from shaft shrink-fits.

In 1933, Smith [21] presented the results of a comprehensive analytical and experimental study into self-excited whirl due to shaft internal damping.

A number of significant findings resulted from this investigation. For a simple Jeffcott-rotor, it was shown how the inclusion of rotor (shaft internal) damping could result in instability at a shaft speed ω_i dependent upon the amount of stationary (support or other external source) damping present:

$$\omega_i = \omega_c \cdot (1 + b'/b'')$$

where,

ω_i = Shaft speed at onset of instability

ω_c = Lowest critical speed

b' = Stationary (support) damping coefficient

b'' = Rotary (shaft) damping coefficient.

Investigation of this simple model shows that if the external damping is small in comparison with the shaft internal damping ($b'/b'' \approx 0$), then the shaft motion will be unstable above the shaft first critical speed. If the support damping is increased, then the onset of instability may be shifted to a higher shaft speed.

The instability onset speed could also be increased by accentuating the support asymmetric properties.

Although this latter phenomenon was observed by Newkirk [33] earlier, he did not fully appreciate that the factor influencing the shaft stability was that of support asymmetry as opposed to increased support flexibility.

Many of these early investigations into the stability problem have since been confirmed and further extended by a number of researchers [35,36,37].

Another type of shaft whirl similar to that due to shaft internal friction can be caused by bearing oil-film forces. In fact, Newkirk [38] later decided that the instability he had initially attributed to shaft internal friction [33] actually resulted from 'oil-whirl'.

Oil-whirl is probably the most common cause of rotor instability today, the concepts of which were established by Hori [39]. A common feature of this phenomenon is the occurrence of instability-onset at a shaft speed of approximately twice the first critical, resulting in non-synchronous shaft motion with a frequency equal to that of

the system first natural frequency. A fatigue situation arises due to the cyclic stresses set up within the shaft. Hori showed that after initiation, the oil-whirl instability could be maintained even when the shaft speed was reduced to a value less than that at the onset of instability.

Other researchers investigated the effect of varying certain bearing oil-film parameters on the instability onset speed. Hagg and Warner [40] and Newkirk and Lewis [41] found that the introduction of low bearing clearances and increased oil supply pressures helped delay the onset of instability. They also discovered that it was possible for the instability to be maintained at shaft speeds many times greater than the onset speed.

Tondl [37] presented the results of analytical and experimental studies of the resistance to oil-whirl instability of a variety of oil-film bearing types and showed the cylindrical bearings to be inefficient in this respect.

Nowadays a number of procedures are available [42] for prediction of rotor instability speeds resulting from various destabilising effects.

For the analysis of real rotor systems, a numerical approach is normally necessary. The system eigenvalues, which in general are functions of rotor speed, are predicted and the speed at which the real part of any of the system eigenvalues becomes zero is termed the instability onset speed. This condition is effectively equivalent to the case of zero system damping, instability

occurring when the real part of the eigenvalue becomes positive. The imaginary component of the relevant eigenvalue represents the rate of rotor precession at instability.

On the whole, good agreement has been achieved using these methods in a laboratory environment. Recently, a number of researchers have utilised the transfer-matrix method, in various manners, to allow determination of system instability characteristics. Dostal [43] achieved good agreement with experimental onset-speeds, making use of a number of graphical techniques. In Ref. [44], use was made of a graphical procedure suggested by Dostal and a number of experimental rotor systems analysed. Reasonable results were obtained in most cases. Murphy and Vance [45] presented a novel approach to the problem by determining, explicitly, the system frequency polynomial, thus eliminating the need for sophisticated and problematic, root-searching routines, such as that employed by Lund [46]. Under certain conditions, the method showed reduced execution times when compared to conventional methods.

Of course, the above linear methods are very useful for estimating the threshold of instability, but can give no indication of the rotor response at greater speeds since shaft displacements may become excessive, invalidating the inherent linearising assumptions. One procedure is to determine the speed at which the shaft becomes unstable using linear methods and then to employ non-linear, transient analysis methods [47] to investigate

the shaft orbit growth with time.

However, such approaches are normally prohibitively time-consuming and therefore, normally only adopted where absolutely necessary.

The foregoing covers only some of the types of shaft whirling encountered in practice, from a mainly linear point of view and is certainly not intended to be a totally comprehensive survey encompassing all aspects of this complex subject. Ref. [48] gives some insight into the many different causes of shaft lateral vibration encountered in many real present-day high-speed rotors.

2.3 Vibration Control

For the purpose of this review, the main methods of vibration attenuation as applied to laterally vibrating rotors, will be categorised as follows:

1) System Design.
2) Rotor Balancing.
3) Application of Control Devices.

2.3.1 System Design

Although this is not often thought of as a method of control and may appear too obvious to mention, it is clear that it is the first and most crucial part of the control process. With proper choice of design parameters and sufficient knowledge of the system dynamics, it should be possible to produce a design which will, to a certain extent, minimise and in some cases eliminate, potential sources of vibration.

2.3.2 Rotor Balancing

It is often not fully appreciated that by far the largest proportion of rotor vibrations in the field may be attributed to lack of balance.

Flexible-rotors generally require balancing in a number of planes for a number of speeds since, for speeds higher than about half of the first critical, the rotor assumes deformations which can no longer be neglected, as they set-up new centrifugal forces in addition to the ones caused by the original unbalance.

The practice of flexible rotor balancing can be ascribed to one of two chief methods (and in some cases a combination of both) - the Influence Coefficient Method and the Modal Method.

The influence coefficient method is based on the fact that for a linear system, the rotor unbalance and resulting vibration amplitudes are related as shown:

$$\underline{x} = \underline{\alpha} \cdot \underline{U}$$

where α are the complex linear coefficients which relate rotor lateral displacement at location j due to unbalance at location p.

The displacement quantities x are also complex.

The rotor may be run at a number of speeds, trial weights positioned on each balancing plane in turn and the unbalance response measured. From this data the influence coefficients, α, can be obtained and the correction weights for a given rotor response estimated.

The method was first described by El Hadi [49] in 1962, then again in 1964 by Goodman [50] who expanded upon

the correction procedure with the least-squares method which accommodates additional balance data.

More recently, a number of refinements have been proposed. Larson [51] and Dreschlen [52] showed how the utilisation of surplus information could lead to increased efficiency over the normal method. The balancing problem may also be cast in the form of an optimisation problem [53], where constrained correction masses may be chosen such that the resulting rotor response is minimised over a speed range which could exceed that used for data collection.

Modal methods are based on elimination of residual unbalance effects mode by mode through the operating speed range, in a manner which carefully avoids the re-introduction of previously balanced modes when balancing a given mode.

The basic theory of Modal Balancing and its developments were given by Bishop, Parkinson and Gladwell in a series of papers [54,55] around the early nineteen sixties. Practical application of the method has been described in a number of papers [56,57].

Suggestion that rotor balancing be performed in two stages [58], where the rigid-body modes are balanced first, then the flexible-rotor modes, does not appear conclusive. In fact, in some cases [59] rigid-body mode correction effects may result in an inferior balance state at speeds where flexible-rotor effects are predominant.

The key to this method appears to be a good pre-hand knowledge of the rotor modal response.

Recent work in the field of flexible rotor balancing has indicated that the best approach may be to combine the advantages, while eliminating the disadvantages of both conventional methods to give a so-called Unified Balancing Aproach (UBA). In 1979, Parkinson et al [60] investigated the theoretical basis of such an approach and in a paper a year later with Darlow and Smalley [61], outlined the procedure and presented experimental results which verified the effectiveness of this method and illustrated its advantages in a practical application.

2.3.3 Application of Control Devices

Most real vibrating systems and in particular flexible-rotor systems, contain passive control devices which help attenuate vibration amplitudes and transmitted forces.

In the case of high-speed shafting subjected to lateral vibrations, these passive controllers generally appear in the form of fluid-film bearings. This type of bearing may be successful in limiting the system response under a variety of conditions, but its effectiveness may well deteriorate if the operating conditions alter slightly. In such circumstances, it may be advisable, if possible, to employ active control techniques.

Active controllers require energy input, whereas passive controllers do not and function purely according to the response of the vibrating system.

2.3.3.1 Passive Controllers

2.3.3.1.1 Hydrodynamic (Oil-film) Bearings

In many cases, for all practical purposes, the only system damping present, in many modern-day rotating shaft applications, is that resulting from the bearing oil-film.

The magnitude and orientation of the force exerted by the oil-film on the shaft journal are dependent mainly on the shaft eccentricity-ratio, with the result that the force vector is a non-linear function of the shaft displacement and velocity vectors.

However, a number of reseachers [23] have shown that if the vibration amplitude is sufficiently small, then the force-displacement/velocity relationship may be linearised, the resulting bearing oil-film force equations being expressed in the form:

$$\begin{bmatrix} F_x \\ F_y \end{bmatrix} = \begin{bmatrix} K_{xx} & K_{xy} \\ K_{yx} & K_{yy} \end{bmatrix} \begin{bmatrix} x \\ y \end{bmatrix} + \begin{bmatrix} C_{xx} & C_{xy} \\ C_{yx} & C_{yy} \end{bmatrix} \begin{bmatrix} \dot{x} \\ \dot{y} \end{bmatrix}$$

where

F_x, F_y are the x and y components of the bearing oil-film force

x, y are small journal displacements from the steady running position

K_{ij}, C_{ij} are the linear displacements and velocity coefficients respectively.

The stiffness and damping coefficients may be estimated either by numerical solution of the Reynold's equation [23], or experimentally by employing some of the currently available identification techniques [62]. The bearing coefficients are dependent upon a number of factors including the shaft rotational speed, frequency, oil

viscosity, magnitude and direction of the steady load and the shape and size of the bearing and journal surfaces.

Angular stiffness/damping and oil inertial effects may be included in the analysis [25], but are normally neglected with no significant loss of accuracy.

Another device also employing a viscous fluid-film and widely used in gas turbine applications, is the squeeze-film bearing.

2.3.3.1.2 Squeeze-Film Dampers

The squeeze-film damper was first employed in a practical installation at the end of the last century by C.A. Parsons, on their turborotor systems and enjoys extensive application in the gas turbine field.

The construction of the device is such that normally a rolling element type bearing is mounted on the shaft journal with its outer race held stationary, the cavity between this outer race and the bearing housing containing the oil. Because of the arrangement, the oil-film lacks inherent stiffness and it is sometimes necessary to simulate this effect [64].

Squeeze-film bearings have shown real benefits in reducing rotor response, transmitted bearing force and non-synchronous components [66], although their effect may be localised [64] and in some instances problems of a non-linear nature might be introduced [65].

It has been demonstrated [66] that for efficient operation, the damper characteristics should be sized for the particular application.

Even though the squeeze-film damper has enjoyed

practical application for some time now, it is clear that much more experimental work is required to enable a more complete understanding of this complex device.

2.3.3.2 Active/Adaptive Controllers

Passive devices, such as tuned vibration absorbers and Lanchester dampers, have been employed for vibration control in mechanical systems for many years now [67], but their benefits can only be realised in limited cases.

In many instances, it may be possible to improve on passive control performance by manipulating certain system parameters such that the system response is maintained at low levels even when operating conditions vary. So-called adaptive control may be employed under such circumstances.

Sandler [68], analysing the vibrations of a uniform shaft, demonstrated how the employment of a variable-location flexible support could result in shifting the system's critical speed. Although original, the principle is certainly not a feasible proposition for most real systems - access and rotor geometry being the major limiting factors.

Burrows et al [69] have shown that a simple 'on-off' control strategy may be efficient in controlling rotor response when a squeeze-film damper is utilised as an actuator with oil supply pressure as the control variable. Switching of the damping constant between two values, at the system's 'fixed-points', overcomes the need for continuous active control.

Employing a similar concept, Goodwin et al [70] showed how alteration of the dynamic characteristics of a hydrostatic bearing could result in shifting of the system critical speeds leading to reduced steady-state response.

The use of active feedback in vibration control is fairly old [71], the controllers taking various forms including Electrodynamic [72], Electromagnetic [73], Hydraulic [73], Pneumatic [74] and Eddy-current [75] type. Hydraulic and pneumatic actuators have been employed mainly in the field of vibration isolation [74,76], generally where fairly large control forces are required.

In the past, electrodynamic devices have been shown to be effective in reducing resonant amplitudes in vibrating components. In Refs. [72,77] the steady-state responses of a flexibly-mounted beam and single degree of freedom torsional system, respectively, were shown to be attenuated substantially by the incorporation of electrodynamic actuators within an active control loop.

Roorda [73] presented results for a number of experiments on a variety of simple structures where feedback control was employed, using different types of actuators. One of the most interesting cases was that of electromagnetic control of a vertically-mounted, harmonically excited, cantilever beam. The control force magnitude and phase were adjusted until the minimum response was achieved. The optimum phase angle was found to correspond to a control force of pure damping.

Seto and Yamanouch [75] studied the eddy-current braking effect as a possible means of damping in a

dynamic absorber fitted to a machine tool of ram-structure form. Although the absolute magnitude of the damping was found to be very small, a reduction by a factor of approximately 10 of vibration amplitude at the system fundamental frequency was observed.

The desirability of introducing control forces to a vibrating system, particularly a system with rotating components, without the need for physical contact, is obvious. Of the controllers described above, only the eddy-current and electromagnetic type satisfy the above requirements. For efficient performance, the application of eddy-current type dampers is really restricted to those cases where the system inherent damping is negligible [75]. In real flexible-rotor systems, some damping will normally be present due to the oil-film bearings.

2.3.3.2.1 Electromagnetic Controllers

Electromagnets are inherently highly non-linear devices and consequently require special consideration when being employed as the actuator component in a control system where linear characteristics are to be preferred.

For an electromagnet positioned close to an iron surface, the force relationship may be given [78] by:

$$F = K \cdot (I/G)^2$$

where K may be approximated as a constant, the value of which is dependent upon the particular magnet construction and geometry. I and G are the magnet current and air-gap respectively. The non-linearity in the force versus current-gap relationship is clearly evident.

Klimek [79] suggested pre-magnetising the

electromagnets using a constant current upon which is superimposed the control current. This helps linearise the force-current relationship as long as the control current is a small proportion of the pre-magnetising current. This set-up, however, leads to the introduction of a static instability [80] and it is therefore necessary to incorporate some counter measures. In addition, the force production capacity of the electromagnet will obviously be reduced somewhat due to the (pre-magnetising + control) current - sharing of the magnet windings.

It is possible to eliminate the gap-effect from the above relationship. In their work on vehicle electromagnetic levitation, Jayawant et al [81], demonstrated how partial-linearisation of the electromagnet characteristics could be performed by feeding back a voltage, proportional to flux density at the magnet face, resulting in a considerable improvement in the system stability margin.

Although initially the choice of electromagnets as bearing elements in rotating systems appeared to result from a need for low-friction supports in high-speed shaft applications, where the lack of lubricant was a major advantage [82], it has recently become clear that the potential of such a device may be more fully exploited when employed as an actuator within an active feedback control loop, thus enabling optimisation of the system dynamics in some form [83].

Schweitzer has shown how the destabilising effect of shaft internal damping could be offset by the introduction

of low-level external electromagnetic damping. System resonant amplitudes were also substantially reduced.

In Ref. [84], the electromagnet force-current-gap relationships were developed for a radial controller and comparisons made with experimental calibrations. It was shown how current pre-magnetisation and the assumption of constant air-gap provided a means of approximating the controller as a linear device, thus enabling the employment of linear control theory. Reasonable agreement was achieved between predicted and measured electromagnetic forces. Because of its design, the radial electromagnet was found to introduce a counter-productive moment. The authors stated that in most cases its effect would be insignificant.

More recently Ellis and Mote [85] studied the role of electromagnets in feedback control of circular saws. A proportional-derivative algorithm was employed resulting in an increase in the stiffness and damping of test-discs of the order of 400 percent. Control circuits of an analog nature were used. Linearisation and static stability problems were minimised by the inclusion of pre-magnetising current and position feedback respectively. Magnetic hysteresis, only one of the complexities exhibited by electromagnets, appears to have created substantial problems [86].

Nikolajsen et al [87] showed how an electromagnetic damper could be used to control the synchronous and instability response of a flexible-rotor system. The electromagnetic damper was positioned about one-third of

the span from one end of the transmission shaft and was designed to introduce radial damping forces. The control force was made independent of the air-gap by the incorporation of a flux-feedback technique similar to that used in Ref. [81], thus leaving the force dependent upon the square of the control current. Reduction in the shaft synchronous response at the first critical speed along with suppression of the system instability due to the oil-film bearings and second-order vibrations, provided proof of the practical possibility of utilising electromagnets as an aid in the vibration control of high-speed flexible-rotors. Linearisation of the electromagnetic damping forces used in the numerical prediction of rotor response was shown to provide fairly accurate agreement between calculated and measured rotor response.

Habermann and Liard [88] presented details of the design and operation of an active magnetic bearing system. Practical magnetic bearing applications were cited.

In Ref. [89] the authors proposed the concept of decentralised control, whereby the complexity of the control system could be reduced by considering a number of sub-systems. The approach was adopted with a view to utilising digital control through the use of microprocessors.

Recently, Salm and Schweitzer [90] outlined a design procedure, based on modal analysis, for determining the electromagnet feedback gain values which would ensure stable modes, by using a reduced order system model. The analysis of simple examples confirmed the effectiveness of

the approach, however, no guidance was given as regards the choice of location of controller. Significant reduction in resonance amplitudes was also claimed, although no detailed information was presented.

More recently, Gondhalekar et al [111] presented design details of a radial electromagnetic bearing used to control the vibrations of a flexible transmission shaft. A linear control force-current relationship was achieved through software control using a microprocessor, thus eliminating the need for pre-magnetisation of the magnets [84]. The electromagnet was similar to that used earlier by Nikolajsen [87], constructional improvements having been incorporated. Because of the magnet geometry, special techniques were utilised to eliminate flux-linking problems. Results indicated the effectiveness of the device in shifting system undamped critical speeds and attenuating resonant response.

2.4 Selection of Magnitude and Location of Control Force

The choice of controller force magnitude (the optimum control force) is considered fully in Chapter 5. Some studies into the effect of controller location on the response of flexible rotor systems have already been performed although scope exists for more comprehensive investigations.

Dostal et al [91], employed the theory of 'fixed-points' to determine the optimum location for a radial damper when applied to a flexible-rotor mounted on a variety of supports. The optimum location for the case

analysed, was found at one-eighth span from one of the shaft supports. The optimum location depends greatly upon the number and type of shaft modes encountered. One of the many interesting findings was that the rotor resonant amplitudes appeared to be much more sensitive to the damping magnitude than to its location.

Schweitzer [83] found the optimum location, for suppression of instability, for an external electromagnetic damper when applied to a vertically mounted flexible-rotor, by employing modal methods to define a factor representative of the 'stabilisability' of a number of unstable modes. The optimum damper location thus corresponded to the location where the stabilisability was largest. Theoretical investigation of a rotor system showed, not surprisingly, that optimal control could be achieved when the vibration could be controlled at an anti-node.

Burrows and Sahinkaya [92], adopted a statistical approach in finding the optimum control location for a multi-mode rotor system. The optimisation consisted of a weighted least-squares approach, whereby the residuals to be minimised were a direct function of rotor response. The technique was applied to the case of a 3-disc shaft supported at its ends on hydrodynamic oil-film bearings. The optimum controller location was found to be close to the shaft centre, this consistent with the mode shapes encountered within the chosen speed range. The method employed provided useful additional information regarding the sensitivity of the optimisation parameters.

2.5 Limitation of Previous Work

The general approach so far in attempting to introduce some means of external control, active or passive, in flexible-rotor systems, has been to apply the control force at some position along the shaft span in a radial sense [43,87,91].

In addition, the most suitable location (optimum location) for the controller may, because of the nature of the equipment, e.g. turbomachinery, be inaccessible.

In certain cases, radial control may be achieved through manipulation of the support characteristics [69, 70], although ineffective control of shaft flexural criticals and/or the introduction of relatively large static displacements in such instances may rule out this option.

The need for an efficient means of control, which may assist in overcoming the above problems, is clear.

The employment of electromagnets as active force-generators in a feedback control circuit, for limiting flexible-rotor dynamic response, has not yet been fully exploited. Although much consideration has been given to utilising these devices as damping elements within rotor systems [83,87], their ability to exert a stiffness influence has, by comparison, been neglected. In recent years, fast, efficient and relatively inexpensive microprocessors have become readily available, but their application to electromagnetic control has been limited.

In the work to date, where electromagnets have been used to control shaft vibrations, the control circuits

appear to be unnecessarily complex as a result of the electromagnet design. The electromagnets have been mounted around the shaft [83,87,111], with arguably the parameter with greatest influence on control system performance, i.e. the gap geometry (size) fixed at the design stage, thus making extremely difficult the possibility of adjustment of control system characteristics through alteration of this parameter.

2.6 Aim of This Work

The main aims of the work described herein are as follows:

1. The creation of computer software to allow dynamic analysis of flexible-rotor systems when external control is employed.
2. To assess theoretically, the performance of a novel Angular Controller, in comparison to the conventional Radial Controller, when employed on a variety of flexible-rotor systems.
3. Design and construction of a flexible-rotor test rig incorporating an Angular Electromagnetic Controller.
4. The experimental investigation of the performance of an Angular Controller, when utilised as an external damper/stiffener, on various rotor arrangements and comparison with predicted performance.

CHAPTER 3

METHODS OF ANALYSIS IN ROTOR-DYNAMICS

Nowadays the need for accurate rotor system critical speed, stability and in some cases even transient reponse data, has led to the requirement for efficient analysis methods. Since real rotor-bearing systems are often very complex structures, exact solutions are, in most cases, not possible and it is necessary to make use of available numerical techniques.

The real system will have distributed mass and elasticity and is said to be continuous, whereas the system to be analysed will be a modelled version of this and will normally consist of a number of discrete rigid masses connected by massless beam elements. It is clear therefore, that the modelling process plays a most crucial role in the overall analysis procedure. It is important to realise that, irrespective of the level of sophistication of the numerical method, the solution obtained will at best, be an approximation to the exact solution for the model.

The most commonly applied methods today are:

1) The Transfer Matrix Method.
2) The Influence Coefficient Method.
3) The Finite-Element Method.
4) The Modal Method.

3.1 The Transfer Matrix Method

The Transfer Matrix technique evolved from the work of Myklestad [10] and Prohl [11] who presented a tabular

procedure for the dynamic analysis of beams and shafts respectively.

The general approach when employing this method is to first set-up, in matrix form, the recurrence relationships for each element type and then to combine these by successive matrix multiplication. The resulting overall transfer matrix will represent implicitly the system frequency equation. The natural frequencies are determined as those frequencies at which the system boundary conditions are satisfied.

The similarity between this method and the Holzer technique [12] is immediately evident where, in the latter case, a torsional natural frequency is determined when the residual torque becomes zero.

The mode shapes are easily obtained by making use of the relationships between the non-zero parameters in the initial state vector and appropriately normalising the resultant relative shaft displacements at the calculated frequencies. System forced-analysis requires little additional effort and is achieved through inclusion of forcing terms in the element recurrence equations leading to the introduction of an additional row and column in the basic transfer matrix.

The transfer matrix method is ideally suited to the analysis of rotor systems because of its applicability to chain-like structures and minimal demand on computer memory. Although the method is susceptible to numerical problems under certain conditions, various procedures may be employed [17] to minimise and possibly even eliminate these effects.

3.2 The Influence Coefficient Method (ICM)

This method evolved from the early matrix methods developed and employed mainly by Argyris [93] for the structural analysis of aircraft frames.

Although influence coefficients in the strictest sense refer to the system flexibility coefficients, it is quite common also to make reference to the system stiffness influence coefficients. The two approaches are described here.

The method, in contrast to the Transfer Matrix Method, when employed for dynamic analyses, necessitates expressing the system equations of motion in an explicit matrix form, i.e. for a linear system:

$$\underline{M}\,\ddot{\underline{x}}(t) + \underline{C}\,\dot{\underline{x}}(t) + \underline{K}\,\underline{x}(t) = \underline{P}(t) \qquad (3.1)$$

making use of the stiffness matrix $\underline{K}$, or:

$$\underline{F}\,\underline{M}\,\ddot{\underline{x}}(t) + \underline{F}\,\underline{C}\,\dot{\underline{x}}(t) + \underline{I}\,\underline{x}(t) = \underline{F}\,\underline{P}(t) \qquad (3.2)$$

if the flexibility coefficient matrix $\underline{F}$ is used. The vector $\underline{x}(t)$ contains the system generalised displacements (linear and angular), all other parameters are as defined in the nomenclature.

The stiffness matrix $\underline{K}$ contains the system stiffness influence coefficients where the stiffness coefficient k_{ij} is defined as the force required, at a point $x = x_i$, to produce a unit displacement, $u_j = 1$, at a point $x = x_j$, such that the displacements at all other points are zero. By analogy, the flexibility influence coefficients, f_{ij}, contained in matrix $\underline{F}$, are defined as the displacement at a point $x = x_i$ due to the application of a unit force, $Q_j = 1$, at a point $x = x_j$.

It is clear that if the flexibility matrix $\underline{F}$ can be inverted, then $\underline{K} = \underline{F}^{-1}$ and equations (3.1) and (3.2) are identical. However, caution needs to be exercised when adopting this approach, since under certain circumstances [47], the flexibility matrix may become ill-conditioned making an inversion unreliable or impossible.

Normally, the stiffness coefficient method is adopted since the $\underline{K}$ matrix is inherently of a banded form leading to possible savings in computer memory.

If we let $\underline{y} = \begin{bmatrix} \dot{\underline{x}} \\ \underline{x} \end{bmatrix}$

then for free vibrations, $\underline{P}(t) = \underline{0}$, from equation (3.1)

$$\underline{A}\,\dot{\underline{y}} + \underline{B}\,\underline{y} = \underline{0}$$

where $\underline{A} = \begin{bmatrix} \underline{0} & \underline{M} \\ \underline{M} & \underline{C} \end{bmatrix}$ and $\underline{B} = \begin{bmatrix} -\underline{M} & \underline{0} \\ \underline{0} & \underline{K} \end{bmatrix}$

Reducing still further, if $\underline{H} = -\underline{A}^{-1}\,\underline{B}$

then $$\dot{\underline{y}} - \underline{H}\,\underline{y} = \underline{0} \qquad (3.3)$$

Assuming the solution of equation (3.3) is of the form $\underline{y} = \underline{\bar{y}}e^{\lambda t}$ then

$$(\underline{\lambda}\,\underline{I} - \underline{H})\underline{\bar{Y}} = \underline{0} \qquad (3.4)$$

and for a non-trivial solution of equation (3.4) we obtain the well known characteristic equation:

$$\left|\underline{\lambda}\,\underline{I} - \underline{H}\right| = \underline{0}$$

which may be solved using a number of available techniques. The eigenvalues, $\underline{\lambda}$, are the system natural frequencies and are, in general, complex functions which vary with rotor speed [46]. For an n-degree-of-freedom system, $\underline{H}$ will be a 2n x 2n matrix.

For the analysis of forced vibrations if external

forcing is assumed to be of the form $\underline{P} = \underline{\bar{P}}e^{i\Omega t}$, then the system response may be described by $\underline{x} = \underline{\bar{X}}e^{i\Omega t}$ and from equation (3.1) may be expressed in the form:

$$\underline{\bar{X}} = \left[\underline{K} - \underline{M}\,\Omega^2 + i\Omega\,\underline{C}\right]^{-1}\underline{\bar{P}}$$

$$= \underline{\bar{R}} \cdot \underline{\bar{P}}$$

where $\underline{\bar{R}}$ is termed the system receptance matrix and must be determined at each appropriate rotor speed.

The above method has been employed with success for rotor-dynamic analysis in a number of cases, e.g. Ref. [94]. Reference [95] describes the procedures for setting-up the system stiffness or flexibility matrices.

3.3 The Finite-Element Method (FEM)

When using this technique, a complex structure is considered as a finite assemblage of discrete elements, where every such element is a continuous structural member. The only significant difference between this method and the Influence Coefficient Method is that in the latter case, the shaft elements exhibit discrete dynamic properties which, due to the approach, can only be considered to appear at the shaft stations or nodes, whilst the former method allows for the inclusion of distributed effects.

Effectively, this means that the system stiffness and mass matrices become densely populated when using the FEM, whereas when the ICM is employed, these matrices are sparsely populated and in the case of the mass matrix, of diagonal form.

In order to incorporate this 'distributed parameter

effect' into the analysis, it is necessary to define a displacement function which will suitably describe the displacement pattern of the elements used. The element stiffness, mass and damping matrices can then be derived and the assembled system matrices set-up.

Solution procedures identical to those shown earlier for the Influence Coefficient Method may be employed.

The FEM has only recently [18] been applied to rotor-bearing systems and although the demand for computer memory is generally much greater than that of the Transfer Matrix Method, it has been shown [96] that fewer elements can be used to model a system, a high level of accuracy being maintained.

The FEM becomes a very powerful tool where systems of great complexity are to be analysed, in fact, in such circumstances, it may be the only accurate method available.

3.4 The Modal Method

The Modal Method has been employed by a number of workers in the field of rotor-dynamics [97] and in particular has been applied to the problem of flexible rotor balancing for a number of years now [55,60].

The method is based on the principle of orthogonality of principle modes and consequently makes possible the determination of the response of a multi-degree-of-freedom system, to some general excitation, by means of the superposition of the responses of a number of single-degree-of-freedom systems.

Considering again the response of a multi-mode system, the equations of motion of which may be written:

$$\underline{M} \cdot \ddot{\underline{x}}(t) + \underline{C} \cdot \dot{\underline{x}}(t) + \underline{K} \cdot \underline{x}(t) = \underline{P}(t)$$

$\underline{x}(t)$ being the system generalised co-ordinates. If a free-vibration analysis, such as that described in Section 3.2, is performed, the system eigenvalues and corresponding eigenvectors can be obtained. Remembering that

$$\underline{y} = \begin{bmatrix} \dot{\underline{x}} \\ \underline{x} \end{bmatrix} \tag{3.5}$$

The resulting eigenvectors may be placed in a matrix $\underline{u}$ where each column in the matrix represents the system mode shape at each of the corresponding system eigenvalues. It is now possible to define a set of principle co-ordinates $\underline{v}$, where:

$$\underline{y} = \underline{u} \cdot \underline{v}(t) \tag{3.6}$$

then

$$\underline{A} \cdot \underline{u} \cdot \dot{\underline{v}}(t) + \underline{B} \cdot \underline{u} \cdot \underline{v}(t) = \underline{P}(t)$$

Pre-multiplying the above by the transposed modal matrix $\underline{u}^T$ and considering orthogonality, leads to the diagonalised matrices $\underline{A}'$ and $\underline{B}'$ and thus renders the solution of the above equation as the simple solution of 2n independent linear equations, in an n-degree-of-freedom system. Thus:

$$\underline{A}' \cdot \dot{\underline{v}}(t) + \underline{B}' \cdot \underline{v}(t) = \underline{u}^T \cdot \underline{P}(t) \tag{3.7}$$

The solution in the generalised co-ordinates x(t) is obtained from the relationships shown in equations (3.5) and (3.6).

Of considerable interest, particularly in the context

of flexible rotor balancing, is the right-hand side of equation (3.7) which determines the distribution of forcing according to its effectiveness in exciting the principle mode motions. In many cases therefore, by suitable choice of $\underline{P}(t)$ vector, it may be possible to improve the balance of particular vibration modes without affecting the others.

The Modal Method was recently [98] applied in a slightly modified fashion (termed quasi-modal analysis) to a number of rotor systems including one employing sub-levels. The technique is in principle identical to that outlined above, but considers the system mode shapes to consist of the combination of two vibration mode shapes: 1) that for an undamped system with the rotor considered pinned at the supports and 2) a static deflection mode shape. The approach adopted is certainly a novel one and eliminates the need for repeated eigenvector analysis due to the change in rotor speed, this being necessary in general, when the conventional modal method is used.

3.5 Discussion of Numerical Methods

It is clear that each of the analysis techniques just described may be effectively applied to the general problem of shaft whirling. However, the suitability of these methods is greatly dependent upon the particular type of system under investigation.

In the case of the Finite-Element and Influence Coefficient Methods, rotor systems of considerable complexity can be analysed, but if the number of elements

required for system modelling is fairly large, then excessive demands may be made on computer memory. This results from the fact that the order of the system matrices employed in the analysis is directly proportional to the number of degrees-of-freedom of the system to be analysed. Both methods are easily applied to systems incorporating multiple sub-levels. In addition, the FEM is ideally suited to shaft arrangements where complex geometrical aspects have to be considered. In fact under these circumstances it may be the only method to provide sufficiently accurate results.

Modal methods appear to have their benefits in cases where the total system response can be ascribed to that resulting from a finite number of vibration modes and where sufficient information regarding the system mode shapes is available. When this is the case, a reduction in the number of degrees-of-freedom of the model is possible. If the mode shapes (eigenvectors) are to be determined accurately using, for example, a method similar to that described in Section 3.4, then a greater number of degrees-of-freedom may be required resulting in the loss of one of the method's main advantages. The method may also easily be applied to systems with sub-levels as described in [98], although contrary to the authors' remarks such arrangements <u>can</u> be analysed using Transfer Matrix Techniques [17].

The order of the matrices employed when using the Transfer Matrix Method is dependent only on the number of degrees-of-freedom at any single shaft node, the matrix

size remaining fixed no matter how many elements are chosen to model the system. This is a significant advantage since effectively it results in little change in computer memory requirements irrespective of the size (number of degrees-of-freedom) and complexity of the system to be analysed. The influence of rotor support/foundation dynamics, of varying complexity,may be easily included in the analysis [17].

Numerical problems, which may be encountered in systems where high-order natural frequencies are required or where intermediate supports exhibit very low flexibility, may be minimised and possibly even eliminated [17,99] by applying a number of available corrective procedures.

Since the numerical method adopted would be used mainly to investigate the dynamic response of a laboratory test-rotor described later, taking into account the above, it was felt that the Transfer Matrix Method would be the most suitable in this case. As a consequence the method is used extensively in the work described herein.

CHAPTER 4

MODELLING THE SYSTEM DYNAMICS - THE TRANSFER MATRIX METHOD

4.1 General Approach

Any real structure subjected to dynamic loading may be idealised as an assembly of sub-elements each in general possessing mass, stiffness and damping properties. When using the Transfer Matrix Method the structure is normally idealised such that a number of similar elements are joined end to end in chain fashion. Making use of the laws of dynamics whilst ensuring inter-element compatibility leads to a set of equations which provide a means of relating the element end-conditions. Transfer matrices are thus obtained for each element type. The parameters required to define the condition of an element at it's ends are expressed in the form of a state vector. The order of the state vector is dependent upon the system to be analysed. For a beam-like structure, since at least two generalised forces and displacements are required at each node, the minimum order is four for planar motion and eight for the most general case.

For the sake of illustrating the general approach the case of an undamped, laterally-vibrating beam (Fig. 4.1) will be considered frequently throughout this chapter. The beam is simply-supported at both ends and, as usual, may be idealised as a number of discrete

rigid masses joined by elastic massless beam elements. From elementary beam theory [Section 4.6] the deflection and force parameters at the left of section i can be related to those at the right of section i - 1 using the transfer matrix $\underline{F}_i$ so that

$$\underline{Z}_i^L = \underline{F}_i \cdot \underline{Z}^R{}_{i-1}$$

Similarly, the parameters to the right and left of any point i are related as shown,

$$\underline{Z}_i^R = \underline{P}_i \cdot \underline{Z}_i^L$$

The matices $\underline{F}_i$ and $\underline{P}_i$ are termed the system field and point sub-element transfer matrices respectively. Transfer matrices for other element types may be obtained following an identical procedure [Section 4.6.3].

Once the basic transfer matrices for a particular arrangement have been developed the system overall transfer matrix $\underline{U}$ is easily obtained by appropriate multiplication of the relevant element transfer matrices. For instance, in the above case the relationship

$$\underline{Z}_7 = \underline{U} \cdot \underline{Z}_0 \qquad (4.1)$$

exists where,

$$\underline{Z}_7 = [\ \underline{F}_7\ \underline{P}_6\ \underline{F}_6\ \underline{P}_5\ \underline{F}_5\ \cdots\ \underline{P}_1\ \underline{F}_1\ ]\cdot \underline{Z}_0$$

Intermediate state vectors are obtained using a similar procedure.

Having obtained the overall transfer matrix $\underline{U}$ the system boundary conditions may then be employed to enable determination of the system natural frequencies and, with a little effort, forced response data.

4.2 Free Analysis

When the overall transfer matrix has been determined and boundary conditions are applied an implicit frequency polynomial of order 2n, where n is the system number of degrees of freedom, is obtained. The roots of this polynomial correspond to the system eigenvalues. It is also possible to obtain an explicit expression for the frequency polynomial [45] although this method is not normally employed.

For a rotor-bearing system a critical speed analysis and stability assessment may be performed by calculation and investigation of the eigenvalues.

In general the transfer matrix coefficients will be of a complex, frequency-dependent and speed-dependent form. The components of all state vectors are assumed to vary harmonically with time so that

$$\underline{Z} = \underline{\bar{Z}} e^{\lambda t}$$

where $\underline{\bar{Z}}$ is an amplitude vector and λ is in general a complex variable ($\lambda = \alpha + i\omega$). The system complex

eigenvalues λ have great practical significance since their imaginary parts represent the damped natural frequencies whilst the real parts provide the level and sense of system damping present. The critical speeds are those speeds at which the shaft rotational frequency coincides with a, generally damped, system natural frequency.

It is well known that in certain damped vibrating systems, for instance in rotor systems where oil-film bearings are employed, instability regions may occur within the shaft operating speed range.

Instability onset speeds may be predicted from linear theory by considering the sign of the real part of the system eigenvalues.

Where the real part of a system eigenvalue is positive ($\alpha > 0$) unstable behaviour will be exhibited, i.e. the system effective damping becomes negative, leading to growth of vibration amplitude with time. If the real part is negative ($\alpha < 0$) stability will be maintained, the degree of which will be dependent upon the amount of residual damping present. The shaft speed at which the eigenvalue has no real part ($\alpha = 0$) is termed the instability onset speed since the system will then be on the threshold of instability, the imaginary component representing the corresponding rate of precession, ω, of the shaft.

When the structure is undamped all complex eigenvalues will be replaced by purely imaginary ones

and the system response may be described as

$$\underline{Z} = \underline{\bar{Z}} e^{i\omega t}$$

where ω now denotes the system undamped natural frequencies. In any case the eigenvalues, whether real or complex, may be obtained when the following conditions are fulfilled. Considering once more the simple beam in bending (Fig. 4.1) and equation (4.1), as a result of the boundary conditions,

$$w_7 = 0 \quad ; \quad M_7 = 0 \quad ; \quad w_0 = 0 \quad ; \quad M_0 = 0$$

Therefore

$$\left.\begin{aligned} U_{12}\Phi_0 + U_{14}V_0 &= 0 \\ U_{32}\Phi_0 + U_{34}V_0 &= 0 \end{aligned}\right| \qquad (4.2)$$

Those, generally complex, frequencies λ which result in non-trivial zero values of the frequency determinant

$$\begin{vmatrix} U_{12} & U_{14} \\ U_{32} & U_{34} \end{vmatrix}$$

are the system eigenvalues.

Since the coefficients U_{ij} are, in general, speed-

-dependent the eigenvalues λ must be determined at each speed. A number of efficient techniques are available for the extraction of the system complex eigenvalues [46, 108]. These methods basically entail incrementing the value of the complex frequency λ until a root is encountered i.e. the frequency determinant changes sign. Subsequent application of an iterative interpolation procedure results in the reduction of the determinant to a practically zero value - the corresponding frequency is a system eigenvalue. In the simplest case this may be achieved by performing a linear interpolation until some pre-defined criterion is met.

A powerful root-finding technique, termed Muller's Method, has been employed with success [108]. The method is based on the approximation of the frequency polynomial, over a specified range, as a quadratic. The nearest root is taken as an estimate of the actual root, convergence being achieved by successive iteration. Alternatively if use is made of the polynomial derivatives [46] then the rate of convergence on a root may also be somewhat increased. However, if system stability alone is to be assessed then a graphical procedure may be employed [43, 44].

When the eigenvalues have been determined the mode shapes may be found easily by back substitution. For instance in the previous example, referring to equation (4.2), one of the initial state variables (Φ_0, V_0) may be expressed in terms of the other, given an arbitrary

value and transfer matrix multiplication performed as before. The system state vectors then provide details of the relative shaft deformations.

4.2.1 Residual Method

Another approach, similar to that employed by Holzer [12] in torsional systems, is to make use of the system boundary conditions to create a residual term. The residual is a function of certain system parameters which are necessarily zero at all system natural frequencies. As with the frequency determinant, the residual is calculated for a range of vibration frequencies and the points at which the residual becomes zero are the natural frequencies.

The procedure will be shown for the vibrating beam of Fig. 4.1. The overall transfer matrix is obtained as explained earlier and from the first equation (4.2) we can write,

$$\Phi_0 = -(U_{14}/U_{12}).V_0$$

Substituting this into the second equation gives

$$(U_{34} -(U_{32}.U_{14}/U_{12})).V_0 = 0$$

or $$R.V_0 = 0$$

where R is termed the residual. For other than the

trivial case $V_0 \neq 0$ and thus $R = 0$ if the assumed value of λ corresponds to a natural frequency. Again an iterative procedure can be employed to find λ when $R \approx 0$.

The same procedure is followed for any rotor arrangement irrespective of the boundary conditions since for different configurations only the number and magnitude of the coefficients in the homogeneous equations will change. The normal modes may be determined using the methods described earlier.

4.2.2 Numerical Problems

When using transfer matrices, unless special precautions are taken, numerical difficulties can be experienced mainly under two circumstances: when computing higher-order natural frequencies and when intermediate elastic supports become very stiff. Fortunately, in the majority of practical cases only the first few natural frequencies are of any interest and thus one potential source of error may be disregarded.

A number of procedures aimed at eliminating the above problems have been proposed [17, 99]. An effective correction method, created by Furke and described in [17], makes use of so-called delta matrices and is based on expressing the system frequency-determinant in terms of a number of smaller determinants. The system determinant is more accurately computed by calculating and combining the individual sub-determinants. However, one of the main disadvantages

of this approach is the large number of sub-determinants, required even for relatively low-order systems. It's application to real rotor systems, where in general non-planar motion can exist is not really feasible. Additionally, the nature of the method is such that normal modes cannot be obtained.

Another correction technique, more suitable for rotordynamic analysis and lacking many of the severe limitations of the delta matrix method, is the modified transfer matrix method developed by Pestel and Mahranholtz [17].

4.2.3 The Modified Transfer Matrix Method

The modified method of analysis eliminates the problem of the small differences of large numbers, which normally occurs as a result of the aforementioned conditions, through a technique whereby the components of the initial state vector are estimated close to their actual values.

The initial estimation of this vector need not be close to the actual vector since convergence is rapid and in many instances after one iteration only the estimated vector is very close to the actual one.

In order to allow for modification of the estimated values correction terms, K, are added to a number of the non-zero initial state vector parameters. For an n^{TH} order problem in which the initial state vector $\underline{Z}_0$ consists, in general, of n/2 components equal to

zero, $\underline{Z}_0$ would be written as follows,

$$\underline{Z}_0 = \begin{bmatrix} 0 \\ 0 \\ \vdots \\ 0 \end{bmatrix}_{\frac{n}{2}} + K_1 \begin{bmatrix} 0 \\ 0 \\ \vdots \\ 0 \end{bmatrix}_{\frac{n}{2}} + K_2 \begin{bmatrix} 0 \\ 0 \\ \vdots \\ 0 \end{bmatrix}_{\frac{n}{2}} + \ldots + K_{(\frac{n}{2}-1)} \begin{bmatrix} 0 \\ 0 \\ \vdots \\ 0 \end{bmatrix}_{\frac{n}{2}}$$

$$\begin{bmatrix} \delta_0 = 1 \\ \delta_1 \\ \delta_2 \\ \vdots \\ \delta_{(\frac{n}{2}-1)} \end{bmatrix} \quad \begin{bmatrix} 0 \\ 1 \\ 0 \\ \vdots \\ 0 \end{bmatrix} \quad \begin{bmatrix} 0 \\ 0 \\ 1 \\ \vdots \\ 0 \end{bmatrix} \quad \begin{bmatrix} 0 \\ 0 \\ 0 \\ \vdots \\ 1 \end{bmatrix}$$

Where δ_i represent actual numbers which are the estimated values for the corresponding parameters which make up the state vector $\underline{Z}_0$, whereas the correction factors K_i are initially unknown and the values δ_0 to $\delta_{(\frac{n}{2}-1)}$ are normally initially arbitrarily set equal to unity.

Once again this method is probably best illustrated by analysing the simple beam system investigated earlier, (Fig. 4.1). Consider the initial state vector parameter values at point 0. Since, for free vibration analysis, the absolute values of these parameters is not of any importance the slope Φ_0 may be given a value of

unity. Now $V_0 \neq 0$ and the shear force V_0 will be linearly related to Φ_0 therefore say;

$$V_0 = \delta . \Phi_0$$

Thus, in matrix notation, introducing the correction factor for the shear force term we can write,

$$\underline{Z}_0 = \begin{bmatrix} 0 \\ 1 \\ 0 \\ \delta \end{bmatrix} + K \begin{bmatrix} 0 \\ 0 \\ 0 \\ 1 \end{bmatrix}$$

and when K is a small quantity $V_0 = \delta$. Assuming initially that $\delta = 1$ and multiplying through by the overall transfer matrix $\underline{U}$ gives:

$$\underline{Z}_7 = \begin{bmatrix} w \\ \Phi \\ M \\ V \end{bmatrix}_7 = \begin{bmatrix} b_1 \\ b_2 \\ b_3 \\ b_4 \end{bmatrix} + K \begin{bmatrix} c_1 \\ c_2 \\ c_3 \\ c_4 \end{bmatrix}$$

Now applying the boundary conditions at point 7,

$$M_7 = 0 \text{ and } w_7 = 0$$

and we obtain two equations

$$b_3 + Kc_3 = 0 \qquad (4.3)$$

$$\text{and } b_1 + Kc_1 = 0 \qquad (4.4)$$

Letting K in equation (4.3) be K_a and K in equation (4.4) be K_b,

$$K_a = -b_3/c_3$$

$$\text{and } K_b = -b_1/c_1$$

If both equations yield the same value for K_a and K_b they would be interdependent, i.e. their determinant would be zero so that the value of λ used in the numerical computation would correspond to a natural frequency of the beam. Normally, however, the above equations give different values for K_a and K_b and in this case the revised value of K is taken as the mean of K_a and K_b. That is,

$$K = \frac{K_a+K_b}{2}$$

The residual R in this case is taken as the difference of the K values,

$$R = K_a-K_b$$

The revised K value is now added to the shear force term in the intial state vector to give

$$V_0 = \delta + K$$

The revised value of δ is thus

$$\delta = 1 + K$$

The foregoing calculation is repeated for the same frequency and new values of K_a and K_b obtained. The latest K value should now be found to be extremely small but the value of R at this frequency will remain unchanged. It should be noted that using this approach, with reasonable estimates of initial state vector parameters, the resulting residual will be determined from the addition of two numbers of identical sign.

The above procedure is repeated, with increasing values of frequency λ, over the desired frequency range until a change in the sign of the residual occurs, indicating a natural frequency between the relevant λ values. By performing linear (or some other means of) interpolation with a smaller frequency increment the system natural frequencies may be determined with sufficient accuracy.

The normal transfer-matrix method may be easily extended to incorporate the above correction routine. The increase in computer memory requirements for all practical purposes may be neglected.

In reference [17] it is shown how the modified method was employed to analyse the case of a turbine-

-generator set mounted on a flexible foundation. The first six system natural frequencies were easily obtained using only eight digits whilst even when 18 digits were employed it was impossible to accurately determine the first five eigenvalues using the normal 'uncorrected' transfer matrix technique.

It is important to note that application of modified method will not necessarily ensure numerical stability in all cases [99]. However, during the numerous analyses performed throughout this investigation no such problems were encountered.

4.2.4 Dynamic Stiffness

Instead of calculating a residual or frequency determinant an alternative approach is to make use of the concept of dynamic stiffness. In contrast to the above two parameters dynamic stiffness has a distinct physical meaning and provides a useful means of estimating system response through utilisation of sub-element dynamic stiffness data [100]. The dynamic stiffness at a system location, depending on the boundary conditions, is defined as either M/Φ or V/w and is thus the inverse of receptance. It has a zero value at a system natural frequency and tends to infinity between any two natural frequencies. This latter characteristic can lead to problems in determining system natural frequencies where a number of such frequencies are closely grouped, due to the substantial

rate of change of dynamic stiffness in this area.

4.3 Forced Analysis

For the analysis of forced vibration all transfer matrices can be expressed in an extended form, i.e. an extra row and column are added to the standard transfer matrix. With this modification the inclusion of forcing terms independent of the state vector parameters is accomplished very easily. The method of analysis is best shown with reference to the uniform beam in Fig. 4.1. Considering the introduction of an external force F at, say, point 3 varying harmonically with time so that,

$$F = \overline{F}e^{i\omega t}$$

and, in general, all state variables are complex and considered to vary in the same manner such that,

$$w = \overline{w}e^{i\omega t}$$
$$\Phi = \overline{\Phi}e^{i\omega t}$$
$$M = \overline{M}e^{i\omega t}$$
$$V = \overline{V}e^{i\omega t}$$

Because of this a new (point) transfer matrix, relating state vectors at points 3^L and 3^R, needs to be introduced. Neglecting moment discontinuities [see section 4.6.3.2]

$$\underline{P}_3 = \left[\begin{array}{cccc|c} 1 & 0 & 0 & 0 & 0 \\ 0 & 1 & 0 & 0 & 0 \\ 0 & 0 & 1 & 0 & 0 \\ -m\omega^2 & 0 & 0 & 1 & \bar{F} \\ \hline 0 & 0 & 0 & 0 & 1 \end{array}\right]$$

Again we obtain the relationship

$$\underline{Z}_7^R = \underline{U}.\underline{Z}_0^L$$

Where the system overall transfer matrix this time is extended and the terms U_{15}, U_{25}, U_{35}, and U_{45} are, in general, non-zero. The coefficients U_{51}, U_{52}, U_{53} and U_{54} are all zero. This time introduction of the beam end conditions provided the non-homogeneous equations:

$$-U_{15} = U_{12}\Phi_0 + U_{14}V_0$$
$$-U_{35} = U_{32}\Phi_0 + U_{34}V_0$$

The equations may be solved for Φ_0 and V_0 and all other system parameters obtained by multiplication of the initial state vector by the relevant transfer matrices.

The complete procedure can be repeated for a range of frequency values and the system frequency response obtained.

Irrespective of the number, type and order of the

system elements employed the above method may be applied without modification.

With the response parameters at each shaft section computed, a detailed description of the shaft motion, in whirl orbit form, may be easily obtained (Appendix A).

4.4 Intermediate Rigid Supports and Pinned-Joints

The introduction of system intermediate flexible supports is easily dealt eith simply by the inclusion of the relevant stiffness values in the appropriate transfer matrices. However, where the stiffness becomes so large that the support must be considered rigid or where other discontinuities, e.g. a hinge or pinned-joint, occur it will be necessary to utilise the resulting intermediate boundary conditions. This, of course, means that the 'straight-through' matrix multiplication approach described earlier cannot now be maintained, although very little hardship will result as shall be seen.

Consider now the introduction of a radially-rigid support and pinned-joint to the vibrating beam of Fig. 4.1. If the support is placed at point 4 and the hinge at point 5 two additional boundary conditions occur;

$$\text{At point 4} \qquad w_4 = 0$$

and let the force transmitted to the support be P.

At point 5 $\quad M_5 = 0$

and let the change in beam slope at this point be Q.

For forced vibrations the following relationships hold;

$$\begin{bmatrix} w \\ \Phi \\ M \\ V \\ 1 \end{bmatrix}_4^R = \begin{bmatrix} U'_{11} & U'_{12} & U'_{13} & U'_{14} & U'_{15} \\ U'_{21} & \cdot & \cdot & \cdot & U'_{25} \\ U'_{31} & \cdot & \cdot & \cdot & U'_{35} \\ U'_{41} & \cdot & \cdot & \cdot & U'_{45} \\ 0 & 0 & 0 & 0 & 1 \end{bmatrix} \begin{bmatrix} w \\ \Phi \\ M \\ V \\ 1 \end{bmatrix}_0^L + P \begin{bmatrix} 0 \\ 0 \\ 0 \\ 1 \\ 0 \end{bmatrix}$$

or

$$\underline{Z}_4^R = \underline{U}' . \underline{Z}_0^L + \underline{P}_4^R$$

and

$$\begin{bmatrix} w \\ \Phi \\ M \\ V \\ 1 \end{bmatrix}_5^R = \begin{bmatrix} U''_{11} & U''_{12} & U''_{13} & U''_{14} & U''_{15} \\ U''_{21} & \cdot & \cdot & \cdot & U''_{25} \\ U''_{31} & \cdot & \cdot & \cdot & U''_{35} \\ U''_{41} & \cdot & \cdot & \cdot & U''_{45} \\ 0 & 0 & 0 & 0 & 1 \end{bmatrix} \begin{bmatrix} w \\ \Phi \\ M \\ V \\ 1 \end{bmatrix}_0^L P \begin{bmatrix} a_1 \\ a_2 \\ a_3 \\ a_4 \\ 0 \end{bmatrix} Q \begin{bmatrix} 0 \\ 1 \\ 0 \\ 0 \\ 0 \end{bmatrix}$$

or

$$\underline{Z}_5^R = \underline{U}'' . \underline{Z}_0^L + \underline{P}_5^R + \underline{Q}_5^R$$

Where $\underline{U}'$ and $\underline{U}''$ are the system transfer matrices relating conditions between points 0 and 4 (right) and points 0 and 5 (right) respectively.

Making use of end and intermediate boundary conditions two additional equations are obtained;

$$0 = U'_{12}\Phi_0 + U'_{14}V_0 + U'_{15}$$

$$0 = U''_{32}\Phi_0 + U''_{34}V_0 + U''_{35} + a_3.P$$

The two equations here, when combined with those resulting from the boundary conditions at the beam right hand end (point 7), allow for complete solution of the four unknowns Φ_0, V_0, P and Q. As before, all other relevant system parameters may be determined by back substitution.

In general the total number of simultaneous equations to be solved, N_t will be

$$N_t = N_e + N_i$$

Where N_i is the total number of equations resulting from intermediate rigidities or releases. N_e is the number of equations obtained from the system end conditions. $N_e = n/2$ where n is the state vector order.

A similar procedure may be employed when a free analysis is to be performed. Each intermediate rigidity or release introduces an additional equation

which allows for elimination of the resulting unknown variable. When this is achieved transfer matrix multiplication is continued as before until the end of the system is reached where application of the boundary conditions will enable estimation of the frequency determinant (or residual).

4.5 Treatment of System Sub-Levels

In real rotating machinery applications many instances occur where accurate modelling of the system dynamics may be achieved only when the characteristics of, for instance, the bearing oil-film, machine casing and foundation are incorporated into the analysis. In such cases these components may be considered as possessing mass/inertia, stiffness and damping qualities. Although, in such circumstances, the simple 'chain-like' structural form is modified, with some additional effort the transfer matrix method may still be employed to analyse such complex systems.

4.5.1 Derivation of Transfer Matrices from Measurement

Before describing the general analysis technique it is worth mentioning that in some cases, where for example system modelling techniques may be limited, incorporation of relevant experimental data may lead to improved accuracy.

For instance, consider a rotor system with the complex multi-level support arrangement as shown in

Fig. 4.2. If the beam is assumed to vibrate in a single plane only then ideally one would wish to describe the support assembly in terms of a simple (4x4) transfer matrix so that the conventional 'straight-through' form of T.M. method is maintained. This could be achieved by measuring the support system receptances, r, and by further manipulation obtaining the required transfer matrix such that:

$$\begin{bmatrix} w \\ \Phi \\ M \\ V \end{bmatrix}_R = \begin{bmatrix} 1 & 0 & 0 & 0 \\ 0 & 1 & 0 & 0 \\ \frac{r_{21}}{(r_{12}r_{21} - r_{11}r_{22})} & \frac{r_{11}}{(r_{11}r_{22} - r_{12}r_{21})} & 1 & 0 \\ \frac{r_{22}}{(r_{11}r_{22} - r_{12}r_{21})} & \frac{r_{12}}{(r_{12}r_{21} - r_{11}r_{22})} & 0 & 1 \end{bmatrix} \cdot \begin{bmatrix} w \\ \Phi \\ M \\ V \end{bmatrix}_L$$

Where r is in general complex and frequency-dependant. Referring to the support shown in Fig. 4.3,

F = Harmonically varying force at point 2.

C = Harmonically varying couple at point 2.

d_{11} = Displacement at point 2 due to force F.

d_{12} = Displacement at point 2 due to couple C.

d_{21} = Slope at point 2 due to force F.

d_{22} = Slope at point 2 due to couple C.

$r_{11} = d_{11}/F$

$r_{12} = d_{12}/C$

$r_{21} = d_{21}/F$

$r_{22} = d_{22}/C$

4.5.2 General Case

The above approach is useful for a system having supports such as those shown in Fig. 4.2 but where inter-support coupling exists, an alternative procedure must be developed. The general case of a rotor mounted on bearings which are in turn located on a flexible casing having mass, subsequently supported on a massless flexible foundation is shown in Fig. 4.4. Although this constitutes a system with only one sub-level the following analysis method can easily be extended to a system with multiple sub-levels. The possibility of damping at all levels necessitates the use of complex transfer matrices. Normally it is assumed that motions in a direction along the shaft rotational axis x have no influence on the system response in the other two planes resulting in the employment of transfer matrices of size (8x8) for free vibration analysis and (9x9) for forced response calculations.

The general approach will be described for the free-vibration analysis of the system shown in Fig. 4.4 making use of the modified transfer matrix method to aid numerical stability. Prediction of the system response as a result of the application of periodic excitation, e.g. mass unbalance, may be achieved by adopting a similar procedure (Section 4.3).

Although not shown for sake of clarity, (Fig. 4.4) radial and angular coupling between the x-z and x-y

planes at the support points may be assumed to exist. Each support is assumed to exhibit stiffness and damping characteristics but in the extreme case may be considered as a rigid link exerting a reaction force or moment P.

For this case the shaft (level I) and machine frame (level II) end conditions will be considered free-free (M = V = 0) but this is not a limitation since any condition can be simulated simply by altering the initial state vectors.

As before, the non-zero parameters in the ititial state vector(s) are given initial estimates $\delta_1, \delta_2 \ldots \ldots \delta_{\frac{n-1}{2}}$ and corresponding correction factors $K_1, K_2 \ldots K_{\frac{n-1}{2}}$, where n is the state vector order at the relevant system level. Normally the state vector parameter expected to have the greatest value is initially guessed as unity, for numerical stability purposes, and left uncorrected.

Consider initially the state vector for the shaft at point 1.

$$\underline{Z}_1 = \begin{bmatrix} w \\ \Phi \\ M_y \\ V_z \\ v \\ \Phi \\ M_z \\ V_y \end{bmatrix}_1 = \begin{bmatrix} \delta_1 \\ \delta_2 \\ 0 \\ 0 \\ \delta_3 \\ 1 \\ 0 \\ 0 \end{bmatrix} + K_1 \begin{bmatrix} 1 \\ 0 \\ 0 \\ 0 \\ 0 \\ 0 \\ 0 \\ 0 \end{bmatrix} + K_2 \begin{bmatrix} 0 \\ 1 \\ 0 \\ 0 \\ 0 \\ 0 \\ 0 \\ 0 \end{bmatrix} + K_3 \begin{bmatrix} 0 \\ 0 \\ 0 \\ 0 \\ 1 \\ 0 \\ 0 \\ 0 \end{bmatrix}$$

Following the usual procedure the intermediate shaft state vectors are obtained by successive multiplication of the appropriate transfer matrices. The process is continued until a support is reached where:

$$\underline{Z}_3^{I_L} = \begin{bmatrix} a_1 \\ a_2 \\ a_3 \\ a_4 \\ a_5 \\ a_6 \\ a_7 \\ a_8 \end{bmatrix} + K_1 \begin{bmatrix} b_1 \\ b_2 \\ b_3 \\ b_4 \\ b_5 \\ b_6 \\ b_7 \\ b_8 \end{bmatrix} + K_2 \begin{bmatrix} c_1 \\ c_2 \\ c_3 \\ c_4 \\ c_5 \\ c_6 \\ c_7 \\ c_8 \end{bmatrix} + K_3 \begin{bmatrix} d_1 \\ d_2 \\ d_3 \\ d_4 \\ d_5 \\ d_6 \\ d_7 \\ d_8 \end{bmatrix}$$

Thus the complete state vector at the left of the support becomes:-

$$\underline{Z}_3^{L} = \begin{bmatrix} \underline{Z}^{I} \\ \hline II\ \underline{Z} \\ \vdots \\ N1\ \underline{Z} \end{bmatrix}_3^{L} = \begin{bmatrix} w \\ \Phi \\ M_y \\ V_z \\ v \\ \theta \\ M_z \\ V_y \\ \hline w \\ \Phi \\ M_y \\ V_z \\ v \\ \theta \\ M_z \\ V_y \\ \vdots \\ \hline \end{bmatrix}_3^{L} = \begin{bmatrix} a_1 \\ a_2 \\ a_3 \\ a_4 \\ a_5 \\ a_6 \\ a_7 \\ a_8 \\ \hline \delta_4 \\ \delta_5 \\ 0 \\ 0 \\ \delta_6 \\ \delta_7 \\ 0 \\ 0 \\ \vdots \\ \hline \end{bmatrix} + K_1 \begin{bmatrix} b_1 \\ b_2 \\ b_3 \\ b_4 \\ b_5 \\ b_6 \\ b_7 \\ b_8 \\ \hline 0 \\ 0 \\ 0 \\ 0 \\ 0 \\ 0 \\ 0 \\ 0 \\ \vdots \\ \hline \end{bmatrix} + K_2 \begin{bmatrix} c_1 \\ c_2 \\ c_3 \\ c_4 \\ c_5 \\ c_6 \\ c_7 \\ c_8 \\ \hline 0 \\ 0 \\ 0 \\ 0 \\ 0 \\ 0 \\ 0 \\ 0 \\ \vdots \\ \hline \end{bmatrix} + K_3 \begin{bmatrix} d_1 \\ d_2 \\ d_3 \\ d_4 \\ d_5 \\ d_6 \\ d_7 \\ d_8 \\ \hline 0 \\ 0 \\ 0 \\ 0 \\ 0 \\ 0 \\ 0 \\ 0 \\ \vdots \\ \hline \end{bmatrix} + K_4 \begin{bmatrix} 0 \\ 0 \\ 0 \\ 0 \\ 0 \\ 0 \\ 0 \\ 0 \\ \hline 1 \\ 0 \\ 0 \\ 0 \\ 0 \\ 0 \\ 0 \\ 0 \\ \vdots \\ \hline \end{bmatrix} + \ldots K_7 \begin{bmatrix} 0 \\ 0 \\ 0 \\ 0 \\ 0 \\ 0 \\ 0 \\ 0 \\ \hline 0 \\ 0 \\ 0 \\ 0 \\ 0 \\ 0 \\ 1 \\ 0 \\ \vdots \\ \hline \end{bmatrix}$$

Note the introduction of additional δ and K variables for the non-zero parameters in the lower level state vector. Although the machine casing is shown here as having no overhang in addition to being located within the shaft length these aspects are in no way limitations of the method.

When any form of support is encountered such as that at point 3 the following steps must be taken,

1) Set-up the support point transfer matrix relating all parameters, at all levels. . Where supports are such that rigidities, P, are introduced the corresponding matrix damping and stiffness coefficients should be set to zero. The order of this matrix will be equal to the sum of the order of matrices employed for each level - in this case sixteen.

2) Make use of any relevant boundary conditions at the support to set-up equations relating the system unknowns. These additional relationships result from two main sources:-

a) The Introduction of Support Rigidities. The number of additional equations introduced will be equal to the number of support rigidities. If N1 is the number of system levels then the maximum number of equations which can be introduced at any point is 4.(N1)

for a two-plane analysis, resulting in a maximum of eight more equations in this case.

b) The Introduction of Discontinuities in the Sub-Levels.

In general the sub-level(s) (machine frame in this case) may not be of a continuous nature and additional intermediate boundary conditions occur. Here the maximum possible number of equations at any location, resulting from such a situation is $4.(N_l-1)$. For example, in the case considered if the beam representing the machine casing was removed then the maximum number of equations would result at each support since $M_{zA}=M_{yA}=V_{zA}=V_{yA}=M_{zB}=M_{yB}=V_{zB}=V_{yB}=0$.

Considering the above points and returning to the system shown in Fig. 4.4 the state vector to the right of point 3 in it's most general form may be written as shown on the following page.

The P vectors can be eliminated if no rigidities are present, or if the rigidities can be simulated using high stiffness values. However, if care is not taken this latter option may lead to numerical problems (4.2.2). The subscript prefix m denotes a reaction moment. Considering location A in Fig. 4.4 the following additional equations may result depending on specific support conditions:-

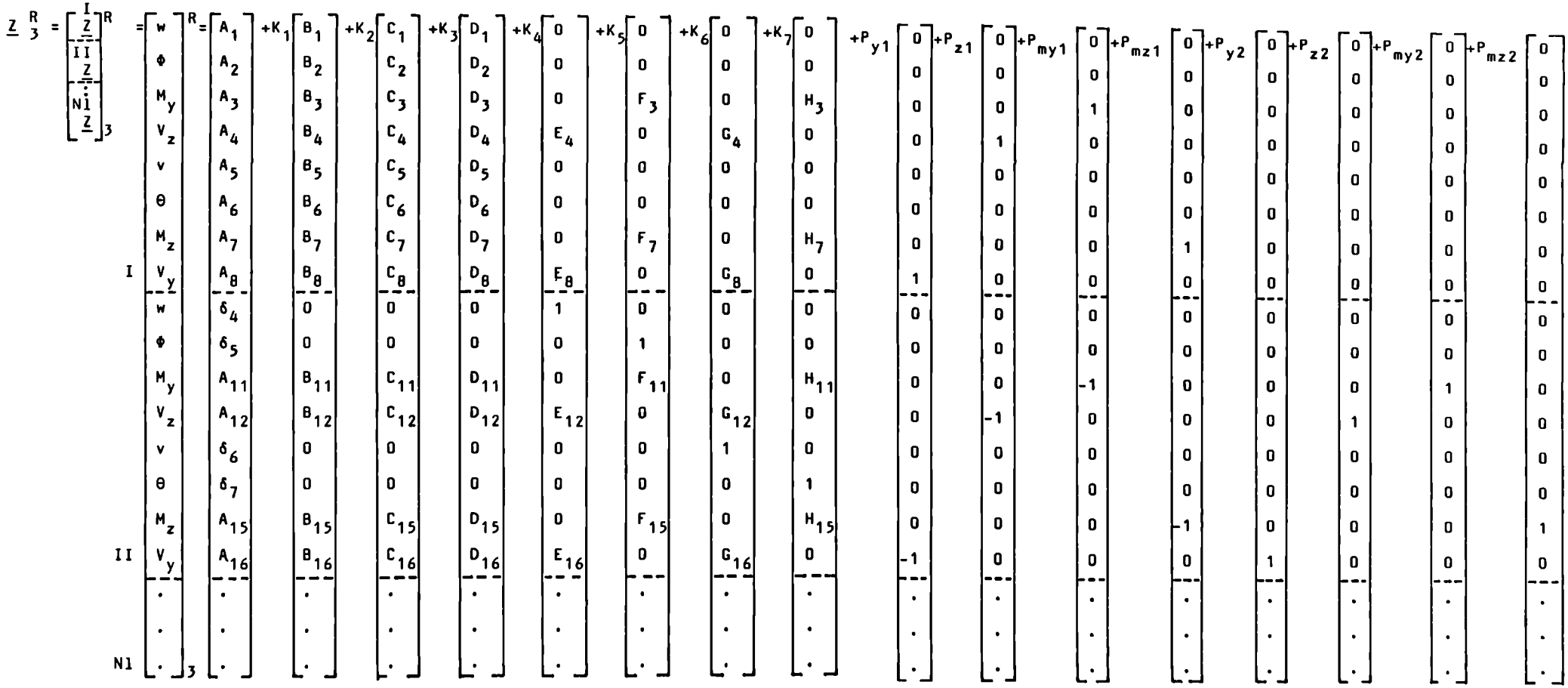
Z R 3 = I Z II Z N1 Z 3 R
w φ My Vz v θ Mz Vy
A1 A2 A3 A4 A5 A6 A7 A8
B1 B2 B3 B4 B5 B6 B7 B8
C1 C2 C3 C4 C5 C6 C7 C8
D1 D2 D3 D4 D5 D6 D7 D8
0 0 0 E4 0 0 0 E8
0 0 F3 0 0 0 F7 0
0 0 0 G4 0 0 0 G8
0 0 H3 0 0 0 H7 0
δ4 δ5 A11 A12 δ6 δ7 A15 A16
0 0 B11 B12 0 0 B15 B16
0 0 C11 C12 0 0 C15 C16
0 0 D11 D12 0 0 D15 D16
1 0 0 E12 0 0 0 E16
0 1 F11 0 0 0 F15 0
0 0 H11 0 1 0 H15 0
0 0 0 G12 0 1 0 G16
+K1 +K2 +K3 +K4 +K5 +K6 +K7 +Py1 +Pz1 +Pmy1 +Pmz1 +Py2 +Pz2 +Pmy2 +Pmz2
I II N1 3 3

If $w_1=w_2$ $\quad K_4=A_1-\delta_4+B_1K_1+C_1K_2+D_1K_3$

If $v_1=v_2$ $\quad K_6=A_5-\delta_6+B_5K_1+C_5K_2+D_5K_3$

If $\Phi_1=\Phi_2$ $\quad K_5=A_2-\delta_5+B_2K_1+C_2K_2+D_2K_3$

If $\theta_1=\theta_2$ $\quad K_7=A_6-\delta_7+B_6K_1+C_6K_2+D_6K_3$

If $w_2=w_3=0$ $\quad \delta_4=0;\ K_4=0$

If $v_2=v_3=0$ $\quad \delta_6=0;\ K_6=0$

If $\Phi_2=\Phi_3=0$ $\quad \delta_5=0;\ K_5=0$

If $\theta_2=\theta_3=0$ $\quad \delta_7=0;\ K_7=0$

If the bending moments and shear forces to the right of point A are zero as described in paragraph 2b earlier then the following additional relationships result.

At II

$$M_y=0=A_{11}+B_{11}K_1+C_{11}K_2+D_{11}K_3+F_{11}K_5+H_{11}K_7-P_{my1}+P_{my2}$$

$$V_z=0=A_{12}+B_{12}K_1+C_{12}K_2+D_{12}K_3+E_{12}K_4+G_{12}K_6-P_{z1}+P_{z2}$$

$$M_z=0=A_{15}+B_{15}K_1+C_{15}K_2+D_{15}K_3+F_{15}K_5+H_{15}K_7-P_{mz1}+P_{mz2}$$

$$V_y=0=A_{16}+B_{16}K_1+C_{16}K_2+D_{16}K_3+E_{16}K_4+G_{16}K_6-P_{y1}+P_{y2}$$

Thus consideration of the support details for a particular case will result in the selection of certain of the above relationships. The normal transfer matrix procedure is continued as before until another support is encountered and the same procedure adopted. When the end of the system is reached another set of relationships result from application of the boundary conditions. In this case,

At I, at point 11

$M_y = V_z = M_z = V_y = 0$

and similarly,

At II, point B

$M_y = V_z = M_z = V_y = 0$

In general the end conditions always provide $\frac{1}{2}(n_I + n_{II} + \ldots + n_{Nl})$ homogeneous equations where n represents the matrix order for the respective system level. The introduction of a number of intermediate rigidities or releases N_r, results in an additional N_r homogeneous equations. Since the number of K variables employed is $(\frac{n_I}{2} + \frac{n_{II}}{2} + \ldots \frac{n_{Nl}}{2} - 1)$ it is obvious that the number of equations available for solution always exceeds the number of system unknowns by one. Thus the procedures described in section 4.2.3 may be applied directly to enable modification of the initial state vectors thereby allowing accurate determination of the system natural frequencies.

4.6 Derivation of Transfer Matrices

4.6.1 Rotor System Modelling

The usual approach of idealising the shaft/rotor system as a series of elastic massless beam elements joined by rigid point masses is adopted here. The lumped mass at each shaft section is determined by summing half the mass of the section to the right of

the station and half the mass of the section to the left of the station.

The following assumptions are made in setting up the system transfer matrices:

1) The rotor system exhibits linear characteristics.
2) The rotor is axi-symmetric.
3) Torsional and axial load effects have no influence on the shaft lateral vibrations.

The analysis allows for the inclusion of the following effects:

1) Shaft mass unbalance.
2) Shaft initial bend.
3) Asymmetric multi-level supports possessing radial and angular mass/inertia, stiffness and damping characteristics. For each support any combination of rigid/flexible elements can be selected.
4) Gyroscopic Couples.
5) Rotary Inertia.
6) Shear Deflection.

4.6.2 Sign Convention

The Cartesian right-handed co-ordinate system is employed (Fig. 4.5), the x-axis coinciding with the mean steady-state position of the shaft rotational axis at each shaft station and the y and z axes coinciding with the principal axes of inertia of shaft cross-sectional area. The displacements in the horizontal (y) and

vertical (z) direction are v and w respectively.

4.6.3 Transfer Matrices

In setting up the system matrices the shaft motion is assumed harmonic such that system parameters can be expressed in the following complex form:

$$w = \bar{w}e^{\lambda t}$$
$$\Phi = \bar{\Phi}e^{\lambda t}$$
$$M_y = \bar{M}_y e^{\lambda t}$$
$$V_z = \bar{V}_z e^{\lambda t}$$

and

$$v = \bar{v}e^{\lambda t}$$
$$\theta = \bar{\theta}e^{\lambda t}$$
$$M_z = \bar{M}_z e^{\lambda t}$$
$$V_y = \bar{V}_y e^{\lambda t}$$

and only the real parts apply. $\lambda = \alpha + i\omega$ where α is the damping exponent and ω the rate of free vibrations of the system. The shaft angular speed of rotation is represented by Ω , so that in the special case of forced vibration due to mass unbalance $\lambda = i\Omega$.

From the above

$$\dot{w} = \lambda \bar{w}\, e^{\lambda t}$$
$$\text{and } \ddot{w} = \lambda^2\, \bar{w}\, e^{\lambda t}$$

and similarly for the other system parameters.

In the following the superscripts L and R represent the conditions at the left and right hand sides of the element respectively.

4.6.3.1 Elastic Massless Field

Referring to Figs. 4.6(a) and (b), and from equilibrium and the theory of elasticity:

$$\left.\begin{aligned}
\bar{w}^R &= \bar{w}^L - \bar{\Phi}^L L - \bar{M}_y^L \frac{L^2}{2EI} - \bar{V}_z^L \left[\frac{L^3}{GEI} - \frac{L}{GA}\right] \\
\bar{\Phi}^R &= \bar{\Phi}^L + \bar{M}_y^L \frac{L}{EI} + \bar{V}_z^L \frac{L^2}{2EI} \\
\bar{M}_y^R &= \bar{M}^L + \bar{V}_z^L L \\
\bar{V}_z^R &= \bar{V}_z^L
\end{aligned}\right\} \quad (4.5)$$

and

$$\left.\begin{aligned}
\bar{v}^R &= \bar{v}^L + \bar{\Theta}^L L + \bar{M}_z^L \frac{L^2}{2EI} - \bar{V}_y^L \left[\frac{L^3}{GEI} - \frac{L}{GA}\right] \\
\bar{\Theta}^R &= \bar{\Theta}^L + \bar{M}_z^L \frac{L}{EI} - \bar{V}_y^L \frac{L^2}{2EI} \\
\bar{M}_z^R &= \bar{M}_z^L - \bar{V}_y^L L \\
\bar{V}_y^R &= \bar{V}_y^L
\end{aligned}\right\} \quad (4.5)$$

where E and G are the elasticity and shear modulii, for

the shaft material, respectively. The shaft cross-sectional area and second moment of area are represented by A and I respectively.

The effect of shaft internal damping may be dealt with [17] by the introduction of complex shaft modulii $\bar{E}$ and $\bar{G}$ where,

$$\bar{E} = E\ (1+ig)$$

and $$\bar{G} = G\ (1+ig)$$

where g is described as the material loss factor generally having values of the order of .005, depending on the material employed and structure type. This effect will not be considered further in the analysis.

When equations (4.5) are expressed in matrix form the flexible field matrix is obtained (section 4.7).

4.6.3.2 Point Mass/Inertia

Fig. 4.7 shows the free body diagram for a concentrated mass and thin disc at a shaft station. The mass m is a combination of shaft lumped mass, determined as described earlier, and disc mass. I_P and I_T are the disc polar and transverse moments of inertia respectively. Employing D'Alembert's principle to set up the system equations we obtian

$$\left.\begin{aligned}
\bar{w}^R &= \bar{w}^L \\
\bar{\Phi}^R &= \bar{\Phi}^L \\
\bar{M}_y^R &= \bar{M}_y^L + I_T\lambda^2\bar{\Phi}^L + I_P\lambda\Omega.\bar{\Theta}^L \\
\bar{V}_z^R &= \bar{V}_z^L + m\lambda^2\bar{w}^L
\end{aligned}\right| \qquad (4.6)$$

and,

$$\begin{aligned}
\bar{v}^R &= \bar{v}^L \\
\bar{\theta}^R &= \bar{\theta}^L \\
\bar{M}_z^R &= \bar{M}_z^L + I_T\lambda^2\bar{\theta}^L - I_P\lambda\Omega\,\bar{\Phi}^L \\
\bar{V}^R &= \bar{V}^L + m\lambda^2\bar{v}^L
\end{aligned} \qquad (4.6)(\text{cont.})$$

If a circular whirl orbit results then $\theta = -i\Phi$ (Appendix A). Considering a thin circular disc where $I_P = 2I_T$ and synchronous excitation ($\lambda = i\Omega$) then from equations (4.6) we obtain,

$$\begin{aligned}
\bar{M}_y^R &= \bar{M}_y^L + I_T\Omega^2\bar{\Phi}^L \\
\bar{M}_z^R &= \bar{M}_z^L + I_T\Omega^2\bar{\theta}^L
\end{aligned}$$

where the gyroscopic couples clearly introduce an additional stiffening influence on the shaft.

With equations (4.6) expressed in matrix form the point mass/inertia transfer matrix is obtained (section 4.7).

4.6.3.3 Point Support

The case of a support with one sub-level is considered here since such an arrangement may be simulated on the test rotor used in the experimental work. All possible dynamic support coefficients are considered in the analysis, including stiffness/damping at each level, although many of the coefficients

will be eliminated depending on the particular system to be investigated. Referring to the shaft support arrangement shown in Fig. 4.8 and making use of D'Alembert's principle the following equations are obtained.

In the x-z plane

At Level 1

$$\bar{w}_1^R = \bar{w}_1^L$$

$$\bar{\Phi}_1^R = \bar{\Phi}_1^L$$

$$\bar{M}_{y1}^R = \bar{M}_{y1}^L + (K_{1\Phi\Phi} + \lambda C_{1\Phi\Phi}).(\bar{\Phi}_1 - \bar{\Phi}_2) + (K_{1\Phi\Theta} + \lambda C_{1\Phi\Theta}).(\bar{\Theta}_1 - \bar{\Theta}_2)$$

$$\bar{V}_{z1}^R = \bar{V}_{z1}^L + (K_{1zz} + \lambda C_{1zz}).(\bar{w}_1 - \bar{w}_2) + (K_{1zy} + \lambda C_{1zy}).(\bar{v}_1 - \bar{v}_2)$$

At level 2

$$\left.\begin{aligned}
&\bar{w}_2^R = \bar{w}_2^L \\
&\bar{\Phi}_2^R = \bar{\Phi}_2^L \\
&\bar{M}_{y2}^R = \bar{M}_{y2}^L - (K_{1\Phi\Phi} + \lambda C_{1\Phi\Phi})\bar{\Phi}_1 \\
&\quad + (K_{1\Phi\Phi} + \lambda C_{1\Phi\Phi} + K_{2\Phi\Phi} + \lambda C_{2\Phi\Phi} + I_{Fy}\lambda^2)\bar{\Phi}_2 \\
&\quad - (K_{1\Phi\Theta} + \lambda C_{1\Phi\Theta})\bar{\Theta}_1 \\
&\quad + (K_{1\Phi\Theta} + \lambda C_{1\Phi\Theta} + K_{2\Phi\Theta} + \lambda C_{2\Phi\Theta})\bar{\Theta}_2
\end{aligned}\right\} \quad (4.7)$$

$$\bar{V}^R_{z2} = \bar{V}^L_{z2} - (K_{1zz}+\lambda C_{1zz})\bar{w}_1 + (K_{1zz}+\lambda C_{1zz}+K_{2zz}+\lambda C_{2zz}+M_F\lambda^2)\bar{w}_2 - (K_{1zy}+\lambda C_{1zy})\bar{v}_1 + (K_{1zy}+\lambda C_{1zy}+K_{2zy}+\lambda C_{2zy})\bar{v}_2 \quad (4.7)\ (\text{cont.})$$

In the x-y plane

At level 1

$$\bar{v}^R_1 = \bar{v}^L_1$$

$$\bar{\theta}^R_1 = \bar{\theta}^L_1$$

$$\bar{M}^R_{z1} = \bar{M}^L_{z1} + (K_{1\theta\theta}+\lambda C_{1\theta\theta}).(\bar{\theta}_1-\bar{\theta}_2) + (K_{1\theta\Phi}+\lambda C_{1\theta\Phi}).(\bar{\Phi}_1-\bar{\Phi}_2)$$

$$\bar{V}^R_{y1} = \bar{V}^L_{y1} + (K_{1yy}+\lambda C_{1yy}).(\bar{v}_1-\bar{v}_2) + (K_{1yz}+\lambda C_{1yz}).(\bar{w}_1-\bar{w}_2)$$

At level 2

$$\bar{v}^R_2 = \bar{v}^L_2$$

$$\bar{\theta}^R_2 = \bar{\theta}^L_2$$

$$\bar{M}^R_{z2} = \bar{M}^L_{z2} - (K_{1\theta\theta}+\lambda C_{1\theta\theta})\bar{\theta}_1 + (K_{1\theta\theta}+\lambda C_{1\theta\theta}+K_{2\theta\theta}+\lambda C_{2\theta\theta}+I_{Fz}\lambda^2)\bar{\theta}_2 - (K_{1\theta\Phi}+\lambda C_{1\theta\Phi})\bar{\Phi}_1 + (K_{1\theta\Phi}+\lambda C_{1\theta\Phi}+K_{2\theta\Phi}+\lambda C_{2\theta\Phi})\bar{\Phi}_2 \quad (4.8)$$

$$
\begin{aligned}
\bar{V}^R_{y2} &= \bar{V}^L_{y2} - (K_{1yy}+\lambda C_{1yy})\bar{v}_1 \\
&+(K_{1yy}+\lambda C_{1yy}+K_{2yy}+\lambda C_{2yy}+M_F\lambda^2)\bar{v}_2 \\
&-(K_{1yz}+\lambda C_{1yz})\bar{w}_1 \\
&+(K_{1yz}+\lambda C_{1yz}+K_{2yz}+\lambda C_{2yz})\bar{w}_2
\end{aligned}
\qquad (4.8)\text{(cont.)}
$$

Expression of the above equations in matrix form results in a complex extended transfer matrix (section 4.7) of size (17x17). However, where individual supports are uncoupled the following boundary conditions may be utilised to enable reduction of this matrix to it's 'normal' (9x9) form.

$$V^R_{z2}=V^L_{z2}=M^R_{y2}=M^L_{y2}=V^R_{y2}=V^L_{y2}=M^R_{z2}=M^L_{z2}=0$$

If we let $\begin{bmatrix} \bar{w}_1 \\ \bar{v}_1 \\ \bar{\Phi}_1 \\ \bar{\Theta}_1 \\ \hline \bar{w}_2 \\ \bar{v}_2 \\ \bar{\Phi}_2 \\ \bar{\Theta}_2 \end{bmatrix} = \left[\begin{array}{c} \underline{\bar{Z}}_1 \\ \hline \underline{\bar{Z}}_2 \end{array}\right]$

Then from equations (4.7) and (4.8)

$$\left[\begin{array}{c|c} \underline{A} & \underline{B} \end{array}\right] \left[\begin{array}{c} \underline{\bar{Z}}_1 \\ \hline \underline{\bar{Z}}_2 \end{array}\right] = \left[\begin{array}{c} \underline{0} \\ \hline \underline{0} \end{array}\right]$$

where,

$$\underline{A} = \begin{bmatrix} -(K_{1zz}+\lambda C_{1zz}) & -(K_{1zy}+\lambda C_{1zy}) & 0 & 0 \\ 0 & 0 & -(K_{1\Phi\Phi}+\lambda C_{1\Phi\Phi}) & -(K_{1\Phi\theta}+\lambda C_{1\Phi\theta}) \\ -(K_{1yz}+\lambda C_{1yz}) & -(K_{1yy}+\lambda C_{1yy}) & 0 & 0 \\ 0 & 0 & -(K_{1\theta\Phi}+\lambda C_{1\theta\Phi}) & -(K_{1\theta\theta}+\lambda C_{1\theta\theta}) \end{bmatrix}$$

and,

$$\underline{B} = \begin{bmatrix} (K_{1zz}+\lambda C_{1zz} & (K_{1zy}+\lambda C_{1zy} & 0 & 0 \\ +K_{2zz}+\lambda C_{2zz} & +K_{2zy}+\lambda C_{2zy}) & & \\ +M_F\lambda^2) & & & \\ 0 & 0 & (K_{1\Phi\Phi}+\lambda C_{1\Phi\Phi} & (K_{1\Phi\theta}+\lambda C_{1\Phi\theta} \\ & & +K_{2\Phi\Phi}+\lambda C_{2\Phi\Phi} & +K_{2\Phi\theta}+\lambda C_{2\Phi\theta}) \\ & & +I_{Fy}\lambda^2) & \\ (K_{1yz}+\lambda C_{1yz} & (K_{1yy}+\lambda C_{1yy} & & \\ +K_{2yz}+\lambda C_{2yz}) & +K_{2yy}+\lambda C_{2yy} & 0 & 0 \\ & +M_F\lambda^2) & & \\ 0 & 0 & (K_{1\theta\Phi}+\lambda C_{1\theta\Phi} & (K_{1\theta\theta}+\lambda C_{1\theta\theta} \\ & & +K_{2\theta\Phi}+\lambda C_{2\theta\Phi}) & +K_{2\theta\theta}+\lambda C_{2\theta\theta} \\ & & & +I_{Fz}\lambda^2) \end{bmatrix}$$

Therefore $\underline{Z}_2 = \underline{B}^{-1} . -\underline{A} . \underline{Z}_1$

Let $\underline{C} = \underline{A} . \left[-\underline{\underline{I}} + \underline{B}^{-1} . -\underline{A} \right]$

Since, in both planes at the shaft level, the displacement and slope to the right and left of the support are identical then by making use of coefficients from the $\underline{C}$ matrix a 9x9 support transfer matrix is obtained (section 4.7)

4.6.3.4 Unbalance Mass

The effect of mass unbalance at a general shaft station is considered in Fig. 4.9 where O is the mean steady state position of the shaft centre, G is the shaft geometric centre and M the centre of mass of the shaft. Since shaft motion is being considered at a point then

$$\bar{w}^R = \bar{w}^L$$
$$\bar{\Phi}^R = \bar{\Phi}^L$$
$$\bar{v}^R = \bar{v}^L$$
$$\bar{\theta}^R = \bar{\theta}^L$$

and, ignoring angular inertia effects,

$$\bar{M}_y^R = \bar{M}_y^L$$

$$\bar{M}_z^R = \bar{M}_z^L$$

Now considering forces in the z and y directions respectively,

$$\bar{V}_z^R = \bar{V}_z^L - m_u\Omega^2(\bar{w}^L + r(\sin\alpha - i\cos\alpha))$$

$$\bar{V}_y^R = \bar{V}_y^L - m_u\Omega^2 \ (\bar{v}^L + r(\cos\alpha + i\sin\alpha))$$

Expressing the above equations in matrix form results in the unbalance mass matrix (section 4.7).

4.6.3.5 Shaft Initial Bend

The inclusion of shaft bend in the analysis leads to modification of the elastic massless field matrix. The point mass matrix needs no alteration since the usual displacements $\bar{w}$ and $\bar{v}$ this time are assumed to include the bend effect.

Referring to Fig. 4.10 it is seen that the effect of shaft initial bend is to modify the displacement and slope relationships so that forcing terms are introduced.

If the section initial bends and slopes are denoted by ϵ and $\overline{\epsilon S}$ respectively then,

$$\bar{w}^R = \bar{w}^L + \epsilon^R(\sin\gamma^R - i\cos\gamma^R) - \epsilon^L(\sin\gamma^L - i\cos\gamma^L) - \bar{\Phi}^L L + \overline{\epsilon S}_\Phi^L L - \bar{M}_y^L \frac{L^2}{2EI} - \bar{V}_z^L \left[\frac{L^3}{6EI} - \frac{L}{GA}\right]$$

$$\bar{\Phi}^R = \bar{\Phi}^L + \overline{\epsilon S}_\Phi^R - \overline{\epsilon S}_\Phi^L + \bar{M}_y^L \frac{L}{EI} + \bar{V}_z^L \frac{L^2}{2EI}$$

$$\bar{M}_y^R = \bar{M}_y^L + \bar{V}_z^L L \qquad (4.9)$$

$$\bar{V}_z^R = \bar{V}_z^L$$

and

$$\bar{v}^R = \bar{v}^L + \epsilon^R(\cos\gamma^R + i\sin\gamma^R) - \epsilon^L(\cos\gamma^L + i\sin\gamma^L)$$

$$+ \bar{\Theta}^L L - \overline{\varepsilon S}^L_\Theta L + \bar{M}^L_z \frac{L^2}{2EI} - \bar{V}^L_y \left[\frac{L^3}{6EI} - \frac{L}{GA}\right]$$

$$\bar{\Theta}^R = \bar{\Theta}^L + \overline{\varepsilon S}^R_\Theta - \overline{\varepsilon S}^L_\Theta + \bar{M}^L_z \frac{L}{EI} - \bar{V}^L_y \frac{L^2}{2EI} \qquad (4.9)\ (\text{cont.})$$

$$\bar{M}^R_z = \bar{M}^L_z - \bar{V}^L_y L$$

$$\bar{V}^R_y = \bar{V}^L_y$$

When equations (4.9) are expressed in matrix form the modified elastic massless field transfer matrix is obtained (section 4,7).

If initial bend at any point n is written as

$$\bar{\varepsilon}_{wn} = - i\varepsilon_n e^{i\gamma n}$$

$$\bar{\varepsilon}_{vn} = \varepsilon_n e^{i\gamma n}$$

The resulting shaft slopes may be estimated from the initial bends as follows:-

$$\overline{\varepsilon S}_{\Theta n} = \left[\frac{(\bar{\varepsilon}_{v(n+1)} - \bar{\varepsilon}_{vn})}{L_n} + \frac{(\bar{\varepsilon}_{vn} - \bar{\varepsilon}_{v(n-1)})}{L_{n-1}}\right] \Big/ 2$$

$$\overline{\varepsilon S}_{\Phi n} = \left[\frac{(\bar{\varepsilon}_{wn} - \bar{\varepsilon}_{w(n+1)})}{L_n} + \frac{(\bar{\varepsilon}_{w(n-1)} - \bar{\varepsilon}_{wn})}{L_{n-1}}\right] \Big/ 2$$

where n is the shaft station number, increasing from left to right.

4.7 Catalogue of Transfer Matrices

Elastic Massless Field Matrix (Straight Shaft)

$$\underline{U} = \begin{bmatrix} 1 & -L & -\frac{L^2}{2EI} & -\left[\frac{L^3}{6EI} - \frac{L}{GA}\right] & 0 & 0 & 0 & 0 & 0 \\ 0 & 1 & \frac{L}{EI} & \frac{L^2}{2EI} & 0 & 0 & 0 & 0 & 0 \\ 0 & 0 & 1 & L & 0 & 0 & 0 & 0 & 0 \\ 0 & 0 & 0 & 1 & 0 & 0 & 0 & 0 & 0 \\ 0 & 0 & 0 & 0 & 1 & L & \frac{L^2}{2EI} & -\left[\frac{L^3}{6EI} - \frac{L}{GA}\right] & 0 \\ 0 & 0 & 0 & 0 & 0 & 1 & \frac{L}{EI} & -\frac{L^2}{2EI} & \\ 0 & 0 & 0 & 0 & 0 & 0 & 1 & -L & 0 \\ 0 & 0 & 0 & 0 & 0 & 0 & 0 & 1 & 0 \\ 0 & 0 & 0 & 0 & 0 & 0 & 0 & 0 & 1 \end{bmatrix}$$

Point Mass/Inertia Matrix

$$\underline{U} = \begin{bmatrix} 1 & 0 & 0 & 0 & 0 & 0 & 0 & 0 & 0 \\ 0 & 1 & 0 & 0 & 0 & 0 & 0 & 0 & 0 \\ 0 & I_T\lambda^2 & 1 & 0 & 0 & +I_P\lambda\Omega & 0 & 0 & 0 \\ m\lambda^2 & 0 & 0 & 1 & 0 & 0 & 0 & 0 & 0 \\ 0 & 0 & 0 & 0 & 1 & 0 & 0 & 0 & 0 \\ 0 & 0 & 0 & 0 & 0 & 1 & 0 & 0 & 0 \\ 0 & -I_P\lambda\Omega & 0 & 0 & 0 & I_T\lambda^2 & 1 & 0 & 0 \\ 0 & 0 & 0 & 0 & m\lambda^2 & 0 & 0 & 1 & 0 \\ 0 & 0 & 0 & 0 & 0 & 0 & 0 & 0 & 1 \end{bmatrix}$$

$\underline{U}$ =

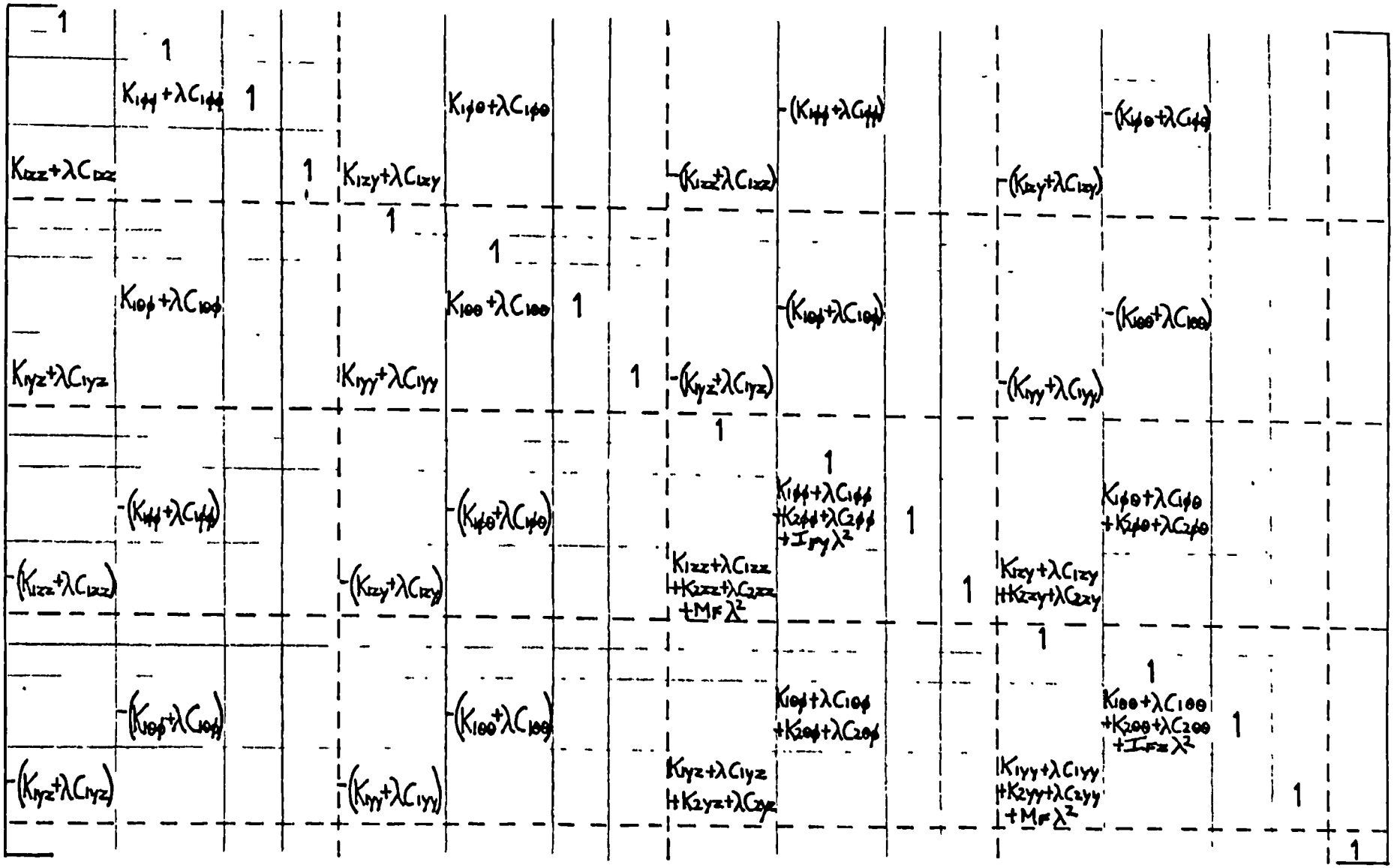

POINT-SUPPORT MATRIX (UNREDUCED)

Point Support Matrix (Reduced)

$$\underline{U} = \begin{bmatrix} 1 & 0 & 0 & 0 & 0 & 0 & 0 & 0 & 0 \\ 0 & 1 & 0 & 0 & 0 & 0 & 0 & 0 & 0 \\ \underline{C}_{21} & \underline{C}_{23} & 1 & 0 & \underline{C}_{22} & \underline{C}_{24} & 0 & 0 & 0 \\ \underline{C}_{11} & \underline{C}_{13} & 0 & 1 & \underline{C}_{12} & \underline{C}_{14} & 0 & 0 & 0 \\ 0 & 0 & 0 & 0 & 1 & 0 & 0 & 0 & 0 \\ 0 & 0 & 0 & 0 & 0 & 1 & 0 & 0 & 0 \\ \underline{C}_{41} & \underline{C}_{43} & 0 & 0 & \underline{C}_{42} & \underline{C}_{44} & 1 & 0 & 0 \\ \underline{C}_{31} & \underline{C}_{33} & 0 & 0 & \underline{C}_{32} & \underline{C}_{34} & 0 & 1 & 0 \\ 0 & 0 & 0 & 0 & 0 & 0 & 0 & 0 & 1 \end{bmatrix}$$

The Coefficients $\underline{C}$ are as defined in section 4.6.33

Unbalance Mass Matrix

$$\underline{U} = \begin{bmatrix} 1 & 0 & 0 & 0 & 0 & 0 & 0 & 0 & 0 \\ 0 & 1 & 0 & 0 & 0 & 0 & 0 & 0 & 0 \\ 0 & 0 & 1 & 0 & 0 & 0 & 0 & 0 & 0 \\ -m_u\Omega^2 & 0 & 0 & 1 & 0 & 0 & 0 & 0 & -m_u\Omega^2 r(\sin\alpha - i\cos\alpha) \\ 0 & 0 & 0 & 0 & 1 & 0 & 0 & 0 & 0 \\ 0 & 0 & 0 & 0 & 0 & 1 & 0 & 0 & 0 \\ 0 & 0 & 0 & 0 & 0 & 0 & 1 & 0 & 0 \\ 0 & 0 & 0 & 0 & -m_u\Omega^2 & 0 & 0 & 1 & -m_u\Omega^2 r(\cos\alpha + i\sin\alpha) \\ 0 & 0 & 0 & 0 & 0 & 0 & 0 & 0 & 1 \end{bmatrix}$$

$$\underline{U} = \left[\begin{array}{cccc|cccc|c}
1 & -L & -\frac{L^2}{2EI} & -\left[\frac{L^3}{6EI} \; \frac{-L}{GA}\right] & 0 & 0 & 0 & 0 & -i\varepsilon^R e^{i\gamma R} + i\varepsilon^L e^{i\gamma L} + \overline{\varepsilon S}_\Phi^L \; L \\
0 & 1 & \frac{L}{EI} & \frac{L^2}{2EI} & 0 & 0 & 0 & 0 & \overline{\varepsilon S}_\Phi^R - \overline{\varepsilon S}_\Phi^L \\
0 & 0 & 1 & L & 0 & 0 & 0 & 0 & 0 \\
0 & 0 & 0 & 1 & 0 & 0 & 0 & 0 & 0 \\
\hline
0 & 0 & 0 & 0 & 1 & L & \frac{L^2}{2EI} & -\left[\frac{L^3}{6EI} \; \frac{-L}{GA}\right] & \varepsilon^R e^{i\gamma R} - \varepsilon^L e^{i\gamma L} - \overline{\varepsilon S}_\Theta^L \; L \\
0 & 0 & 0 & 0 & 0 & 1 & \frac{L}{EI} & -\frac{L^2}{2EI} & \overline{\varepsilon S}_\Theta^R - \overline{\varepsilon S}_\Theta^L \\
0 & 0 & 0 & 0 & 0 & 0 & 1 & -L & 0 \\
0 & 0 & 0 & 0 & 0 & 0 & 0 & 1 & 0 \\
\hline
0 & 0 & 0 & 0 & 0 & 0 & 0 & 0 & 1
\end{array}\right]$$

ELASTIC MASSLESS FIELD MATRIX (INCLUDING SHAFT BEND)

4.8.1 Analysis Programme

A computer programme, incorporating the procedures described in this chapter, was created and employed for the rotordynamic analyses performed and described in this thesis.

The programme enables the prediction of system undamped critical speeds, corresponding mode shapes and damped unbalanced response taking into account the effects described in section 4.6.1. In addition, the programme was used as part of an optimisation algorithm later developed and described in Chapter 5.

Free-vibration analyses were performed utilising the modified transfer matrix method, described in section 4.5.2, to aid numerical stability.

When using this method simulation of intermediate shaft-level rigid supports as high-stiffness flexible supports was found necessary to ensure elimination of possible ill-conditioning of the solution equations. Although this approach posed no problems in any of the analyses performed a more suitable procedure might be to employ the normal transfer matrix method where only rigid intermediate (shaft-level) supports are introduced and to apply the modified method in all other cases.

The programme could be employed to analyse rotor systems of significant complexity with minimal demand on computer memory.

In addition to shaft displacement data other output information included: Bearing/support forces,

shaft deflected form, dynamic stiffness at any point and system receptances.

A brief description of the programme structure is presented in the form of a flow chart in Fig. 4.13.

4.8.2 Validation of The Analysis Programme

Accuracy of the analysis programme was assessed in a number of ways. First, the case of a uniform beam mounted on simple supports (Fig. 4.11a) was analysed and the first five undamped natural frequencies (including rotary inertia effects) predicted using the programme and compared to the exact values calculated using the Timoshenko beam theory, viz:

$$\omega_n = \frac{\frac{D}{4}\left[\frac{n\pi}{L}\right]^2 \sqrt{\frac{E}{\rho}}}{\sqrt{[1 + R]}} \qquad (4.10)$$

where ω_n is the n^{TH} natural frequency (rad/sec) and R is the term representing rotary inertia effects,

$$R = \frac{D^2}{16}\left[\frac{n\pi}{L}\right]^2$$

Values of the other parameters used were as follows:-

E = Young's Modulus = 210×10^9 N/m^2

ρ = Material Density = 7860 kg/m^3

D = Shaft Diameter = .0254 m

L = Shaft Length = .956 m

n = Mode Number = 1,2,3....∞.

The beam frequencies are compared in table 4.1 where the influence of number of shaft elements on the modelling accuracy is shown

Table 4.1

Natl. Freq. N°.	Beam Theory (Equ.4.10) rad/sec	Transfer Matrix Programme rad/sec	N°.of Shaft Elements	% Error
1	354.37	354.17	6	.06
		354.18	8	.05
		354.19	10	.05
		354.19	16	.05
2	1416.57	1411.91	6	.33
		1413.10	8	.25
		1413.42	10	.22
		1413.62	16	.21
3	3183.83	3143.77	6	1.26
		3161.93	8	.69
		3166.15	10	.56
		3168.62	16	.48
4	5651.56	5412.23	6	4.23
		5557.63	8	1.66
		5586.92	10	1.14
		5602.32	16	.87
5	8813.43	7696.79	6	12.67
		8479.44	8	3.79
		8622.42	10	2.17
		8689.34	16	1.41

When a sufficient number of shaft elements are employed in the model excellent agreement with predicted

frequencies using equation 4.10 is observed. A small number of elements is seen to provide good accuracy at the lower frequencies where, for instance, the use of eight elements results in a maximum error of less than one percent for the first three natural frequencies. The analysis of higher-frequency necessitates the employment of a greater number of elements if reasonable accuracy is to be maintained. However, it is seen that even when only eight elements are used the first five natural frequencies can still be accurately predicted to within four percent, the same beam was then considered mounted on flexible supports (Fig.4.11b) and the calculated natural frequencies compared (Table 4.2) with those estimated using other numerical techniques [91,101].

Table 4.2

	ω_{c1}	ω_{c2}	ω_{c3}	ω_{c4}
Transfer Matrix Method	339	1190	2129	3007
O.S.Turkay Ref [101]	338	1198	1976	2476
Dostal et al Ref [91]	350	1200	1950	2500

Agreement between the results obtained using the various numerical method is found to be very good at

the lower frequencies with some disparity at the higher ones.

The effectiveness of the analysis programme in predicting the damped response of a shaft system, due to some pre-defined unbalance distribution, was assessed by analysing the arrangements shown in Fig. 4.11. These systems were earlier investigated by Dostal et al [91] and relevant graphical results from their paper are presented for comparison (Fig. 4.12). As with the free analyses, agreement is excellent for shaft cases (a) and (c) and for case (b) over the major part of the shaft speed range.

In addition to the above, the case of a simple Jeffcott rotor mounted on flexible supports with central unbalance and damping was analysed using the programme since, for this arrangement, the exact shaft response, bearing forces and influence coefficients are easily computed for comparison. The agreement was excellent with little discernable difference in the results.

Later comparisons with experimental measurement taken from a test rotor also confirm the validity of the programme.

Although, in all shaft cases analysed during these investigations, the normal and modified transfer matrix methods were found to agree almost exactly when predicting the first six shaft critical speeds, it was observed that at higher support stiffness values employment of the normal method resulted in failure to

accurately predict the higher frequency mode shapes.

4.8.3 Residual 'Jumps'

When employing the modified transfer matrix method for the free-vibration analysis of certain systems the calculated residual has been observed to tend to infinity then change sign, or 'jump', within specific frequency ranges.

This effect has been shown, in the literature [17] , to occur in systems comprising a number of branches and where a resonance exists in one of the sub-systems.

However, during the present investigations the phenomenon has been encountered in rotordynamic systems lacking sub-levels but incorporating flexible supports.

The 'jump' occurs because specific coefficients in the system transfer matrix tend to zero resulting in the decoupling of certain system boundary parameters. The characteristic is directly related to system rigid-body motions and thus does not appear in shaft arrangements where such motions do not occur e.g. a shaft mounted on rigid supports.

The frequencies at which these 'jumps' occur are not necessarily natural frequencies (Fig. 4.14) and consequently an effective means of discrimination must be sought. One suggestion [17] is the use of a different residual in the event of a 'jump', but from the author's experience there is no guarantee that this alternative residual will not also 'jump' and

unfortunately this will not be known until an analysis has been performed.

A more effective approach might be to monitor the signs of the coefficients making up the frequency determinant. If a 'jump' is encountered then at least one coefficient has changed sign. To fulfill the requirements for a natural frequency other coefficient(s) would also have had to undergo a change in sign. For example, referring to the case considered in section 4.2 and assuming the coefficient U_{12} to have changed sign (resulting in a residual jump) then for a system natural frequency to have been passed the polarity of one or both of the coefficients U_{14} and U_{32} must have similarly altered.

CHAPTER 5

VIBRATION REDUCTION OF FLEXIBLE ROTORS

Because of the extent of the work presented here, a brief summary of the principle findings is included at the end of this Chapter.

5.1 Radial Versus Angular Control

In practice, the introduction of control forces to rotor-dynamic systems should be accomplished with the minimum of alteration to the machine structure. This could be best achieved by mounting the controller at the shaft bearings/supports. Unfortunately, in many cases, this location is very inefficient when employing conventional control methods.

In an attempt to overcome some of the limitations which exist when using current control methods, a different approach to the vibration reduction of flexible rotors is proposed.

The introduction of a control moment (Angular Control), to a shaft system, is assessed and compared to the conventional procedure whereby a Radial Control force is employed. In this Chapter a theoretical investigation of radial/angular controller performance is presented for a number of test cases.

5.2 Simple Jeffcott Rotor

The effectiveness of angular control may be examined first by considering the case of a Jeffcott rotor (Fig. 5.1) mounted on simple supports. Viscous damping C_2 is

included in the model to represent system inherent damping due to, for example, oil-film bearings. Allaire et al [102] reported the effect of central radial feedback control on such a system and reached the obvious conclusion that derivative and proportional feedback could be employed to attenuate the resonant response and alter the system critical speed respectively. Here, a more general approach is adopted whereby the effect of location and type of control can be assessed. First, consider the synchronous response of the shaft due to central unbalance.

If a control couple M_c (or control force F_c) is located at some position along the shaft as shown in Fig. 5.1, then making use of simple beam deflection formulae [103], it is possible to define a central control force, F_e, to replace the radial and angular 'forces', F_c and M_c respectively. Thus, for the radial controller, the effective force would be:

$$F_{er} = F_c \cdot \alpha_1$$

and for the angular controller: (5.1)

$$F_{ea} = M_c \cdot \alpha_2$$

α_1 and α_2 are appropriate influence coefficients [103]:

$$\alpha_1 = (3L^2a - 4a^3)/L^3$$

$$\alpha_2 = \frac{48}{L^3}\left(\frac{L^2}{16} - \frac{a^2}{4}\right)$$

where a is the distance of the control element from the left-hand bearing and L is the shaft length.

The radial and angular effective central feedback control 'forces' may be expressed as:

$$F_{er} = [G_3 y + G_4 \dot{y}] \cdot \alpha_1 \quad \text{(a)}$$
$$F_{ea} = [G_1 \theta + G_2 \dot{\theta}] \, r^2 \cdot \alpha_2 \quad \text{(b)} \qquad (5.2)$$

where y and θ are the radial and angular displacements at the controller location and G represents the relevant controller feedback gain.

For the analysis here, the effective radius of the angular controller, r, is chosen as 0.03L since this value is approximately that used later, on the laboratory rig. It is felt to be an acceptable minimum value for most practical cases and could be increased substantially in many other instances.

The equation of motion for the system incorporating radial and angular control at any location is:

$$m\ddot{x} + C_2\dot{x} + K_2 x = F_u - F_{er} - F_{ea} \qquad (5.3)$$

where F_u is the external force due to unbalance ($me\omega^2$), K_2 ($= 48EI/L^3$) is the shaft stiffness and C_2 is the system damping.

Substitution of equations (5.2) in equation (5.3) and further manipulation (see Appendix B) leads to a relationship between the non-dimensional unbalance response ($\frac{x}{e}$) and other relevant system parameters, for the angular and radial control cases.

Because, in general, the controller location does not correspond to the shaft centre, the resulting equations (Appendix B) are not as simple as those obtained in Ref. [102]. Figs. 5.2 show the influence of radial and angular derivative control on the shaft non-dimensional response ($\frac{x}{e}$) for various levels of inherent system damping (C_2).

Figure 5.2a illustrates the effect of angular damping control with the controller mounted at a support ($b = \frac{a}{L} = 0$), whilst in Fig. 5.2b the case of radial control damping, applied at the shaft centre ($b = 0.5$), is considered. In both figures the uncontrolled response is shown for comparison. As expected, greater control damping is required for the angular damper in order to obtain the same reduction in response as its radial counterpart. For the cases shown, angular damping requirements are seen to be approximately one hundred times those of the radial controller.

At first sight these results appear to 'rule-out' the employment of an angular controller. However, comparisons made with the radial controller mounted at the shaft mid-span are, in many cases, only of academic interest since, in many real rotor systems, access to the shaft at this point would be impossible. In addition to the question of accessability, consideration of the shaft mode shapes encountered in real systems may necessitate the placement of a radial controller at a shaft section close to the supports. Further comparison of the two damper requirements (again using equations (B.8) and (B.9)), with the radial damper this time positioned more realistically at locations $b = 0.2$ and $b = 0.1$, shows that the required angular damping rate is now only approximately twenty times and eleven times respectively, that of the radial damper. It is important to note that this requirement is also inversely proportional to the square of the radius r, so that the angular damping

requirements reduce substantially when this parameter is increased. Similar conclusions may be drawn for the case of stiffness control, where the system critical speed can be shifted by employing proportional feedback control.

Equations (B.8) and (B.9), in Appendix B, were used to predict the non-dimensional control damping forces required to reduce the system peak response (i.e. at $\omega = \omega_{CR}$) to a variety of pre-defined levels. These forces were computed for both control types and a range of controller locations covering the shaft span and the results presented in Fig. 5.3. Figs. 5.3a and Fig. 5.3b represent two levels of inherent system damping, C_2 (ρ_2 = 0.05 and 0.1 respectively). The results are shown for a range of 'controlled magnification factor' values. Inspection of these figures highlights the increasing efficiency of the angular controller as its point of application approaches a shaft support. The trend is reversed for radial control - best performance being achieved with control implemented at the shaft mid-span. With each damper mounted at its respective optimum location, the force requirement of the angular damper is approximately eleven times greater than the radial version, to give the same reduction in displacement at the rotor centre. However, as would be expected, locating the radial controller at a shaft support or the angular controller at shaft centre results in the elimination of effective control.

The system free-vibration response is not easily assessed by examination of the equations developed in Appendix B and so another approach is necessary. If the

shaft deflected form is not appreciably altered by the introduction of control damping [91], then the following simple relationships may be used.

Radial Control

For central unbalance the shaft deflected form is defined [103] by the relationship:

$$y = (3b - 4b^3)\ x$$

Substituting for y and α_1 in (5.2a) gives:

$$F_{er} = [G_3 + i\omega G_4] \cdot (3b - 4b^3)^2\ x \qquad (5.4)$$

Angular Control

Again from the shaft deflectd form:

$$\theta = 3\ \left(\frac{1 - 4b^2}{L}\right) \cdot x$$

Substituting for θ and α_2 in (5.2b) and setting $R = \frac{r}{L}$

$$F_{ea} = [G_1 + i\omega G_2] \cdot R^2 \cdot 9\ (1 - 4b^2)^2 \cdot x \qquad (5.5)$$

Inserting equations (5.4) and (5.5) in the system equation and taking the Laplace transform, leads to the system transfer function:

$$\frac{x}{F_u} = \frac{1}{m\ [s^2 + 2\omega_{cr}\ S\rho + \omega_{cr}^2 + \omega_{cr}^2\ h]}$$

where

$$\rho = [\rho_2 + \rho_{f2}\ (3b - 4b^3)^2 + \rho_{f1}\ (9R^2\ (1 - 4b^2)^2)]$$

and $$h = [h_{f2} \cdot (3b - 4b^3)^2 + h_{f1} \cdot (9R^2\ (1 - 4b^2)^2)]$$

The parameters are as defined in Appendix B. The damped eigenvalues are obtained by setting the denominator equal to zero.

Therefore: $$S_{1,2} = -(\rho)\ \omega_{cr} \pm i\omega_{cr} \sqrt{(1 + h) - (\rho)^2}$$

The damped critical speed is:

$$\omega_d = \omega_{cr} \sqrt{(1 + h) - (\rho)^2}$$

and the exponential growth/decay factor is:

$$p = -\rho\omega_{cr}$$

The logarithmic decrement is given by:

$$\delta = \frac{-2\pi\rho\omega_{cr}}{\omega_d}$$

Therefore:

$$\delta = \frac{2\pi\ (\rho)}{\sqrt{(1 + h) - (\rho)^2}} \qquad (5.6)$$

Thus, the relative effects of radial and angular control can be assessed by substituting specific values for the system parameters. Equation (5.6) shows how the inclusion of derivative feedback increases the system stability, whilst the opposite is true for proportional feedback.

Considering the case where only damping control is utilised and the radial controller is mounted at a shaft position corresponding to b = 0.1 with the angular controller located at a support (b = 0), then assuming R = 0.03:

$$\rho = \rho_2 + 0.0876\ \rho_{f2} + 0.0081\ \rho_{f1}$$

and if the radial and angular feedback gains are identical then:

$$\frac{\text{Effective Radial Control Damping}}{\text{Effective Angular Control Damping}} = \frac{0.0876}{0.0081} = 10.8$$

which agrees with the earlier findings.

The analysis presented for the simple Jeffcott rotor is effective in providing some insight into the relative merits of each type of control, but lacks many of the characteristics found in a real flexible rotor system, e.g. multiple critical speeds, support flexiblity and damping, etc.

5.3 Multi-Mode Systems

5.3.1 Synchronous Response

In the case above, the choice of criterion for controller performance was simple and obvious - namely to reduce the central deflection of the rotor. However, in real multi-mass systems, this choice is far more complex because minimisation of the shaft response at a particular location will not necessarily lead to minimised response at other shaft locations. If a comparison is to be made of the efficiency of radial and angular controllers when employed on such a system, it is necessary to choose a suitable Performance Index (PI). Two main PI's have been employed in the past by other workers - shaft maximum displacement response [91] and sum of squares of shaft response [92], although no indication has been given of the relationship between these and other possible PI's.

In the present investigation, three performance indices are examined:

1) Shaft Maximum Displacement Response (i.e. the largest displacement to occur on the shaft).
2) Sum of Squares of Shaft Response (SSSR).
3) Total Bearing Force (arithmetic sum of bearing forces).

Three shaft systems, as previously investigated by Dostal [91] and shown in Fig. 4.11, were used in the analyses. These consisted of a uniform shaft of diameter 25.4 mm and length 956 mm, loaded parabolically to allow excitation of all modes within the selected frequency range and mounted on:

a) Pinned Supports.

b) Flexible Supports.

c) Damped Flexible Supports.

The creation of a basis for performance comparison of radial and angular type actuators requires careful consideration due to the multivariable nature of the problem.

The following procedure was adopted here and applied to each of the three shaft configurations in turn.

1. In general for each type of control (radial/angular) the performance indices are functions of the controller location a, the damping value C and the shaft speed Ω. That is:

$$PI = f(a, C, \Omega)$$

For both types of controller with C and a fixed, each performance index was computed as a function of Ω, over a shaft speed range covering the first three rigid-bearing critical speeds (0 - 3500 rad/sec) and (PI_{max}) computed. The objective was to minimise this value. Thus a was held constant and the minimum value of (PI_{max}), denoted by $(PI_{max})_{min}$, was obtained by varying C. This procedure was repeated for a range of values of a to obtain the lowest value of $(PI_{max})_{min}$, that is $(PI_{max})_{min\text{-}min}$.
Thus, adopting this approach, the optimum controller location and damping rate for a passive, or fixed-gain active device can be determined.

2. The radial and angular dampers were considered at their optimum locations and the damping controlled as

a function of rotor speed such that the system response was minimised continuously. In practice this would require the use of an adaptive [68] controller.

3. The procedure described in (1) above was repeated with each controller mounted at the left-hand support - this representing an ideal practical location for a controller. The effect of support stiffness on controller performance was examined.
4. The effect of introducing radial/angular stiffness control at the optimum control locations as determined in (1) was assessed.

For the purpose of the numerical analysis, the shaft was modelled as described in Section 4.6.1, nine elastic-massless elements being employed to ensure the removal of vibration nodes from the shaft stations within the specified frequency range.

In the initial stages of the work, a procedure described by Dostal et al [91] and making use of the theory of 'fixed-points' [104], was used to determine the system optimum passive damping value and corresponding controller location. The method entailed:

i) Determining the system response at the highest fixed-point within the operating speed range for each damper location.
ii) Comparing the response values obtained in (i) for a range of damper positions. The optimum damper location corresponds to the minimum response value.
iii) Estimating the control damping required to give a

zero-slope response at the highest fixed-point, with the damper at its optimum location. The resulting control damping value is the system optimum damping rate.

5.3.1.1 A Note on 'Fixed-Points'

The fundamental theory of fixed-points is sufficiently described elsewhere [91,104], but a number of observations, relevant to the investigations described here, are felt to be worthy of mention.

In addition to the necessary restraints as described by Dostal [91], exact fixed-points occur only when the response at a single rotor section, or some direct function of this, is considered. If any other response function is chosen, then fixed-points will not occur in an exact sense but the approach may still be used as an approximate design tool in some cases.

That approximate 'fixed-points' should occur in the case of shaft maximum displacement (all other fixed-point conditions being satisfied) is fairly obvious if it is assumed that the introduction of control damping does not significantly alter the shaft deflected form. This is due to the fact that the receptance relating the shaft displacement, at the point of maximum displacement, to the control force, is the same in both the controlled and uncontrolled shaft states. Thus effectively, within specific speed ranges, the response at one station only is being considered.

The shaft sum of squares of response will be directly related to shaft maximum displacement for relatively low

damping [91] and hence approximate 'fixed-points' would be expected to occur in both cases at the same shaft speeds. It follows that both criteria would be expected to produce identical optimum control damping values.

Continuing this line of thought, it seems reasonable that, in an experimental environment, in many cases direct measurement of shaft maximum response, necessitating continual repositioning of response measuring probes (or the employment of a greater number of probes), may be eliminated through measurement of a reduced SSSR using a smaller number of fixed-location probes. Of course, care would have to be taken to ensure that probe locations do not coincide with shaft nodal points.

The relationship between total bearing force and the above two performance indices is not so clear and it would appear that, in general, the control damping required to minimise the total bearing force may be different, its magnitude dependent upon the shaft-support dynamic relationship. For instance, consider the case of a flexible shaft vibrating in one of its free-free modes. If the bearings are inadvertently placed at, or close to, shaft nodes, then it is clear that although a large shaft response may occur, the bearing forces may be very small or, in the extreme case, even non-existent. Thus it does appear possible that minimisation of the former two performance indices will not necessarily lead to minimisation of the total bearing force.

In shaft cases (Figs. 4.11a and 4.11b) where all necessary fixed-point conditions are satisfied (except for

the choice of response function), in general, extremely good 'fixed-points' were found to occur for control damping levels over a fairly large region ($0.5C_{opt} < C < 2C_{opt}$) in the vicinity of the optimum control damping values, for all three performance indices. Variations in the extent of this damping range occur depending on the exact location of the control damping - the above representing a minimum range for the cases investigated.

For very low ($C \to 0$) or very high ($C \to \infty$) control damping values, certain 'fixed-points' tend to degenerate, their degree of deterioration being determined by the location of the controller in relation to the anti-nodes of the modes to be controlled. Figs. 5.4a and 5.4b illustrate the effect of control damping magnitude on the existence of 'fixed-points', with the radial and angular controllers at their respective optimum locations, for the pinned-pinned shaft case (Fig. 4.11a).

It is interesting to note that irrespective of the control damping level, the first 'fixed-point' is always clearly defined in both control cases. The optimum control damping values for the cases presented in Fig. 5.4 are 4500 Ns/m and 24 Nms for radial and angular control respectively. The influence of control damping magnitude on the maintenance of 'fixed-points" as displayed in Fig. 5.4 is typical of that observed in the other rotor systems investigated for both control types and various controller locations.

However, where the motion of shaft orthogonal planes is coupled due to, for example, the introduction of oil-

film bearings (Fig. 4.11c) additional violations of the 'fixed-point' theory [91,104] lead to further deterioration of the 'fixed-points', particularly at higher shaft rotational frequencies.

Although effective, when studying a large number of combinations of shaft configurations and controller locations, the 'fixed-point' method was found excessively time-consuming. Additionally, the unsuitability of this method for determining local optimum (frequency-dependent) control damping/stiffness values, along with the other limitations resulting from violations of the 'fixed-points' theory, necessitated the introduction of a more suitable optimisation procedure.

5.3.1.2 Optimisation of Control Parameters

A few optimisation procedures have been developed for use with rotor-bearing systems [92,94,105]. These methods, however, make use of the system equations of motion in explicit form, viz:

$$\underline{M} \cdot \ddot{\underline{q}} + \underline{C} \cdot \dot{\underline{q}} + \underline{K} \cdot \underline{q} + \underline{U} = \underline{F}$$

With $\underline{U}$ normally chosen such that $\underline{q}$, or some related function, may be minimised. Because the transfer matrix method was initially used for the dynamic analysis of the test rotor, the above approach was deemed unsuitable.

The following method, created specifically for this investigation, is simple but effective. In addition demands on computer memory are minimal because of the nature of the optimisation formulation.

In a linear system the response due to mass unbalance may be assumed harmonic and thus can be expressed in the

form of rotating vectors:

$$\text{i.e.} \quad \underline{q}(t) = \underline{\bar{Q}} e^{i\Omega t}$$
$$\text{where} \quad \underline{\bar{Q}} = \underline{Q}_r + i\underline{Q}_i \qquad (5.7)$$
$$\text{and} \quad \underline{\bar{Q}} = [\underline{\bar{w}}, \underline{\bar{v}}]^T$$

where the shaft radial displacements are:

$$\underline{w}(t) = \text{Re}\{\underline{\bar{w}} e^{i\Omega t}\} = \underline{w}_c \cos \Omega t - \underline{w}_s \sin \Omega t$$
$$\text{and} \quad \underline{v}(t) = \text{Re}\{\underline{\bar{v}} e^{i\Omega t}\} = \underline{v}_c \cos \Omega t - \underline{v}_s \sin \Omega t \qquad (5.8)$$

The controlled response $\underline{q}_c(t)$ may be expressed in terms of the uncontrolled response $\underline{q}_u(t)$, control force vector $\underline{f}_c(t)$ and system receptances $\underline{\bar{r}}$ as follows:

$$\underline{q}_c(t) = \underline{q}_u(t) - \underline{\bar{r}} \cdot \underline{f}_c(t) \qquad (5.9)$$

where

$$\underline{\bar{r}} = \begin{array}{c} \text{Radial Control} \quad\quad\quad\quad\quad\quad\quad\quad \text{Angular Control} \\ \left[\begin{array}{ccc|ccc} \bar{r}_{11} & \cdots & \bar{r}_{1(mx2)} & \cdots & \bar{r}_{1(mx4)} \\ \bar{r}_{21} & & & & \\ \vdots & & & & \\ \bar{r}_{(mx2)1} & \cdots & \bar{r}_{(mx2)(mx2)} & \cdots & \bar{r}_{(mx2)(mx4)} \end{array}\right] \end{array}$$

$$; \quad \underline{f}_c(t) = \underline{\bar{F}}_c e^{i\Omega t} \qquad (5.10)$$
$$\text{and} \quad \underline{\bar{F}}_c = [\underline{\bar{F}}_{cz}, \underline{\bar{F}}_{cy}, \underline{\bar{M}}_{cy}, \underline{\bar{M}}_{cz}]^T$$

where the control force vectors $\underline{\bar{F}}_{cz}$, $\underline{\bar{F}}_{cy}$, $\underline{\bar{M}}_{cy}$ and $\underline{\bar{M}}_{cz}$ may be expressed in the same form as the shaft response vectors (5.8). The vector $\underline{\bar{F}}_c$ will be of maximum order 2m where m is the number of shaft stations. However, the number of external control forces, n, will generally be much less than this. The maximum size of the receptance matrix $\underline{\bar{r}}$ is (mx2).(mx4), assuming that only the shaft

radial response will be required. The actual size of $\underline{\bar{r}}$ will be determined by the number of stations at which the shaft response is to be computed, l,and the actual number of control forces n and is therefore (l x n). Normally either radial or angular control will be employed resulting in elimination of one half of the system receptance matrix $\underline{\bar{r}}$.

Substituting equations (5.7) and (5.10) in (5.9) gives:

$$\underline{\bar{Q}}_c = \underline{\bar{Q}}_u - \underline{\bar{r}} \cdot \underline{\bar{F}}_c \qquad (5.11)$$

and

$$\underline{\bar{F}}_c = \underline{\bar{Z}} \cdot \underline{\bar{Q}}_{ce} \qquad (5.12)$$

where $\underline{\bar{Z}}$ is the control dynamic stiffness matrix and $\underline{\bar{Q}}_{ce}$ is the controlled response at the controller locations e.

Substituting (5.12) in (5.11) and considering the response at controller locations,

$$\underline{\bar{Q}}_{ce} = [\underline{I} + \underline{\bar{r}}_e \cdot \underline{\bar{Z}}]^{-1} \cdot \underline{\bar{Q}}_{ue}$$

$\underline{I}$ is a unity matrix. Substituting this equation back into (5.11) we obtain:

$$\underline{\bar{Q}}_c = \underline{\bar{Q}}_u - \underline{\bar{r}} \cdot \underline{\bar{A}} \cdot \underline{\bar{Q}}_{ue} \qquad (5.13)$$

where

$$\underline{\bar{A}} = \underline{\bar{Z}} \cdot [\underline{I} + \underline{\bar{r}}_e \cdot \underline{\bar{Z}}]^{-1} \qquad (5.14)$$

The subscript e refers to conditions at the points of location of the external control forces.

Therefore, with the system uncontrolled response and relevant receptance known, $\underline{\bar{Z}}$ may be chosen so that the control response $\underline{\bar{Q}}_c$, or some related parameter, is minimised. The relevant data is obtained through a two-stage transfer-matrix analysis. In the first stage the shaft uncontrolled response, due to a pre-defined unbalance distribution, is determined. Next, the system

response to a unit harmonic force of frequency equal to shaft speed and located at the controller positions is obtained, thus providing the shaft dynamic influence coefficients, or receptances. A computer program was created incorporating equations (5.13) and (5.14) in a sub-routine called by Nag library routine E04JAF which is designed to perform a numerical multivariable optimisation. A flow chart illustrating the main structure of the optimisation procedure is presented in Fig. 5.12.

Although not considered here, the method could just as easily be employed to determine the necessary external support-stiffness magnitudes required to ensure sufficient removal of system undamped critical-speeds from shaft operating speeds. This would be extremely useful in the many practical cases where system damping is small. In such circumstances, the difference between damped and undamped critical speeds will be negligible. In fact, even if significant system damping is present, the above procedure may still be useful as the first stage of a more comprehensive optimisation strategy.

The optimisation method described has the following advantages:

1. Repetitive shaft analyses are avoided since the system characteristics (receptances and uncontrolled responses) are obtained initially using a two-stage procedure. This effectively ensures that the optimisation program run-time is independent of that of the main analysis program.
2. High computational efficiency due to minimal computer storage demands since:

a) Initial rotor analysis is performed using the well known transfer-matrix technique.

b) Only the relevant system receptances are utilised, thus eliminating the need for storage of redundant data. In most cases, control inputs are restricted to one or two shaft locations. For a rotor system with coupling at the supports employing a single controller, at most 2 m components of receptance and uncontrolled response are required (at each shaft frequency).

3. As well as allowing for prediction of optimum control parameters and minimised performance indices, the technique enables the computation of system response for any linearly defined control force arrangement.

Minimised shaft maximum response and sum of squares of response were obtained using equation (5.13). Although the minimised total bearing force could also be obtained using this approach the method would fail when rigid bearings were present. A more suitable procedure is to make use of equations (5.13) and (5.14), replacing the shaft response terms with bearing forces keeping in mind that the new 'receptances' have units of (N/N). The analysis is then identical to that described earlier.

When employing the optimisation technique to determine optimum adaptive control parameters, in certain instances within particular frequency ranges (mainly around the 'fixed-points'), the chosen performance index was found to be insensitive to the magnitude of the

selected control parameters. This phenomenon poses few practical problems, however, since it merely indicates the lack of benefit in applying control at that location under such circumstances. To enable assessment of the reliability of the optimisation search routine, the control parameters were given three separate starting values, each within the specified operating range. Continual convergence of the minimised PI and optimum control parameters to within a specified tolerance band indicated a successful optimisation analysis.

The accuracy of the method was confirmed by performing a number of analyses on the three shaft arrangements (Fig. 4.11) and comparing the results to those obtained using the 'fixed-point' approach. Excellent agreement was achieved.

5.3.1.3 Results of the Controller Comparison

The results of a number of computer runs using the above approach are presented here.

The investigation highlighted the necessity for a suitable choice of shaft speed increment in the computer program, particularly in the region of those shaft critical speeds insensitive to the controller influence. Failure to take account of this could have led to gross errors in the predicted optimised damping constant and minimised performance index, although in some cases, where only relative comparisons are required, the effect may be less critical.

As a result of the relatively high support stiffness and damping rates the shaft system described in Fig. 4.11c

was found to behave in a very similar fashion to the pinned-pinned shaft arrangement (Fig. 4.11a). Consequently, in general, conclusions drawn for the latter case are also applicable to the former. Because of this, the following discussions will be directed mainly at the first two shaft systems (Figs. 4.11a and 4.11b) - reference being made to the third system where appropriate.

In all cases examined, performance indices 1 and 2 (shaft maximum displacement and sum of squares of displacement) were found to produce the same optimum damping values and optimum controller locations, whilst this was generally not true when total bearing force was considered. These findings confirm the views expressed in Section 5.3.1.1.

5.3.1.3.1 Optimum Control Location

Figures 5.5a and 5.5b show the effect of controller location on the minimised performance indices for the shaft systems with rigid and flexible-undamped supports respectively and for both controller types. Because of the nature of the shaft excitation, the magnitudes of the minimised PI's are not symmetrical about the shaft centre, but their relative positions are, thus allowing the following general conclusions to be drawn:

1. For radial control and all rotor configurations, the minimum value of each PI is realised when the controller is mounted at the stations adjacent to the supports (stations 2 and 9). However, it should be noted that when support flexibility is present, minimisation of the total bearing force could be

achieved almost to the same extent, by mounting the radial controller at one of the supports.

2. For angular control, the optimum controller location, for minimisation of shaft maximum displacement and sum of squares of response, is at the supports for large support stiffness and moves inward when flexible supports are introduced.

3. The optimum location for angular control when minimising total bearing force is, in general, different to that required to minimise the other PI's, the ideal application occurring between the supports and shaft centre. The optimum location for angular control would appear to be more sensitive to the value of shaft support stiffness than that resulting from radial control.

5.3.1.3.2 Optimum Control Damping and Corresponding Minimised PIs

Figure 5.6 shows the variation of minimised performance indices with control damping for the shaft employing rigid supports. The radial and angular controllers are considered mounted at their respective optimum locations (i.e. for minimisation of maximum deflection/sum of squares of shaft response). Examination of this figure and similar data for the other shaft cases leads to the following additional conclusions:

1. In general, values of the minimised PI's resulting from radial control are found to be lower than those achieved using angular control.

2. Minimisation of shaft maximum response and sum of squares of shaft response could be simultaneously

achieved using one optimum damping constant. However, employment of this optimum damping rate will not necessarily lead to minimisation of the total bearing force. For instance, considering angular damping control at station 1 for the shaft on pinned-supports, Figs. 5.7 demonstrate the effect on the shaft maximum displacement of minimising the bearing-force and vice-versa. It is seen that by choosing the control damping to minimise the bearing force, the minimum possible value of shaft maximum displacement would be increased by approximately 55% - this increase occurring at the first critical. However, if the shaft maximum displacement was minimised, the optimum bearing force would be inceased by only 25% at the top end of the frequency range. Thus, it is seen that the selection of an appropriate system performance index requires careful consideration and in practice would depend, mainly, upon the relative importance of a variety of system response functions (e.g. shaft displacement, bearing force etc.).

Table 5.1 provides a quantitative comparison of the minimised responses ($(PI_{max})_{min-min}$) which may be obtained by utilising optimally designed, passive and radial/angular dampers. The corresponding optimum damping rates are also shown. The parameters are presented more meaningfully when non-dimensionalised with reference to radial controller performance. To enable direct comparison the effective radius r of the angular

controller is set, as before, to 0.03L and the equivalent linear damping coefficient calculated.

Table 5.1 Radial/Angular Control Optimisation Comparison

$$\text{Amplitude Ratio} = \frac{(PI_{max})_{min\text{-}min} \text{ - Angular Control}}{(PI_{max})_{min\text{-}min} \text{ - Radial Control}}$$

$$\text{Damping Ratio} = \frac{\text{Optimum Angular Damping Rate}/r^2}{\text{Optimum Radial Damping Rate}} \; ; \; \frac{r}{L} = 0.03$$

	Shaft on Rigid Supports (Fig. 4.11a)				Shaft on Flex Supports (Fig. 4.11b)			
PI	Amp Ratio	Damp Ratio	Damp Loc Rad	Damp Loc Ang	Amp Ratio	Damp Ratio	Damp Loc Rad	Damp Loc Ang
Shaft Max Defn	1.7	6.5	St.2	St.1	2.5	15.8	St.2	St.2
Total Brg Force	3.5	3.0	St.2	St.1	2.6	15.8	St.2	St.2

The results shown in Table 5.1 indicate the possible benefits of radial control, particularly when substantial support flexibility is present. However, before a realistic comparison of both control methods (Radial/Angular) can be made, a number of very important considerations must be borne in mind:

1. The control capability of the angular device is inversely proportional to the square of the radius r. Thus, considering the pinned-pinned shaft, if the controller radius r is doubled (and this would not be excessive in a large number of cases) then radial and angular optimum damping requirements would be of the same order of magnitude. Although the radially-minimised performance indices would be smaller than

those resulting from angular control, the angular damper would still be capable of significantly attenuating the rotor system response.

2. The above comparison is made with each controller placed at its optimum location. Practical considerations may preclude the siting of a radial controller at its optimum location (on the shaft span) and thus invalidate the results of the simulation. The shaft supports present the ideal location for controller mounting from both an access and structural point of view. In fact, the implementation of angular control at <u>each</u> support is conceivable in many practical installations, whilst the possibility of including an additional radial controller on the shaft span would probably be remote at best.

   Because of this and in order to allow a more realistic comparison, the performance of the radial and angular controllers is later assessed with both considered mounted at one of the shaft supports.

3. It has been assumed so far that:

   a) No additional hardware advantages are obtained by introducing control in an angular fashion.

   b) That the choice of actuator type, e.g. hydraulic, pneumatic, electromagnetic etc., will not affect the relative performance of radial and angular controllers.

   Both of these points are of significance and are discussed in greater detail in Chapter 6.

5.3.1.3.3 Controller Power

Proper assessment of controller performance demands not only evalution of vibration attenuation characteristics but, in addition, consideration of resulting controller energy dissipation rates (power levels).

In Fig. 5.8, radial and angular controller power requirements are illustrated for two shaft support stiffness values, with the controllers mounted at their respective optimum locations (i.e. for minimisation of shaft maximum deflection/sum of squares of response) and optimum passive damping levels employed.

It is seen that, in general, because of the greater shaft response both controllers dissipate higher energy rates when flexible supports are introduced. Exceptions occur in specific frequency ranges (angular control: 1200-1800 rad/sec; radial control: 3100-3500 rad/sec), where the controllers are in close proximity to shaft vibration nodes.

Of particular interest is the fact that each controller type has superiority over the other, in terms of power consumption, within specific speed ranges. Indeed instances occur (Figs. 5.4 and 5.8, 1800-2400 rad/sec) where even though radial control provides best response attenuation, correspondingly greater controller power levels are demanded.

5.3.1.3.4 Controllers Mounted at LH Shaft Supports

With both types of controller mounted at the shaft left-hand support, intuition suggests that at high

support-stiffness values, the radial controller will become ineffective whilst the angular controller may still give some measure of control. At relatively low stiffness values, this trend would be expected to reverse. Consequently, at some intermediate support stiffness, the two should perform equally well. Fig. 5.9 demonstrates the influence of shaft support stiffness on the performance of radial and angular passive dampers. Results are presented for shaft speeds encompassing the range 0-3500 rad/sec. The minimised system response $((PI_{max})_{min-min})$ and corresponding optimum damping rates are shown for the three performance indices.

The stiffness ratio, defined as the ratio of support stiffness to shaft stiffness, at which both controllers give the same minimised response will be termed the 'critical stiffness ratio' (CSR).

The CSR, as expected, is the same for maximum deflection and sum of squares of displacements criteria, but different in the case where total bearing force is minimised. In calculating the stiffness ratio, the representative shaft stiffness K_s is determined for the case where the shaft is subjected to a central concentrated force ($K_s = 48EI/L^3 = 2.36 \times 10^5$ N/m).

From Fig. 5.9a, the CSR is estimated as approximately 15 and 33 for maximum displacement and total bearing force respectively. Thus, the choice of control damping type, when employed at the supports in a passive sense, would depend not only on the operating stiffness ratio, but also on the performance index adopted.

At a stiffness ratio of just less than 10, the angular damper is seen to become relatively ineffective. This is due to the introduction of a shaft mode where practically zero-slope occurs at the shaft ends.

The optimum damping rate for angular control is seen to be insensitive to the stiffness ratio (Fig. 5.9b), whereas the radial damping rate decreases significantly at low stiffness ratios.

According to Dostal et al [91] many present-day real rotor systems employ bearings with a stiffness of the order 21.6×10^6 N/m. If this support stiffness was used here, the resultant operative stiffness ratio would be approximately 90, indicating the possible practical advantages of angular control in such a system.

It is worth noting that reduction of the maximum shaft speed, to a value enclosing the first two rigid-bearing criticals, would result in an extension of the stiffness ratio range over which the angular controller would be superior. This is because the radial controller efficiency is mainly determined by the system reponse at the first critical speed - a region where, by comparison, the angular controller is extremely effective.

Consequently, under such circumstances the CSR would be decreased significantly, thus validating the benefits of angular control for a greater range of shaft-support configurations.

5.3.1.3.5 Adaptive Damping Control

The effect of introducing control damping as a function of shaft speed (adaptive control), in order to

minimise system response, is illustrated in Fig. 5.10, where relevant shaft passively-controlled response is presented for comparison. The response plots of Fig. 5.10a demonstrate the effect of locating the controllers at their respective optimum positions, whilst those of Figs. 5.10b-e are for the controllers mounted at the shaft left-hand support. In the cases where control damping was optimised continuously, the maximum and minimum control damping values were chosen as the appropriate optimum passive damping rate and zero respectively.

Some interesting conclusions may be drawn from these investigations.

When the shaft supports exhibit high stiffness (shaft configurations corresponding to Figs. 4.11a and 4.11c) and dampers are located at their optimum positions (Fig. 5.10a) although the radial damper is seen to be more effective than its angular counterpart, especially at the first critical speed, the difference in performance is not excessive and, in fact, over a large proportion of the speed range, both perform equally well. Because these two shaft systems were found to respond in the same manner, with slight differences at high shaft speeds, only the response of the 'pinned-pinned' shaft is shown.

When the supports contain substantial flexibility (Fig. 5.10a) angular control is observed to be much less effective than radial control, over an extensive central portion of the speed range. As in the high support stiffness case, speed zones exist where both means of control result in the same response, although in this

instance, the zones are more dispersed and represent a smaller portion of the complete speed range. Response attenuation at the first critical speed is almost identical for both means of control.

For the shaft arrangements investigated here, it was found that the employment of adaptive control resulted in the required control damping essentially switching between the pre-defined maximum and minimum values. Fig. 5.10c demonstrates this effect and is typical of the form of control damping required for the systems analysed. It is clear that the system response may be continuously minimised (Fig. 5.10b) through the introduction of an 'on-off' control strategy (Fig. 5.10c), controller switching occurring around the system 'fixed-points'. These results are in agreement with those of Burrows et al [69] though different optimisation procedures were employed. It is worth noting that in the cases shown and in general, the 'angular fixed-points' do not occur at the same frequencies as the 'radial fixed-points'.

The influence of radial and angular adaptive damping control on the shaft response, with both controllers incorporated at the shaft left-hand support, is shown in Fig. 5.10e. Two levels of shaft support stiffness (K_b = 2.13×10^2 N/m and 5.0×10^6 N/m, i.e. stiffness ratios of approximately 9 and 21 respectively) are considered. At the top half of the speed range, the superiority of radial control is evident whilst at the lower speeds, this trend is reversed with substantial benefits resulting from the employment of angular damping. As the support stiffness

is decreased, the effective range of the radial controller is extended in direct contrast to that of the angular controller. However, even with a relatively low support stiffness, the angular approach is seen to offer a distinct advantage over at least the lower 20% of the shaft operating speed (i.e. the speed range covering the shaft first bending critical speed).

For the support stiffness values considered, there appears to be little advantage in employing the angular controller as an adaptive device, since its passive performance is almost as effective (Figs. 5.10d and 5.10e). This is also true for the radial damper when a large support stiffness is present. Referring to Figs. 5.10d and 5.10e, it is clear that there exist definite speed ranges where radial control provides best system performance, whilst in other speed ranges angular control is to be preferred. Consequently, under such circumstances, some advantage may result from the introduction of a unified control strategy whereby the control mode (radial/angular) could be chosen according to the shaft speed and implemented in either a passive or adaptive form.

5.3.1.3.6 Stiffness Control

The application of external spring-like elements to a rotor-bearing arrangement leads to displacement of the system critical speeds. The effect of introducing radial and angular passive stiffness control to the pinned-pinned shaft case of Fig. 4.11a, at the previously determined optimum locations, is illustrated in Figs. 5.11a and

5.11b. The shaft response for three control stiffness magnitudes is shown. Due to the increase in shaft effective stiffness, the critical speeds are augmented - the extent of modification being dependent upon the level of stiffness control employed and the effectiveness of external control on the particular whirling mode under consideration.

The introduction of a passive stiffness element may lead to significant shaft response attenuation even in cases where system damping is small. For example, cases occur in practice where a shaft operating speed inadvertently coincides with, or occurs close to, a system critical speed. Even a small displacement of the critical speed in such a case may result in a large reduction of the vibration response. Of course it would still be necessary to ensure safe passage of the shaft through other critical speeds which might be encountered during run-up to the design speed.

This latter problem may be minimised or even satisfactorily removed by implementing an adaptive stiffness control strategy. Referring to Fig. 5.11b, it is observed that by suitable application of a simple 'on-off' type control procedure, the shaft response may be considerably reduced over the complete speed range. This may be achieved by employing maximum control stiffness at low shaft speeds up to a speed just above the first uncontrolled critical speed where the control is then 'switched-off'. At another point below the next uncontrolled critical speed, maximum control is once more

introduced and maintained until the unstiffened second critical speed has been passed whereby control is again eliminated. With this trend extended over the complete speed range, the shaft critical speeds are effectively avoided and a comparatively low response level achieved even in the absence of system damping. However, at least a small amount of damping is desirable if only to ensure elimination of the possibility of rotor instability which may occur in various forms [42,109].

5.3.1.3.7 Damping-Stiffness Control

A natural extension to the control procedures described earlier would be the introduction of a combined damping/stiffness control approach.

Kaya et al [94] studied the effect of applying such a technique, in a radial sense, to the shaft arrangement shown in Fig. 4.11a. Optimum frequency-dependent control damping and stiffness rates were determined and it was found that for an inherently undamped system, the resulting optimum control force tended to be predominantly either in phase or 180° out of phase with the excitation forces (i.e. stiffness control). The introduction of some system damping altered this situation and led to the requirement of an optimum control force in the form of combined stiffness and damping. It was observed that the minimisation of system response may be best achieved, in certain instances, when the control stiffness/damping parameters are allowed to take on negative values. In such circumstances, the rotor-bearing minimised response would approach the Limiting Performance Characteristic

[105,110] for the arrangement.

Of course, practical realisation of such a concept would necessitate the employment of an active control strategy - a passive device being unable to supply the required negative stiffness and damping coefficients. However, application of the above procedure, in the form of active feedback control, would require great care since the presence of negative system coefficients may lead to system destabilisation. This fact was recognised by Burrows et al [92] who suggested the implementation of an open-loop adaptive control strategy employing a radial magnetic bearing as the force actuator. Simultaneous control and system parameter identification could be realised by the injection of an additional multifrequency test signal and application of frequency domain estimation techniques [62].

The procedures described above, although not considered further, may also be adopted where angular control is employed and so the conclusions formed above would be, in general, equally applicable.

5.3.2 System Stability

A number of potential causes of rotor instability exist in much of the high-speed machinery in operation today. The presence of any of the following elements - oil-film bearings, shaft internal friction, asymmetric rotor support configurations or aerodynamic excitation forces, may lead to destabilisation.

Of the above, probably the most common cause of rotor

instability is that resulting from the employment of journal bearings. When the shaft rotational frequency reaches a particular value, determined by the bearing parameters and other operating conditions, the system damping becomes negative and the shaft whirls at a frequency of around half the rotational frequency.

It has been shown [43,87] how the introduction of even a small amount of external damping in such a system can lead to a significant increase in the instability onset speed. The effectiveness of employing angular damping for system stabilisation will be assessed here by considering its application to the rotor system analysed by Burrows et al [92] and shown in Fig. 5.13. The shaft arrangement consists of a symmetrical flexible rotor carrying three rigid discs and supported on oil-film bearings.

Journal bearing parameters are presented in Fig. 5.13 and the eight linearised bearing coefficients are calculated from equations developed by Holmes [23]. System stability is assessed by examining the real part of the speed-dependent eigenvalues which are calculated using a numerical program based on the stiffness coefficient method [101].

The imaginary parts of the eigenvalues plotted against shaft speed, for the uncontrolled case, are shown in Fig. 5.14a. Those modes exhibiting relatively small variation in frequency with shaft speed and shown dashed in Figs. 5.14a, c and d, are predominantly shaft bending modes, whilst the others are representative of shaft

rigid-body motion. The characteristic splitting of the modes is due to the asymmetric nature of the bearing oil-film. The degree of system stability is indicated by the magnitude and sense of the logarithmic decrement which is shown at selected points. The appearance of a change in sign of the logarithmic decrement for the first shaft bending mode indicates the occurrence of instability at a shaft speed of 361 rad/sec. The shaft precession rate, 137.5 rad/sec, at this speed, is less than half of the rotational frequency in line with the observations of other workers [46,108].

The application of external damping as a means of suppressing the rotor instability is investigated by considering first the incorporation of a radial damper, then that of an angular damper at the left-hand bearing. For the purpose of comparison, the radial and angular damping levels, required to increase the instability onset speed by more than a factor of two, to 800 rad/sec, are computed and compared. Fig. 5.14b illustrates the variation of the real part of the relevant eigenvalue with radial and angular control damping levels for a shaft speed of 800 rad/sec. The radial and angular control damping rates required to stabilise the system are found to be 5700 Ns/m and 10.5 Nms respectively.

Setting the angular damper radius to shaft length ratio, (r/L), equal to 0.03, as before, allows direct comparison of the required damping rates. The equivalent linear damping coefficient for the angular controller (3700 Ns/m) is approximately 65% of that demanded from the

radial device. Of course, as noted earlier, increasing the (r/L) ratio would lead to a substantial decrease in the required angular damping coefficient. For instance, doubling this ratio leads to a radial damping requirement of more than six times that for the angular controller.

Figs. 5.14c and 5.14d show the effect, on the system damped natural frequencies, of introducing radial and angular damping values of 5700 Ns/m and 10.5 Nms respectively. Stable operation of the shaft-bearing arrangement, within the desired speed range, is indicated by the complete removal of negative logarithmic decrements.

It is interesting to note that in the case of radial control (Fig. 5.14c), at almost all speeds and shaft flexural modes illustrated, the effect of additional damping, whilst leading to elimination of the oil-whirl instability, leads to a substantial reduction in system damping. This is in direct contrast to the angular damping effect, where in general, a significant increase in modal damping is observed (Fig. 5.14d). For example, referring to Figs. 5.14c and 5.14d and considering the shaft third flexural mode at a speed of 450 rad/sec, the logarithmic decrements corresponding to radial and angular control are approximately 0.065 and 0.236 respectively. Synchronous excitation of these modes due to mass unbalance would thus lead to greater attenuation of system response in the case of angular control. Examination of damping levels at other modes indicates even more substantial benefits from angular control.

The application of external damping (radial and angular) is seen to greatly influence the two 'rigid-body' modes, i.e. those modes running almost parallel with the synchronous forcing line shown in Fig. 5.14a. Although angular damping substantially increases the damped natural frequencies corresponding to the above modes, the lower mode is actually eliminated at a shaft speed equal to 275 rad/sec, when radial control is employed. However, even with the system in the uncontrolled state, these modes are extremely well damped and therefore should pose no problems regarding the presence of unbalance response peaks (i.e. if they are excited - Figs. 5.14a and 5.14c).

The shaft flexural-modal frequencies are influenced to a lesser extent by the implementation of external control. Although external angular damping produces substantial splitting of the modes, the critical speeds resulting from synchronous excitations are barely altered. This is not the case when radial damping is employed. Reference to Figs. 5.14a and 5.14c shows an increase of approximately 6% in the first three critical speeds when radial control is introduced.

5.3.3 Chapter Summary

From the results of the analyses performed in this Chapter, the following main conclusions can be drawn:

1. An efficient optimisation procedure has been developed and utilised to determine optimum control locations and damping rates.

2a) Radial control is most effective when introduced at a

location on the shaft span between the supports.

b) Angular control is highly efficient when introduced at a shaft support when the support stiffness is fairly high. If support stiffness is low, then better performance can be achieved when the angular controller is located on the shaft span between the supports.

3. Angular control is a viable means of synchronous vibration reduction and instability suppression in flexible rotor systems. Optimum passive radial and angular damping rates are of the same order of magnitude when a reasonable controller radius is selected.

4. The choice of performance index can greatly influence the optimum control force magnitude and location.

5. Effective control, angular or radial, may be implemented at all shaft speeds by the incorporation of an adaptive 'on-off' control approach.

It is clear from the investigations performed and discussed in this Chapter that both radial and angular control have their merits in differing circumstances and that the choice of control method would greatly depend upon the particular system being considered. In fact, it may even be possible to combine both means of control to create an efficient 'unified control strategy'.

CHAPTER 6

EXPERIMENTAL EQUIPMENT

A brief summary of the main aspects of the work covered here is presented at the end of this Chapter.

6.1 Test Rotor

6.2 Rig Requirements

When designing the test-rotor, taking into account the type of investigations to be performed, the following were considered as essential features:

1. Shaft maximum operating speed greater than the first critical speed.
   This is a fundamental requirement for the simulation of a flexible rotor system.
2. The test arrangement should exhibit characteristics which may exist in a full-scale, practical system.
   In much modern-day high-speed machinery, the effect of gyroscopic moments and support-flexibility, mass and damping may play a major role in influencing the system dynamic response.
3. Easily adjustable system characteristics.
   System mass/stiffness/damping parameters should be amenable to alteration to enable investigation of the influence of these variables on the overall system characteristics.
4. Provision for accurate system response measurement and the introduction of external control forces.
   Access to a number of shaft locations for the purpose

of response measurement and control can be a major difficulty where substantial alteration of the test configuration must be allowed for. In such circumstances the acceptance of a compromise solution is normally necessary.

To ensure fulfilment of the above requirements, the test rotor was designed as follows.

6.3 Rig Design

The main test rig consisted of a 1290 mm long, 15 mm diameter, uniform carbon-steel shaft mounted on double-row, self-aligning ball-bearings with bearing centres of 1050 mm. A variety of shaft configurations, some employing intermediate discs and different levels of bearing-support stiffness, were investigated throughout the test program. The rotor design was such that in the majority of test cases, the shaft maximum operating speed (≈ 3000 rpm) was approximately two times the system first critical speed. The general layout of the test rotor, including the drive-system, is shown in Fig. 6.1a.

In some instances, discs of varying mass/inertia were rigidly mounted on the shaft between the bearings. The purpose of the discs was generally two-fold:

a) to enable the application of unbalance masses, and
b) to allow the introduction of gyroscopic/rotary inertia effects.

Investigation of the influence of electromagnetic control necessitated the employment of a special 100 mm diameter, low-loss, silicon-steel disc mounted on the

shaft adjacent to the drive-end bearing (Fig. 6.1b). All discs were such that they could easily be axially re-positioned on the shaft if necessary.

A 0.75 kW, direct-current, variable-speed motor was employed to drive the test-shaft. Using a timing-belt, pulley-drive arrangement, the test-shaft, driven through a stub-shaft assembly, could be run at a speed approximately 3.5 times that of the drive-motor. The introduction of a flexible pin-cord type coupling, between the stub-shaft and test-shaft, helped ensure the elimination of vibrations transmitted from the drive.

The complete system was supported on cast-iron blocks which were in turn rigidly attached to a large steel table having substantial mass.

The test-shaft was located axially at the drive-end bearing and allowed to move freely at the non-drive end to avoid axial stressing of the shaft (Fig. 6.2).

The bearing support structure (Figs. 6.3 and 6.4) was designed such that flexibility in the horizontal and vertical planes could be easily altered by introducing a range of thin steel-rings of fixed diameter and varying thickness. The rings could be pre-loaded as required by the adjustment of four screws within each pedestal. In addition, the rings were effectively utilised as proving-rings, through the application of electrical resistance strain-gauges, thus allowing measurement of the transmitted bearing force. Because of the fairly extensive use of strain-gauges in the construction of a variety of force transducers employed during the test

program, details of the construction of the components utilised are provided in Appendix C. Replacement of the bearing rings with solid steel cylinders enabled the simulation of rigid supports.

Simulation of support sub-level characteristics could be accomplished by the introduction of flexible mountings at the bearing pedestal. This was achieved using helical springs mounted in parallel with two high-precision linear ball-bearings (Fig. 6.3).

Non-contact eddy-current displacement probes were employed to measure the shaft response at various locations as specified in Chapter 7.

The test-shaft speed was monitored using a Sodenco magnetic pick-up which produced an output in the form of a series of pulses. The occurrence of each pulse resulted from the passing of a shaft protrusion. This signal was relayed to a Racal universal counter timer which provided a digital display of rotational frequency within the range 0 - 1.2 Mc/s. The shaft speed signal was simultaneously stored on an FM recorder.

During all rotating-shaft tests the shaft orbit, at appropriate locations, was displayed on a dual-beam monitor by suitably combining the displacement signals in the shaft horizontal and vertical planes. The orbit data could be stored on a digital oscilloscope and passed to a suitable x-y plotter to provide 'hard-copy' information.

As in other tests, the measured response data was initially stored on magnetic tape using a 7-channel FM recorder. The recorder incorporated low-frequency filters

which could be employed to remove any DC bias present in the response signals.

6.3.1 Component Calibrations

A series of calibration tests was performed to allow determination of the dynamic characteristics of a number of test rig components. This was thought necessary to ensure accurate system modelling.

The stiffness characteristics of the bearing rings (20 mm OD, 0.5 mm thick) and bearing pedestal springs were determined from static deflection measurements using linear regression analysis. Representative results are presented in Fig. 6.5. Some variation in the stiffness of similar components is observed. When mounted on the test-rig these spring elements were arranged so as to minimise the difference in flexibility characteristics of the two bearing-support structures. The measured ring and spring mean stiffness values were 140 N/mm and 143 N/mm respectively. The resulting effective support stiffnesses, for each test configuration, are specified in Chapter 7. One bearing ring in each plane, at each support, was fitted with strain-gauges (Appendix C) and calibrated in a similar manner. The strain-gauge signals were augmented using a high-quality DC amplifier, thus ensuring a large signal to noise ratio. With bridge input volts set at 2.25 V and amplifier gain of 2 V/mV, the resulting overall calibration factor was approximately 1 volt/Newton.

In order to assess the level of damping present and

to determine the natural frequencies, the bearing housing and bearing pedestal assemblies were each, in turn, tested dynamically. This entailed the employment of an electromagnetic vibrator (described in the next section) which was used to excite the above systems sinusoidally over a large frequency range. To ensure repeatability, in both calibrations and test situations, the pedestal springs and bearing rings were pre-loaded before each test, to appropriate pre-defined levels. The bearing-pedestal (Fig. 6.3) measured natural frequency was found to be approximately 2½% lower than the calculated value of 5660 cyc/min. The inherent damping was found to be extremely small as observed from the transient reponse shown in Fig. 6.6. Dynamic testing of the bearing-ring assembly produced some unexpected results. Figure 6.7 represents a system receptance plot and indicates the presence of a number of closely-grouped resonances, the major one occurring around 123 Hz.

Analysis and presentation of the test data in receptance form enables accurate determination of natural frequencies and damping levels for vibration modes which may be closely spaced [112], an advantage not realised when using some other methods [112]. Kennedy and Pancu [113] showed how for a single-degree-of-freedom system with hysteretic damping, the receptance versus frequency plot on an Argand diagram is a circle. Structural or material damping can be represented mathematically in a variety of forms [114], most common of which is the assumption of a restoring force 180^{o} out of phase with the

velocity and with magnitude proportional to the system stiffness. Thus, for a single-degree-of-freedom system the combined stiffness-damping force is defined as a complex stiffness $\bar{K} = K(1 + ig)$. The term g is a proportionality constant dependent upon the specific material properties. Based on this approach for a single-degree-of-freedom, the receptance $\bar{\alpha}$ can be expressed as:

$$\bar{\alpha} = \mu e^{i\Phi}$$

where

$$\mu = \frac{1}{K\sqrt{[(1 - \beta^2)^2 + g^2]}} \quad ; \quad \beta = \frac{\omega}{\omega_c}$$

and $$\Phi = \tan^{-1}[-g/(1 - \beta^2)]$$

At the natural frequency, $\omega = \omega_c$ and $\beta = 1$, so that

$$\mu = 1/Kg$$

Thus, measurement of the relevant receptance circle diameter [112] will provide details of the system structural damping. Material damping is normally very small and the assumption of viscous damping under such circumstances leads to an almost circular receptance plot. The equivalent (frequency dependent) viscous damping coefficient is given by $C = Kg/\omega$. From the plot shown in Fig. 6.7 g is estimated as 0.0076 and the equivalent viscous damping rate at the natural frequency is calculated as 3.4 Ns/m. These figures indicate the low level of structural damping available.

The emergence of numerous resonance peaks is thought to be mainly due to the inability of the shaker arrangement to excite only the housing translational mode

of vibration. The calculated system natural frequency of 110.7 Hz is substantially lower than the measured predominant value since for estimation purposes, only the rings in the direct line of motion of the housing were considered. As a result, for modelling purposes, an effective bearing-ring stiffness of 350 N/mm was computed from the measured frequency. A typical response plot resulting from a transient test on an individual bearing-ring is presented in Fig. 6.8 where again the lack of internal damping is self-evident.

The above test results clearly show the bearing-support structural damping to be extremely small so that for modelling purposes these elements could be safely considered as pure springs.

The eddy-current proximity probes were calibrated on a sample section of the test shaft. The gap versus output voltage data was recorded using a Vernier/clock gauge arrangement and digital voltmeter. Four of the eight probes were calibrated and a nominal sensitivity of 266 mV/THOU obtained (Fig. 6.9). The probes had a linear range of 1.5 mm (0.060 ins) and linearity of $\pm$ 1% over the frequency range 0 - 20 kHz.

6.4 Vibrator Arrangement

Throughout the experimental work, a number of shaker-tests were performed on a variety of rig components. Figure 6.10 shows a schematic diagram of the equipment, including instrumentation, used for such tests.

The force was produced by a Goodman's electromagnetic

vibrator. A sinusoidal signal of variable frequency supplied by a function generator was augmented, using a power amplifier, before being fed to the electromagnetic shaker.

System response was measured, in general, using non-contact displacement probes.

The force, where possible, was measured using a Piezo-electric force transducer with overall nominal sensitivity of 10 mV/N. A charge amplifier, transforming transducer electrostatic charges into proportional output voltages, was required for use with the Piezo-electric transducer. However, during the early stages of the work, this type of device was not available and it was necessary to construct an axial force transducer. The conflicting requirements of high-rigidity and high sensitivity led to the employment of semi-conductor strain gauges having a gauge factor of approximately 140. Such components are fairly sensitive to temperature effects. However, this influence was minimised by proper utilisation of a four-arm Wheatstone bridge arrangement (Appendix C, Section C.1.2). Signal (low-frequency) drift was eliminated by introducing a high-pass filter with lower cut-off frequency of approximately 5 Hz.

A DC strain gauge amplifier was employed to boost the force signal. Calibration of the constructed transducer was effected by physically connecting, in series, a Piezo-electric transducer, introducing an axial dynamic force and measuring the transfer function: strain gauge transducer output voltage/Piezo-electric transducer output voltage, using a real-time frequency analyser. Knowing

accurately the calibration factor for the Piezo-electric device enabled that for the new transducer to be determined (Fig. 6.11). Repeatability checks at normal ambient air temperatures ($20^{o} \pm 10^{o}C$) confirmed the transducer's relative insensitivity to temperature effects within this temperature range. Connection of the strain gauges in a specific manner (Appendix C) ensured the elimination of the influence of bending moments resulting from inevitable small misalignments, an advantage not available when using a Piezo-electric type transducer. With an amplifier gain setting of 2.28 V/mV and bridge input-volts set at 2.25 V, the nominal overall calibration factor was measured as 51 mV/Newton.

Throughout the tests a digital oscilloscope was used to observe the system response and input force signals to ensure the elimination of any unexpected peculiarities.

All relevant signals were recorded on a 7-channel FM tape recorder for later analysis on a digital computer.

6.5 Mechanical Dampers

A number of commercially available 'Kinetrol' rotary vane-type, viscous dashpots were employed to enable the introduction of external radial damping at various shaft locations.

Initially, adjustable PTFE pads were utilised to provide the necessary low-friction contact between the damper arms and shaft as suggested by other workers [91]. However, severe problems, including excessive pad wear and the emergence of large vibration components having

frequencies corresponding to integer multiples of shaft running speed, resulted in the use of a modified damper arrangement.

Fig. 6.12 shows the re-designed set-up where a shaft-mounted, self-aligning ball-bearing is located within a nylon housing which is free to slide, in one direction only, within the damper-arm assembly. With this arrangement, shaft external frictional forces were minimised and the need for decoupling of the control damping in the two planes could be practically achieved.

The modified damper assembly performed very well as long as certain setting-up procedures were adhered to (Section 7.5.2).

An attempt to introduce damping to the rotor, in an angular fashion, using the configuration shown in Fig. 6.13, was largely unsuccessful for much the same reasons as for the original radial damper design. After a number of attempts to overcome the problems, it was decided that mechanical application of angular damping to the test-rotor posed so many problems that extensive rig alterations would be necessary if this approach were to be followed through. Since a large portion of experimental work would be concerned with the performance of a contactless angular electromagnetic controller, mechanical angular damping was considered no further.

6.5.1 Damper Calibrations

The radial mechanical dampers were calibrated 'in-situ', i.e. mounted on the test-shaft, by exciting the

shaft using an electromagnetic shaker arrangement as described in Section 6.4 and by measuring the resulting system response at a number of locations. By determining the undamped/damped test rotor characteristics, the device's dynamic parameters could be estimated.

The calibration procedure adopted was based on the utilisation of system dynamic influence coefficients and is described in Appendix D.

Many unexpected problems were experienced during the calibrations. For instance, in an effort to reproduce test conditions, the dampers were set-up as described in Section 7.5.2. However, this resulted in the (necessary) presence of a small clearance in the damper slider mechanism leading to some deterioration of the harmonic response waveform. This was overcome, to some extent, by locking the damper slider arrangement. The results, although probably not wholly representative of a rotating shaft situation, were at least repeatable (for a fixed input force level) and the waveform distortion had been eliminated. The damper was found to be capable of exerting a greater influence on the system response using the latter approach, as would be expected.

Further investigations were performed to assess the linearity of the Kinetrol dampers. Fig. 6.14 shows the measured system receptances for three levels of input force, with the damping rate set at maximum. The extent of the non-linearity is indicated by the degree of disparity of the response plots. It is clear that the choice of force level will have a marked effect on the

calibration results. Consequently, in an effort to obtain more meaningful data in all subsequent damper calibration tests, the force level was chosen so as to provide a system response of the same order as that measured during the rotating shaft tests.

During calibrations the damper arm length was set at 110 mm, this corresponding to the setting used throughout the rotational tests.

The measured damping rates (Fig. 6.15) are shown to reduce drastically with increasing frequency, thus rendering the dampers ineffective at the higher shaft speeds.

6.6 Electromagnetic Actuator

6.6.1 Design and Construction

The size of the magnets employed was determined mainly by test-rig access limitations and the availability of suitable laminations. The angular controller consisted of a set of four small, 'u-shaped', silicon-steel, laminated electromagnets rigidly mounted on a high-reluctance Tufnol support stand (Fig. 6.16) to minimise flux leakage effects.

The laminations used for the magnet cores were obtained by modifying commercially available 'E-type' laminations. With the lamination size fixed (Fig. 6.18), the magnet coil, mounted on one limb, was designed to allow for maximisation of the number of turns. Effective utilisation of the available space resulted in a compromise between the number of coil turns and coil size

(current-rating). The final coil design was based on 200 turns of 22 SWG enamelled copper wire giving a total resistance of approximately 0.9Ω.

A number of parameters need to be considered in the design of electromagents viz; force requirements, flux density limitations and heat dissipation rate. All of these variables are of course greatly affected by the choice of air-gap.

Based on a maximum coil-current of 2 amps, the magnets were designed to produce corresponding electromagnetic forces in the range 7.5 - 93 Newtons for gap and flux density ranges of 0.035 - 0.010 ins (0.89 - 0.25 mm) and 0.28 - 0.98 TESLA respectively. This design resulted in the attainment of reasonable magnet force levels, whilst ensuring minimisation of magnetic saturation (for silicon steels $B_{SAT} \approx 1.0 - 1.2$ TESLA). For the above conditions, the computed coil maximum heat dissipation rating is approximately 0.2 W/cm^2, which is half the recommended maximum allowable value [106] for intermittent but frequent use. The magnet cores were placed equi-distant from the shaft centre-line and mounted at 90 degrees to each other with their pole-faces extended in a direction parallel to the shaft axis (Figs. 6.1b and 6.17). The magnetic circuit is completed when the flux is linked axially from both limbs of each magnet to a shaft-mounted disc. Thus, the introduction of an axial magnetic force offset from the shaft axis produces a control moment at the disc.

When an alternating magnetic flux field is set-up in

an electrical conductor, eddy-currents are created resulting in energy loss in the form of heat. The power dissipated due to such losses is proportional to the square of the frequency of the alternating field and thus can be significant at high frequencies. The introduction of laminated cores helps to minimise this effect. In the conventional arrangement [87] where the magnetic flux follows a radial path, the rotor component of the magnetic actuator may be constructed in a laminated form without much trouble. However, when the flux path is orientated as in this case, lamination of the magnet rotor component is much more difficult. To overcome this problem, it was decided that a solid disc having special magnetic properties, would be utilised for transmission of the magnetic forces from the magnets to the shaft. A high-resistivity, silicon steel, shaft mounted disc was thus employed to minimise eddy-current and hysteresis effects. This arrangement eliminated the need for costly and time-consuming manufacturing processes and in fact, was later found to function extremely well even at fairly high frequencies (100 Hz).

Because electromagnets can pull but not push, the magnets were controlled in diametrally-opposing pairs. Each magnet-pair is controlled individually according to the measured shaft-slope signal in that plane. Arrangement of the control actuator in the form of two sub-systems, one in each orthogonal plane, is in line with the princples of decentralised control as described by Schweitzer [89]. Such an approach simplified the control

strategy considerably. The control forces in the shaft horizontal and vertical planes are practically uncoupled and at any instant in time a maximum of one electromagnet per plane is operational. In addition to the above, the introduction of such a magnet configuration eliminates the need for extra measures which would be required to remove the inherent flux-leakage/linkage problems [87].

Levelling of the magnet pole-faces, a factor critical to the operation of the actuator, was achieved through the use of a surface-grinder. The magnets were rigidly fixed to the support stand and then all machined to the same height.

6.6.2 Control Hardware

In formulating a suitable control procedure to allow investigation of the influence of angular control, great emphasis was placed on simplicity.

In this early stage of development of the angular electromagnetic controller, no hardware linearisation techniques were employed. The effectiveness of a pre-magnetising current as a control-current linearising tool has been described elsewhere [84]. However, using this approach, a static instability will be introduced (Section 6.6.3) unless counter measures are taken. Additionally, the force producing capacity of the electromagnet may be reduced significantly due to the current-sharing of the windings, thus confirming the desirability of some other means of current linearisation.

The electromagnetic force is also a non-linear

function of the air-gap which alters according to the specific system response.

In radial systems this variation in gap may be significant and may necessitate the introduction of some counter-measures [87]. When employing an angular controller, however, the location of the device may be chosen (see Section 6.6.4.1) so that during normal shaft running the air-gap is sensibly constant.

Shaft-slope is sensed in each plane by suitably summing two shaft displacement signals, obtained using non-contact eddy-current type probes (Fig. 6.19a).

Each resulting slope signal was introduced to an analogue circuit designed to create a signal phase lag in the range 90^{o} - 180^{o}, thus providing as output, a combined proportional-derivative feedback signal. The magnitude of the feedback signals could be altered by varying the gains of the operational amplifiers. These gains were controllable through utilisation of an outer digital control loop employing a micro-computer (Fig. 6.19a). Controller damping and stiffness could thus be adjusted manually by keyboard input or automatically through software control. The hardware employed is illustrated in Fig. 6.19b.

Each magnet-coil was served by a 30 Watt DC power amplifier, necessary for boosting the control current to an acceptable level.

Considering any two electromagnets in the same plane (Figs. 6.17 and 6.19a) by appropriate signal rectification, the positive part of the feedback signal

may be used for one and the negative part for the other magnet, this ensures that only one magnet per plane is operational at any one time.

Current feedback was employed to minimise the effect of variation of electromagnet impedance with frequency, thus effectively ensuring a fixed coil-current for a given shaft displacement amplitude irrespective of signal frequency.

6.6.3 System Control

For simplicity, consider the application of the above angular control system to the single-degree-of-freedom system represented in Fig. 6.20. 0 is the centre of rotation of the system. The system may be represented, in general, by the following differential equation:

$$I_s\ddot{\theta} + C_s\dot{\theta} + K_s\theta = Me - Mf \qquad (6.1)$$

where I_s, C_s and K_s are the system inertial, damping and stiffness properties

Me is an external excitation moment

Mf is the resultant feedback control moment

and $$Mf = C_F\dot{\theta} + (K_F - K_P)\,\theta$$

K_P is the magnet 'negative-stiffness' due to the presence of a DC pre-magnetising current

C_F and K_F are the effective feedback damping and stiffness coefficients and for the sake of this analysis are assumed constant.

Let: $$C_F = C_N \pm C_L$$

and $$K_F = K_N \pm K_L$$

where C_N and K_N are the nominal damping and stiffness feedback coefficients to be selected by appropriate choice

of op-amp gains (Section 6.6.2). These would represent the resultant system damping and stiffness coefficients if the control circuit components did not introduce undesirable phase lags to the feedback response.

In real systems this is not possible and response lags occur. The coefficients C_L and K_L represent this effect, their signs being determined by the degree of lag present. The phase lag $\Phi_L = \text{ARCTAN}\left[\frac{C_L}{K_L}\right]$.

Substituting the above in equation (6.1) and considering the system to vibrate freely, Me = 0 and

$$I_S\ddot{\theta} + (C_S + C_N \pm C_L)\dot{\theta} + (K_S + K_N \pm K_L - K_P)\theta = 0$$

or $$I_S\ddot{\theta} + C\dot{\theta} + K\theta = 0$$

where $$C = C_S + C_N \pm C_L$$

and $$K = K_S + K_N \pm K_L - K_P \qquad (6.2)$$

The signs and relative magnitudes of the coefficients C and K in equation (6.2) will clearly determine the system stability state.

A number of interesting cases can be considered.

In the calibrations which follow (Section 6.6.63), in all cases $0 < |\Phi_L| < 90^\circ$ and thus in the following cases, where applicable, the signs of C_L and K_L will be set accordingly.

1. Shaft with no internal damping ($C_S = 0$) subjected to magnetic damping control ($C_N \neq 0$)

Consider the magnet without pre-magnetisation:

($K_P = 0$)

$K_N = 0$ and C_L is -VE ; K_L is +VE

Therefore from equation (6.2):

$C = C_N - C_L$ and $K = K_S + K_L$

Thus no system instability will occur provided

$C_N > C_L$.

In addition, the introduction of magnetic damping is seen to increase the system effective stiffness.

2. Shaft with no internal damping ($C_S = 0$) subjected to magnetic stiffness control ($K_N \neq 0$)

Consider the magnet without pre-magnetisation:

($K_P = 0$)

$C_N = 0$ and again C_L is -VE ; K_L is +VE

From equation (6.2):

$C = -C_L$; $K = K_S + K_N + K_L$

This time a dynamic instability is introduced due to the negative damping term. Again the system stiffness is increased. For such a system if C_L is small, then the introduction of a small amount of magnetic damping would remove the above problem.

It is obvious that the effect of the component phase lag Φ_L could be counteracted using some form of lead compensation. In addition, it is clear that the use of a pre-magnetising current, although useful in linearising the force-current relationship, will always have a destabilising influence and thus some of the proportional feedback may have to be utilised just to eliminate this effect.

The above two cases were considered because of their relevance to the experimental work described in Chapter 7.

The special case of magnetic levitation may be considered by setting $C_S = K_S = 0$ and considering lead

compensation to be present, $C_L = K_L = 0$.

Therefore from equation (6.2):

$$C = C_N \quad \text{and} \quad K = K_N - K_P$$

Thus, if $K_N < K_P$ the system is statically unstable - a well known fact.

Although the above analysis is presented for a simple single-degree-of-freedom system, the conclusions reached are also applicable in principle to multi-degree-of-freedom systems.

6.6.4 Electromagnet Theory

Consider the flux field between an active electromanget and the shaft disc with the disc in its mean position (Fig. 6.21). Ignoring flux fringing and leakage, the flux path would be as shown.

For a magnetic circuit, the line integral of the magnetic field strength H taken around any complete line is equal to the current enclosed [107], thus:

$$\int Hdl = \Sigma I = N.i. \qquad (6.3)$$

where N is the number of coil turns and i is the coil current.

Since the relative permeability, μ_r, of the magnet lamination material is much greater than the permeability of free space, μ_o, it is safe to assume that the magnetic-circuit reluctance can be approximated as that of the air-gap.

The electromagnetic attraction force F may be determined by considering a small change in the air-gap, G and equating the work done in displacing the magnet to the

change in air-gap magnetic energy [84].

Following this approach it can be shown that:

$$F = \frac{\mu_o A N^2 i^2}{8 G^2} \qquad (6.4)$$

where A is the magnet pole face area. For the magnet design employed here:

$$N = 200$$

$$A = 2 \times 8 \times 16 \times 10^{-6} \ m^2$$

so that $$F = 1.609 \ (i/G)^2 \qquad (6.5)$$

with the gap G in millimetres and current i in amps.

6.6.4.1 Electromagnets in Angular Form

Because of the inherently simple physical arrangement of the electromagnets in the case of angular control, the possibility exists for simple adjustment of the air-gap to improve, for instance, performance inadequacies created at the design stage. In addition, the magnet air-gap could, conceivably, be introduced as an additional variable within an adaptive control strategy. Such a procedure could not easily be employed for a radial controller due to the intrinsic geometrical limitations. Further, when applying radial control to a flexible shaft system, the trend has been to locate the device at a point on the shaft span where a large uncontrolled response (i.e. an anti-node) exists. This highlights an additional advantage when using angular control. To illustrate the point, consider again the Jeffcott-rotor considered in Chapter 5 (Fig. 5.1). Consider the electromagnet air-gap G, to be selected proportional (proportionality constant - d) to the uncontrolled response q_u at that location.

This seems reasonable since some clearance must be allowed to exist in the event of controller failure.

Then $G = d.q_u$.

Referring to equation (6.4) the magnetic force F may be estimated from:

$$F = k.(i/G)^2 = \frac{k}{d^2} \cdot \frac{(i)^2}{(q_u)^2}$$

where k is a constant dependent mainly on the magnet geometry.

With the subscripts r and a referring to radial control at the shaft centre and angular control at a support respectively, then the ratio of force production capacities for the controllers would be:

$$\frac{F_a}{F_r} = \frac{(q_{ur})^2}{(q_{ua})^2} \cdot \frac{(i_a)^2}{(i_r)^2}$$

and for a shaft central unbalance, $\frac{(q_u r)^2}{(q_u a)^2} = 123.5.$

Thus, $$\frac{F_a}{F_r} = 123.5 \times \frac{(i_a)^2}{(i_r)^2}$$

Therefore, even though the system demands greater control force levels from the angular device it is evident that with equal control currents, in theory, greater forces may be obtained from this controller because of the smaller gap. However, an increased magnet core area would be required to cope with the greater flux and thus a better alternative would be to employ a larger gap with a subsequent benefit in linearisation of the device.

Alternatively, a smaller current may be applied with a consequent reduction in control power consumption.

6.6.5 Controller Modelling and Calculation of the Effective Linear Electromagnetic Coefficients

Due to the nature of the techniques employed for simulation of test rotor performance (Chapter 4) a linear model of the electromagnetic controller is required.

Since the magnet pairs in orthogonal planes are controlled individually according to their respective slope feedback signals, a maximum of four control coefficients are considered to be present at any instant in time. The possibility of coupling between orthogonal planes is minimised as a result of the size and location of the individual magnets. When the dynamic axial displacement of the shaft-mounted silicon-steel disc is very small in comparison to the air-gap (Chapter 7) the assumption of constant gap is a reasonable one so that any coupling effect should be negligible. If the control current i is a linear function of the shaft-slope feedback signals Φ and θ then the control moments M_y and M_z are, in general:

$$M_y = K_\Phi \ (\Phi)^2 + C_\Phi \ (\dot{\Phi})^2$$

and

$$M_z = K_\theta \ (\theta)^2 + C_\theta \ (\dot{\theta})^2$$

The linearised damping and stiffness coefficients C_L and K_L may be obtained by equating the terms:

$\int M_y \cdot \dot{\Phi} dt$ ($\int M_z \cdot \dot{\theta} dt$) and $\int M_y \Phi$ ($\int M_z \cdot \theta dt$)

respectively, for the linear and non-linear cases.

i.e. $[\int M_y \cdot \dot{\Phi} dt]_{linear} = [\int M_y \cdot \dot{\Phi} dt]_{non\text{-}linear}$ to obtain

$C_{L\Phi}$ and

$[\int M_y \cdot \Phi dt]_{linear} = [\int M_y \cdot \Phi dt]_{non\text{-}linear}$ to obtain $K_{L\Phi}$ and similarly for $C_{L\theta}$ and $K_{L\theta}$.

In the following analysis, only the plane containing slope Φ is considered since the results may be applied directly to the other plane.

If the integral terms are considered as positive quantities, then the following convention may be used.

Let $\Phi = \hat{\Phi} \sin(\omega t + P)$.

Therefore: $\dot{\Phi} = \omega\hat{\Phi} \cos(\omega t + P) = \hat{\dot{\Phi}} \cos(\omega t + P)$

The phase angle P may be expressed as:

$$P = P_C + P_L \qquad (6.6)$$

where P_C represents the phase angle of the control moment relative to the shaft negative slope velocity signal $(-\dot{\Phi})$ and is selected according to the type of control employed, i.e. stiffness ($P_C = 90^o$) or damping ($P_C = 0$). The phase angle P_L represents the undesirable phase-lag component of the magnet and control-circuit transfer function and is measured experimentally using the calibration rig described in Section 6.6.6.1.

The control moment M_y is assumed to be of the following form:

for $\frac{-\pi}{2} < \omega t < \frac{\pi}{2}$; $M_y = M \cos^2 \omega t$

and for $\frac{\pi}{2} < \omega t < \frac{3\pi}{2}$; $M_y = -M \cos^2 \omega t$

When damping control is utilised, $M = C_{NL\Phi} \cdot \hat{\dot{\Phi}}^2$.

Whilst for stiffness control, $M = K_{NL\Phi} \cdot \hat{\Phi}^2$.

If the control hardware introduces negligible unwanted time delay ($P_L \approx 0$), then:

for damping control

$$\int M_y \cdot \Phi dt = 0 \qquad (\text{i.e. } K_{L\Phi} = 0)$$

and for stiffness control (6.7)

$$\int M_y \cdot \dot{\Phi} dt = 0 \qquad (\text{i.e. } C_{L\Phi} = 0)$$

In general,

$$\int_0^{2\pi} M_y \cdot \dot{\Phi} dt = \frac{1}{\omega} \int_{\frac{-\pi}{2}}^{\frac{\pi}{2}} M \cos^2 \omega t \cdot \hat{\dot{\Phi}} \cos(\omega t + p)\, d\omega t - \frac{1}{\omega} \int_{\frac{\pi}{2}}^{\frac{3\pi}{2}} M \cos^2 \omega t \cdot \hat{\dot{\Phi}} \cos(\omega t + p)\, d\omega t \tag{6.8}$$

and

$$\int_0^{2\pi} M_y \cdot \Phi dt = \frac{1}{\omega} \int_{\frac{-\pi}{2}}^{\frac{\pi}{2}} M \cos^2 \omega t \cdot \hat{\Phi} \sin(\omega t + p)\, d\omega t - \frac{1}{\omega} \int_{\frac{\pi}{2}}^{\frac{3\pi}{2}} M \cos^2 \omega t \cdot \hat{\Phi} \sin(\omega t + p)\, d\omega t \tag{6.9}$$

Upon integration, the above equations yield the following:

$$\int_0^{2\pi} M_y \cdot \dot{\Phi} dt = \frac{8}{3} \frac{M\hat{\dot{\Phi}}}{\omega} \cos p \tag{6.10}$$

and

$$\int_0^{2\pi} M_y \cdot \Phi dt = \frac{8}{3} \frac{M\hat{\Phi}}{\omega} \sin p \tag{6.11}$$

respectively.

Now, considering an equivalent linear system and employing damping and stiffness control respectively.

Then:

$$\int_0^{2\pi} M_y \cdot \dot{\Phi} dt = \frac{C_{L\Phi}}{\omega} \int_0^{2\pi} \hat{\dot{\Phi}}^2 \cos^2 \omega t \cdot d\omega t = \frac{\pi \hat{\dot{\Phi}}^2}{\omega} C_{L\Phi} \tag{6.12}$$

and

$$\int_0^{2\pi} M_y \cdot \Phi dt = \frac{K_{L\Phi}}{\omega} \int_0^{2\pi} \hat{\Phi}^2 \sin^2 \omega t \cdot d\omega t = \frac{\pi \hat{\Phi}^2}{\omega} K_{L\Phi} \quad (6.13)$$

Now equating (6.10) to (6.12) and (6.11) to (6.13) gives:

$$C_{L\Phi} = \frac{8}{3\pi} \frac{M}{\hat{\Phi}\omega} \cos p \quad (6.14)$$

and

$$K_{L\Phi} = \frac{8}{3\pi} \frac{M}{\hat{\Phi}} \sin p \quad (6.15)$$

Thus the effective linearised stiffness and damping coefficients, K_L and C_L, to be used in the simulations may be determined by utilising the magnet calibration data and the experimentally measured shaft-slope response (Φ and θ) at the controller, at each shaft speed.

6.6.6 Electromagnetic Controller Calibration

6.6.6.1 Calibration Rig

A specially designed and constructed calibration rig was employed (Fig. 6.22) to obtain the dynamic characteristics of the electromagnetic actuator. The rig enabled the measurement of electromagnetic bending moment by utilising semi-conductor strain-gauges in a 'four-arm' bridge arrangement (Appendix C, Section C.1.3). An output voltage proportional to bending moment was obtained. The transducer was calibrated using the same techniques as those discussed in Section 6.4, where calibration of the axial force transducer is described. Fig. 6.23 shows the frequency response of the device. With the strain gauge amplifier gain set at 5 V/mV (bridge input volts = 3 V), the overall transducer-amp sensitivity was 7.24 V/Nm in the range of 10 - 40 Hz (magnet radius = 44.5 mm). The transducer sensitivity is seen to increase

substantially above 40 Hz due to a system resonance around 167 Hz. This effect was taken into account in subsequent magnet calibrations.

6.6.6.2 Calibration Procedure

Throughout the electromagnet calibrations the following parameters were varied in turn to allow investigation of their influence on the controller performance.

1. Control feedback gain and control type (i.e. damping and/or stiffness).
2. Magnet air-gap.
3. Control signal frequency.
4. Amplitude of simulated shaft-slope signal.

The calibrations entailed the use of a function generator to provide a sinusoidal voltage (V) at input to the control circuitry. This was used to simulate the shaft-slope feedback signal. During each test the air-gap was held constant. Measurement of the magnet control current was made possible by monitoring the voltage drop across a small (0.1Ω) resistance placed in series with the coil.

A number of tests, covering the frequency range 0 to 100 Hz, were performed. Throughout these tests three signals were recorded:

a) Electromagnet control moment.
b) Magnet control current (i(t)).
c) Simulated shaft-slope volts (V(t)) (input to control circuits).

This data was recorded on magnetic tape and later

processed on digital computer providing signal amplitude and phase information for subsequent estimation of the electromagnetic damping and stiffness parameters.

The input voltage V(t) is related to the simulated shaft-slope $\Phi(t)$ through the relationship:

$$V(t) = k \cdot \Phi(t) \qquad (6.16)$$

where k is the effective gain of the shaft displacement transducer arrangement, relating shaft-slope at the controller to voltage input to the control circuitry and was found to be a real constant over the test frequency range (0 to 100 Hz). Using equation (6.16) $\Phi(t)$ could be calculated from the measured V(t) values.

The electromagnet/control-circuit was considered as a 'black-box' and for pre-determined operational amplifier gain and control-type (stiffness or damping) settings, its characteristics were determined by measuring the overall system transfer function. Having obtained the moment amplitude M, phase p_m (relative to input volts V(t)) and the slope signal V(t), application of equations (6.6), (6.14), (6.15), (6.16) and (6.17) enabled computation of the magnetic stiffness and damping coefficients.

During the calibrations, it was observed particularly at the higher frequencies, that unwanted time delays were introduced (Section 6.6.6.3) to the control moment signal as a result of control-circuit/magnet component phase-lags ($p_L \neq 0$). This had the effect of creating an additional stiffening moment when damping control was employed and vice-versa.

The phase angle p_L was calculated from the measured

phase p_m as follows:

$$\begin{aligned} &\text{for damping control} \quad p_L = |p_m| - 90 \\ &\text{for stiffness control} \quad p_L = |p_m| - 180 \end{aligned} \tag{6.17}$$

Throughout the tests p_L, although fairly small, was found to be in the first quadrant (Section 6.6.6.3) i.e. $0 \rightarrow 90^o$.

Considering this effect in equations (6.14) and (6.15) for damping and stiffness control in turn, we obtain:

For damping control ($p_c = 0^o$)

$$0 < C_{L\Phi} < \frac{8}{3\pi}\frac{M}{\hat{\Phi}}$$

$$0 < K_{L\Phi} < \frac{8}{3\pi}\frac{M}{\hat{\Phi}}$$

For stiffness control ($p_c = 90^o$)

$$\frac{-8}{3\pi}\frac{M}{\hat{\Phi}} < C_{L\Phi} < 0$$

$$0 < K_{L\Phi} < \frac{8}{3\pi}\frac{M}{\hat{\Phi}}$$

Thus, positive control stiffness is always maintained but negative damping may occur (Section 6.6.6.3).

Because of the nature of the procedures employed during rotating shaft tests (Chapter 7), the linearised control coefficients estimated using the methods described here required further modification in accordance with the techniques described in Appendix E.

6.6.6.3 Magnet/Control-Circuit Calibration Results

At various stages during the calibrations, a number of the signals recorded were monitored using a real-time frequency analyser. The signals were observed to be

practically harmonic, as expected, except for the electromagnet bending moment signal which although periodic, displayed a number of harmonics illustrating the non-linearity of the devices.

Following the procedures described in Sections 6.6.5 and 6.6.6.2, the linearised electromagnetic damping and stiffness coefficients were determined for a range of control signal amplitudes and frequencies. Some typical results obtained from the calibration are presented in Fig. 6.24. The graphs show the magnetic damping coefficients to be a linear function of control signal frequency and amplitude, whilst the stiffness coefficients are dependent only on the latter parameter. The characteristics validate the magnet force-current square-law relationship (equations (6.14) and (6.15)). Thus for damping and stiffness control respectively, the coefficients are expected to be of the form:

$$C_{L\Phi} = b_C \, \omega \hat{V}$$

$$K_{L\Phi} = b_K \, \hat{V}$$

where $\hat{V}$ is the shaft slope control signal amplitude and b_C, b_K are constants dependent upon the circuit gain settings.

To aid in computation of the coefficients, for use in later system simulation, linear regression analysis was performed through utilisation of the least-squares method. Examination of the calibration data presented in Fig. 6.14 shows that in general the straight-lines fitted to the data, if projected, do not pass through the graph origin. Thus, the magnet coefficients may be more accurately

predicted using the following relationships:

$$C_{L\Phi} = a_c + b_c \, \omega \hat{V} \quad \text{Nms/rad}$$
$$K_{L\Phi} = a_K + b_K \, \hat{V} \quad \text{Nms/rad} \qquad (6.18)$$

where ω is the signal frequency (Hz).

The coefficients a and b in equations (6.18) were computed using a least-squares approach and are shown in Table 6.1 for a range of calibration settings. The corresponding correlation coefficient R is also presented. This parameter gives an indication of the reliability of the above relationships in their representation of the control hardware characteristics. A value of R in the range 0.8 to 1.0 would provide confirmation of the validity of these expressions [116]. Analysis of the calibration results showed that the data could be best represented by considering two separate frequency ranges as shown.

The angular damping and stiffness coefficients which may be predicted using equations (6.18) and the information supplied in Table 6.1, are based on a mean electromagnet radius of 44.5 mm. This was also the radius setting employed in the rotating/vibrating shaft tests described later.

Table 6.1

Control Type	Micro-Computer Digital Gain Setting	Magnet Air-Gap mm (THOU)	Freq Range (Hz)	Coeff a	Coeff b	R
Damping	70	0.9 (35)	$0<\omega<40$	0.3912	0.0415	0.986
"	"	"	$40<\omega<80$	0.2623	0.0387	0.884
"	90	"	$0<\omega<40$	0.8784	0.1067	0.987
"	"	"	$40<\omega<80$	0.5937	0.1015	0.921
"	110	"	$0<\omega<40$	1.0378	0.1739	0.99
"	"	"	$40<\omega<80$	0.8186	0.1582	0.95
Stiffness	100	"	$0<\omega<40$	66.95	145.13	0.996
"	"	"	$40<\omega<80$	37.68	166.93	0.874
"	110	"	$0<\omega<40$	71.3	159.0	0.995
"	"	"	$40<\omega<80$	21.2	211.0	0.876
Damping	70	1.1 (43)	$0<\omega<30$	0.2938	0.0285	0.986
"	"	"	$30<\omega<50$	0.2213	0.0281	0.998
"	90	"	$0<\omega<30$	0.5669	0.0777	0.997
"	"	"	$30<\omega<50$	0.4822	0.076	0.982
"	110	"	$0<\omega<30$	0.7519	0.1245	0.997
"	"	"	$30<\omega<50$	0.5613	0.1239	0.981

The above information was stored on computer and used in conjunction with data obtained from shaft controlled response measurements to enable computer simulation of the test conditions (Chapter 7).

As far as is known, the principle of angular control has never been considered elsewhere. As a result, researchers will have little 'feel' for the units of angular damping and stiffness. Expression of the angular coefficients in a more conventional form is therefore desirable. In the test and calibration environments, bending moments are imposed upon the system by introducing

forces parallel with, but offset from, the principle bending axes of a shaft-mounted disc. Thus, the angular coefficients $C_{L\Phi}$ and $K_{L\Phi}$ may be replaced by axial coefficients C_{LA} and K_{LA} acting at a mean radius r. If the shaft motion is small, then the axial and angular coefficients are related as follows:

$$C_{LA} = C_{L\Phi}/r^2$$
$$K_{LA} = K_{L\Phi}/r^2$$

and in particular substituting the value of r used in these investigations (r = 0.0445 m) we obtain:

$$C_{LA} = 505\ C_{L\Phi}\ \text{Ns/m}$$
$$K_{LA} = 505\ K_{L\Phi}\ \text{N/m}$$

The maximum attainable electromagnetic stiffness and damping coefficient values were determined by power amplifier DC supply current limitations. The current limit was set slightly above 2 amps. Under these circumstances and for the cases considered, the maximum attainable magnet coefficients in the 0 to 100 Hz frequency range were found to be as follows:

$C_{L\Phi}$ (max) $\approx$ 12.6 Nms/rad (C_{LA} (max) $\approx$ 6360 Ns/m) (Fig. 6.24c)

$K_{L\Phi}$ (max) $\approx$ 800 Nm/rad (K_{LA} (max) $\approx 4 \times 10^5$ N/m) (Fig. 6.24e)

It is seen that the electromagnets, though small in overall size, are capable of introducing reasonable magnitudes of control damping and stiffness, even in the presence of a relatively large air-gap.

Typical plots of the control hardware frequency-response are presented in Fig. 6.25. The measured

bending moment phase angle, relative to the shaft-slope signal, is denoted by p_1 whilst that of the magnet current is represented by p_2. Figs. 6.25a and 6.25b illustrate the effect on these phase angles of utilising damping control and stiffness control respectively.

For each control case at low signal frequencies, undesirable component phase-lags are negligible and the bending moment signal is of a pure damping and pure stiffness form respectively. However, as the frequency is increased, such unwanted phenomena are introduced. For example, when damping control is employed, the system phase-shift is approximately 108^{o} and 124^{o} ($p_L = 18^{o}$ and 34^{o}) at 50 Hz and 100 Hz respectively, thus effectively leading to the presence of a stiffness control effect. It is seen that approximately half of the overall unwanted lag, p_L, is due to the main control circuitry and the other half due to the magnet coil arrangement. When stiffness control is introduced, p_L is less than that which results when damping control is employed. This improvement is observed to occur mainly in the analogue control section of the hardware, i.e. phase p_2 has decreased significantly. This indicates the presence of an additional phase component in the circuitry used to perform signal differentiation, i.e. when damping control is utilised.

In the majority of test cases, described in Chapter 7, the operational range of the electromagnetic controller was limited to 0 to 3000 rpm (0 to 50 Hz). In these circumstances, the maximum undesirable control system

phase-shifts, p_L, would be approximately 18^o and 9^o for damping and stiffness control respectively. These values are small but system performance could be improved if necessary by introducing some form of lead compensation.

In Fig. 6.26 the measured and predicted electromagnet bending moments are compared for a range of control currents and three air-gap settings. The theoretical curves were plotted using equation (6.5). Although some discrepancy between theoretical and experimental results is evident, examination of the experimental data confirms the validity of the form of the magnet force-current-gap relationships presented in Section 6.6.4. The maximum bending moment which can be produced without current overloading and with an air-gap setting of 0.9 mm (0.035 ins) is approximately 0.45 Nm. This corresponds to a magnet force of 10.1 Newtons. The electromagnet measured force capability is, surprisingly, greater than that predicted from theory. This may be due, to some extent, to fringing at the magnet pole-faces leading to an increase in the effective pole-face area.

The calibration data obtained in this section is sufficient to enable the creation of a suitable model for the electromagnetic controller for use in later rotor simulations as described in Chapter 7.

6.7 Instrumentation

Because of the wide variety of tests performed throughout the experimental investigation, relevant details of the instrumentation employed are provided in

the appropriate sections throughout this chapter and Chapter 7. In many of the tests conducted, the HP 3582A Spectrum Analyser was found to be extremely useful in providing instant information regarding the signal frequency content.

6.8 Data Analysis Equipment

Analysis of the data stored on tape was performed using an FFT algorithm available on the MINC 23 digital computer. The analogue data was processed using the computer's A/D converters which had an input voltage range of -5 V to +5 V providing a resolution of 2.44 mV.

The software was designed such that the signal employed for phase reference purposes (shaft speed signal in rotating-shaft tests and excitation force signal in vibrating-shaft tests) was used to trigger the A/D conversion process. The shaft rotational (vibrational) frequency was computed by averaging the measured period of vibration over a suitable number of cycles (normally 10 cycles unless significant speed fluctuations were suspected). Other shaft response data, e.g. shaft displacement, bearing forces etc. was analysed, employing time averaging techniques to enhance the signal-to-noise ratio, using 128 samples per period where possible. However, at frequencies greater than approximately 35 Hz, sampling-rate limitations necessitated the use of 64 samples/period. These sampling rates were more than adequate for accurate signal digitisation. Before processing test data, proper functioning of the algorithm was verified by analysing a sinusoidal waveform, of known

amplitude and frequency, produced using a function generator.

6.9 Chapter Summary

The work described in detail in this chapter may be briefly summarised as follows:

1. A laboratory rig comprising a high-speed shaft mounted on rolling-element bearings was designed and constructed. The rig was designed such that investigation of system response, on a number of test configurations, could be easily achieved.
2. A number of displacement/force transducers, employing electrical resistance strain gauges, were constructed and tested and found to perform satisfactorily.
3. Vibration testing of the bearing flexible-support assembly showed the material inherent damping to be negligible.
4. Calibration of the Kinetrol mechanical dashpots presented many problems due to the device's inherent non-linear characteristics. In addition, severe deterioration in damper performance was observed as the excitation frequency was increased.
5. A simple, small and robust angular electromagnetic actuator was constructed and, along with the associated control hardware, calibrated using a specially constructed rig. Damping and stiffness coefficients were obtained and the following observations made:
   a) Damping and stiffness forces were always

evident, irrespective of the type of control demanded, due to the introduction of undesirable control signal time lags. Although in certain circumstances this effect could result in system instability problems, these could easily be eliminated by slightly increasing the control damping rate.

b) The measured damping and stiffness coefficients were found to be in accordance with a magnet-moment/current/gap relationship of the form $M = k.\ (i/G)^2$ as predicted by theory.

c) The measured electromagnet force capacity was found to be in fair agreement with that predicted from theory.

CHAPTER 7

EXPERIMENTAL RESULTS AND THEORETICAL COMPARISON

7.1 General

In this chapter, results obtained from a number of tests performed on a laboratory rig (Figs. 6.1) are presented and a comparison made with theoretical data produced using the transfer matrix program described in Chapter 4. The test procedures employed are described in detail along with the shaft arrangements investigated.

The main aims of the experimental portion of the work were as follows:

1. To verify the accuracy of the analysis program developed and described in Chapter 4.
2. To examine the effectiveness of the application of external control forces (radial and angular) in attenuating rotor system response.
3. To investigate, in particular, the performance of a new type of contactless angular electromagnetic actuator when employed to implement different control strategies.

In each test, eddy-current proximity displacement probes were mounted at convenient locations along the shaft in the horizontal and vertical planes. Results, in the main, are presented for measurements made in the horizontal direction, although where appropriate, details of shaft response in the vertical plane are also shown.

The displacement probe locations were fixed for each test case and chosen such that they were always displaced

from any nodal points appearing within the specified frequency range. In each plane the response measured at each probe was combined with that of the other probes to enable calculation of a root-mean-square (rms) value which was chosen as the representative system response function. This eliminated the need for measurement of the shaft maximum response (Chapter 5) which would generally require re-positioning of the displacement transducers during test-runs [91]. A similar procedure was adopted when the shaft system was subjected to external excitation using an electromagnetic shaker. However, here a more meaningful parameter, rms-receptance, was chosen as the system response function.

Transmitted bearing forces and bearing pedestal displacements were recorded in certain test cases by making use of electrical resistance strain gauges and eddy-current displacement probes respectively.

In addition to the above, when vibratory shaft tests were performed (as opposed to rotating shaft tests), it was necessary also to record the external excitation force using an axial Piezo-electric force transducer. In rotating shaft situations, non-contact measurement of shaft rotational speed was performed using a Sodenco magnetic pick-up as described in Chapter 6. These latter two signals were each used for phase reference purposes in their respective cases.

Since the test shaft was found to possess significant initial-bend (0.164 mm maximum) in certain cases (e.g. Test 3), a procedure was adopted to enable elimination of

this effect. This was achieved, for each shaft configuration, by recording shaft response data for two test-runs, each run corresponding to a different pre-defined unbalance distribution. Subsequent vectorial subtraction of the measured data led to elimination of the influence of shaft permanent bend.

In addition to the normal forced response tests, in a number of cases transient 'hammer tests' were performed and system response analysed with the aid of a real-time frequency analyser. This allowed estimation of system natural frequencies.

At intermediate stages throughout the seies of tests described here, repeatability checks were implemented to ensure meaningful results. The test data was recorded on magnetic tape and later analysed using an FFT algorithm on digital computer as described in Chapter 6.

Although the majority of the tests were performed with the shaft rotating, in some cases additional vibrating shaft tests were conducted. The latter approach was included because of the resulting benefits, viz:

i) Test results become totally independent of shaft-bend/residual-unbalance effects.

ii) System response levels may be selected to suit prevailing safety and other important considerations by appropriate adjustment of the external excitaton force.

iii) The test frequency range can be extended considerably without the need for special safety measures (shaft

maximum running speed = 3000 rpm).

iv) A number of extraneous effects may be eliminated, e.g. undesirable multi-frequency excitation from the drive system and unwanted friction effects resulting from physical contact with mechanical dampers.

v) The approach enables comparison of the relevant system receptances for various positions of excitation source, thus providing information regarding the most suitable locations and types of external control, irrespective of the form of controller to be employed, e.g. mechanical, electromagnetic etc.

Of course, when such test methods are employed, the results must be considered with care and account taken of any rotor-dynamic effects which have been eliminated as a result of the test procedure, e.g. the gyroscopic influence of shaft-mounted discs. In all instances where such tests were performed, an attempt was made to maintain the external excitation force level constant over the frequency range.

7.2 Auxilliary Test Rig - Rig A

An additional test rotor having the dimensions shown in Fig. 7.1 was utilised at an early stage of the research work, mainly for balancing studies, before the laboratory rig described in Chapter 6 became available.

The test rig consisted of a uniform low-carbon steel shaft supported on single deep-groove ball-bearings which were mounted in steel bearing-housings. The nature of

the construction of the bearing-housings resulted in support anisotropy, the greater stiffness prevailing in the horizontal plane. Three pulleys equally spaced were clamped to the shaft by means of taper-lock bushes. Each pulley had provision for the addition of balance weights at eight equally-spaced axial drilled and tapped holes. Rotor stiffness/inertia dissymmetries were present as a result of geometric irregularities in the pulley bushes. The complete rotor-bearing system was rigidly bolted to a solid lathe-bed, which in turn was isolated by means of a layer of compressed cork, from the supporting foundation. Proximity probes were employed to measure the shaft dynamic response.

The measured shaft first (synchronous) critical speeds were 560 rpm and 580 rpm in the vertical and horizontal planes respectively. Maximum shaft speed was limited to 1800 rpm for safety reasons.

This test-rig displayed some interesting phenomena which are discussed later in the relevant sections.

In the remainder of this chapter, all results pertain to the test-rig arrangement as described in Chapter 6, unless specific reference is made to Rig A.

Throughout the test program rotor-balancing was found necessary in a number of instances, to minimise inherent shaft/rotor mass unbalance. The procedures adopted were as described in the following section.

7.3 Test Rotor Balancing

The relative merits of currently available flexible-

rotor balancing methods are discussed in Chapter 2. Because of its simplicity and suitability for programming on digital computer, the Influence Coefficient Method was selected for the purpose of balancing the laboratory rig. A computer program based on the work presented by Goodman [50], was created and tested by performing balance measurements on a number of rotor arrangements.

The effectiveness of the balance program was initially assessed by considering test-rig A. The balance procedure allows for multi-plane, multi-speed correction through a least-squares approach. The rotor was balanced at three planes and two shaft speeds (545 rpm and 750 rpm), i.e. one above and one below the first critical speeds. Before balancing, the lack of inherent system damping meant that the critical speeds could only be traversed by applying external damping, whilst simultaneously ensuring rapid rotor acceleration.

The balancing procedure was as follows:

1. Measure displacement amplitude and phase at each balance plane and speed. This is termed the zero-rotor data.
2. Apply a trial-mass to each balance plane in turn and at each balance speed measure displacement amplitude and phase at the corresponding locations. This is termed the trial-mass data.
3. The zero-rotor and trial mass information obtained from Steps 1 and 2 is used as input data to the balance program. The data provides details of the system influence coefficients from which the program

predicts the required magnitudes and locations of the correction masses.

The correction masses are then applied to the rotor and Steps 1 and 3 above repeated if necessary.

After one balance correction, it was found that the test rotor could be run through its first critical(s) fairly rapidly, without the need for external damping and without excessive vibration. Following another balance correction, the first critical(s) could be traversed without external damping, even with small acceleration, with a low level of shaft vibration. Fig. 7.2 shows the measured shaft response at the central pulley in the horizontal plane before and after balancing. The characteristic peak at the first critical speed is clearly observed, but the response has been attenuated considerably as a result of balancing. Another large response peak present at a speed approximately equal to half of the first critical speed is shown to be insensitive to balancing. The phenomenon is termed a 'secondary critical' and is discussed in greater detail later.

An example of the measured shaft zero-rotor, trial-mass and final balance data is presented in Fig. 7.3. Reductions in unbalance response at the two balancing speeds are seen to be generally of the order of 90% and in one case as much as 95%. Output data from the balancing program is displayed in Fig. 7.4. Correction mass magnitude and location requirements are seen to be different when the shaft is to be balanced only at the

low speed. It is observed that after the second balance correction, the calculated maximum residual vibration is somewhat larger than the rms residual, even though the overall residual vibration level is low. This indicates the possibility of further reducing the maximum residual vibration (Plane 1, 750 rpm) through employment of a weighted least-squares procedure such as that described in Ref. [50].

The above results, along with those obtained from the main laboratory rig throughout the research work described herein, confirm the effectiveness of the balancing method adopted.

One criticism of the above procedure is that in some instances, the magnitudes of the computed correction masses were relatively large because of their angular orientation. Thus, although the nett correction effect was acceptable, an optimum mass distribution was not achieved. Although this posed no problems in a laboratory environment,the possible disadvantages in a practical situation are evident. However, if necessary, this problem could be overcome to a certain extent by, for example, employing linear programming techniques [117] so that constraints on the correction mass size may be introduced.

7.4 Asynchronous Vibrations and Secondary Criticals

Frequently throughout the experimental work when the shaft was run without external control damping the resulting response, although in the majority of cases of a predominantly synchronous form, was found to consist of a

number of non-synchronous harmonic components. This characteristic was particularly evident when running close to a shaft critical speed and in some cases even resulted in the appearance of a low-frequency beat. Although from a data analysis point of view its influence could be sufficiently minimised, the problem was further investigated.

The source of the problem became apparent when the test-shaft was uncoupled, the motor/pulley-drive arrangement run on its own and the response measured. Even under the above circumstances, excitation of the test shaft system resonances was found to occur at almost any motor speed. Although the shaft response was initally extremely small, if left for a sufficient period of time the displacement amplitude was found to become quite large.

Further investigation showed the cause could be attributed to two main factors: i) emanation of a broadband excitation from the drive system (Fig. 7.5) and ii) lack of inherent test system damping.

The effect of the above undesirable features was minimised by: a) supporting the drive motor on anti-vibration mounts and b) suitable adjustment of the drive-belt tension.

In addition to the above, secondary-criticals [67] were frequently observed throughout the test program. A secondary-critical occurs when an excitation component with frequency equal to some multiple, or sub-multiple, of the shaft rotational frequency coincides with a system

natural frequency. The phenomenon has been found to occur in practical rotor systems with horizontally mounted shafts and low damping. The absence of the effect in vertical shaft arrangements confirms the contributory role of gravity.

The most common type of secondary-critical is that where a shaft non-synchronous excitation occurs at a frequency equal to two times the shaft rotational frequency, thus leading to a 'critical-speed' at a shaft speed of approximately half the first primary critical-speed. The secondary-critical in this case is often termed the 'half-critical' and was observed in this form frequently in the test work described in this chapter.

It may be shown [118] that if a rotating horizontal shaft has unsymmetrical elastic properties about the two principle axes, then the gravitational force will induce a secondary resonance at a shaft speed equal to the mean of the primary critical speeds. Den Hartog [67] showed how the same effect could result from the interaction of unbalance and gravity forces, even in the absence of shaft asymmetries.

Den Hartog suggested shaft balancing as a means of differentiating between the above two possible causes. The principle is that if after proper balancing at the primary-critical speed, the secondary-critical remains unaltered, then shaft asymmetry is the culprit. This approach seems reasonable but certain limitations exist. If system damping is effectively zero, then even a very low level of shaft unbalance will be sufficient to produce

a large resonant response at the 'half-critical'. In addition, since secondary-criticals appear within a very small shaft speed range, i.e. they are very sharp in form, exceptional speed control may be required to ensure a valid pre and post-balance response comparison.

Investigation of secondary-criticals found to occur in the laboratory rigs examined indicated their cause, in general, to be a combination of the above two factors. Fig. 7.2 shows the effect of balancing the system shown in Fig. 7.1. Although the response around the primary-critical speed (≈ 580 rpm) is seen to be attenuated considerably after balancing, that at the 'half-critical' (≈ 290 rpm) remained almost unchanged. It is evident from this plot that, in certain circumstances, shaft response at a secondary-critical may be more severe than that which would result when running at a primary critical. In other cases, the application of balance correction masses was found to reduce to some extent the 'half-critical' response. More detailed investigation showed the shaft response at the 'half-critical' to be influenced by the flexibility of the coupling. The couplings employed throughout the experimental work were of the pin and chord type (Fig.7.6), where an elastic-band was used as the flexible torque-transmitting element. Close examination of this set-up highlights the inherent asymmetric stiffness properties. Altering the grade of elastic-band employed confirmed this view, the most flexible arrangement resulting in the best performance in terms of secondary-critical response. However, a compromise was

necessary, regarding the coupling stiffness, to ensure good torque-transmission characteristics and so it was never possible to eliminate secondary-criticals without the use of external damping (see Test 3).

7.5 Tests

A range of tests were performed on the rig shown in Fig. 6.1 and described in Chapter 6. The effect of external radial and angular control, using mechanical dashpots and an electromagnetic actuator respectively, was investigated. The influence of shaft initial-bend was considered first.

7.5.1 Test 1 - Shaft Response Due to Permanent Bend

The response of a uniform, initially-bent, rotating shaft was investigated. Displacement probe positions are shown in Fig. 7.7a, although for comparison purposes, only probes 4, 5 and 6 were used to compute the measured rms response.

The shaft support configuration employed was that designed to simulate radially-rigid bearings (Section 6.3).

The magnitude and orientation of the shaft bend was measured by recording the displacement at suitable locations along the shaft length whilst slowly rotating the shaft. The shaft bend data used in the analysis program to enable prediction of shaft response was a computed average of bend measurements taken before and after each test run. This approach was found necessary since variations in the magnitude of the shaft initial-

bend were observed throughout the experimental work. This phenomenon, also reported by other workers [91], was of a transient nature since it was found that, after each test run, if the shaft was left unrotated for a sufficient length of time, e.g. 24 hours, then the initial-bend would resort to its original form.

Details of the average shaft bend for this test are given in Fig. 7.7b, where the bend is observed to be almost planar.

The shaft maximum speed was restricted to 3000 rpm for safety reasons.

During testing the lack of inherent system damping was evident (Figs. 7.7c-e) since response measurements above the first critical speed could only be obtained after introducing external damping to allow safe passage to the higher shaft speeds where the damping was subsequently removed.

Fig. 7.7c is a plot of measured and predicted shaft rms displacement response obtained from probes 4, 5 and 6 (Fig. 7.7a). The theoretical plot agrees very well with the experimental data, thus confirming the validity of the system model. The measured first critical speed is observed to be slightly greater than the predicted value and is estimated from the response plot as 1630 rpm. Similar plots are presented in Figs. 7.7d and 7.7e, where the individual displacements at probes 4 and 5 respectively are illustrated for comparison. As would be expected, agreement between theory and experiment, on the whole, is very good, particularly at probe 5.

To assess the accuracy of the analysis program in predicting the complete shaft response, the shaft displacement was measured at various locations along its length. At zero shaft speed the predicted shaft deflected form should agree identically with the measured shaft bend. This was indeed found to be the case and provided confirmation of the ability of the transfer-matrix program to take account of shaft lack of straightness. The measured and predicted shaft deflected forms, at three selected speeds (520, 1400 and 2000 rpm) are shown in Fig. 7.7f. Experimental and theoretical data are observed to correspond extremely well. The greatest disparity is seen to occur at a shaft location corresponding to displacement probe number 4. The cause appears to be related to inaccuracy in the measurement of shaft bend at this position, since at low and high shaft speeds the magnitude of the error is almost constant.

In addition to the above, transient tests were performed in order to:

1. Determine the system natural frequencies, and
2. Assess the influence of the coupling arrangement on the dynamic characteristics of the test shaft.

The natural frequencies in the vertical plane were found to be consistently greater than those in the horizontal plane, although only marginally. With the shaft rotating at 1200 rpm, the natural frequencies were measured as 27.2 Hz (1632 cyc/min) and 27.4 Hz (1644 cyc/min) in the horizontal and vertical planes respectively. Since in this case, gyroscopic effects

could be safely ignored, the measured natural frequencies would be expected to coincide with the shaft critical speeds. This was indeed the case. The bearing-supports appeared to exhibit greater flexibility in the horizontal plane. Examination of the physical aspects of the support arrangement justified this conclusion (Figs. 6.3 and 6.4).

The first four, static-shaft, natural frequencies in the horizontal plane, with coupling removed, were measured as 27.0, 98.0, 172.0 and 274.0 Hz (1620, 5880, 10320 and 16440 cyc/min). The corresponding theoretical values are 26.9, 96.7, 168 and 274.6 Hz respectively (i.e. 1614, 5801, 10078 and 16477 cyc/min). These figures demonstrate the validity of the system model, all four natural frequencies being estimated to within approximately 2%.

The influence of the coupling on the shaft dynamics was assessed by comparing measured natural frequencies for the coupled and uncoupled shaft cases. With the coupling removed, the shaft fundamental natural frequencies were recorded as 27.0 Hz and 27.2 Hz in the horizontal and vertical planes respectively. Comparing these values with those above, it is clear that the coupling did in fact have a restraining effect on the test shaft, leading to an increase in the system natural frequencies. However, the effect was minimal and indeed resulted in, at most, a fundamental frequency shift of less than 1%. Consequently, in all subsequent computer analyses, this effect was excluded.

In the tests just described, the absence of

gyroscopic influences along with the employment of rolling-element bearings resulted in de-coupling of the shaft motion in orthogonal planes.

7.5.2 Test 2 - Effect of External Mechanical Damping

The shaft system employed in Test 1 was again utilised to enable examination of the effect on system synchronous response of applying external damping to the shaft.

The influence of damper location was investigated by introducing radial damping at three shaft positions in turn using mechanical vane-type dashpots as described in Section 6.5.

The three damper locations corresponding to Tests 2a, 2b and 2c are shown in Fig. 7.8a where the displacement measuring positions are also indicated.

The measured shaft initial-bend, recorded with the dampers 'in-situ' is presented in Fig. 7.8b.

Three levels of damping were selected during each test-run and the shaft response recorded. The incorporation of a rolling-element bearing between the damper arms and shaft helped minimise rotary-friction forces and for all practical purposes, ensured decoupling of the rotor response in the horizontal and vertical planes.

Adjustment of clearance within the damper sliding-block assembly (Fig. 6.13) was found to critically affect the shaft response. As a result, in an effort to ensure consistency, an appropriate pre-test set-up procedure had

to be devised.

Initially, the damper clearance in both planes was adjusted such that no external damping was applied to the shaft. Next, the shaft was run constantly at a speed close to the first critical speed to provide a substantial shaft response. The resulting response was monitored in both planes and the corresponding damper clearances adjusted until a point was reached where a small reduction in response level was observed, thus indicating the elimination of clearance within the relevant damper assembly.

Shaft measured and predicted rms displacement response, computed from the displacements at locations corresponding to probe positions 4, 5 and 6, are presented in Figs. 7.8c-e.

Although agreement between theory and experiment is, on the whole, seen to be poor, at least the predicted and measured response trends correspond. Similar problems were experienced by Kaya [94] who also used Kinetrol dampers in an experimental study.

The results obtained in Test 1 suggest the lack of agreement observed here to be mainly due to inaccurate modelling of the damper arrangement. The nature of the problems experienced throughout the damper calibrations (Chapter 6) strengthens this view.

The inability of the analysis program to accurately predict the damped system response is felt to be mainly due to the following contributory factors:

1. Inherent non-linearity of dashpots (Fig. 6.15).

2. Presence of excessive clearance within the damper sliding-block arrangement (Fig. 6.12).
3. Influence of undesirable friction effects emanating from the damper sliding-block assembly.

The inherent complexities of the mechanical dampers were further illustrated when an attempt was made to predict the damper characteristics required to ensure correspondence between the location of experimental and theoretical 'fixed-points'. This resulted in the computation of an extremely large effective damper inertia which could not be accounted for from assessment of the device's physical dimensions.

As a result of time limitations, it was not possible to investigate this problem further. However, a number of useful observations may still be made regarding the application of external control measures, from the results obtained.

Referring to Figs. 7.8c(i) to 7.8e(i), the application of external damping can lead to significant reductions in system response, the degree of attenuation being greatly dependent upon the damper location. As expected, control of the shaft first mode of vibration is best achieved with radial damping applied at the shaft centre (Test Arrangement 2c). The ineffectiveness of the radial damper when employed at a location close to a shaft support is demonstrated in Fig. 7.8c(i). In this case the shaft first critical speed could not be traversed, even with maximum damping employed.

The ability of the damper to substantially displace

the shaft response peaks (Figs. 7.8d(i) and 7.8e(i)) suggests the presence of relatively large damping forces.

The appearance of clearly-defined 'fixed-points' in the response plots, in these circumstances, provides confirmation of the views expressed in Chapter 5. There it was suggested that even though the choice of response function (in this case a reduced shaft rms displacement) could lead to invalidation of the fixed-point theory, fairly accurate 'fixed-points' would result for a large range of damping values.

In Chapter 5, it was discussed how an optimum control damping rate could be chosen to minimise the system maximum response over a specified shaft speed range. In order to ahieve this, the damping level would have to be selected so that the response plot would pass, with zero slope, through the highest system fixed-point. Considering the response plots resulting from Test 2c (Fig. 7.8e(i)), the optimum damping level is seen to correspond approximately to a damper setting of 2. Similar conclusions may be drawn for the case investigated in Fig. 7.8d(i) where the optimum damper setting appears to be somewhere between minimum and 2.

The relatively small variation in optimum damping levels with respect to damper location over a central section of the shaft is in agreement with the findings of Dostal et al [91]. One would expect the optimum damping requirements to increase as the damper location approaches the shaft supports and the disparity between the results of Tests 2b and 2c in this regard, is probably due to the

non-linear nature of the damper arrangement.

Looking at Figs. 7.8c(i) to 7.8e(i), it is clear that the system response can be minimised at each shaft speed by following a procedure whereby the damping is switched between two levels, this switching occurring at the 'fixed-point(s)'. Considering the speed range 0 - 2750 rpm, best control is achieved if the largest damping rate (setting 4) is selected at low shaft speeds and maintained up to a shaft speed corresponding to the first 'fixed-point' (i.e. approximately 1650 rpm for test case 2c). At this speed the damping is removed (or reduced to a minimum) resulting in minimum shaft response at all higher speeds up to the next 'fixed-point'. These findings are in complete agreement with the results of a theoretical investigation presented in Chapter 5 and indicate the possible benefits of employing an adaptive 'on-off' control strategy. In such circumstances, no advantage is realised when a continuous form of control is employed.

Application of angular damping to the above test-shaft arrangement was attempted using a modified damper set-up (Section 6.5). Considerable attenuation of the rotor response was found possible but, although the damper arms incorporated PTFE pads to reduce friction effects at the shaft-disc, problems of excessive pad wear were experienced, even at low shaft speeds. Despite numerous attempts to maintain a constant pad contact-pressure during testing, repeatability of results could not be achieved to an acceptable degree.

The problems experienced here and during Test 2, highlighted the major difficulties resulting from the employment of a control device whose operation necessitates physical contact with a rotating component. In fact, in these latter tests, it was decided that due to the inherent complexities of the damping assembly, extensive modifications, which would be required in an attempt to eliminate the above problems, could not be justified and that angular control could be best achieved by utilisation of a non-contact device.

7.5.3 A Note on the Electromagnetic Controller

The electromagnetic damping/stiffness coefficients were adjusted by altering the control circuit gain settings using a micro-computer. The level and type of control required could be set in two ways: a) through software implementation or b) by keyboard input. The required degree of control was varied by selecting a digital value in the range 0 - 128, these representing the minimum and maximum control settings respectively. The relationship between the digital setting and the resulting level of control is a non-linear one. Controller performance data, for the range of control parameters employed in the following tests, is presented in Chapter 6.

In the next four sections, the appropriate electromagnet digital settings (C_{ref} and K_{ref}) are displayed on the relevant response plots for reference purposes only and should not be confused with the

resulting control damping and stiffness rates. Because of magnet non-linear behaviour, the resulting damping/stiffness rates are not constant, but vary with response amplitude and/or frequency (shaft speed), even when the control gain is fixed. The coefficients have been estimated from the magnet calibration data, measured shaft response and the procedures described in Appendix E (see Chapter 6).

Access limitations and the need to avoid stray magnetic fields dictated the location of the displacement probes employed to provide the feedback (shaft-slope) signal for the control circuitry. Details regarding the position and spacing of these probes are furnished in the relevant figures.

Alignment of the electromagnetic controller with the shaft-mounted, silicon-steel, low loss disc to achieve the desired air-gap was found to be a critical and sometimes time-consuming operation. The procedure employed necessitated positioning the magnet pole-faces hard against the disc, then after locking the magnets in position on the support stand, slowly displacing the magnet assembly axially by employing a jacking-screw arrangement. The required gap was then set using feeler-gauges and the magnet support stand finally locked in position on the baseplate.

The importance of magnet support rigidity was highlighted when some operational problems were experienced. Subsequent modifications led to the elimination of undesirable destabilising influences.

7.5.4 Test 3 - Angular Electromagnetic Control of a Rigidly-Supported Shaft

The purpose of these tests was to assess the ability of a contactless angular electromagnetic controller to attenuate the synchronous unbalanced response of a flexible rotor. Details of the magnet arrangement and allied electronic control circuitry are presented in Section 6.6.

The test-shaft, details of which are presented in Fig. 7.9a, was located on radially-rigid supports as in Tests 1 and 2. However, subsequent raising of the shaft support-structure led to an increased flexibility in the horizontal plane. The electromagnetic actuator was located slightly inboard of the drive-end bearing.

A number of light, wooden discs designed to accept small balance weights were sited at various positions on the shaft. The disc material was chosen to minimise the additional lumped-mass/inertia so that, dynamically, the system would differ only slightly from that analysed in Tests 1 and 2. This was intended to allow some measure of comparison between the various test results.

The electromagnet air-gap was set at 0.89 mm (0.035 in). Test 3 consisted of two parts. The aim of the first part (Test 3a), was to investigate the effect of the application of electromagnetic damping. The second portion of the work (Tests 3b and 3c) was undertaken with a view to studying the influence of electromagnetic stiffness control. Without the application of external control, it was found impossible to run the shaft within

the speed range 1350 rev/min to 1650 rev/min, due to excessive system response.

Results obtained from Test 3a are presented in Fig. 7.9b(i). Shaft rms displacement, computed from the readings of probes 4, 5 and 6, is shown for four levels of electromagnetic damping. The introduction of angular damping is seen to result in considerable attenuation of the system resonant response. The application of low-level damping (C_{ref} = 70) was found to be sufficient to ensure safe passage of the shaft through its first critical speed (1500 rev/min). With maximum damping employed (C_{ref} = 110) the largest measured uncontrolled shaft responses (at 1425 rpm and 1570 rpm) are seen to be reduced by 71% and 63% respectively.

At shaft speeds close to the first critical speed, the test shaft may be considered to act as a single-degree-of-freedom system. If the characteristics of this equivalent, single-mass system can be estimated, then a more realistic assessment of the degree of control present can be made. For a single-mass (Jeffcott) rotor with disc mass M and mass unbalance force of $me\omega^2$ and supported on rigid bearings, the system displacement response may be calculated [119] from:

$$X = \frac{me}{M} \frac{f^2}{\sqrt{(1 - f^2)^2 + (2\zeta f)^2}}$$

where $f = \omega/\omega_{NAT}$

X = displacement response of single-degree-of-freedom system

ζ = dimensionless damping factor

For the test-shaft vibrating in its first mode, the shaft stiffness k may be estimated using the formula for a centrally-loaded uniform shaft ($k = 48EI/L^3$). Making use of the measured first critical speed (1500 rev/min), the system effective mass M is computed as 0.877 kg. Utilising the above equation in conjunction with the measured undamped test-shaft response, a least-squares procedure was employed to determine the system me value (4.6E - 5 kgm).

The same least-squares method was then used to estimate the damping factor ζ from the measured damped response plots illustrated in Fig. 7.9b(i).

The resulting damping factors are 0.05, 0.1 and 0.13 corresponding to the reference settings (C_{ref}) 70, 90 and 110 respectively. The control damping levels may be considered to be relatively small, but would be effective, in terms of system vibration attenuation, in any 'pinned-pinned' shaft arrangement vibrating in its first mode. Additionally, a relatively small increase in the magnet effective radius would lead to substantially greater system damping levels.

The above estimation technique could have been performed more accurately by making use of modal methods (Chapter 3). However, at the time of this work no such procedures were available. The approach adopted is an approximation to the more conventional modal methods.

Referring to Fig. 7.9b(i), an interesting aspect is the appearance of an approximate 'fixed-point' at a speed of 1950 rpm. This 'point' does not coincide with the

uncontrolled response due to an inherent electromagnetic stiffening effect resulting mainly from control-circuit component phase-lags (Section 6.6.3). The employment of an 'on-off' adaptive damping control strategy, as described in Chapter 5, in this case would clearly require the electromagnet 'switching-speed' to be dependent upon the initial damping setting.

The measured damped response at a single shaft location corresponding to probe 4 (Fig. 7.9a) is shown in Fig. 7.9c(i) for comparison. The single-point response plots are of identical form to the shaft rms plots but, in general, of greater magnitude. An approximate 'fixed-point' is also seen to occur, in this case at a speed of 1910 rpm. The predicted rms and single-point shaft displacements are shown in Figs. 7.9b(ii) and 7.9c(ii) respectively. In both cases the agreement between measured and predicted uncontrolled response is excellent.

This close agreement is seen to deteriorate somewhat when control damping is introduced. The theory predicts the presence of approximate 'fixed-points', although these are observed to occur at slightly lower shaft speeds than the corresponding measured 'points".

The lack of agreement between measured and predicted shaft damped response is thought to result from a combination of the following contributory factors:

1. Inherent magnet non-linearity (i.e. inability of the predicted linearised magnet coefficients to reflect the true (non-linear) magnet performance).
2. Variation of the shaft initial-bend with time. This

effect could introduce errors into the procedure for computation of the equivalent linearised magnet coefficients (Appendix E).

3. Variation of electromagnet air-gap.
4. Measurement error.

Where a linear analysis approach is adopted and the test-shaft possesses significant permanent bend, as in this case, then the effects described in paragraphs (1) and (2) are, to a large extent, unavoidable.

The good agreement achieved between measured and predicted shaft uncontrolled response appears to confirm an acceptable level of measurement accuracy (paragraph (4)).

The assumption of constant air-gap was further assessed by examination of the shaft angular response at the controller. Of all the tests performed with the controller in operation, the measured maximum displacement at the magnet air-gap was found to be approximately 0.05 mm (0.001 in), for an air-gap setting of 0.89 mm (0.035 in). This condition occurred with the shaft running at its first critical speed and the reference damping level, C_{ref}, set at 70 (Fig. 7.9b(i)). The largest peak response value present at other damping settings was found to be less than half of this figure. Thus, although the variation in air-gap was not significant, some improvement in the theoretical results may be achieved if the controller was calibrated dynamically.

The influence of magnetic coupling between the shaft horizontal and vertical planes, was investigated during

various tests. With the shaft running close to resonance, maximum damping was introduced in one plane only and any alteration of response in the orthogonal plane noted. This procedure was performed in the shaft horizontal and vertical planes in turn. Only minute changes in response levels were observed, thus confirming earlier assumptions. In fact, some coupling would be expected anyway as a result of gyroscopic influences.

Details of the variation of angular damping with shaft speed, for Test 3a, are presented in Fig. 7.9d. The damping rates were computed from the magnet calibration data presented in Chapter 6, in conjunction with the measured shaft-slope and rotational speed. The maximum damping rate (3.85 Nms/rad at 1600 rpm) shown in the figure corresponds to the highest attainable system damping for this case, since at slightly greater damping (C_{ref}) settings, power supply current-overloading occurs. Magnet power dissipation curves for the above case are shown in Fig. 7.9e. These were also computed using calibration and test data. It is interesting to note that the maximum power dissipated remains almost constant ($\approx$ 4.8 watts) irrespective of the damping reference setting. Reference to Figs. 7.9b(i) and 7.9e indicates that at high shaft speeds (> 1950 rpm) with high damping settings, both magnet power requirements and shaft response are increased. This is in line with the theoretical findings of Chapter 5. At slightly lower shaft speeds, although some system response attenuation occurs, there is substantial increase in power

consumption.

In Test 3b, a large value of electromagnetic stiffness combined with low damping, sufficient to maintain system stability (Section 6.6.3), was introduced over the complete shaft speed range and the shaft response measured. Shaft unbalance details are given in Fig. 7.9a. The effectiveness of stiffness control in displacing the shaft first critical speed is clearly demonstrated in Fig. 7.9f. A shift of approximately 200 rpm (13%) is observed. The shaft response at the 'new' critical-speed is still large since system damping is fairly low. The form of the controlled system response plot is seen to bear some resemblance to the classical 'hardening-spring' characteristic, due to the inherent magnet non-linearities.

Examination of Fig. 7.9f shows that some advantage could result if an adaptive (or variable-gain) stiffness-control strategy were employed. This was the approach adopted in Test 3c. the stiffness and damping reference settings selected in Test 3b were again utilised, this time only up to a shaft speed of approximately 1560 rpm. Above this speed, the electromagnets were switched-off. The magnet 'switching-speed' corresponded to that speed at which the measured controlled and uncontrolled responses were identical and was determined by making reference to Test 3b results (Fig. 7.9f).

The results of Test 3c are presented in Fig. 7.9g(i) where the advantages of adaptive stiffness control, even when system damping is low, are evident. By comparing

Figs. 7.9f and 7.9g(i), the employment of adaptive control is seen to result in a shaft response corresponding to the locus of minimum response. Theoretical plots are presented in Fig. 7.9g(ii) for comparison. Agreement between the measured and predicted response data is reasonably good. The theoretically determined controller 'switching-speed' (1570 rpm) is very close to the measured value (1560 rpm). Damping and stiffness rates for this case are shown as a function of speed in Fig. 7.9h, where the maximum attained values are seen to be 1.54 Nms/rad and 318 Nm/rad respectively.

Even though the adoption of an adaptive stiffness-control strategy alone would be sufficient to ensure considerable attenuation of shaft steady-state synchronous response, consideration must also be given to the system transient-response at the controller 'switching-speed'. Figs. 7.9i-l, show the resulting shaft transients during Test 3c when stiffness control was switched on and off. Two levels of angular damping were introduced in turn for comparison. One major problem encountered during the tests was the inability of the motor speed-control unit to maintain a steady shaft speed. This is evident from the difference in magnitude of the controlled and uncontrolled shaft responses, particularly at the lower damping setting. With very low magnetic damping ($C \approx 0.5$ Nms/rad) the shaft transient response, resulting from switching, varied according to the exact shaft speed at switching, but in general was characterised by large oscillatory displacements taking, typically from 1.5 to 6 seconds to

reach their steady-state values (Figs. 7.9i and 7.9j). Increasing the damping to approximately 1.5 Nms/rad improved the system transient performance considerably (Figs. 7.9k and 7.9l), leading to settling times of the order 0.5 secs. It is clear that in practice, successful implementation of an 'on-off' adaptive stiffness-control procedure would require the presence of a reasonable level of system damping.

A common feature in the lightly-damped rotating shaft tests performed here, was the appearance of secondary criticals [67] most certainly caused by interaction of shaft-stiffness asymmetries and gravity loading. The shaft response at these additional criticals, in many cases, was found to be greater than that at the primary critical speeds. The measured secondary-criticals were characterised by a large shaft response over an extremely small speed range. The effectiveness of the angular damper in eliminating this additional form of vibration was examined and relevant results are presented in Figs. 7.9m-p. Figs. 7.9m and 7.9n show the gradual elimination of a non-synchronous 2 x rpm component in the time and frequency domains respectively. In the example shown, the shaft speed was approximately half the first critical speed leading to the introduction of a 'half-critical'. With sufficient magnetic damping, the non-synchronous component is seen to almost vanish.

Throughout the experimental work, measurement of the shaft whirl-orbit, at various shaft locations, was performed by combining the signals obtained from

displacement probes mounted in the horizontal and vertical planes. A permanent record was acquired by first storing the two ses of data on a digital oscilloscope, then passing this information to an X-Y plotter. Fig. 7.9p is typical of the shaft orbit characteristics exhibited throughout the tests. Non-synchronous response is indicated by the introduction of additional loops in the whirl-orbit (at 750 rpm and 2000 rpm - undamped). The results demonstrate the virtual elimination of shaft non-synchronous vibrations, in addition to the considerable reduction in synchronous response, when angular magnetic damping is utilised.

7.5.5 Test 4 - Angular Electromagnetic Control - Extended Frequency Range

These tests were performed to demonstrate the effectiveness of the angular electromagnetic controller over a broad frequency range. Safety considerations limited the shaft maximum speed to 3000 rpm so that investigation of the controller performance over a larger frequency range could only be achieved by adopting a different approach. The test shaft was shaken, in the horizontal plane, using an electromagnetic vibrator (Section 6.4).

The test configuration used here was identical to that employed in Test 3. Details of the location of displacement probes and electromagnetic shaker are presented in Fig. 7.10a. The electromagnet air-gap was set at 1 mm (0.040 ins) and a frequency range of 0 - 100 Hz covered. Except in the case where no external control

was applied, the excitation force amplitude was maintained with an average value of approximately 3 Newtons, over the specified frequency range.

Two tests were conducted, one to assess the influence of magnetic damping (Test 4a) and the other to study the effect of introducing electromagnetic stiffness (Test 4b).

The results of Test 4a are shown in Fig. 7.10b. The readings from probes 2, 5 and 6 were used in conjunction with the measured excitation force to produce an rms receptance versus shaft vibration frequency plot. The beneficial effect of electromagnetic damping is evident and the angular controller is seen to operate well over the complete frequency range, particularly at the higher shaft frequencies around the second system natural frequency.

If the system natural frequencies are not closely spaced, then in the presence of a single harmonic excitation component with frequency in the region of a system resonance, the resulting response will corespond to that of a single-degree-of-freedom system. For such an arrangement the system receptance can be written [119] as:

$$r = \frac{1}{k\sqrt{(1 - f^2)^2 + (2\zeta f)^2}}$$

where k is the system stiffness, N/m

f is the frequency ratio ($f = \omega/\omega_{NAT}$)

ζ is the damping factor ($\zeta = C/(2\ m\ \omega_{NAT})$)

C is the system damping constant, Ns/m

m is the system mass, kg

Making use of the above and considering a system at

its undamped natural frequency (f = 1):

$$r_N = \frac{1}{2\zeta k}$$

or

$$\zeta = \frac{1}{2k r_N}$$

where r_N is the damped system receptance at f = 1.

Although this approach involves a number of approximations at least it provides a simple means of estimating the degree of damping control achieved. Referring to Fig. 7.10b and considering the first system natural frequency, the stiffness k may be estimated by extrapolating the receptance plot at low frequencies. Following the above procedure, the computed system damping factors, corresponding to the digital damping settings (C_{ref}) of 70, 90 and 110, are 0.03, 0.14 and 0.26 respectively. The influence of external damping on the system resonant response at the second natural frequency is even more pronounced. With maximum damping introduced the characteristic response peak is eliminated completely. The damping factors for this case may be approximated as before. However, the equivalent single-degree-of-freedom stiffness k is different to that employed for analysis of the first natural frequency. A conservative approach is to use the stiffness value corresponding to the minimum occurring in the receptance plots at a frequency of approximately 4200 cyc/min. The resulting computed damping factors are 0.16, 0.36 and 0.58 respectively.

Angular electromagnetic damping is thus seen to be an effective means of attenuating shaft response over a frequency range encompassing two natural frequencies.

Another method capable of achieving significant reductions in system response at, or close to, a natural frquency is based on introducing additional stiffness to the system to displace the resonances. This prinipcle was demonstrated in Test 3 and is given further consideration here. Fig. 7.10c illustrates the effect of angular electromagnetic stiffening on the system rms receptance. Substantial increases in the two system natural frequencies are observed. With maximum stiffness control employed, the fundamental frequency was shifted by approximately 245 cyc/min, i.e. a 17% change. The second shaft mode has its natural frequency altered by 175 cyc/min (3.4%) as a result of stiffness control.

Fig. 7.10d demonstrates how the implementation of stiffness control alone can lead to favourable system performance. The minimum response locus is represented by the dashed lines. Significant vibration attenuation is achieved by utilising maximum stiffness control, over a frequency range encompassing the uncontrolled fundamental natural frequency, up to a frequency of 1600 cyc/min and thereafter removing the control influence.

7.5.6 Test 5 - Angular Electromagnetic Control - Attenuation of Bearing Forces

These tests were undertaken in order to assess the ability of angular electromagnetic control to reduce transmitted bearing forces. The test configuration used was identical to that employed in Tests 3 and 4, but with alterations to the shaft supports as shown in Fig. 7.11a.

It was initially intended that the shaft be rotated as was the case in Test 3. However, after modification, the bearing supports, in addition to introducing the desired radial flexiblity, were found to exhibit axial flexibility. This latter characteristic, not surprisingly, resulted in system stability problems (Section 6.6.3). Elimination of the effect without significantly influencing the radial support stiffness was found to be extremely difficult. Since the problem was directly related to the magnitude of shaft angular response at the electromagnets, it was decided that the best approach would be to excite the shaft using an electromagnetic shaker. In these circumstances, the external excitation force could be easily adjusted to a suitable level.

The location of displacement probes and magnetic shaker are shown in Fig. 7.11a.

Two tests were performed, the first to examine the effect of damping control and the second to investigate the influence of stiffness control.

Following a procedure similar to that employed in Test 4, the bearing transmitted forces are presented in non-dimensional form by dividing through by the excitation force. This is normally termed the transmissibility, although in the strictest sense, it is the sum of the non-dimensional bearing forces which constitutes the system transmissibility.

Figs. 7.11b and 7.11d show the non-dimensional bearing forces as a function of frequency, with different

levels of control damping, for the drive-end (DE) and non-drive-end (NDE) bearings respectively. Considerable attenuation of the bearing forces is observed. The largest uncontrolled response is seen to be reduced by 88% and 85% at the DE and NDE bearings respectively.

For a single-degree-of-freedom system the degree of damping present is best represented by the system damping factor ζ. Applying the assumptions made in Section 7.5.5 an estimate of the non-dimensional control damping, as a proportion of system critical damping, can be made. In a single mass system the transmissibility TR can be calculated [119] from:

$$TR = \frac{\sqrt{1 + (2\zeta f)^2}}{\sqrt{(1 - f^2)^2 + (2\zeta f)^2}}$$

At the system undamped natural frequency f = 1 and we can write:

$$\zeta = \frac{1}{2\sqrt{[(TR)^2 - 1]}}$$

The measured transmissibility TR can be obtained from the response plots of Figs. 7.11b and 7.11d and the damping factor ζ computed using the above equation.

Following this procedure, the damping factors corresponding to the reference settings (C_{ref}) of 70 and 110 were estimated as 0.02 and 0.07 respectively. Thus, although substantial reductions in bearing transmitted force are achieved, the control damping is seen to be small. The low level of control damping is a result of the small shaft response, necessary to ensure system stability in this case.

Comparing the measured bearing force magnification factors at the system undamped natural frequency (≈ 1410 cyc/min), with the control damping set at maximum (C_{ref} = 110), the DE bearing (magnification factor = 5.22) appears to be influenced to a greater extent than the NDE bearing (magnification factor = 5.85) by the application of angular control.

Theoretical plots of the non-dimensional bearing forces are presented in Figs. 7.11c and 7.11e. The agreement with measured response is very good.

The effect on the bearing transmitted force of introducing angular stiffness control, is demonstrated in Fig. 7.11f. The dimensionless drive-end bearing force is plotted as a function of frequency. Bearing forces at the shaft non-drive-end exhibited similar trends. The system natural frequency is seen to be increased by approximately 30 cyc/min, i.e. a change of 2.1%. Again the control influence is small due to the low level of system response. Fig. 7.11g shows the predicted controlled and uncontrolled dimensionless bearing forces and once more agreement with the measured response is very good.

Whilst problems resulting from support inherent axial-flexibility led to limitations on the level of angular control which could be applied to the test system, results from the above tests did illustrate the possible benefits of such a control approach in terms of reduction of transmitted foundation forces.

Because of the non-linear nature of the

electromagnets/mechanical dashpots and due to the introduction of a number of other complexities throughout the experimental work, meaningful comparison of results from different test configurations was limited. As a result, experimental assessment of the relative performances of radial and angular controllers, when employed on a specific shaft system, could not be easily achieved. Consequently, an alternative efficient and rational approach, eliminating the need for experimental investigation of specific controller types, was adopted as follows.

7.5.7 Test 6 - Comparison of Shaft Radial and Angular Receptances

The suitability of various shaft locations for the introduction of external control forces may be assessed by measurement of the relevant system receptances. Referring to the shaft system shown in Figs. 7.12a,b, a number of locations were chosen for application of external harmonic forcing using an electromagnetic shaker. Direct comparison of the appropriate measured receptances gives an indication of the most suitable control position, i.e. the forcing location resulting in the largest receptance value.

Of course, the choice of point of displacement measurement is of critical importance and for the tests conducted here, since the complete system response was of interest, an approach similar to that employed in earlier tests was adopted. The shaft displacement was monitored

at a number of points and a computed rms receptance value used as the system response function.

Steel discs were mounted just outside the bearing assembly at each shaft end to allow the introduction of 'anglar excitation'. This was accomplished by aligning the shaker axis parallel with the shaft rotational axis and clamping the shaker linkage to the disc perimeter through a universal-joint assembly. This arrangement, allowing a small degree of radial misalignment, was found necessary to reduce unwanted bending influences at the Piezo-electric transducer and to minimise the external restraining effect.

Radial excitation of the shaft was achieved by connecting the shaker assembly to a shaft-mounted sleeve.

Two tests were performed, the first (Test 6a) with the shaft resting on 'rigid' supports. Four shaker locations were chosen for excitation of the rotor system (Fig. 7.12a).

During the second test (Test 6b) only two of these points were utilised (Fig. 7.12b) and the shaft was mounted on flexible supports.

The test frequency range, 0 - 90 Hz, was selected to include the first two rigid-bearing natural frequencies. All shaft vibratory motion was restricted to the horizontal plane.

Results from the first test are presented in Fig. 7.12c. The rms receptance, computed using measurements from probes 2, 3, 4 and 5, is plotted against frequency for the four excitation locations (Fig. 7.12a). The

small differences in system natural frequencies are a result of the shaker assembly mass/stiffness effect.

To provide some idea of the relative magnitudes of the control forces which would be required at each of the excitation points, receptance ratios are provided at selected shaft frequencies. The term outside the brackets is calculated from:

$$\frac{\text{rms receptance with excitation at point 2}}{\text{rms receptance with excitation at point 1}}$$

and that inside the brackets is determined from:

$$\frac{\text{rms receptance with excitation at point 4}}{\text{rms receptance with excitation at point 1}}$$

These two values indicate the relative force requirements for angular and radial control at the shaft locations as specified.

As expected the results showed that, at the first natural frequency, best control could be achieved by positioning the controller close to the shaft centre. However, with such an arrangement, controller performance is seen to deteriorate considerably at frequencies in the region of the second natural frequency. In agreement with the findings of a theoretical investigation performed in Chapter 5, radial control is seen to perform best (at least up to the second natural frequency) when introduced on the shaft span between the supports. However, the difference between radial and angular forces, required to achieve the same degree of control, is not excessive and in certain frequency bands is fairly small. In addition, the radius employed for angular excitation, 44.5 mm, is not large and could easily be increased substantially.

Theoretical receptance plots are presented in Fig. 7.12d for comparison and excellent agreement with the measured data is observed.

In some practical rotor-dynamic installations, the response at particular shaft stations (e.g. turbine disc locations) may be of greater importance than the overall system response. In such circumstances the choice of type and location of control could be critical. This point is illustrated in Fig. 7.12e where the receptance, as measured at probe 2 only, is shown as a function of frequency for radial and angular excitation. Although the receptance resulting from radial excitation is generally greater than that due to angular excitation, there exists a substantial speed range (2250 - 3350 cyc/min) where application of radial control at the specified location would have little influence on the response at the shaft station corresponding to probe 2. Once more the predicted response plots (Fig. 7.12f) were found to agree extremely well with the measured data.

With the shaft mounted on flexible supports (K_B = 0.309×10^6 N/m), the shaft rms receptance plots for the two points of excitation (Fig. 7.12b) are shown in Fig. 7.12g. Receptance ratios, as defined in Test 6a, are presented for comparison with earlier results at the same shaft frequencies, the introduction of support flexibility is seen to result in an increase in the receptance ratios, thus indicating a relative deterioration in angular control performance in such circumstances. The relative increase in angular force requirements is seen to range

from 24% at low frequency (1100 cyc/min) to 150% at the higher frequencies (4700 cyc/min).

The appearance of a blunt peak in the response plots at a frequency of approximately 2800 cyc/min is a result of the introduction of rigid-body modes. The form of the response plots at this frequency is thought to be due to the small amount of damping present within the shaker assembly, these modes being more sensitive to external damping than the shaft flexural modes (Section 5.3.2).

7.5.8 A Note on Shaft Reverse-Whirls

A number of researchers [46,67,118] have shown theoretically that certain rotor systems may exhibit reverse-whirl characteristics within specific speed ranges. However, the phenomenon is rarely observed in practice [67,120].

Throughout the test program described within this chapter, in certain circumstances the test shaft was seen to vibrate in a distinctly odd manner. The shaft motion appeared to continually change from a 'bobbing' to a whirling type motion. Close examination of the shaft orbit showed that the shaft was whirling alternately in a forward and reverse sense and that a transition point occurred where pure translatory (straight-line) motion ensued.

Pederson [120] showed theoretically how, for an undamped uniform shaft mounted on isotropic supports, the natural frequencies are grouped in pairs with the numerically smallest natural frequency of a pair

corresponding to backward precession and the higher frequency corresponding to forward precession. The introduction of gyroscopic effects further separates the natural frequencies in each pair and thus, given the above conditions, would lead to an extension of the region of reverse whirl.

With the above in mind, a test shaft employing steel, shaft-mounted discs having substantial polar inertia and mounted on anisotropic supports, was examined (Fig. 7.13a).

The shaft first critical speeds in the horizontal and vertical planes were found to occur within the speed range 885 - 900 rpm, more accurate measurement being limited by the degree of speed control available. The measured (using probes 4, 5 and 6) and predicted shaft rms displacement responses are presented in Fig. 7.13b. The theoretical and experimental data agree very well, an error of approximately 1.7% occurring in the predicted peak response speed.

The first two system eigenvalues were predicted and plotted as a function of shaft speed in Fig. 7.13c. The computed critical speeds in the vertical and horizontal planes are 854 rev/min and 864 rev/min respectively. Examination of the real and imaginary components of the correponding eigenvectors, in accordance with the procedures outlined in Appendix A, showed the lower critical speed to be of a retrograde nature. The higher critical speed corresponded to a forward whirl motion. It might be assumed that in the region between these two

critical speeds the shaft would whirl in a reverse direction. This would be the case only if no gyroscopic influences were present since shaft straight-line motion (the point of transition between forward/reverse whirl), would ensue at each critical speed. When gyroscopic effects are included, the region of reverse whirl would be shifted as shown in Fig. 7.13d which is a plot of the orbit semi-axes against shaft speed.

For the above test arrangement (Fig. 7.13a), shaft-orbits were recorded at speeds below, above and between the two critical speeds. The results are presented in Fig. 7.14a where reverse whirl is observed to occur at a shaft speed of 890 rpm.

It was found during testing that the introduction of a small amount (2.0 Nms/rad) of angular electromagnetic damping led to the elimination of shaft reverse whirling (Fig. 7.14b). The presence of significant damping in many practical rotor arrangements probably accounts for the absence of shaft retrograde precession in real systems. In Appendix F the simple case of a damped Jeffcott-rotor with anisotropic supports was considered and the limits for elimination of reverse whirl determined. The results are expressed in graphical form and presented in Fig. F.1. It is shown that relatively low damping levels are effective in eliminating reverse whirl, even when significant support anisotropy is present.

Results of a theoretical analysis of the test rotor

for three different angular damping rates (0, 0.1, 2.0 Nms/rad) are presented in Figs. 7.13e and 7.15. With the damping rate set at 2.0 Nms/rad, reverse whirl is completely eliminated, in agreement with test observations. The introduction of an intermediate damping value (0.1 Nms/rad) is not sufficient to eliminate backward precession but does limit the speed range over which this occurs.

Finally, it is worth noting that although the introduction of gyroscopic effects alone may result in the creation of reverse whirl modes, these will not be excited by synchronous unbalance forces unless some support anisotropy exists [120].

7.5.9 Summary

Dynamic response predictions, for a number of test shaft arrangements, using a transfer-matrix program, showed reasonable and in many cases excellent, agreement with experimental data.

The application of external damping using mechanical dashpots highlighted the inherent disadvantages of employing a device whose construction necessitates physical contact with a rotating element.

In direct contrast angular control of a high-speed rotating shaft using an electromagnetic actuator has been shown to be a feasible and worthwhile proposition. The device can be employed to implement a variety of control strategies leading to significant system synchronous and asynchronous response attenuation.

Measurement of relevant test-shaft receptances has shown that the forces required for implementation of angular control are of the same order of magnitude as and in some instances less than, those demanded using radial control for the same degree of vibration attenuation.

CHAPTER 8

CONCLUSIONS

A summary of the theoretical and experimental work performed during this project, along with important findings, is presented. Suggestions for further research are also provided.

8.1 Theoretical Work

a) A program based on the Transfer Matrix Technique was created and extensively employed for the dynamic analysis of a variety of rotor-bearing systems. A general procedure incorporating the modified TM method, to be used for the free-vibration analysis of multi-level systems, is presented. Using this approach the demands on computer memory are minimal and the possibility of numerical instability is substantially reduced.

The program allows for the investigation of 'real-life' effects such as: i) mass unbalance, ii) multiple multi-level supports possessing radial and angular stiffness, damping and mass/inertia characteristics, iii) shaft initial-bend, iv) gyroscopic/rotary inertia couples and shear deflection.

Using the program to predict critical speeds, unbalanced response and influence coefficients for a number of test-shaft cases, good agreement with the results of other workers, and those from available closed-form solutions, was achieved.

Whilst employment of the modified TM method was shown

to be successful in all cases, in providing accurate high-frequency shaft mode-shapes, in some instances this same accuracy could not be achieved using the normal method.

b) A procedure enabling prediction of optimal control parameters for any number of control devices located at chosen points on the rotor-bearing system was developed. The method entailed the employment of a two-stage transfer matrix analysis in conjunction with a multi-variable optimisation algorithm, allowing minimisation of any chosen system response parameter. Since the transfer matrix technique was utilised, computer memory requirements were reduced significantly in comparison to those of other available methods. Additionally, repetitive shaft-system analyses were avoided thus leading to increased computational efficiency.

Accuracy of the technique was assessed and confirmed through its application to a number of shaft cases incorporating a variety of support configurations. Comparison of results with those obtained using a 'fixed-point' procedure showed excellent agreement.

c) A comprehensive study of the relative performance of angular and radial controllers, when applied to various shaft arrangements, was implemented employing the newly-created optimisation technique. Attenuation of system synchronous response was examined for both modes of control. Three performance indices were considered for comparison:

1. Shaft maximum displacement.
2. Shaft sum of squares of displacement.

3. Total bearing force.

The main findings were as follows:

i) Effect of Choice of Performance Index

Shaft maximum displacement and sum of squares of displacement were found to be equivalent response functions, minimisation of each leading to identical control requirements. Miminisation of total bearing force resulted in the employment of optimum control parameters and controller locations, in general, different from those predicted using either of the above two performance indices.

ii) Optimum Control Locations and Control Coefficients

For a shaft speed range encompassing the first three rigid-bearing critical speeds:

1) The optimum radial controller location is at a point approximately 10% of the shaft span from the supports and appears to be relatively insensitive to the support stiffness magnitude.

2) The optimum location for angular control is seen to depend on the choice of performance index and occurs at the shaft supports and at a position close to the shaft centre when employing the shaft maximum displacement (or sum of squares of displacement) and total bearing force criteria respectively.

3) With the controllers employed at their optimum locations, for a reasonable value of angular controller equivalent radius the optimum angular damping levels are of the same order as those of

the radial controller. Although in these circumstances system response attenuation using radial control was found to be greater than that resulting from angular control, in many circumstances the difference may not be substantial.

iii) Control at Shaft Supports

From a practical point of view the control forces should, ideally, be introduced at the shaft supports. The results of such a study, therefore are of great significance.

The investigation showed that for large support stiffness values, angular control is far superior (both in terms of minimised response and force requirements) to radial control, this trend reversing as the support stiffness is decreased.

However, even for fairly low support stiffnesses, angular control may still be the more effective of the two, particularly over the lower end of the shaft speed range.

When support stiffness is low and angular control is employed, there appears to be little advantage in utilising an adaptive control procedure since passive angular control is almost as effective. Similarly, passive control is to be preferred in the case of radial control of a system with relatively stiff supports.

iv) Adaptive Versus Passive Control

In a number of cases the introduction of an adaptive

control strategy will lead to system response levels significantly lower than those which could be obtained by the employment of an equivalent passive device.

In many of these cases, however, continuous adaptive control may not be necessary and may be replaced by an equivalent simpler approach, whereby the control effect is 'switched' on and off at rotor speeds determined by the system dynamic characteristics.

d) Theoretical studies, performed and described within, have shown that in rotor systems containing elements which may exhibit destabilising characteristics (e.g. oil-film bearings), system stability may be considerably improved by the application of external radial or angular control forces.

Substantial increases in instability threshold speeds can be realised even when low control-damping levels are employed. The introduction of angular damping at an oil-film bearing was found to be an efficient means of system stability control. In contrast, whilst certain shaft modes may be stabilised using radial control at the bearings other modes may in fact have their stability margin considerably reduced. In addition, radial damping requirements were found to be greater than those for the angular device.

A new means of attenuating rotor-system response has been proposed and investigated theoretically. Situations have been shown to exist where angular control would

provide a viable alternative to the conventional radial methods. Indeed, it should be borne in mind that the theoretical analyses undertaken unavoidably provide the radial control procedures with an unfair advantage since access limitations in practice may invalidate many of the desirable features of this approach.

8.2 Experimental Work

An extensive test program requiring the design, construction and experimental analysis of a number of test-shaft arrangements was undertaken to:

1. Enable assessment of the (transfer matrix) analysis program in predicting rotor-system unbalance response.
2. Investigate the effectiveness of external control, particularly angular electromagnetic control, in attenuating system response.

The shaft arrangements investigated were such that, in the operational speed range, a maximum of one critical speed per plane was encountered. The main findings were as follows.

a) The measured response of an initially-bent, uniform shaft mounted on rigid supports was found to agree very closely with the response predicted using a numerical analysis program created specifically for the project.

System natural frequencies were predicted to within a few percent of their measured values.

Shaft non-synchronous vibrations were evident throughout the test work. Their presence was found to be

mainly due to the combination of shaft/coupling stiffness asymmetry and gravitational effect.

b) The effect of introducing radial viscous damping to the bent-shaft system, using mechanical dashpots, was assessed.

With the dampers placed close to the shaft mid-span, a substantial reduction in system response could be achieved. Gradual re-location of the dampers towards the shaft supports resulted in a progressive deterioration of the system response. When the mechanical dampers were positioned at a shaft location corresponding to a distance of one-eighth of the shaft span from a shaft support, the first critical speed could not be traversed.

A representative system response function, computed as the root-mean-square of a number of measured shaft displacements, was plotted and displayed clearly-defined 'fixed-points'. The benefit of switching between control-damping levels at the system 'fixed-points' was evident from the experimental results, thus confirming the validity of the earlier theoretical analyses concerning the application of an adaptive "on-off" control strategy.

The mechanical dampers employed exhibited highly non-linear characteristics making their modelling extremely difficult. In addition, their damping rate was found to decrease significantly with increasing excitation-frequency at high shaft speeds, rendering them relatively ineffective. Because of these effects and other related problems, agreement between predicted and measured shaft response was not as good as for the undamped case.

A number of difficulties experienced with the mechanical dampers highlighted the possible benefits of utilising a non-contact control device.

c) The main portion of the experimental work involved the design, construction and application of an angular electromagnetic actuator on a variety of test-shaft configurations.

The controller was mounted close to the test-rotor drive-end bearing. Throughout the tests reasonably good agreement between predicted and measured, controlled and uncontrolled, system response was observed, even though the inherent non-linear characteristics of this device resulted in a fairly complex analysis procedure.

The controller was capable of simulating damping and or stiffness control forces, the level of which could be easily altered by keyboard input or software instruction using a microprocessor.

When employed as a damper the device was found to be effective in attenuating synchronous and non-synchronous shaft response and transmitted bearing forces - control damping factors of .26 and .58 being recorded for the system first and second modes respectively.

Significant increases in the system natural frequencies (17% in one case) were realised by utilising the electromagnetic actuator as a stiffness element. This led to a considerable reduction in response levels within specific shaft speed/frequency ranges.

The benefits of this type of control were further extended by implementing an adaptive stiffness control

procedure whereby system control was applied up to a shaft speed corresponding to the first 'fixed-point' and thereafter removed. This approach resulted in a reduced system response over the complete shaft-speed range, in agreement with theoretical predictions.

Calibration of the electromagnetic controller, using a specially designed and constructed force-transducer, provided the relevant information regarding the dynamic characteristics of the controller for use in the analysis program. As expected, the linearised damping coefficients were observed to be directly proportional to the shaft-slope feedback signal and excitation frequency, whilst the stiffness coefficients were found to be a linear function only of the former parameter.

The measured force/current/gap relationships showed relatively good agreement with those predicted using simple magnetic-circuit theory.

The control hardware was found to function well over a frequency range of 0 - 100 Hz, although at the higher frequencies, the influence of control circuit component phase-lags did produce some deterioration in performance.

In test-shaft arrangements having bearings possessing anisotropic stiffness properties, shaft reverse-whirl phenomena were observed. In these cases the introduction of a small amount of angular electromagnetic damping resulted in the elimination of this effect.

d) The relative merits of radial and angular control were considered by comparing measured system receptances over a frequency range encompassing two natural

frequencies. Results were in excellent agreement with theory and showed the increase in efficiency of the radial approach when support flexibility was increased.

In summary, results from experimental work on a laboratory rig have shown that angular control is a feasible and practical means of vibration control. The employment of an electromagnetic actuator to implement this type of control results in a number of advantages which may not be realised using other available devices. The lack of physical contact between controller and shaft system, along with the possibility of simple implementation of a variety of control strategies, are just two of the features which make the electromagnetic actuator a most useful tool in the field of vibration control.

8.3 Suggestions for Further Work

The work performed and described within this thesis represents only a small step towards assessing the capabilities of the various means of shaft vibration control and in particular, those of angular control. The following proposals are made with a view to extending the knowledge in this field. Item 1 below is suggested with the main aim of improving the operational aspects of the particular controller utilised for the present studies, items 2 and 3 being of a more general nature.

1. Steps should be taken to modify the electromagnet control circuitry to achieve linear operation of the control device. This would simplify considerably

the analysis procedures, since a much less complex controller model could be utilised. Some form of circuit compensation is also required to eliminate unwanted component phase-lags and to ensure stable controller performance at all times.

2. Experimental investigations into the relative performance of angular/radial electromagnetic controllers need to be conducted on a more realistic rotor system. The rig employed should incorporate oil-film bearings and have a shaft speed range covering at least two shaft critical-speeds.

3. A study should be conducted with the object of rationalising controller performance data, taking into account parameters such as controller size and power (or energy dissipation rate for a passive device) requirement necessary to ensure the attainment of some pre-defined standard criteria. This would allow proper evaluation and comparison of a variety of available control devices.

REFERENCES

1. Rankine, W.J. "On the centrifugal force of rotating shafts". The Engineer, Vol. XXVII, 249, April 1869.

2. Dunkerly, S. "On the whirling and vibration of shafts". Phil. Trans. Royal Society, June 1894.

3. Chree, C. "The whirling and transverse vibrations of rotating shafts", Phil. Mag., 1904.

4. Rayleigh. "The theory of sound". 2nd Edn., London, MacMillan & Co., 1894.

5. Jeffcott, H.H. "The lateral vibration of loaded shafts in the neighbourhood of a whirling speed - the effect of want of balance". Phil. Mag., Vol. XXXVII, March 1919.

6. Kimball, R.L. and Hull, E.H. "Vibration phenomena of a loaded unbalanced shaft while passing through its critical speed". Trans. ASME, Vol. 47, 673, 1925.

7. Stodola, A. "Steam and gas turbines". McGraw-Hill Book Co. Inc., New York, 1927.

8. Bishop, R.E.D. "Unbalanced and initially bent shafts". Engineering, Vol. 190, 735, 1960.

9. Parkinson, A.G., Jackson, K.L. and Bishop, R.E.D. "Some experiments on the balancing of small flexible rotors: Part 2 - Experiments". J. Mech. Engng. Sci., Vol. 5, 133, 1963.

10. Myklestad, N.O. "A new method of calculating natural modes of uncoupled bending vibration of aeroplane wings and other types of beams". Journal of Aero Science, Vol. 11, 153, 1944.

11. Prohl, M.A. "A general method for calculating critical speeds of flexible rotors". ASME Journal of Applied Mechanics, Vol. 12, Sept. 1945, PA142.

12. Holzer, H. "Die berechrung der drehschwingungen". Springer Verlag OGH, Berlin, 1921. Republished by J.W. Edwards Publisher Inc., Ann Arbor, Michigan, USA.

13. Linn, F.C. and Prohl, M.A. "The effect of flexibility of supports upon the critical speeds of high-speed rotors". Trans. SNAME, Vol. 59, 536-553, 1951.

14. Kimball, A. "Vibration prevention in engineering". John Wiley, New York, 1932.

15. Caruso, W.J. "Prediction of critical speeds of steam turbines by dynamic stiffness method". ASME Colloqium on Mechanical Impedance Methods for Mechanical Vibrations, 1959.

16. Gladwell, G.M.L. "The approximation of uniform beams in transverse vibration by sets of masses elastically connected". Proc. 4th US Nat. Congress of Applied Mechanics, Amer. Soc. Mech. Engrs., 169-176, 1962.

17. Pestel and Leckie. "Matrix methods in elastomechanics". McGraw-Hill Book Co. Inc., London 1963.

18. Ruhl, R.L. "Dynamics of distributed parameter rotor systems: transfer matrix and finite element techniques". PhD Thesis, Cornell University, USA, 1970.

19. Koenig, E.C. "Analysis of calculating lateral vibration characteristics of rotating systems with any number of flexible supports: Part 1 - Method of analysis". Journal of Applied Mechanics, Vol. 28, 585, 1961.

20. Guenther, T.G. and Lovejoy, D.C. "Analysis of calculating lateral vibration characteristics of rotating systems with any number of flexible supports: Part 2 - Application of the method of analysis". Journal of Applied Mechanics, Vol. 28, 591, 1961.

21. Smith, D.M. "The motion of a rotor carried by a flexible shaft in flexible bearings". Proc. Roy. Soc. (A), Vol. 142, 92, 1933.

22. Kirk, R.G. and Gunter, E.J. "The effect of support flexibility and damping on the synchronous response of a single-mass flexible rotor". Trans. ASME Jnl. Engng. Ind., Vol. 94, 1972.

23. Holmes, R. "The vibration of a rigid shaft on short-sleeve bearings". Jnl. Mech. Engng. Sci., Vol. 2, No. 4, 337-341, 1960.

24. Lund, J.W. "Review of analytical methods in rotor-bearing dynamics". Tribology Int., Vol. 13, 233-236, 1980.

25. Capriz, G. "On the vibrations of shafts rotating on lubricated bearings". Annali Mat. Pura. Appl., Vol. 4, 5, 1960.

26. Bannister, R.H. "Theoretical and experimental investigation illustrating the influence of non-linearity and misalignment on the eight oil-film force coefficients". Conf. on Vibrations in Rotating Machinery, Inst. Mech. Engrs., Cambridge 1976, Paper No. C219/76.

27. Lund, J.W. and Orcutt, F.K. "Calculations and experiments on the unbalance response of a flexible rotor". Jnl. of Engng. for Ind., 785, 1967.

28. Gasch, R. "Vibrations of large turbo-rotors in fluid film bearings on an elastic foundation". J. Sound Vib., Vol. 47, 53-73, 1976.

29. Ramsden, J.N. and Stoker, J.R. "The solution of a vibration problem on a turbine-compressor set mounted on a steel foundation". Proc. Inst. Mech. Engrs., Vol. 191, 135-145, 1977.

30. Hensman, N., Reeves, C.W., Ruddy, A.V. and Taylor, C.M. "A theoretical and experimental analysis of the rotor-dynamics of a high pressure steam turbine on a large ammonia plant". Conf. on Vibrations in Rotating Machinery, Cambridge 1980, Inst. Mech. Engrs., Paper No. C295/80.

31. Wang, Z. and Lund, J.W. "Calculations of long rotors with many bearings on a flexible foundation". Conf. on Vibrations in Rotating Machinery, York 1984, Inst. Mech. Engrs., Paper No. C291/84.

32. Adams, M.L. "Non-linear dynamics of flexible multi-bearing rotors". Jnl. Sound Vib., Vol. 71, 129-144, 1980.

33. Newkirk, B.L. "Shaft whipping". General Electric Review, Vol. 27, 169, 1924.

34. Kimball, A.L. "Internal friction theory of shaft whirling". General Electric Review, Vol. 27, 244, 1924.

35. Robertson, D. "Hysteretic influences on the whirling of rotors". Proc. Inst. Mech. Engrs., London, Vol. 131, 513, 1935.

36. Dimentberg, F.M. "Flexural vibrations of rotating shafts". Published by Butterworth, London, 1961.

37. Tondl, A. "Some problems of rotor-dynamics". Published by Chapman and Hall, 1965.

38. Newkirk, B.L. "Shaft whipping due to oil action". General Electric Review, 1925.

39. Hori, Y. "A theory of oil whip". Trans. ASME, J. App. Mech., Vol. 81, 189-198, 1959.

40. Hagg, A.G. and Warner, P.C. "Oil whip of flexible rotors". Trans. ASME, Vol. 75, 1339-1344, 1953.

41. Newkirk, B.L. and Lewis, J.F. "Oil-film whirl. An investigation of disturbances due to oil-film in journal bearings". Trans. ASME, Vol. 78, 21-27, 1956.

42. Reiger, N.F. "Rotor-bearing dynamics state of the art". Mechanism and Machine Theory, Vol. 12, 261-270, Pergamon Press, GB, 1977.

43. Dostal, M., Roberts, J.B. and Holmes, R. "Stability control of flexible shafts supported on oil-film bearings". Jnl. Sound Vib., Vol. 35, 361-377, 1974.

44. Kikuchi, K. and Kobayashi, S. "Stability analysis of a rotating shaft system with many bearings and discs". Bull. JSME, Vol. 20, No. 150, 1592, Dec. 1977.

45. Murphy, B.T.and Vance, J.M. "An improved method for calculating critical speeds and rotor-dynamic stability of turbomachinery". Trans. ASME, Jnl. Engng. Power, 82-GT-294, 1982.

46. Lund, J.W. "Stability and damped critical speeds of a flexible rotor in fluid film bearings". Jnl. Engng. Ind., Trans. ASME, Series B, Vol. 96, No. 2, 509, 1974.

47. Kirk, R.G. and Gunter, E.J. "Transient response of rotor-bearing systems". Trans. ASME, Jnl. Engng. Ind., 682-690, May 1974.

48. Smith, D.M. "Recognition of the causes of rotor vibration in turbomachinery". Conf. on Vibrations in Rotating Machinery, Cambridge 1980, Inst. Mech. Engrs., Paper No. C251/80.

49. El-Hadi, I. Zusammenstellung, kritische untersuchung und weiterentwicklung der verfahren zum auswuchten betriebsmabig aufgesttellter maschinen mit starren und mit elastischen laufern, 1962.

50. Goodman, T.M. "A least-squares method for computing balancing corrections". Trans. ASME, Jnl. Engng. Ind., Series B, Vol. 86, No. 3, 273-279, 1964.

51. Larsson, L.O. "On the determination of the influence coefficients in rotor balancing, using linear regression analysis". Conf. on Vibrations in Rotating Machinery, Cambridge 1976, Inst. Mech. Engrs., Paper No. C173/76.

52. Dreschlen, J. "Processing surplus information in computer aided balancing of large flexible rotors". Conf. on Vibrations in Rotating Machinery, Cambridge 1976, Inst. Mech. Engrs.

53. Balda, M. "Balancing flexible rotors as a problem of mathematical programming". Conf. on Vibrations in Rotating Machinery, Cambridge 1976, Inst. Mech. Engrs.

54. Bishop, R.E.D. and Gladwell, G.M.L. "The vibration and balancing of an unbalanced flexible rotor". J. Mech. Engng. Sci., Vol. 1, No. 1, 66-77, 1959.

55. Bishop, R.E.D. and Parkinson, A.G. "Residual vibration in modal balancing". J. Mech. Engng. Sci., Vol. 7, No. 1, 33-39, 1965.

56. Moore, L.S. and Dodd, E.G. "Mass balancing of large flexible rotors". GECJ, Vol. 31, No. 2, 74-83, 1964.

57. Giers, A. "Practice of flexible rotor balancing". Conf. on Vibrations in Rotating Machinery, Cambridge 1976, Inst. Mech. Engrs.

58. Kellenberger, W. "Should a flexible rotor be balanced in N or (N + 2) planes?". ASME Paper No. 71, Vibr. - 55, 1971.

59. Kendig, J.P. "Comparative study of methods for flexible rotor balancing". MSc Thesis, Dept. of Mech. Engng., Rochester Inst. of Techn., Rochester, N.Y., 1975.

60. Parkinson, A.G., Darlow, M.S., Smalley, A.J. and Badgley, R.H. "An introduction to a unified approach to flexible rotor balancing". ASME Paper 79-GT-161, March 1979.

61. Darlow, M.S., Smalley, A.J. and Parkinson, A.G. "A unified approach to the flexible rotor balancing: Outline and experimental verification". Conf. on Vibrations in Rotating Machinery, Cambridge 1980, Inst. Mech. Engrs., Paper No. C340/80.

62. Burrows, C.R. and Stanway, R. "A coherent strategy for estimating linearised oil-film coefficients". Proc. R. Soc. Lond., A370, 89-105, 1980.

63. Lin, Y.K. and Donaldson, B.K. "Brief survey of transfer matrix techniques". Jnl. Sound Vib., Vol. 10, 103, 1970.

64. Cunningham, R.E. "Steady-state unbalance response of a three disc flexible rotor on flexible damped supports". Trans. ASME, Jnl. Mech. Design., Vol. 100, Part 3, 563-573, 1978.

65. Nikolajsen, J.L. and Holmes, R. "Investigation of squeeze-film isolators for the vibration control of a flexible rotor". J. Mech. Engng. Sci., Vol. 21, 247-252, 1979.

66. Gunter, E.J., Barrett, L.E. and Allaire, P.E. "Stabilisation of turbomechinery with squeeze-film dampers - theory and applications". Conf. on Vibrations in Rotating Machinery, Cambridge 1976, Inst. Mech. Engrs., Paper No. C233/76.

67. Den Hartog, J.P. "Mechanical vibrations". 4th Edn., McGraw-Hill, New York, 1956.

68. Sandler, B. "Adaptive mechanisms, (automatic vibration control)". J. Sound Vib., Vol. 73, No. 2, 161-175, 1980.

69. Burrows, C.R., Sahinkaya, M.N. and Turkey, O.S. "An adaptive squeeze-film bearing". Trans. ASME, Jnl. Lubrication Tech., 83-Lub-23, 1983.

70. Goodwin, M.J., Penny, J.E.T. and Hooke, C.J. "Variable impedance bearings for turbogenerator rotors". Conf. on Vibrations in Rotating Machinery, York 1984, Inst. Mech. Engrs., Paper No. C288/84.

71. Olson, H.F. "Electronic control of noise, vibration and reverberation". J. Acoust. Soc. Am., Vol. 28, 966-972, 1956.

72. Abu-Akeel, A.K. "The electrodynamic vibration absorber as a passive or active device". Trans. ASME, Series B, J. Engng. Ind., Vol. 89, 741-753, 1967.

73. Roorda, J. "Experiments in feedback control of structures". Solid Mech. Arch., Vol. 5, No. 2, 131-163, 1980.

74. Sankar, S. and Guntur, R.R. "Pneumatic vibration control using active force generators". The Shock and Vibration Bulletin, May 1981, The Shock and Vibration Information Centre, Naval Research Laboratory, Washington DC, No. 51 Part 1.

75. Seto, K. and Yamanouch, M. "Effect of a variable stiffness type dynamic absorber with eddy current damping". Bull. Jap. Soc. of Mech. Eng., Vol. 21, Part 160, 1482-1489, 1978.

76. Krasnicki, E.J. "The experimental performance of an 'on-off' active damper". The Shock and Vibration Bulletin, May 1981, The Shock and Vibration Informatin Centre, Naval Research Laboratory, Washington DC, No. 51.

77 Rockwell, T.H. and Lawther, J.M. "Theoretical and experimental results on active vibration dampers". Jnl. Acoust. Soc. Am., Vol. 36, No. 8, 1964.

78. Hughes, E. "Electrical technology". 4th Edn., Longman, 1973.

79. Klimek, K. "A contribution to the measurement technique using electromagnetic suspension". (In Germany) Deutsche Luft-und Raumfahrt, Forschungsbericht 72-30, 1972.

80. Braunbeck, W. "Free suspension of bodies in electric and magnetic fields". Z. Phys., Vol. 112, 735-763, 1939.

81. Jayawant, B.V. et al. "Development of 1 ton magnetically suspended vehicle using controlled dc electromagnets". Proc. Inst. Elect. Engrs., Vol. 123, No. 9, 941-948, 1976.

82. Schweitzer, G. and Ulbrich, H. "Magnetic bearings - a novel type of suspension". Int. Conf. on Vibrations in Rotating Machinery, Inst. Mech. Engrs., London, Cambridge 1980.

83. Schweitzer, G. "Stabilisation of self-excited rotor vibrations by an active damper". Dynamics of Rotors, ed. F.I. Niordsen, Springer-Verlag, Berlin, 472-493, 1975.

84. Schweitzer, G. and Lange, R. "Characteristics of a magnetic rotor bearing for active vibration control". Conf. on Vibrations in Rotating Machinery, Inst. Mech. Engrs., Cambridge 1976, Paper No. C239/76.

85. Ellis, R.W. and Mote, C.D. "A feedback vibration controller for circular saws". J. Dyn. Syst. Meas. Control., Trans. ASME, 44-49, March 1979.

86. Ellis, R.W. "Active electromagnetic vibration control in rotating discs". PhD Dissertation, University of California, Dept. of Mech. Engng., Berkeley, Jan. 1977.

87. Nikolajsen, J.L., Holmes, R. and Gondhalekar, V. "Investigation of an electromagnetic damper for vibration control of a transmission shaft". Proc. Inst. Mech. Engrs., Vol. 193, No. 31, 331-336, 1979.

88. Habermann, H. and Liard, G. "An active magnetic bearing system". Tribology Int., Vol. 13, 85-89, 1980.

89. Blueler, H. and Schweitzer, G. "Decentralised control". Applied Control and Identification Symposium, IASTED, Copenhagen, 1983.

90. Salm, J. and Schweitzer, G. "Modelling and control of a flexible rotor with magnetic bearings". Conf. on Vibrations on Rotating Machinery, Inst. Mech. Engrs., York 1984, C277/84.

91. Dostal, M., Roberts, J.B. and Holmes, R. "The effect of external damping on the vibration of flexible shafts supported on oil-film bearings". J. Sound Vib., Vol. 51, 69-87, 1977.

92. Burrows, C.R. and Sahinkaya, M.N. "Vibration control of multi-mode rotor bearing systems". Proc. R. Soc., London, A386, 77-94, 1983.

93. Argyris, J.H. "Energy theorems and structural analysis". Aircraft Engineering, Oct. 1954.

94. Kaya, F. "Vibration control of flexible shafts supported on journal bearings". PhD Dissertation, University of Sussex, 1981.

95. Vernon, J.B. "Linear vibration theory". New York, John Wiley, 1967.

96. Ruhl, R.L. and Booker, J.F. "A finite element model for distributed parameter turborotor systems". Trans. ASME, Jnl. Engng. Ind., Feb. 1972, 126-132.

97. Morton, P.G. "On the dynamics of large turbo-generator rotors". Proceedings Inst. Mech. Engrs., Vol. 180, Part 1, No. 12, 1965-66.

98. Matsushita, O., Ida, M. and Takahashi, R. "Application of quasi-modal concept to rotational ratio response analysis and new balancing". Conf. on Vibrations in Rotating Machinery, York 1984, Inst. Mech. Engrs., Paper No. C319/84.

99. Marguerre, K. and Uhrig, R. "Calculation of multi-term linked systems: 1, the transmission method and its limitations". Zeitschrift Fur Angewandte Mathematik und Mechanik, 44, 1964, (I/2), 1-21 (in German).

100. McLean, R.F. "The analysis of critical speeds using the modified transfer matrix and dynamic stiffness techniques". Conf. on Vibrations in Rotating Systems, Inst. Mech. Engrs., 1972.

101. Turkay, O.S. "Adaptive vibration control using squeeze-film bearing". PhD Dissertation, University of Sussex, 1982.

102. Allaire, P.E., Lewis, D.W. and Jain, V.K. "Feedback control of a single mass rotor on rigid supports". Jnl. Franklin Institute, Vol. 312, No. 1, 1-11, July 1981.

103. Roark, R.J. and Young, W.C. "Formulas for stress and strain". McGraw-Hill Ltd., 5th Edn., 1975.

104. Lewis, F.M. "The extended theory of the viscous vibration damper". Jnl. Applied Mechanics, Trans. ASME, Vol. 77, 377, 1955.

105. Pilkey, W.D., Wang, B.P. and Vannoy, D. "Efficient optimal design of suspension systems for rotating shafts". Jnl. Engng. Ind., Trans. ASME, Aug. 1976.

106. The Electrical Year Book, Model and Allied Publications, Argus Books Ltd., England, 1975.

107. Draper, A. "Electrical machines". 2nd Edn., Longman Group Ltd., London, 1974.

108. Bansal, P.N. and Kirk, R.G. "Stability and damped critical speeds of rotor-bearing systems". Jnl. Engng. Ind., Trans. ASME, Nov. 1975.

109. Rao, J.S. "Rotor dynamics". Wiley Eastern Ltd., 1983.

110. Wang, B.P. and Pilkey, W.D. "Limiting performance characteristics of steady-state systems". Jnl. Applied Mechanics, Trans. ASME, Sept. 1975.

111. Gondhalekar, V. and Holmes, R. "Design of a radial electromagnetic bearing for the vibration control of a supercritical shaft". Proc. Inst. Mech. Engrs., Vol. 198C, No. 16, 1984.

112. Bishop, R.E.D. and Gladwell, G.M.L. "An investigation into the theory of resonance testing". Phil. Trans. A, 255, 241, 1962.

113. Kennedy, C.C. and Pancu, C.D.P. "Use of vectors in vibration measurement and analysis". J. Aero. Sci., 14, 603, 1947.

114. Neumark, S. "Concept of complex stiffness applied to problems of oscillations with viscous and hysteretic damping". RAE Report No. Aero. 1592-ARC 20.038, 1957.

115. MSc class notes. "Experimental stress analysis". Strathclyde University, Glasgow, 1980-81.

116. Manual on Experimental Stress Analysis, 3rd Edn., edited by A.S. Kobayashi, Society for Experimental Stress Analysis, 1978.

117. Little, R.M. and Pilkey, W.D. "A linear programming approach for balancing flexible rotors". Jnl. Engng. Ind., Trans. ASME, Aug. 1976.

118. McCallion, H. "Vibration of linear mechanical systems". Longman Group Ltd., London, 1973.

119. Tse, F.S., Morse, I.E. and Hinkle, R.T. "Mechanical vibrations - theory and applications". 2nd Edn., Allyn & Bacon Inc., London, 1978.

120. Pederson, P.T. "On forward and backward precession of rotors". Ingenieur-Archiv. 42 (1972), S.26-41.

APPENDIX A

SHAFT ORBITAL MOTION

If a rotating shaft is subjected to synchronous excitation due to, for example, mass unbalance then, in general, the shaft journal locus will be an ellipse in space, the centre of which will correspond to the unperturbed steady state shaft position. In fluid-film bearings this relative mean position will vary depending mainly upon the shaft running speed.

Referring to Fig. A.1. we can determine the characteristics of the elliptical orbit as follows.

The shaft motion may be expressed as shown,

$$w = \mathrm{Re}\,[\bar{w}e^{i\lambda t}]$$
$$v = \mathrm{Re}\,[\bar{v}e^{i\lambda t}] \qquad (A.1)$$

where Re denotes the real part of the term in brackets and,

$$\bar{W} = W_c + iW_s$$
$$\text{and } \bar{v} = v_c + iv_s$$

Since $\lambda = \alpha + i\omega$ then equations (A.1) can be rewritten as

$$w = (w_c \cos\omega t - w_s \sin\omega t)e^{\alpha t}$$
$$\text{and } v = (v_c \cos\omega t - v_s \sin\omega t)e^{\alpha t}$$

For forced synchronous motion $\alpha = 0$ and $\omega = \Omega$ so that,

$$\begin{aligned} w &= w_c \cos\Omega t - w_s \sin\Omega t \\ \text{and } v &= v_c \cos\Omega t - v_s \sin\Omega t \end{aligned} \qquad (A.2)$$

where Ω is the shaft rotational frequency. Equations (A.2) can also be written in the form

$$\begin{aligned} w &= A_w \sin(\Omega t + \beta_w) \\ v &= A_v \cos(\Omega t + \beta_v) \end{aligned} \qquad (A.3)$$

where,

$$A_w = \sqrt{w_c^2 + w_s^2} \quad ; \quad A_v = \sqrt{v_c^2 + v_s^2}$$

and

$$\beta_w = \text{ARCTAN}\,(w_c/-w_s) \quad ; \quad \beta_v = \text{ARCTAN}\,(v_s/v_c)$$

A_w and A_v are the amplitudes of the deflections w and v respectively and β_w, β_v are the corresponding phase angles. The phase angles β represent the relative time-lag between the occurence of maximum deflection and the passing of a shaft reference point in the relevant plane.

Equations (A.2) and (A.3) describe the elliptical whirl orbit of the shaft.

Now, the instantaneous orbital radius r is given by

$$r = \sqrt{w^2 + v^2} \qquad (A.4)$$

Substituting for w and v from equations (A.2) in equation (A.4) gives,

$$r = \left[\tfrac{1}{2}\left\{w_c^2+w_s^2+v_c^2+v_s^2+(w_c^2+v_c^2-w_s^2-v_s^2)\cos 2\Omega t - 2(w_s w_c+v_s v_c)\sin 2\Omega t\right\}\right]^{\frac{1}{2}} \qquad (A.5)$$

and r reaches a maximum or minimum when

$$\frac{d}{d(\Omega t)}\left[(w_c^2+v_c^2-w_s^2-v_s^2)\cos 2\Omega t - 2(w_s w_c+v_s v_c)\sin 2\Omega t\right] = 0$$

$$\text{thus } \tan 2\Omega t = \frac{-2(w_s w_c+v_s v_c)}{(-w_s^2-v_s^2+w_c^2+v_c^2} \qquad (A.6)$$

Using equation (A.6) in (A.5) gives

$$a,b = \left[\tfrac{1}{2}\left\{w_c^2+w_s^2+v_c^2+v_s^2 \pm [(w_c^2+v_c^2-w_s^2 v_s^2)^2 + 4(w_s w_c+v_s v_c)^2]^{\frac{1}{2}}\right\}\right]^{\frac{1}{2}}$$

Where a and b are the major and minor semi-axes, of the orbital ellipse, respectively.

The orbital radius r makes an angle ψ with the y axis where,

$$\psi = \text{ARCTAN}\left[\frac{w}{v}\right] = \frac{[w_c\cos\Omega t - w_s\sin\Omega t]}{[v_c\cos\Omega t - v_s\sin\Omega t]} \qquad (A.7)$$

The maximum displacement a occurs at

$$\psi_a = \tfrac{1}{2}\text{ARCTAN}\ \frac{[2(v_c w_c+v_s w_s)]}{[(v_c^2+v_s^2-w_c^2-w_s^2)]}$$

The rotor precession rate $\dot{\psi}$ may be obtained in

terms of w and v and their derivatives by differentiating equation (A.7) with respect to time. Subsequent use of equations (A.2) along with algebraic manipulation leads to

$$\dot{\psi} = \frac{\cos^2\psi\Omega[w_c v_s - v_c w_s]}{v^2}$$

and since the term outside the square brackets is always taken as positive then the direction of shaft whirl may be determined by examination of the sign of the term $[w_c v_s - v_c w_s]$. Thus,

For forward whirl $(w_c v_s - v_c w_s) > 0$

For reverse whirl $(w_c v_s - v_c w_s) < 0$

and $(w_c v_s - v_c w_s) = 0$ indicates shaft straight line motion.

APPENDIX B

GENERAL FEEDBACK CONTROL OF A JEFFCOTT ROTOR

Radial Control ($F_{ea} = 0$)

From equation (5.3), letting $F = F_u - F_{er}$

$$F = m\ddot{x} + C_2\dot{x} + k_2x \qquad (B.1)$$

The radial displacement y at any shaft location may be expressed as:

$$y = \alpha_3[-m\ddot{x} - C_2\dot{x} + F] - \alpha_4[G_3y + G_4\dot{y}]$$

Therefore,

$$F = m\ddot{x} + C_2\dot{x} + y/\alpha_3 + \frac{\alpha_4}{\alpha_3}[G_3y + G_4\dot{y}] \qquad (B.2)$$

Where, from standard beam deflection formulae [103],

$$\alpha_3 = \frac{1}{EI}\left(\frac{L^2a}{16} - \frac{a^3}{12}\right)$$

and $$\alpha_4 = \frac{1}{6EIL}(2a^2L^2 + 2a^4 - 4a^3L)$$

From equations (B.1) and (B.2) we get

$$x = \left[\frac{1}{k_2\alpha_3} + \frac{\alpha_4G_3}{k_2\alpha_3}\right]y + \left[\frac{\alpha_4G_4}{k_2\alpha_3}\right]\dot{y} \qquad (B.3)$$

or $x = Ay + B\dot{y}$

taking the Laplace Transform

$$y = x/(A+BS) \qquad (B.4)$$

Substituting (B.3) in (B.1) and taking the Laplace Transform gives

$$\frac{F}{y} = [mBS^3+(mA+C_2B)S^2+(C_2A+k_2B)S+k_2A] \qquad (B.5)$$

Now,

$$\frac{y}{F_u} = \frac{y}{F+F_{er}} = \frac{1}{F/y+[G_3+G_4S]}\ \alpha_1$$

Therefore,

$$\frac{y}{F_u} = \frac{1}{[mBS^3+(mA+C_2B)S^2+(C_2A+k_2B)S+k_2A+[G_3+G_4S]\alpha_1]} \qquad (B.6)$$

letting, $b = a/L$; $R = \frac{r}{L}$; $f = \omega/\omega_{CR}$;

$$h_{f1} = \frac{G_1}{k_2};\quad \rho_{f1} = \frac{G_2}{2m\omega_{CR}};\quad h_{f2} = \frac{G_3}{k_2}; \qquad (B.7)$$

$$\rho_{f2} = \frac{G_4}{2m\omega_{CR}}$$

Now for forced response $F_u = me\omega^2$ and substituting equations (B.4) in equation (B.6), replacing S with $i\omega$, and making use of the relationships described in (B.7) we obtain,

$$\frac{x}{e} = \frac{f^2[1+h_{f2}E] + i[2f^3\rho_{f2}E]}{[[h_{f2}E(1-f^2)-\rho_{f2}E(4_{\rho 2}f^2)+(1-f^2+h_{f2}H)] + i[h_{f2}E(2\rho_2 f)+\rho_{f2}E(2f-2f^3)+(2\rho_2 f+2f\rho_{f2}H)]]} \qquad (B.8)$$

Where,

$E = (7b^2-32b^3+40b^4-16b^6)$

and $H = (9b^2-24b^4+16b^6)$

As a check on the above consider the following cases,

<u>No Radial Control</u>

$G_3 = G_4 = h_{f2} = \rho_{f2} = 0$

Therefore,

$$\frac{x}{e} = \frac{f^2}{(1-f^2+i2\rho_2 f)}$$

which is correct.

Radial Control at Shaft Centre

b = 0.5 Therefore E = 0 and H = 1

Therefore,

$$\frac{x}{e} = \frac{f^2}{[(1-f^2+h_{f2}) + i2f(\rho_2+\rho_{f2})]}$$

Which is again correct (refer to equation (12) in reference [102]).

Angular Control ($F_{er} = 0$)

Following a procedure similar to that employed for radial control shown above, a similar relationship may be obtained:

$$\frac{x}{e} = \frac{f^2[1+R^2h_{fi}M] + i[2fR^2\rho_{f1}M]}{[[1-f^2(1+4R^2\rho_{f1}\rho_2M)+R^2h_{f1}M(1-f^2+\frac{N}{M}^2)] + i[f(2\rho_2+2R^2\rho_2h_{f1}M)+R^2\rho_{f1}M(2f+2f\frac{N}{M}^2-2f^3)]]} \quad (B.9)$$

where,

$M = (7-48b+120b^2-144b^4)$

and $N = 3(1-4b^2)$

It should be noted that equations (B.8) and (B.9) do not hold for the limiting conditions where the radial and angular controllers are mounted at a shaft support and shaft centre respectively (refer to equation (B.4)).

APPENDIX C

STRAIN GAUGE TRANSDUCERS

C.1 General

The Wheatstone Bridge is widely employed in strain gauge applications because of it's suitability for the measurement of small changes in electrical resistance.

A variety of strain-gauge transducers may be constructed making use of the full bridge arrangement where each arm of the bridge consists of a strain-gauge as shown.

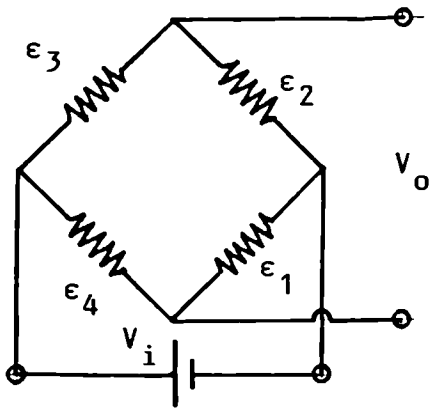

During the experimental work a Fylde D.C. strain-gauge amplifier was used in conjunction with the specially designed and constructed transducers described here. In addition to amplifying the bridge output signal considerably the amplifier also produced a constant D.C. bridge input voltage and allowed for bridge balancing through potentiometer adjustment.

Consider the above arrangement where the gauges have been bonded to the surface of a component subjected, in general, to bending and direct loading. The strain

in any gauge n may be expressed as:-

$$\varepsilon_n = \varepsilon_{Bn} + \varepsilon_{Dn} + \varepsilon_{Tn}$$

where,

ε_{Bn} = Strain due to bending.

ε_{Dn} = Stain due to direct loading.

ε_{Tn} = Strain due to temperature effects (apparent strain).

For a four-arm bridge the bridge output-volts may be expressed [115] as,

$$V_o = \frac{V_i.GF}{4} [\varepsilon_1 - \varepsilon_2 + \varepsilon_3 - \varepsilon_4]$$

$$= \frac{V_i.GF}{4} [(\varepsilon_{B1}-\varepsilon_{B2}+\varepsilon_{B3}-\varepsilon_{B4})+(\varepsilon_{D1}-\varepsilon_{D2}+\varepsilon_{D3}-\varepsilon_{D4}) +(\varepsilon_{T1}-\varepsilon_{T2}+\varepsilon_{T3}-\varepsilon_{T4})]$$

Where GF is the gauge factor and V_i the bridge input volts.

If the four gauges are mounted in close proximity it may be assumed that they are subjected to the same temperature field and generally the same environmental conditions. In these circumstances $\varepsilon_{Tn} = 0$; $n = 1, 4$ and

$$V_O = \frac{V_i.GF}{4}.[(\varepsilon_{B1}-\varepsilon_{B2}+\varepsilon_{B3}-\varepsilon_{B4})+(\varepsilon_{D1}-\varepsilon_{D2}+\varepsilon_{D3}-\varepsilon_{D4})] \quad (C.1)$$

The exact orientation of the gauges on the element under stress will determine the magnitude and sign of the direct and bending strains in equation (C.1). Thus the four-arm Wheatstone Bridge may be used effectively to construct a force transducer with the gauge positions

selected to maximise the performance of the particular device.

C.1.1 Bearing Ring Force Transducers

The strain-gauges were located as shown (i.e. gauges 1 and 3 mounted on the ring outer surface) to enable maximisation of the transducer sensitivity since $\varepsilon_{Bn} > \varepsilon_{Dn}$ for n = 1,4

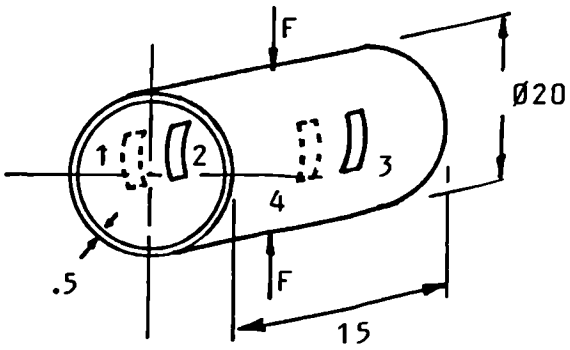

For this case

$\varepsilon_{B2} = -\varepsilon_{B1}$ and $\varepsilon_{B4} = -\varepsilon_{B3}$

$$|\varepsilon_{B1}| = |\varepsilon_{B2}| = |\varepsilon_{B3}| = |\varepsilon_{B4}| = |\varepsilon_{B}|$$

$$\varepsilon_{D1} = \varepsilon_{D2} = \varepsilon_{D3} = \varepsilon_{D4}$$

Therefore substituting the above in equation (C.1) we obtain,

$$V_0 = V_i.GF.(4\varepsilon_B)$$

For this arrangement the gauge factor was approximately 2.0. and gauge resistance 120Ω.

C.1.2 Axial Force Transducer

Since only the direct forces were of interest the gauges were connected such that bending effects could be eliminated.

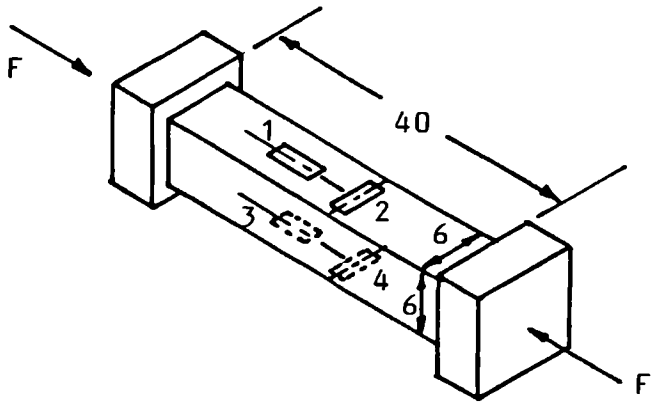

For this case,

$\varepsilon_{B1} = \varepsilon_{B3}$; $|\varepsilon_{B1}| = |\varepsilon_{B3}| = |\varepsilon_B|$

$\varepsilon_{D1} = \varepsilon_{D3} = \varepsilon_D$

$\varepsilon_{B2} = \varepsilon_{B4} = -\mu\varepsilon_B$

$\varepsilon_{D2} = \varepsilon_{D4} = -\mu\varepsilon_D$

where μ is Poisson's Ratio (for steel $\mu = 0.3$)

Substituting these equations into equation (C.1)

$$V_0 = \frac{V_i.GF.}{4}(\simeq 2.6\varepsilon_D)$$

For this arrangement semi-conductor gauges were employed with a gauge-factor of approximately 140 and gauge resistance of 350Ω.

C.1.3 Electromagnet Force Transducer

Here, due to the nature of the magnet calibration technique, only the bending effects were of interest.

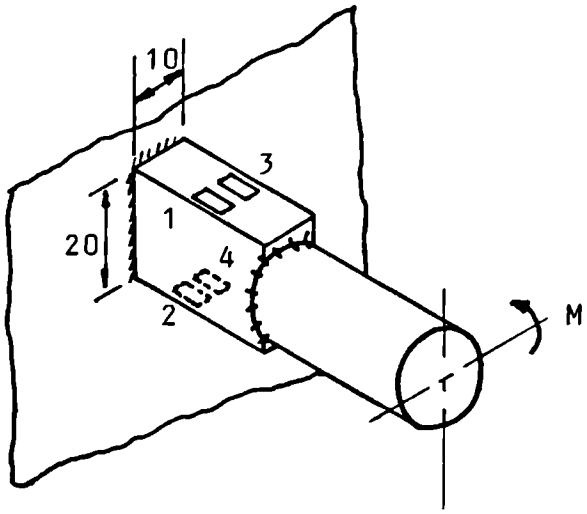

For this case,

$$\varepsilon_{B1} = \varepsilon_{B3} = -\varepsilon_{B2} = -\varepsilon_{B4}$$

$$|\varepsilon_{B1}| = |\varepsilon_{B2}| = |\varepsilon_{B3}| = |\varepsilon_{B4}| = |\varepsilon_{B}|$$

$$\varepsilon_{D1} = \varepsilon_{D2} = \varepsilon_{D3} = \varepsilon_{D4}$$

Therefore substituting these equations in equation (C.1),

$$V_O = \frac{V_i}{4}.GF.\ (4\varepsilon_B)$$

Gauge details were as for case C.1.2.

APPENDIX D

CALIBRATION OF MECHANICAL (KINETROL) DAMPERS

Consider the following linear shaft system subjected to an excitation force p(t) at point F, initially uncontrolled (Fig. D.1a), then controlled using some external device at point D, (Fig. D.1b).

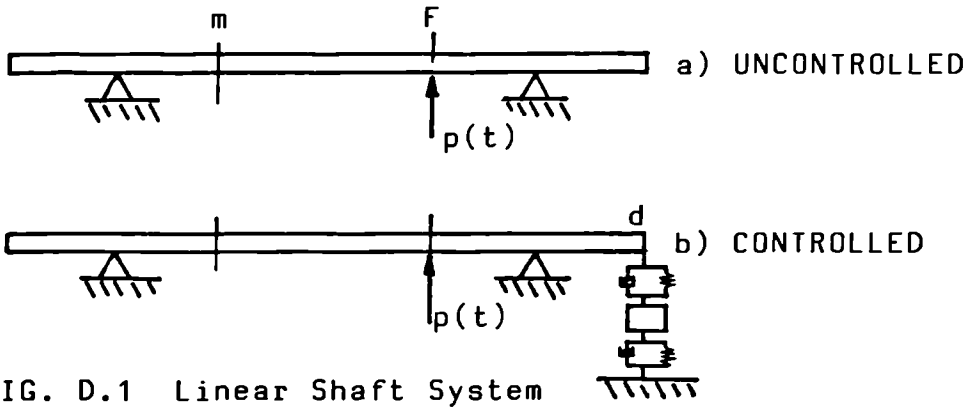

FIG. D.1 Linear Shaft System

If the excitation force is assumed harmonic then,

$$p(t) = \overline{P}.e^{i\omega t}$$

and $$q_m(t) = \overline{Q}_m.e^{i\omega t}$$

where $q_m(t)$ is the shaft displacment at any location m.

Letting the subscripts u and c denote the uncontrolled and controlled states of the shaft system respectively we can write,

$$q_{mc}(t) = q_{mu}(t) - f_c(t).\overline{r}_{mdu}$$

Therefore (D.1)

$$\overline{Q}_{mc} = \overline{Q}_{mu} - \overline{F}_c.\overline{r}_{mdu}$$

where

$f_c(t)$ = instantaneous control force at point d

$$= \overline{F}_c . e^{i\omega t}$$

$\overline{r}_{mdu}$ = Receptance defined by the dynamic displacement at point m due to a unit harmonic force at point d (uncontrolled - i.e. no damper fitted).

Consider the motion at the controller location. Assuming the controller (in this particular case mechanical damper) may be modelled as a single degree of freedom system then

$$\overline{F}_c = \overline{Z} . \overline{Q}_{dc}$$

where (D.2)

$$\overline{Z} = (K - M\omega^2 + i\omega C)$$

Substituting equations (D.2) into equation (D.1) and setting m = d we obtain,

$$\overline{Q}_{dc} = \frac{\overline{Q}_{du}}{(1 + \overline{Z} . \overline{r}_{ddu})} \qquad (D.3)$$

Now substituting equations (D.3) and (D.2) into equation (D.1) gives:

$$\overline{Q}_{mc} = \overline{Q}_{mu} - \frac{\overline{Q}_{du} . \overline{r}_{mdu}}{\frac{1}{\overline{Z}} + \overline{r}_{ddu}} \qquad (D.4)$$

Since all shaft motions are a direct result of the single external excitation force p(t) we can write:

$$\overline{Q}_{mc} = \overline{P} . \overline{r}_{mFc}$$
$$\overline{Q}_{mu} = \overline{P} . \overline{r}_{mFu} \qquad (D.5)$$
$$\overline{Q}_{du} = \overline{P} . \overline{r}_{dFu}$$

Upon substitution of equations (D.5) into (D.4) and some further manipulation we can obtain an expression

for the controller dynamic stiffness $\bar{Z}$ in terms of the measured (controlled and uncontrolled) system receptances:

$$\bar{Z} = \frac{1}{\frac{[-\bar{r}_{dfu} \cdot \bar{r}_{mdu}]}{[\bar{r}_{mFc} - \bar{r}_{mFu}]} - \bar{r}_{ddu}} \qquad (D.6)$$

and

$\bar{r}_{dFu}$ = Receptance defined by the displacement at point d due to a unit force at point F (uncontrolled - i.e. no damper fitted).

$\bar{r}_{mFc}$ = Receptance defined by the displacement at point m due to unit force at point F (controlled - i.e. damper fitted).

$\bar{r}_{mFu}$ = Receptance defined by the displacement at point m due to a unit force at point F (uncontrolled - i.e. no damper fitted.

$\bar{r}_{ddu}$ = Receptance defined by the displacement at point d due to a unit force at point d (uncontrolled - i.e. no damper fitted).

Thus, measurement of the above system receptances enables estimation of the damper characteristics.

APPENDIX E

ESTIMATION OF EQUIVALENT LINEARISED ELECTROMAGNETIC CONTROL PARAMETERS

For modelling purposes accurate prediction of the magnet damping and stiffness coefficients is essential. Because of the effect of shaft residual bend it was found necessary to vectorially subtract the response results of two test runs. In each test run, unbalance masses of known magnitude and location were applied. The situation is further complicated since, for non-linear electromagnetic control, the control forces during each of the two test runs are, in general, different. If an accurate model of the sustem is to be obtained then some means of computing an equivalent or effective control force, and corresponding control parameters, is required.

The following procedure is used.

Consider the initial test run (system A) where the shaft is run without any applied unbalance. Then the response of the system will be due to inherent unbalance resulting mainly from the initial-bend.

In the second test run (system B) a known unbalance is applied to the system and the shaft driven over the same speed range.

Subtraction of response data from these two test runs will result in a set of response data

representative of a shaft arrangement (system C) subjected to the known unbalance but having no other inherent unbalance.

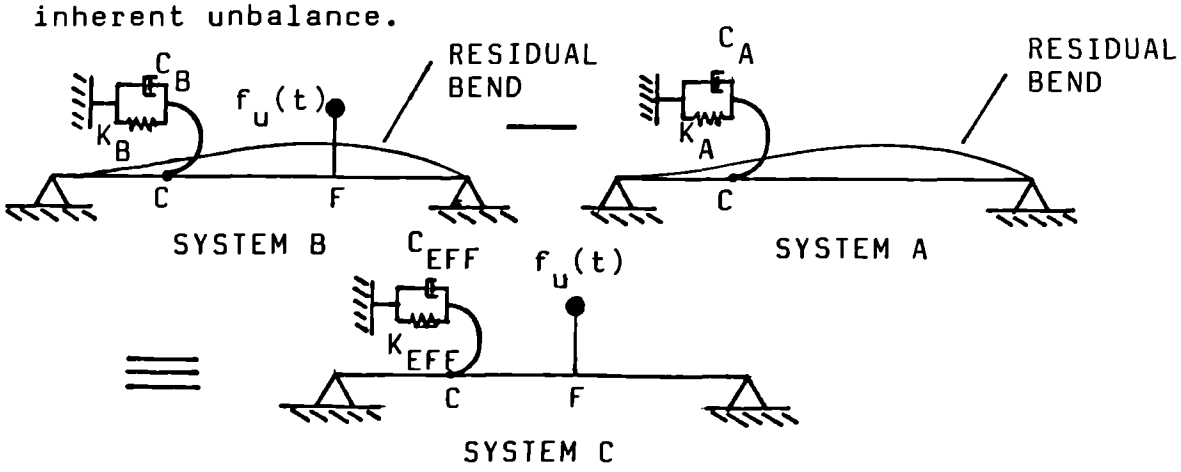

C and K are the electromagnetic linearised damping and stiffness coefficients respectively. $f_u(t)$ is the force, at a shaft rotational speed ω, due to the externally applied unbalance.

Since shaft response due to unbalance is being considered the motion is assumed harmonic, thus,

$$f_u(t) = \overline{F}_u . e^{i\omega t}$$

$$\theta(t) = \overline{\theta} . e^{i\omega t}$$

and similarly for all other harmonically varying parameters.

$\theta(t)$ is the instantaneous shaft slope at the controller (point C).

For System A

$$\overline{\theta}_A = \overline{\theta}_0 - \overline{M}_A . \overline{r}_{cc} \qquad (E.1)$$

where

$\overline{\theta}_A$ is the shaft slope at point C for system A.

$\bar{\theta}_0$ is the shaft slope at point C due to inherent unbalance.

$\bar{M}_A$ is the control moment at point C.

$\bar{r}_{cc}$ is the angular point receptance at C.

and $\bar{M}_A = \bar{\theta}_A\,[K_A+i\omega C_A] = \bar{\theta}_A.\bar{Z}_A$ (E.2)

Similarly,

For System B

$$\bar{\theta}_B = \bar{\theta}_0 - \bar{M}_B.\bar{r}_{cc} + \bar{F}_u.\bar{r}_{cF} \quad (E.3)$$

where,

$\bar{r}_{cF}$ is the receptance defining the slope at point C due to a unit force at point F.

All other terms are defined analogously to those used in system A.

In addition, $\bar{M}_B = \bar{\theta}_B[K_B+i\omega C_B] = \bar{\theta}_B.\bar{Z}_B$ (E.4)

Now from (E.1) and (E.3)

$$\bar{\theta}_B - \bar{\theta}_A = \bar{r}_{cc}[\bar{M}_A-\bar{M}_B] + \bar{F}_u.\bar{r}_{cF} \quad (E.5)$$

Substituting equations (E.2) and (E.4) in (E.5) gives,

$$\bar{\theta}_B - \bar{\theta}_A = \bar{r}_{cc}[\bar{\theta}_A.\bar{Z}_A-\bar{\theta}_B.\bar{Z}_B] + \bar{F}_u.\bar{r}_{cF} \quad (E.6)$$

Considering System C now,

$$\bar{\theta}_c = -\bar{M}_c.\bar{r}_{cc} + \bar{F}_u.\bar{r}_{cF} \quad (E.7)$$

and,

$$\bar{M}_c = \bar{\theta}_c[K_{EFF}+i\omega C_{EFF}] = \bar{\theta}_c.\bar{Z}_{EFF} \quad (E.8)$$

Putting equation (E.8) in equation (E.7)

$$\bar{\theta}_c = \bar{r}_{cc}[-\bar{\theta}_c.\bar{Z}_{EFF}] + \bar{F}_u.\bar{r}_{cF} \quad (E.9)$$

and since $\bar{\theta}_c = \bar{\theta}_B - \bar{\theta}_A$ equation (E.9) can be rewritten as

$$\bar{\theta}_B - \bar{\theta}_A = \bar{r}_{cc}[(\bar{\theta}_A-\bar{\theta}_B).\bar{Z}_{EFF}] + \bar{F}_u.\bar{r}_{cF} \quad (E.10)$$

and equating the right hand sides of equations (E.6) and (E.10) we find,

$$\bar{Z}_{EFF} = \frac{[\bar{\Theta}_A.\bar{Z}_A - \bar{\Theta}_B.\bar{Z}_B]}{[\bar{\Theta}_A - \bar{\Theta}_B]} \qquad (E.11)$$

Thus, in general, solution of equation (E.11) will necessitate the measurement of $\bar{\Theta}_A$ and $\bar{\Theta}_B$ during test runs and the computation of $\bar{Z}_A$ and $\bar{Z}_B$ from calibration data, for each rotor frequency, using the procedures described in sections 6.6.5 and 6.6.6.2. Only then can the equivalent control impedance $\bar{Z}_{EFF}$ be determined and employed in the numerical simulations.

It is seen that if the controller characteristics are assumed linear then $\bar{Z}_A = \bar{Z}_B = \bar{Z}$ and from equation (E.11) $\bar{Z}_{EFF} = \bar{Z}$ and is independant of the system responses thus simplifying the analysis considerably. Alternatively, if the condition $\bar{\Theta}_A = -\bar{\Theta}_B$ is satisfied then again $\bar{Z}_{EFF} = \bar{Z}$.

APPENDIX F

THE INFLUENCE OF EXTERNAL DAMPING AND SUPPORT ASYMMETRY ON REVERSE WHIRLING OF A JEFFCOTT ROTOR

Consider an unbalanced Jeffcott rotor mounted on anisotropic supports and subjected to external viscous damping. Using the co-ordinate system as defined in Chapter 4 we can write the equation of motion for each plane as:-

$$M\frac{d^2}{dt^2}.(v+e\cos\Omega t) + C\frac{dv}{dt} + K_v v = 0$$

$$\text{and } M\frac{d^2}{dt^2}(w+e\sin\Omega t) + C\frac{dw}{dt} + K_w w = 0 \qquad \text{(F.1)}$$

Where M and e are the rotor mass and eccentricity respectively, C the external damping and K_v, K_w the effective shaft/support stiffness in the respective planes.

Equation (F.2) may be expressed as,

$$\ddot{v} + 2\zeta\omega_{nv}\dot{v} + \omega_{nv}^2 v = e\Omega^2\cos\omega t$$

$$\ddot{w} + 2\zeta\omega_{nw}\dot{w} + \omega_{nw}^2 w = e\Omega^2\sin\omega t \qquad \text{(F.2)}$$

Where ζ is the dimensionless damping factor and ω_{nv} and ω_{nw} are the natural frequencies in orthogonal planes defined by,

$$\omega_{nv} = \frac{\sqrt{K_v}}{\sqrt{M}} \; ; \quad \omega_{nw} = \frac{\sqrt{K_w}}{\sqrt{M}}$$

Assuming synchronous harmonic motion with shaft precession rate equal to rotational speed ($\Omega = \omega$) the steady-state solutions of equation (F.2) are

$$v = \frac{eF_v^2}{\sqrt{[(1-F_v^2)^2+(2\zeta F_v)^2]}} \cos\left\{\omega t - \tan^{-1}\frac{(2\zeta F_v)}{(1-F_v^2)}\right\}$$

$$= \bar{v}e^{i\omega t} = [v_c + iv_s]e^{i\omega t}$$

$$w = \frac{eF_v^2}{\sqrt{[(1-F_w^2)^2 + (2\zeta F_w)^2]}} \sin\left\{\omega t - \tan^{-1}\frac{(2\zeta F_w)}{(1-F_w^2)}\right\}$$

$$= \bar{w}e^{i\omega t} = [w_c + iw_s]e^{i\omega t}$$

where

$F_v = \omega/\omega_{nv}$; $F_w = \omega/\omega_{nw}$

Now the displacement cos and sine terms may be written as,

$$\begin{aligned} v_c &= (1-F_v^2) \\ v_s &= 2\zeta F_v \\ w_c &= 2\zeta F_w \\ w_s &= -(1-F_w^2) \end{aligned} \qquad (F.3)$$

The direction of rotor whirl is determined by the sign of the term $(v_s w_c - v_c w_s)$ as described in Appendix A.

Thus, substituting from equation (F.3) in the above leads to the conclusion that

For forward whirl $[4\zeta^2 F_v F_w + (1-F_v^2)(1-F_w^2)] > 0$

For reverse whirl $[4\zeta^2 F_v F_w + (1-F_v^2)(1-F_w^2)] < 0$

Now, since F_v and F_w are always positive it is seen that the introduction of external damping tends to suppress reverse whirling.

Considering first the case of no external damping ($\zeta = 0$) then $[(1-F_v^2)(1-F_w^2)]$ will be positive for forward whirl and negative for reverse whirl. Thus, for isotropic supports ($F_v=F_w$) the above term is <u>always</u> positive, leading to progressive or forward whirl at all speeds.

If, however, $F_v \neq F_w$ then the following conditions will result,

$F_v < 1$; $F_w < 1 \rightarrow$ Forward Whirl

$F_v > 1$; $F_w > 1 \rightarrow$ Forward Whirl

$F_v < 1$; $F_w > 1$ or $F_v > 1$; $F_w < 1 \rightarrow$ Reverse Whirl

It is evident that, for the simple model investigated if damping is not present then shaft retrograde whirling may exist only if supports exhibiting non-isotropic properties are employed. The region of reverse whirl is confined to a speed range between the shaft critical speeds in orthogonal planes.

If system damping is present then clearly the speeds at which retrograde precession may occur will be determined by the relative magnitudes of ζ, F_v and F_w.

The influence of these parameters on the existence of shaft reverse whirls is illustrated in Fig. F.1. The horizontal axis represents the degree of support anisotropy present whilst the vertical axis shows the

shaft running speed as a proportion of the lower critical speed, where only the speed range between the two system critical speeds is examined. The curves drawn show the amount of external damping just necessary to eliminate reverse whirling for a corresponding range of support asymmetry ratios. The region enclosed by the curves and the vertical axis indicates shaft retrograde motion. For example, referring to the case where $\zeta = 0.3$ it is seen that for a critical speed ratio (ω_{nw}/ω_{mv}) greater than approximately .56 the shaft will whirl in the same direction as rotation at any speed between the two system critical speeds, i.e. reverse whirl is completely eliminated. However, as support asymmetry becomes more pronounced ($\frac{F_v}{F_w} \rightarrow 0$) reverse whirling will occur over a portion of the speed range between the two criticals, until at (ω_{nw}/ω_{nv})=.5 the shaft will exhibit retrograde motion within a speed range between $F_{wr} \approx 1.175$ and $F_{wr} \approx 1.7$.

The diagram thus gives a good quick guide to the amount of system damping required to ensure forward whirling for a given degree of support asymmetry.

It is clear that the introduction of even a small amount of external damping is effective in removing reverse whirls. For instance, where the critical speeds in the two planes differ by approximately 20% it is observed that the application of damping of the order of 10% of the system critical damping value will

result in the elimination of shaft reverse whirl. This probably explains why the phenomenon has rarely been observed in practical rotor systems [67].

DIAGRAMS

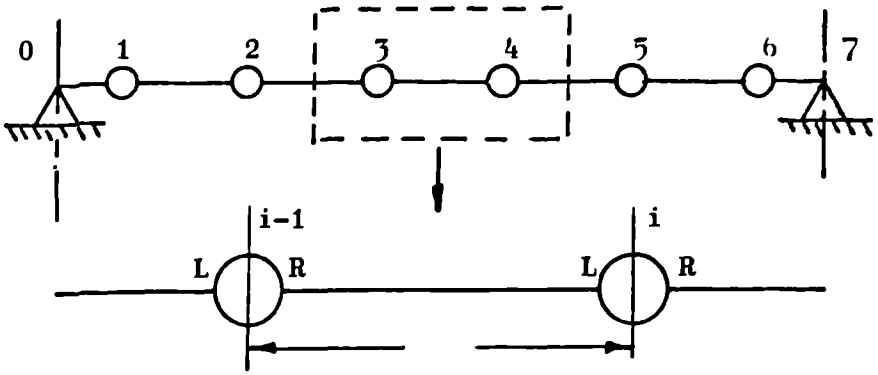

FIG. 4.1 SIMPLE BEAM MODEL

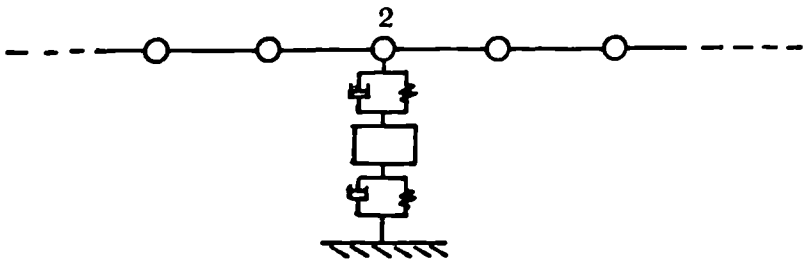

FIG. 4.2 SUPPORT WITH SUB-LEVEL CHARACTERISTICS

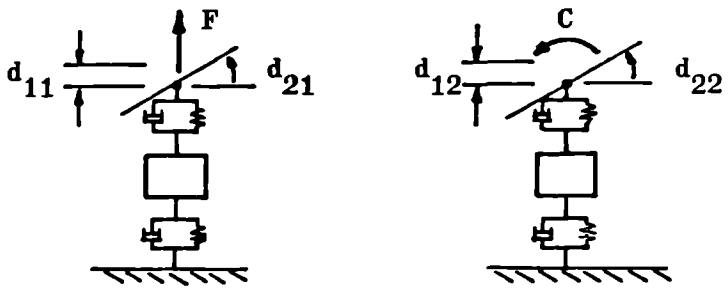

FIG. 4.3 EXPERIMENTAL DETERMINATION OF SUPPORT CHARACTERISTICS

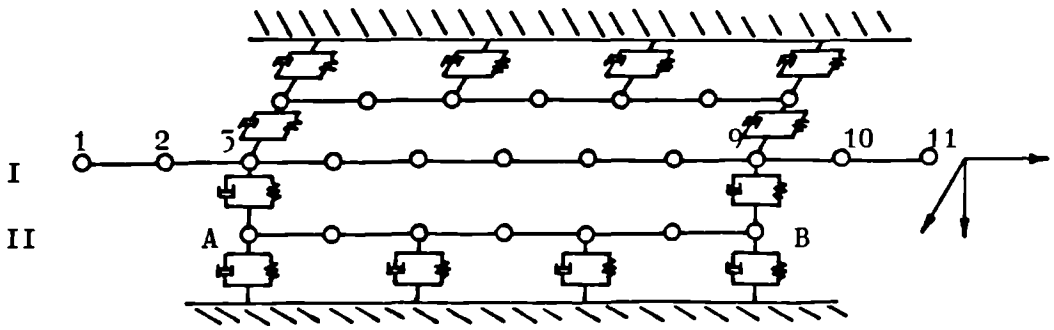

FIG. 4.4 SYSTEM WITH SUPPORT COUPLING

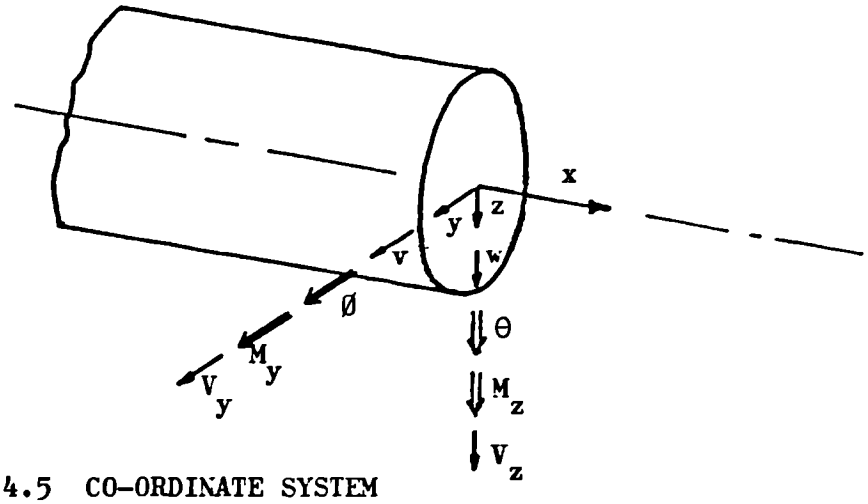

FIG. 4.5 CO-ORDINATE SYSTEM

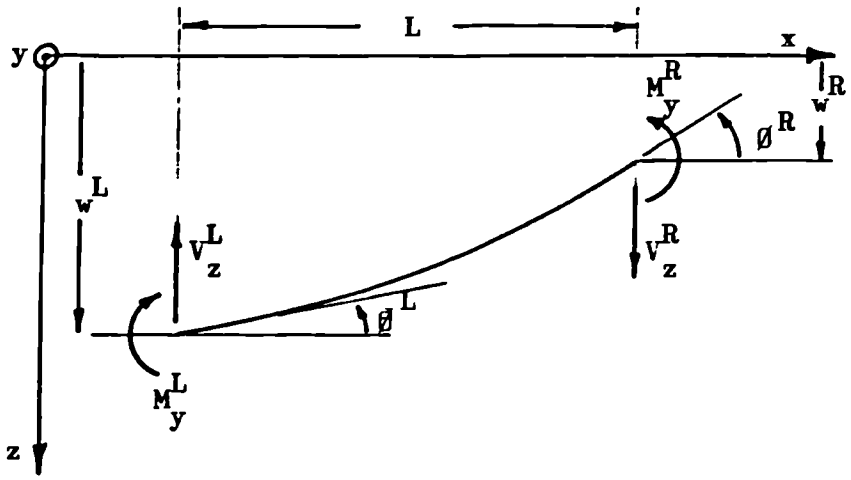

(a) x-z PLANE

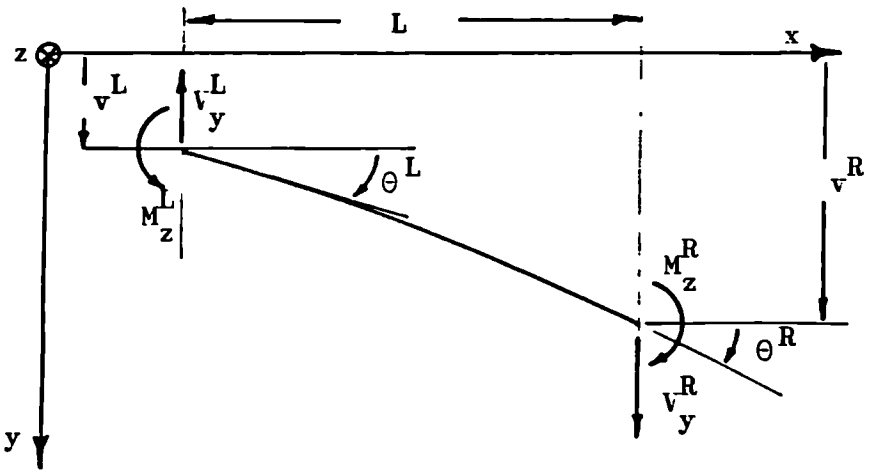

(b) x-y PLANE

FIG. 4.6 ELASTIC MASSLESS ELEMENT

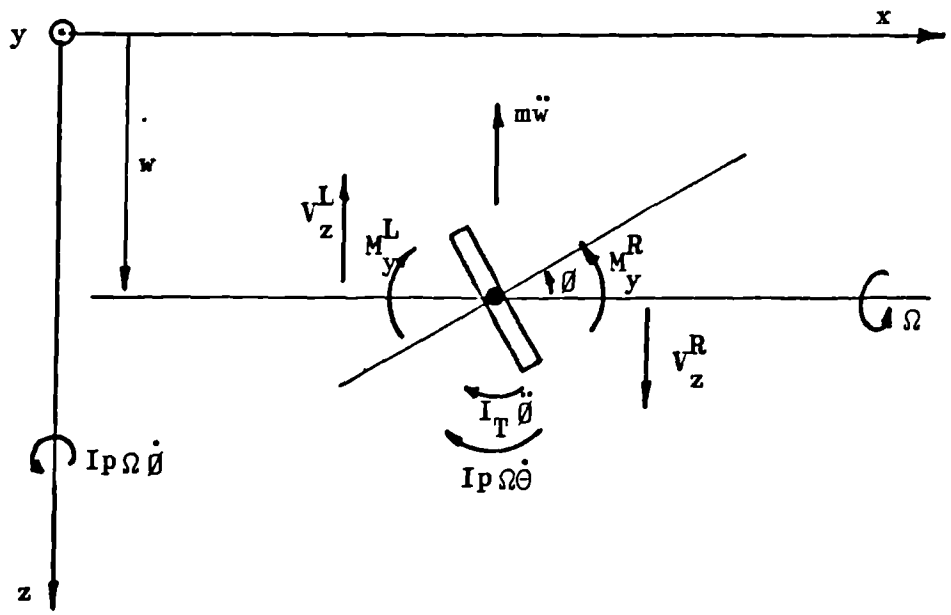

(a) x-z PLANE

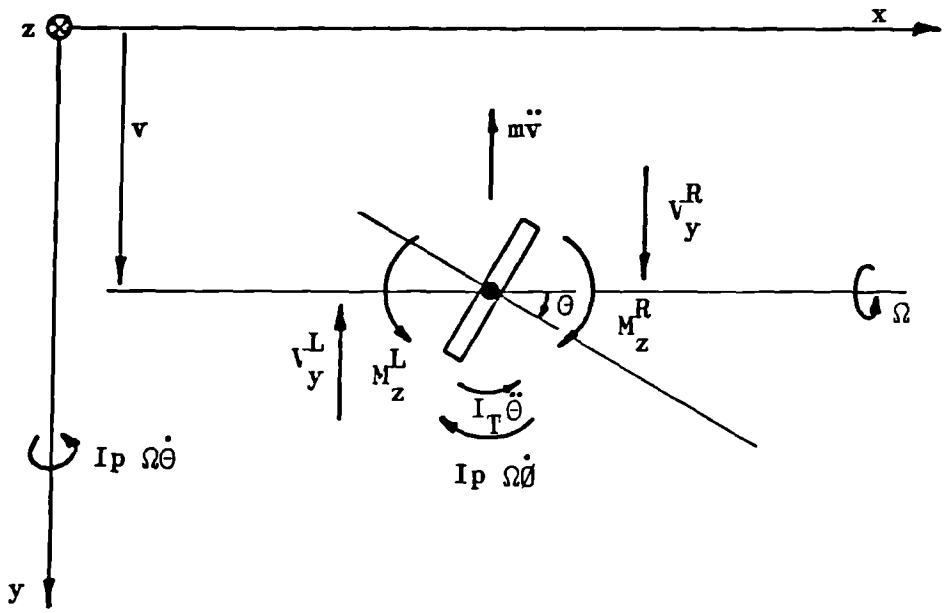

(b) x-y PLANE

FIG. 4.7 POINT MASS/INERTIA ELEMENT

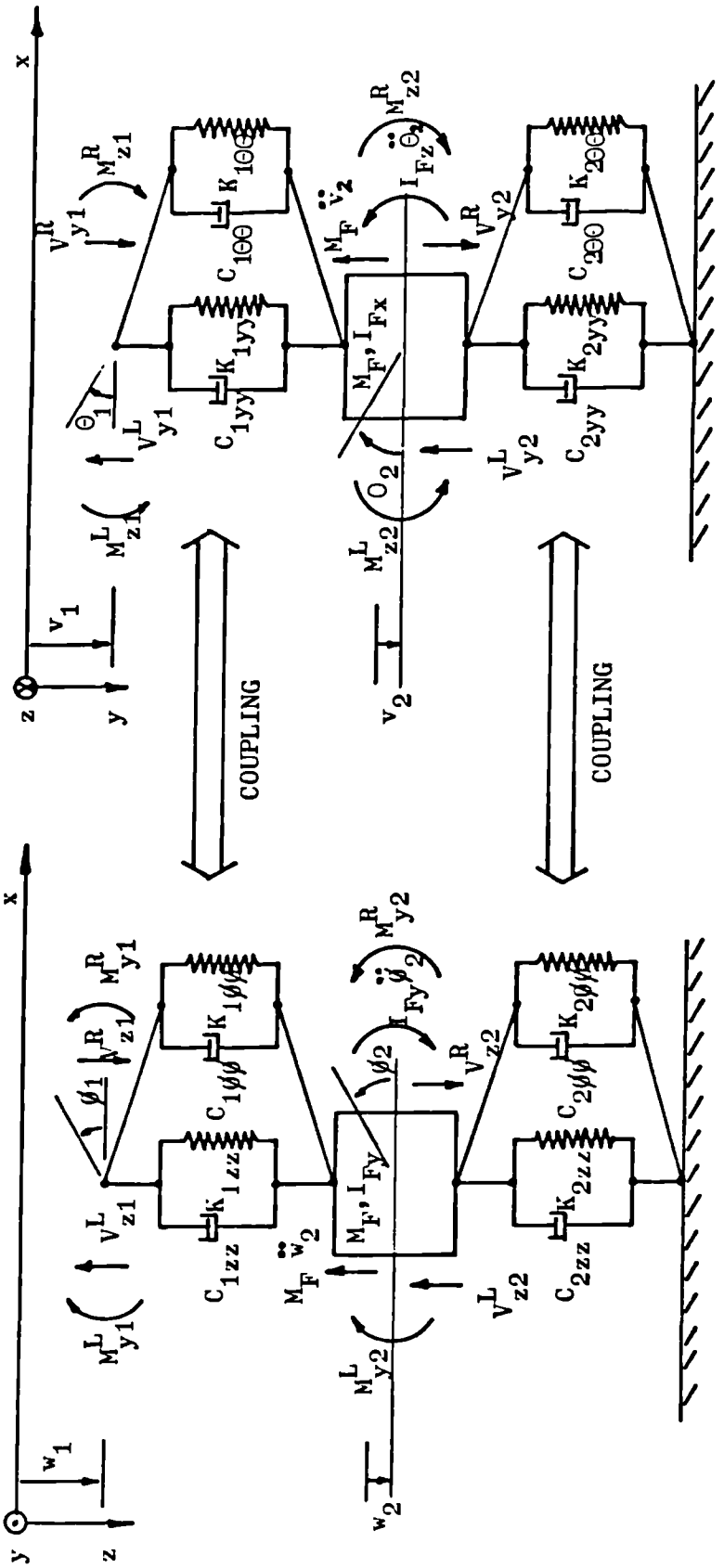

FIG. 4.8 POINT SUPPORT (WITH ONE SUB-LEVEL)

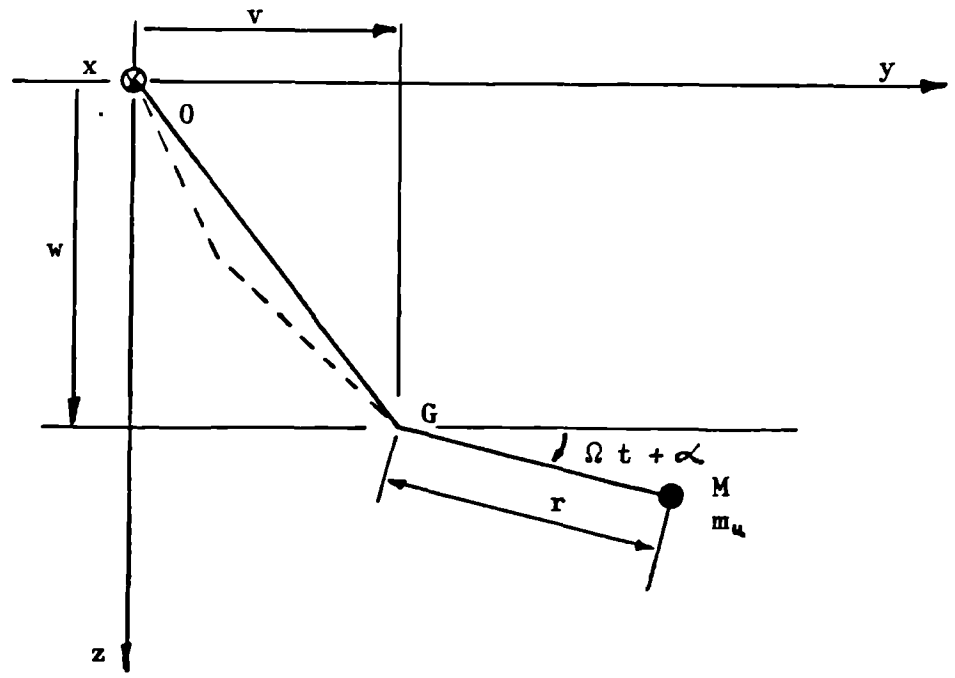

FIG. 4.9 UNBALANCE MASS

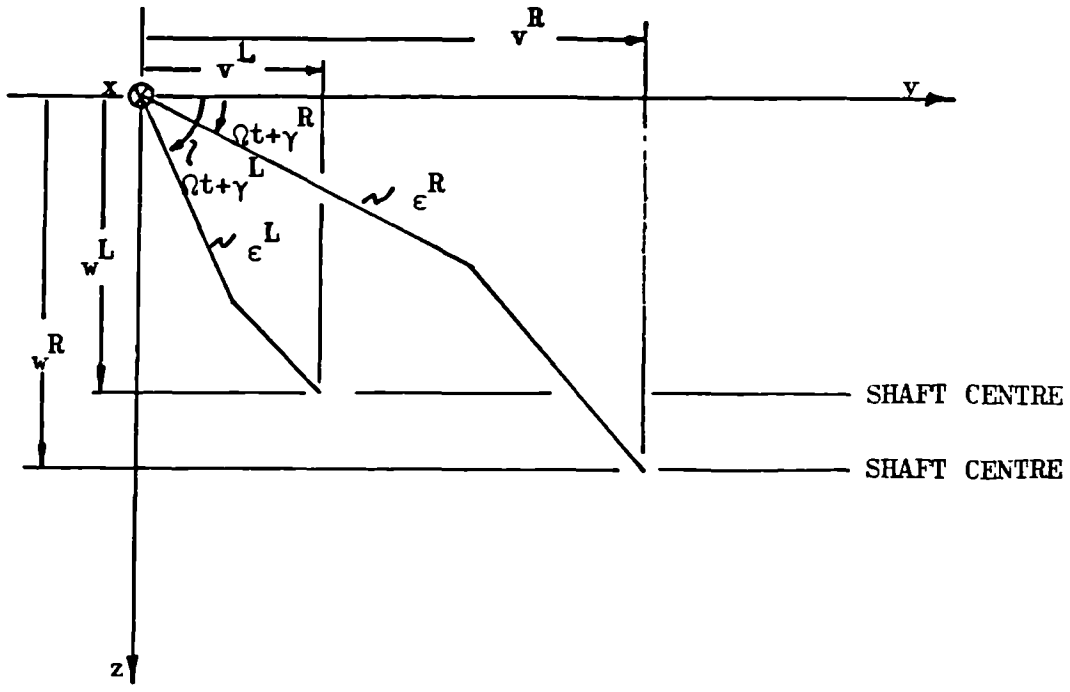

FIG. 4.10 EFFECT OF SHAFT INITIAL-BEND ON ELASTIC MASSLESS ELEMENT

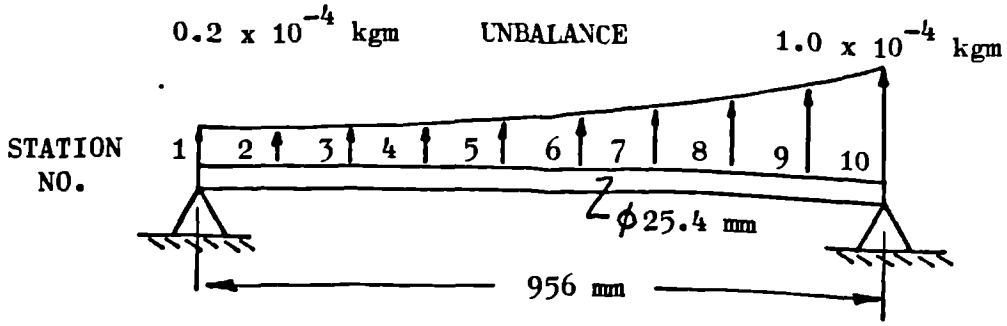

(a) PINNED SUPPORTS

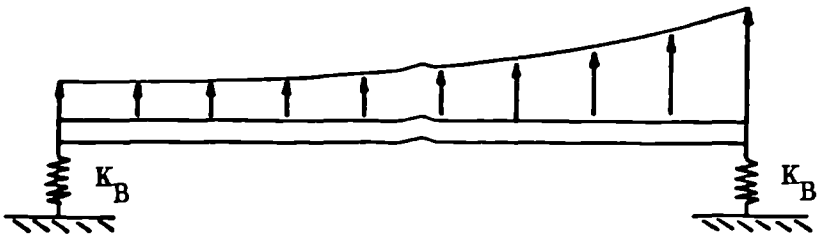

(b) FLEXIBLE SUPPORTS (K_B = 2.13 x 10^6 N/m)

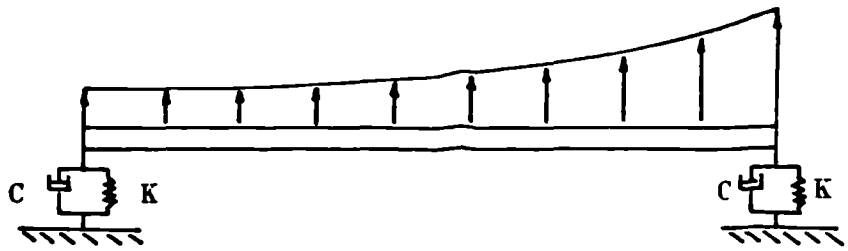

(c) OIL-FILM BEARINGS (C AND K CALCULATED AS PER REF. [91])

FIG. 4.11 SHAFT SYSTEMS FOR ANALYSIS

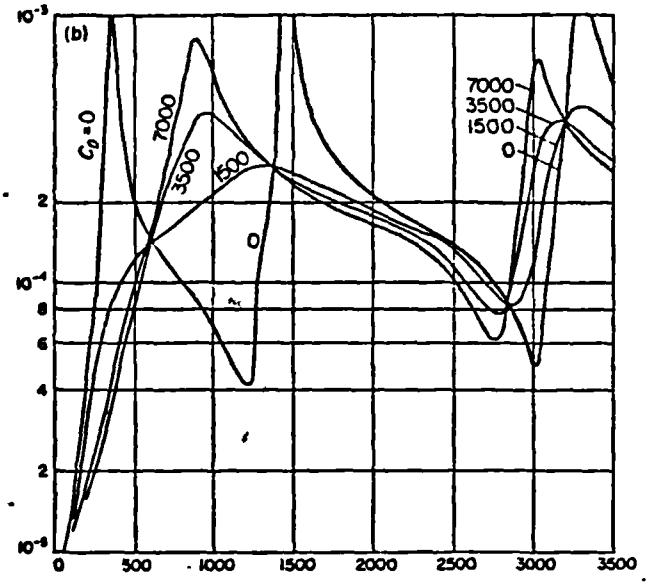

a(i) PINNED SUPPORTS

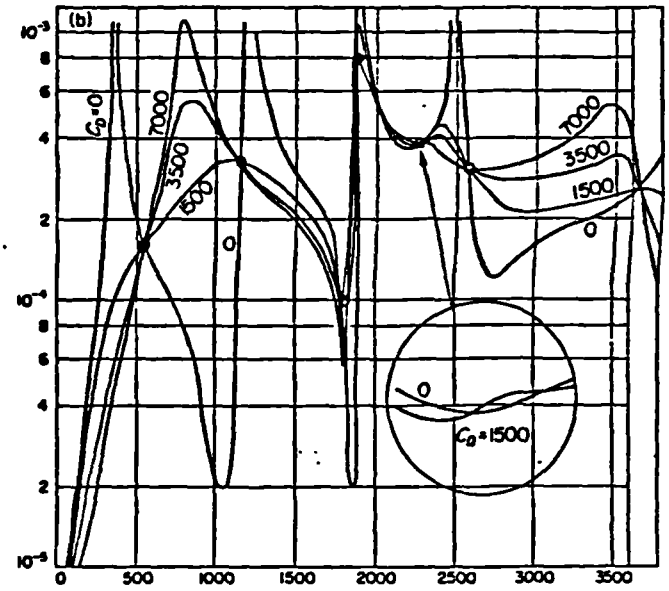

a(ii) FLEXIBLE SUPPORTS

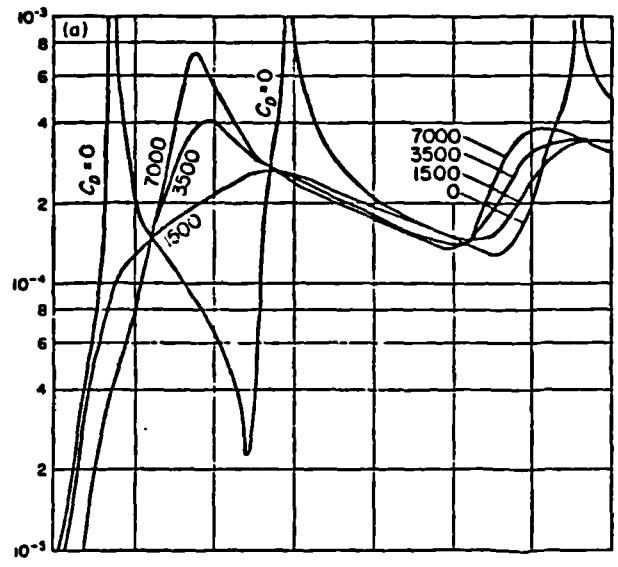

a(iii) OIL-FILM BEARINGS

FIG.4.12a SHAFT RESPONSE FOR DIFFERENT TYPES OF SUPPORTS - DUE TO DOSTAL et al [91]

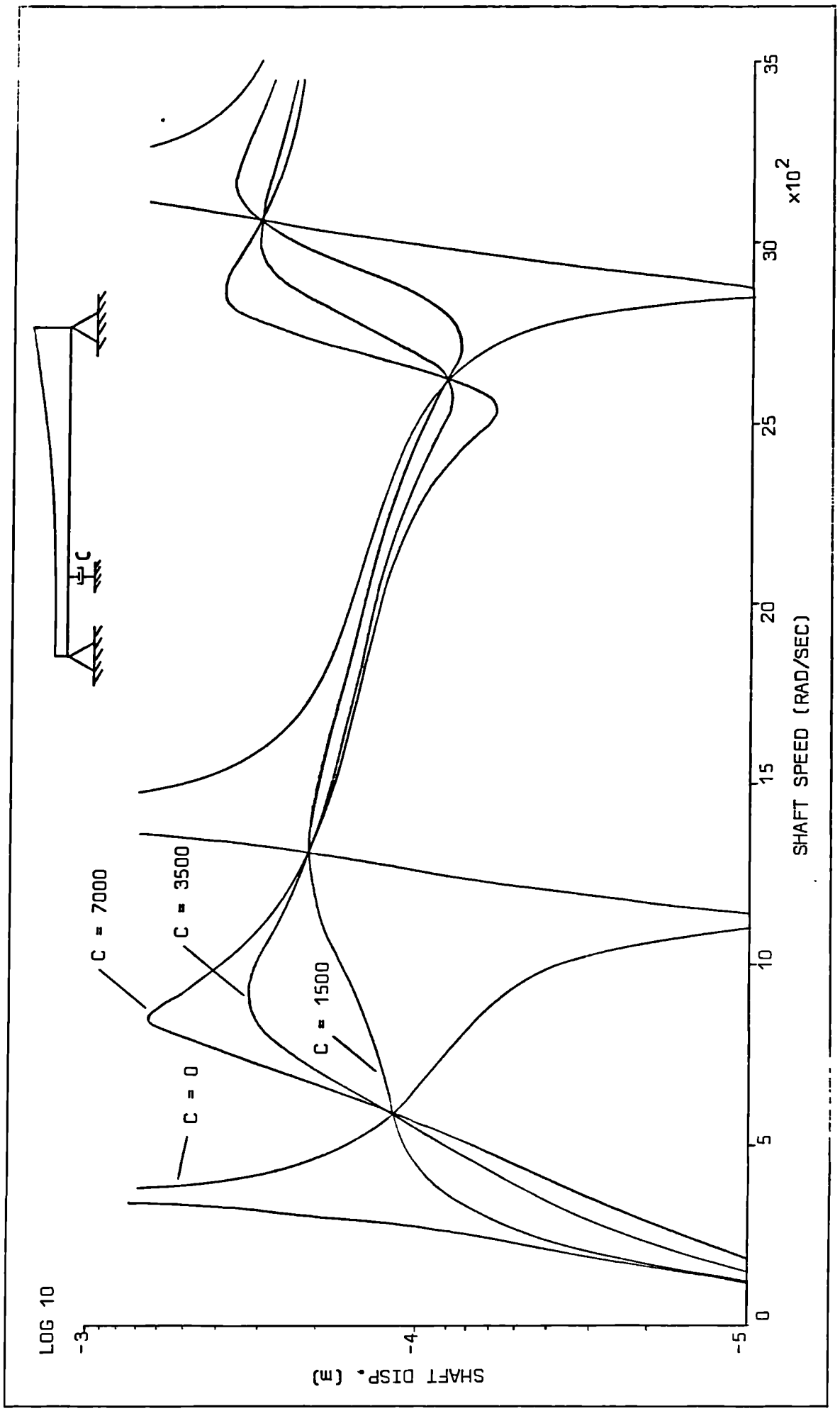

FIG.4.12b(i) SHAFT RESPONSE PREDICTED USING TM METHOD (CHAPTER 4) - PINNED SUPPORTS

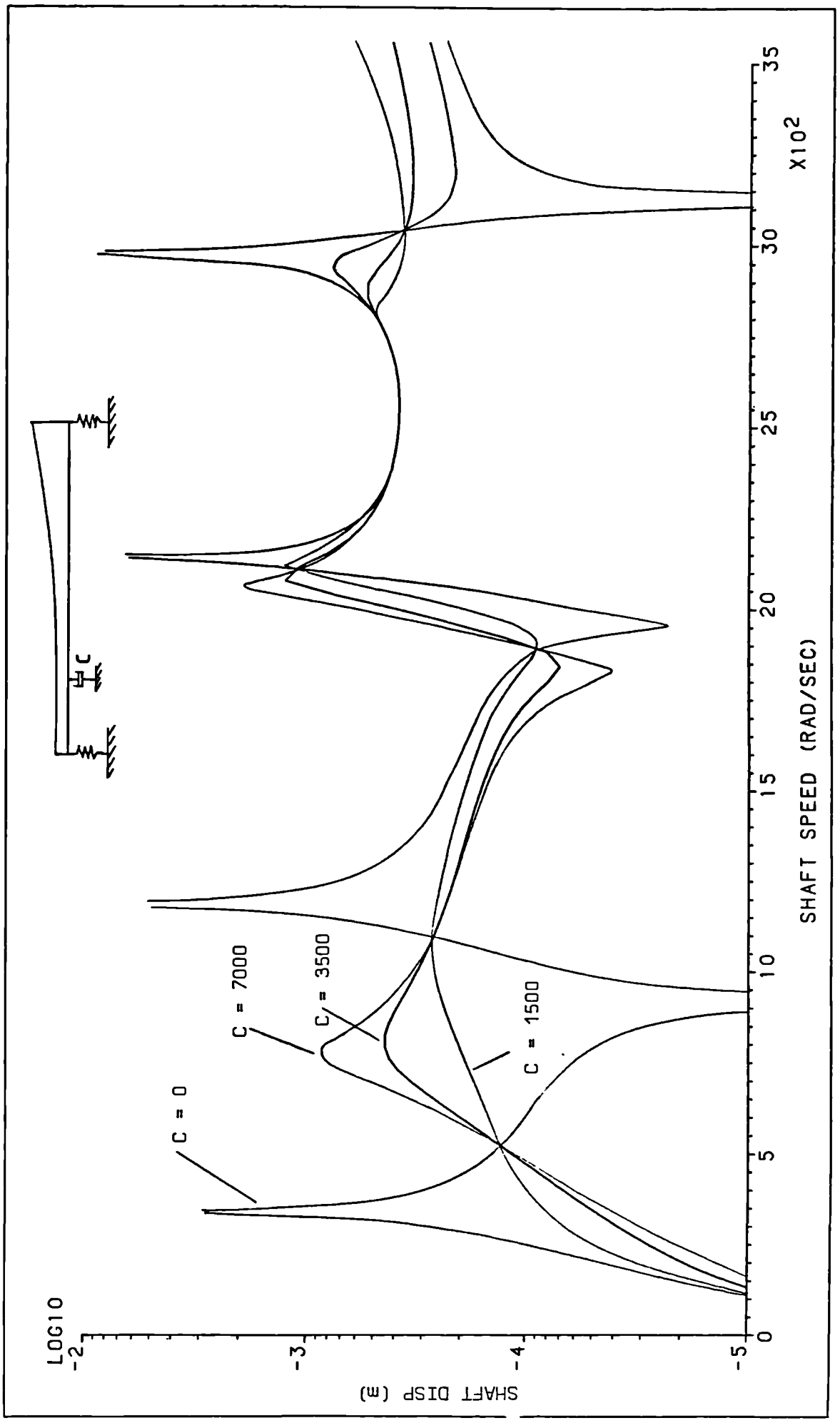

FIG. 4.12b(ii) SHAFT RESPONSE PREDICTED USING TM METHOD (CHAPTER 4) - FLEXIBLE SUPPORTS

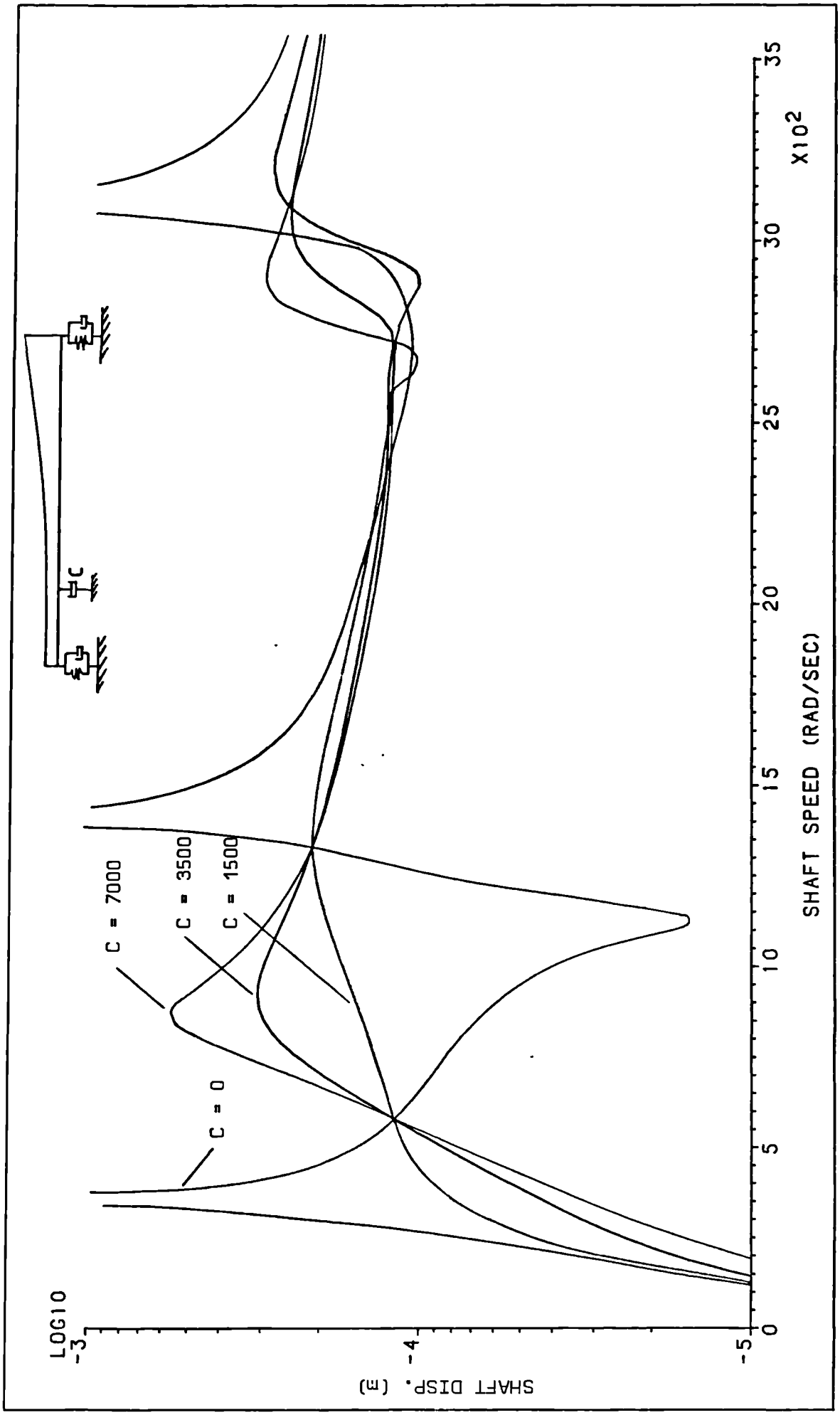

FIG. 4.12b(iii) SHAFT RESPONSE PREDICTED USING TM METHOD (CHAPTER 4) - OIL-FILM BEARINGS

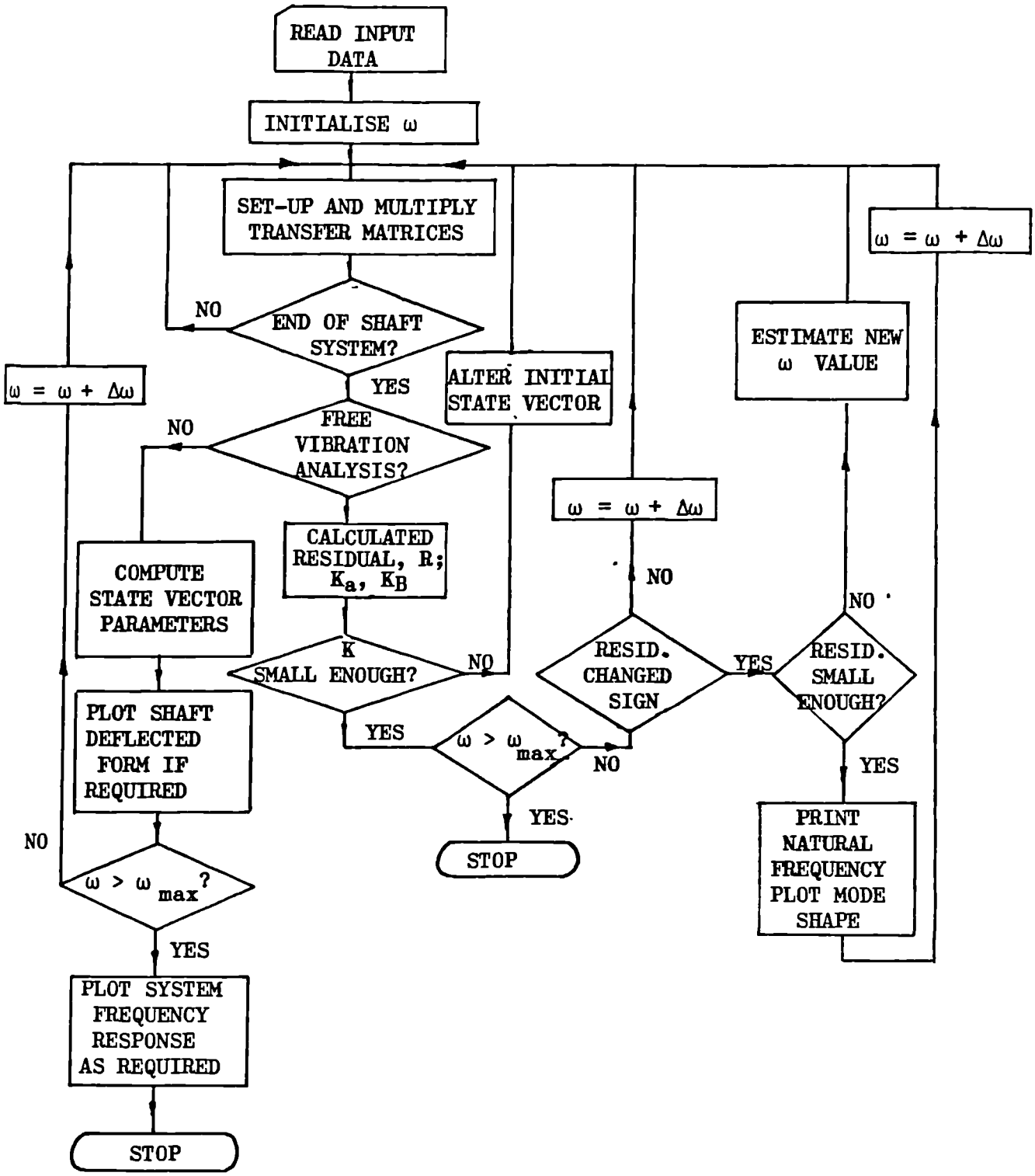

FIG. 4.13 TM PROGRAM FLOW CHART

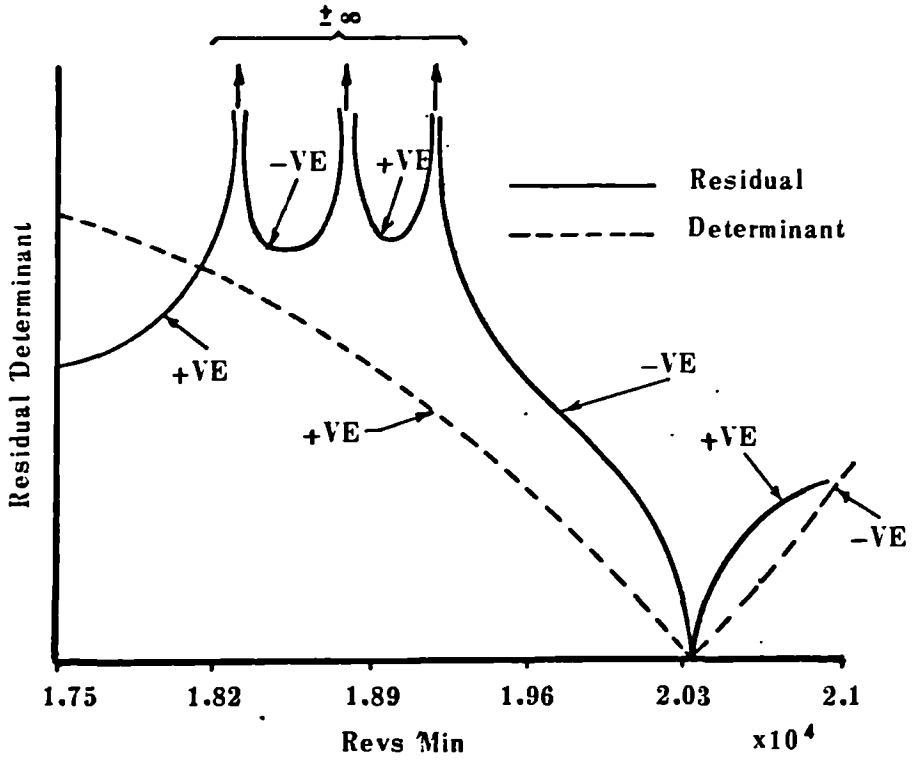

FIG. 4.14 PLOT OF FREQUENCY DETERMINANT AND RESIDUAL FOR SHAFT CASE SHOWN IN FIG. 4.11(b)

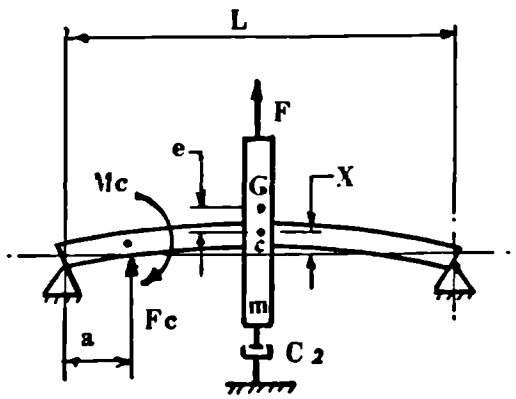

FIG. 5.1 JEFFCOTT ROTOR

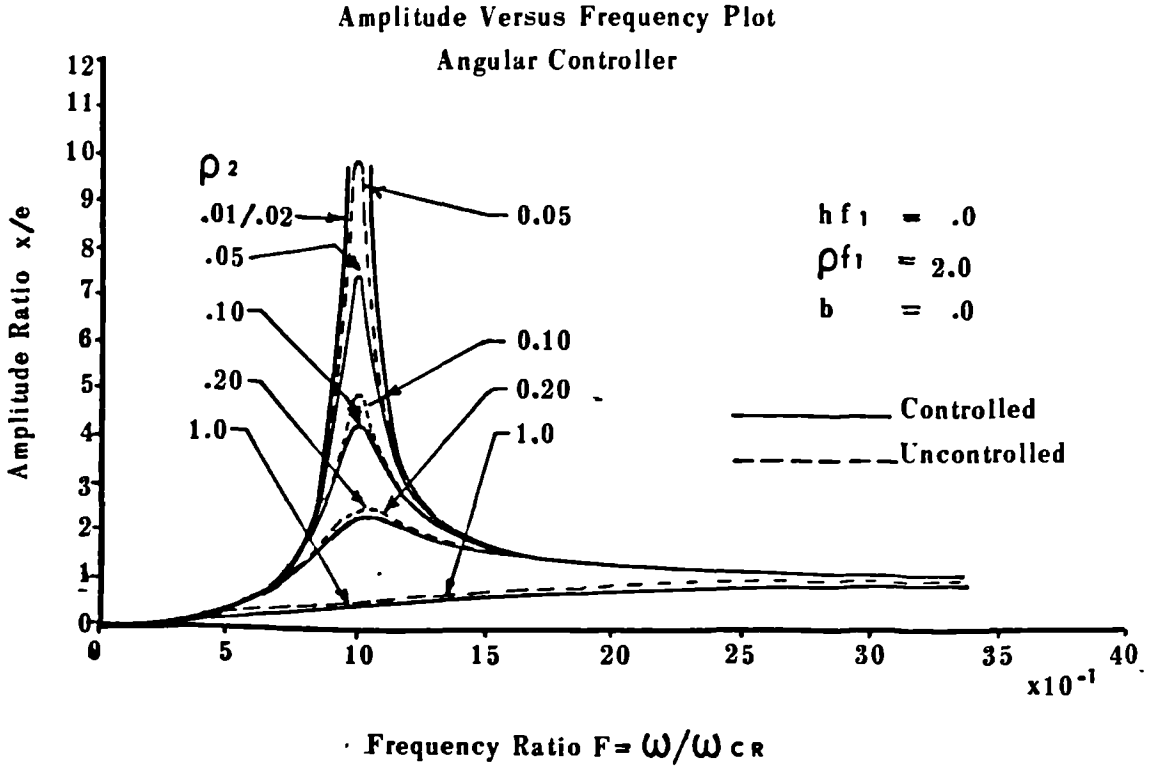

FIG. 5.2a ANGULAR CONTROL ($\rho_{f1} = 2.0$)

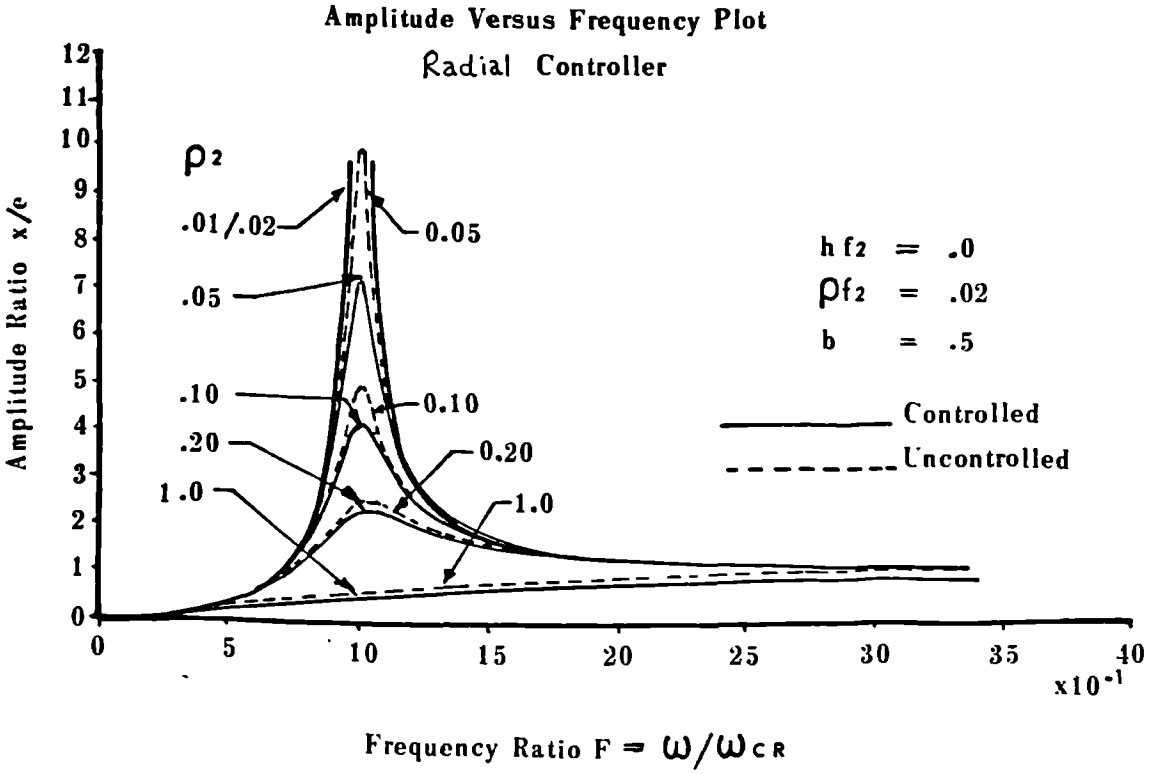

FIG. 5.2b RADIAL CONTROL ($\rho_{f2} = .02$)

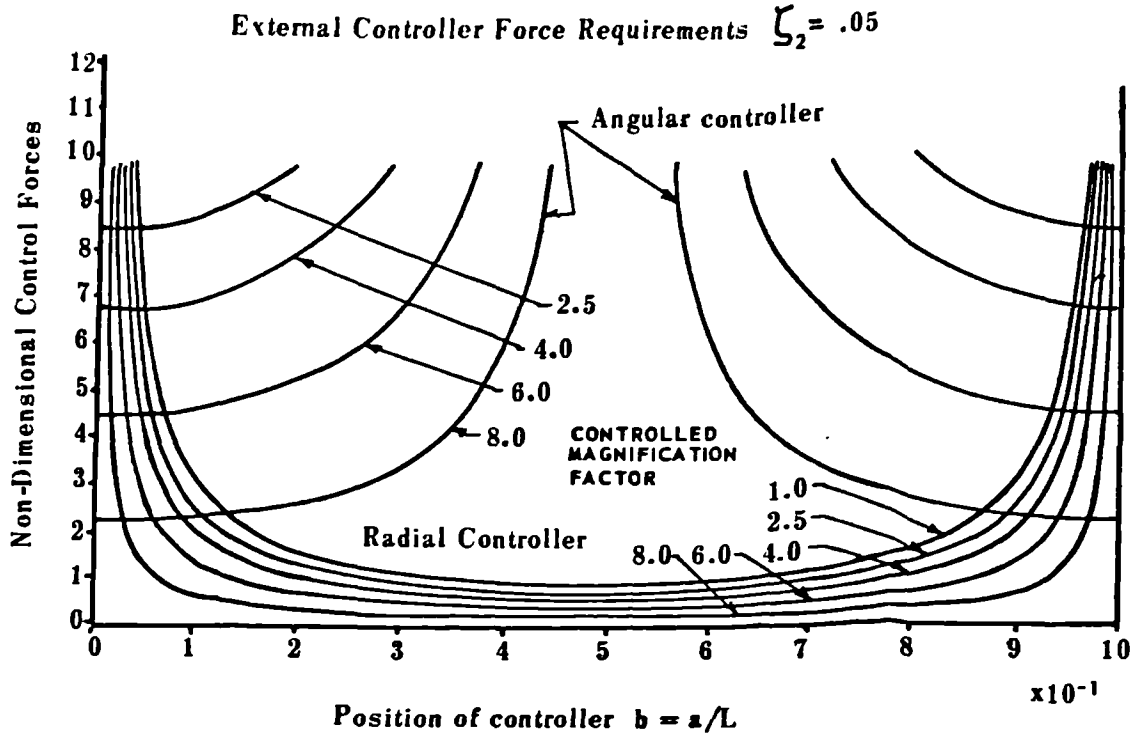

FIG. 5.3a EFFECT OF CONTROLLER LOCATION (ζ_2 = 0.05)

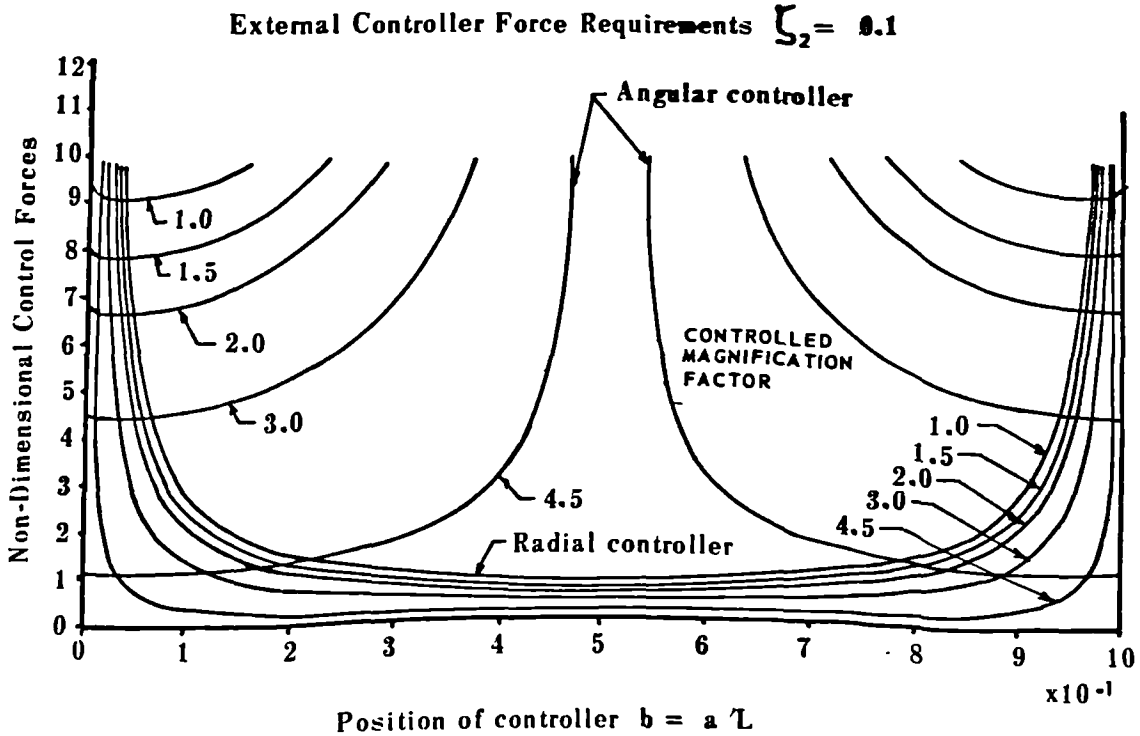

FIG. 5.3b EFFECT OF CONTROLLER LOCATION (ζ_2 = 0.1)

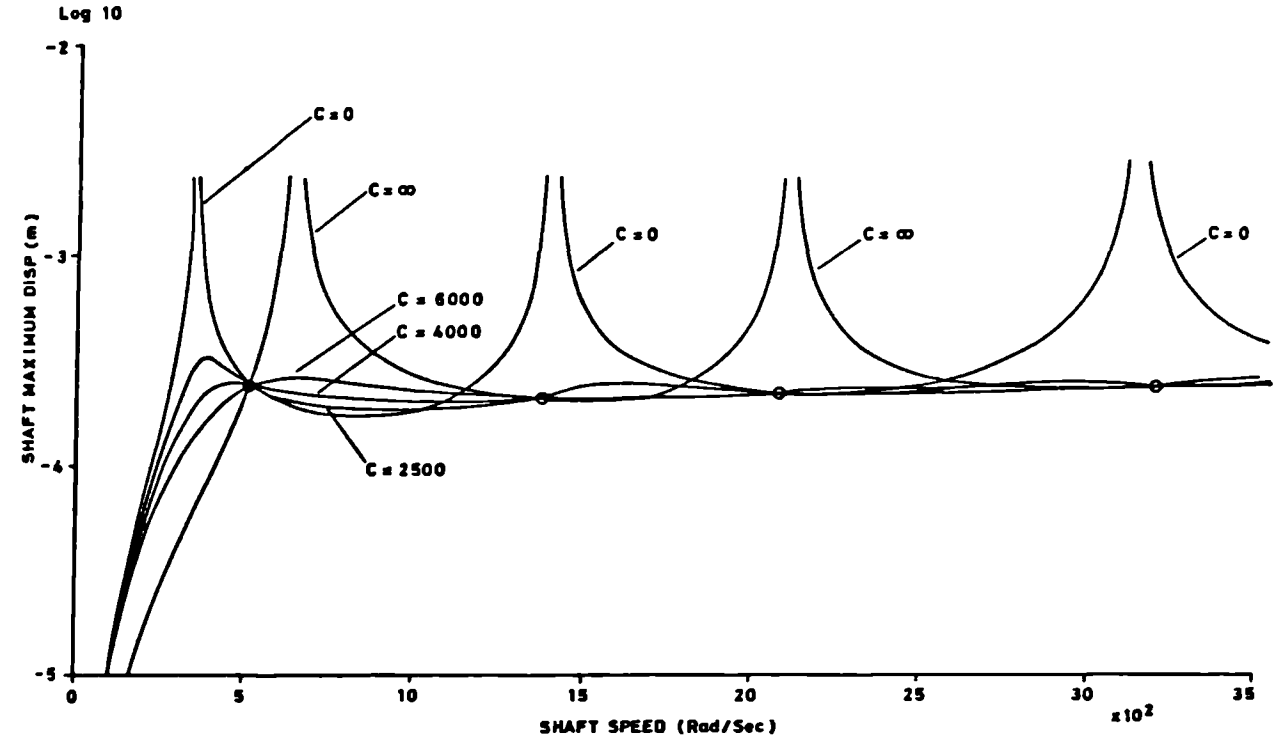

FIG. 5.4a INFLUENCE OF CONTROL DAMPING ON THE 'FIXED-POINTS' - RADIAL CONTROL AT STAT 2

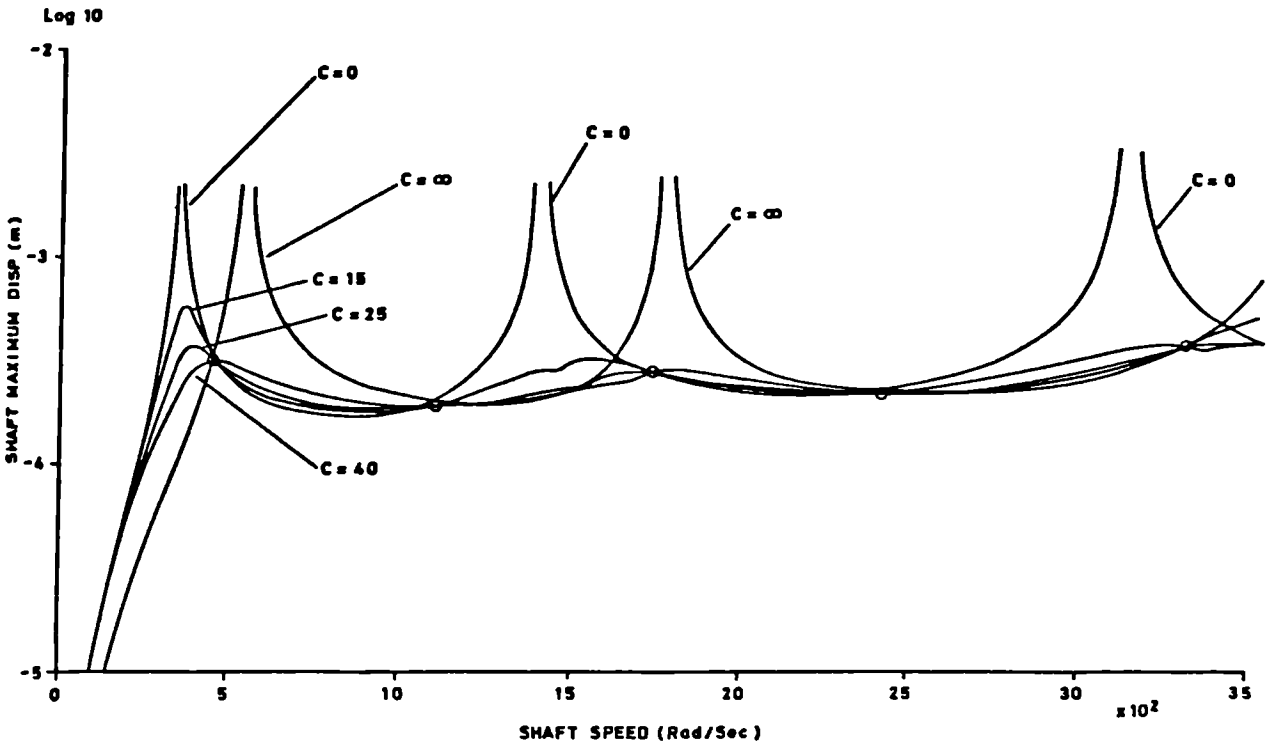

FIG. 5 4b INFLUENCE OF CONTROL DAMPING ON THE 'FIXED-POINTS' - ANGULAR CONTROL AT STAT 1

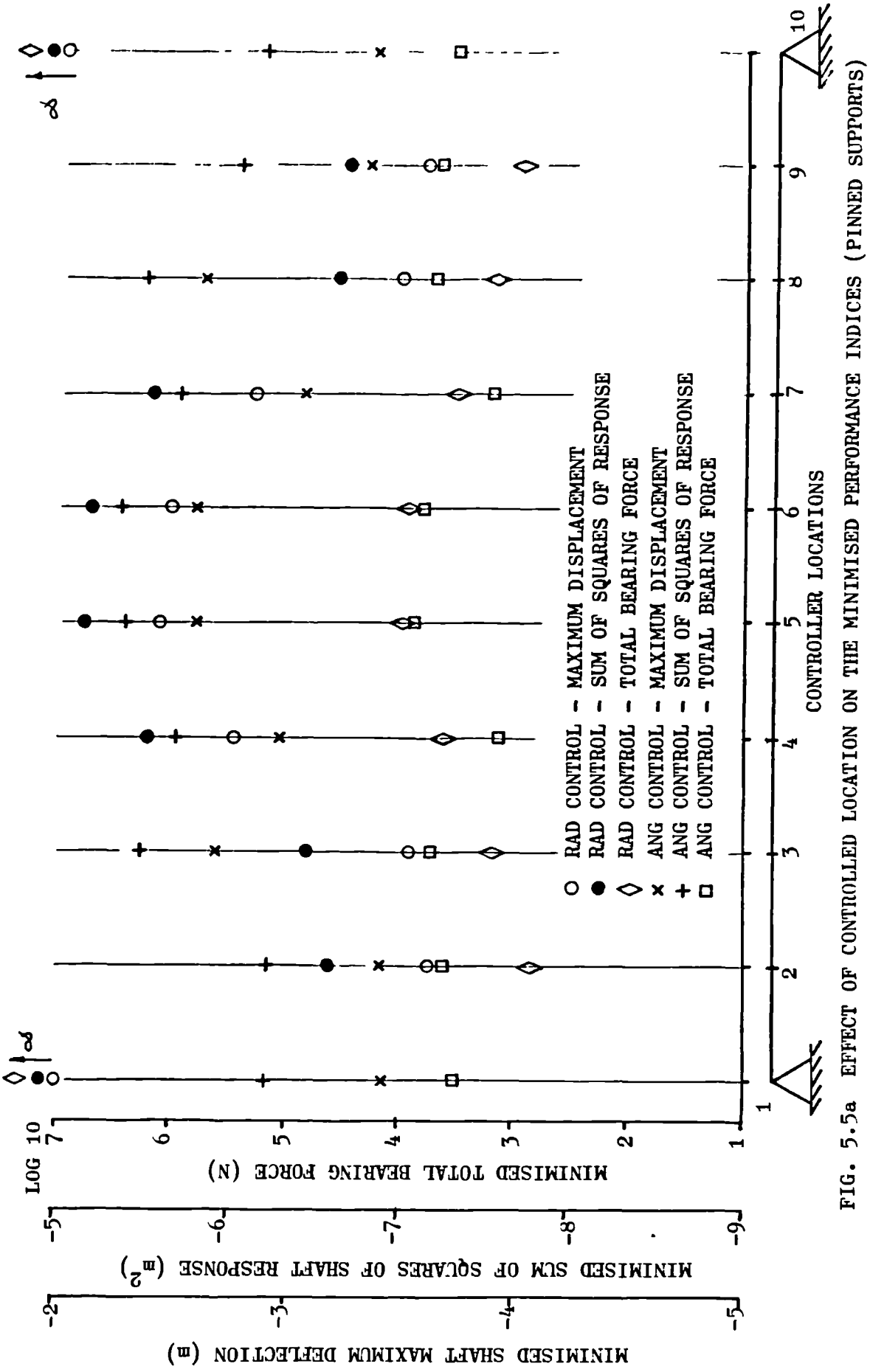

FIG. 5.5a EFFECT OF CONTROLLED LOCATION ON THE MINIMISED PERFORMANCE INDICES (PINNED SUPPORTS)

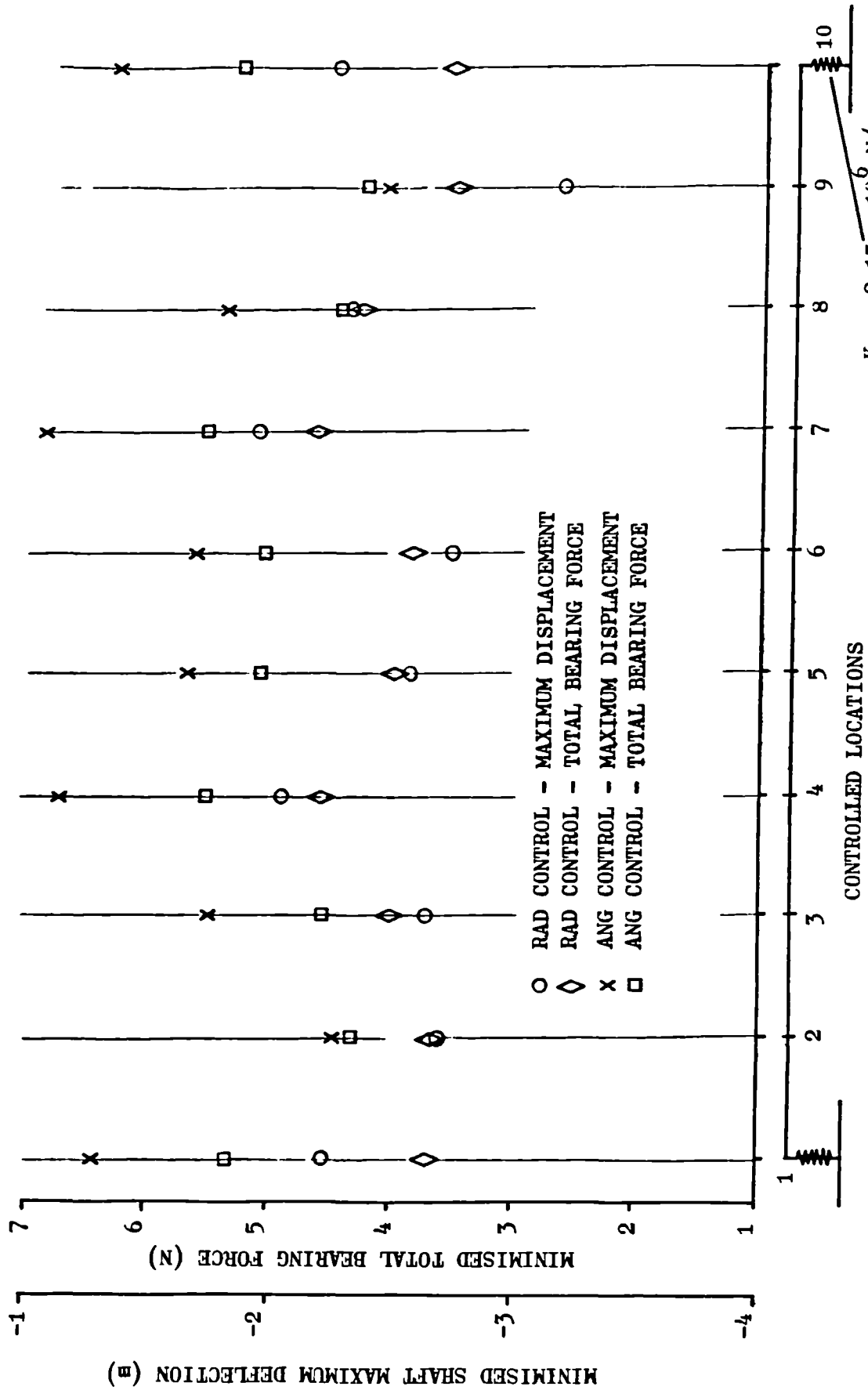

FIG. 5.5b EFFECT OF CONTROLLER LOCATION ON THE MINIMISED PERFORMANCE INDICES (FLEXIBLE SUPPORTS)

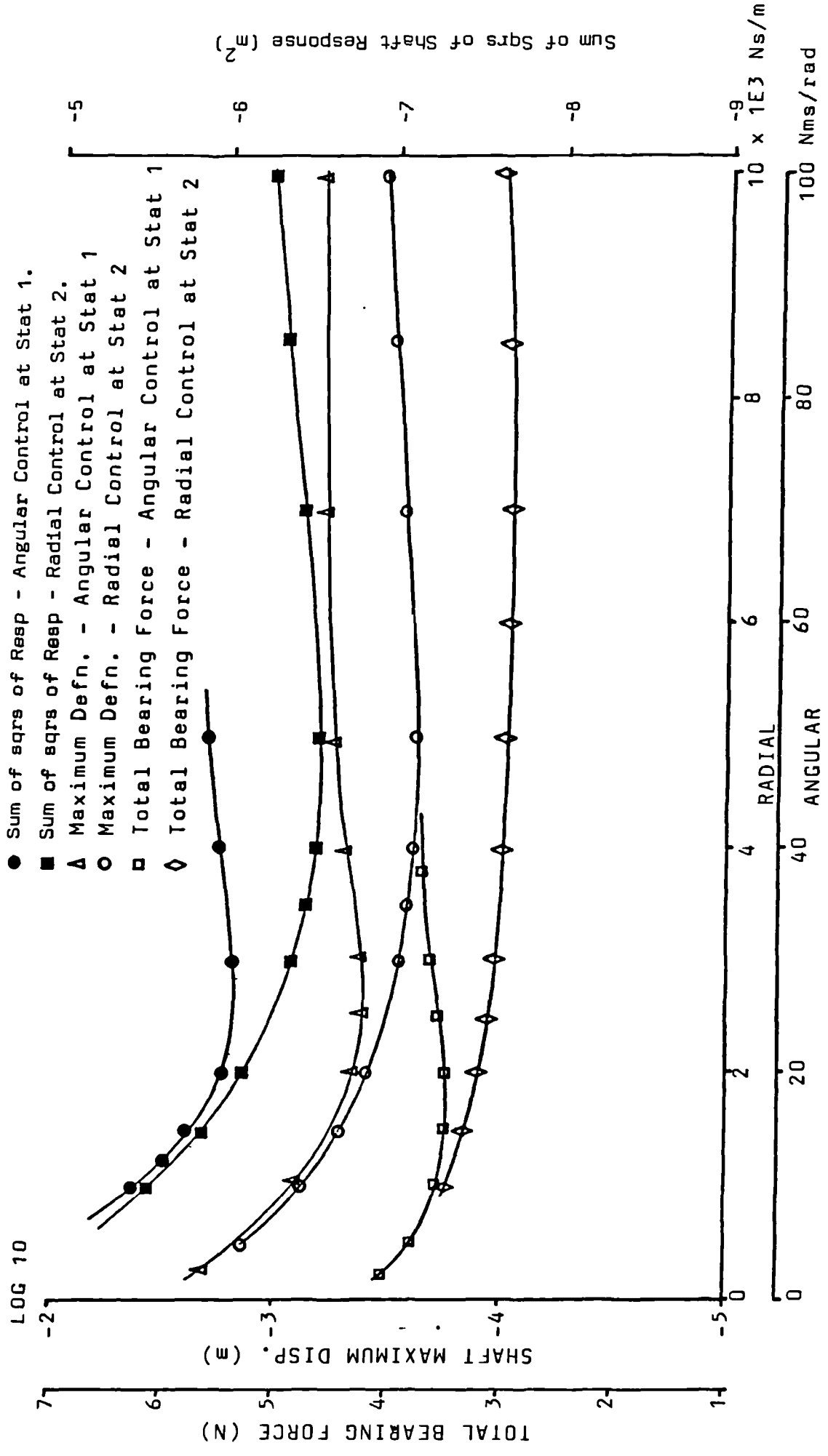

FIG. 5.6 VARIATION OF SYSTEM MAXIMUM RESPONSE WITH CONTROL DAMPING (PINNED SUPPORTS)

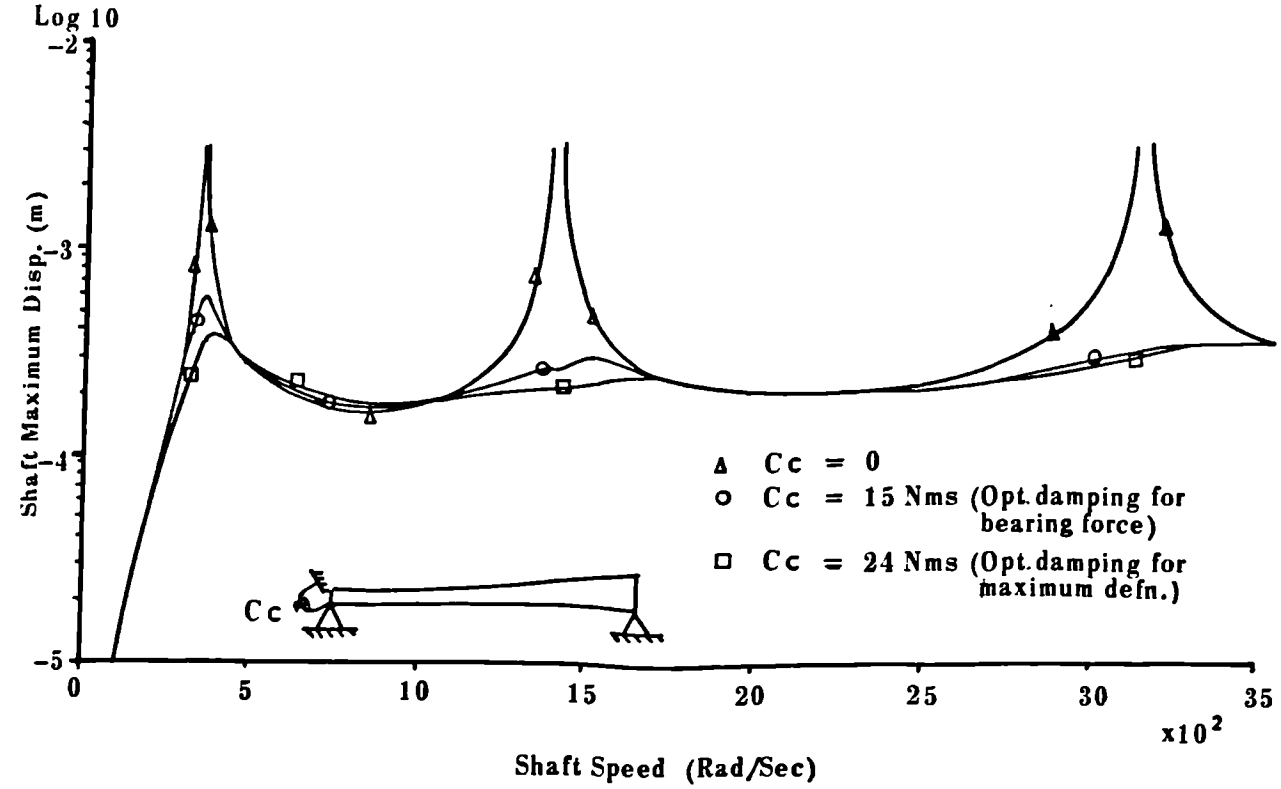

FIG. 5.7a EFFECT OF CHOICE OF PI
– SHAFT MAXIMUM DISPLACEMENT

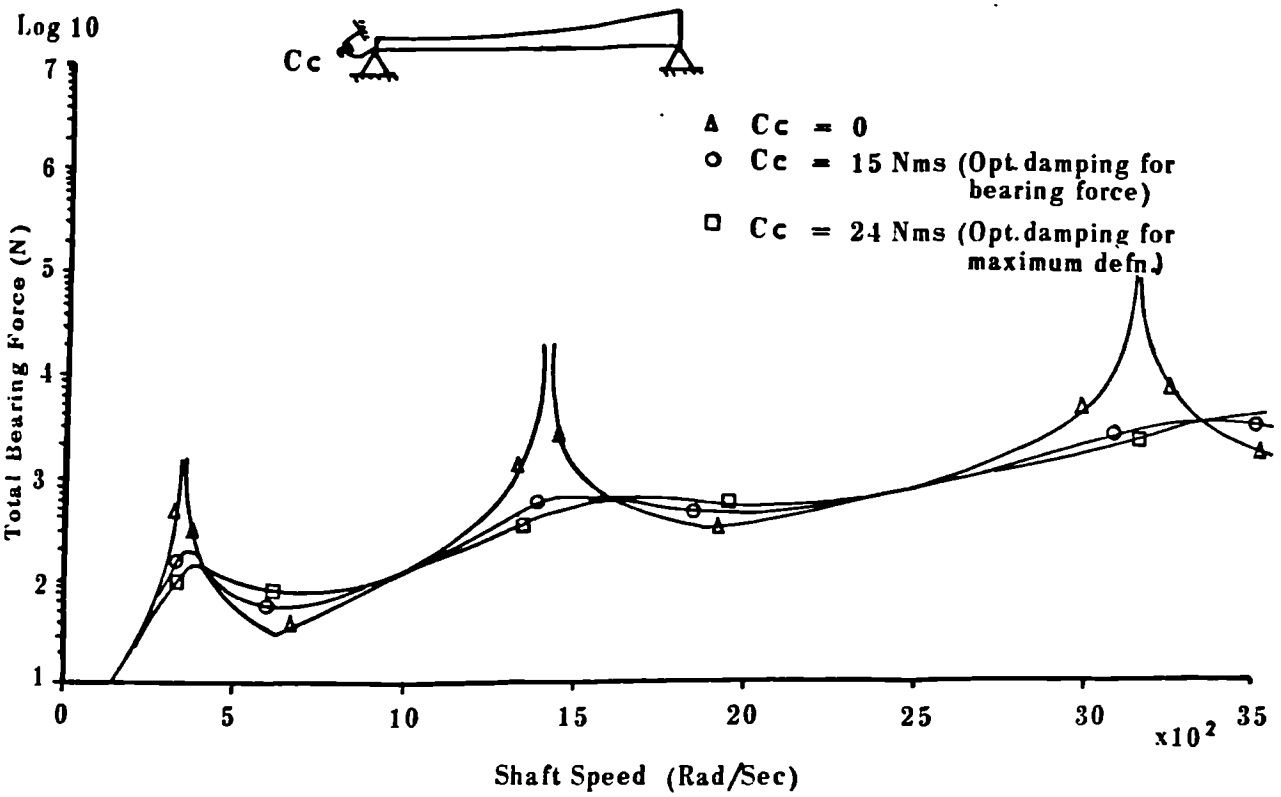

FIG. 5.7b EFFECT OF CHOICE OF PI
– TOTAL BEARING FORCE

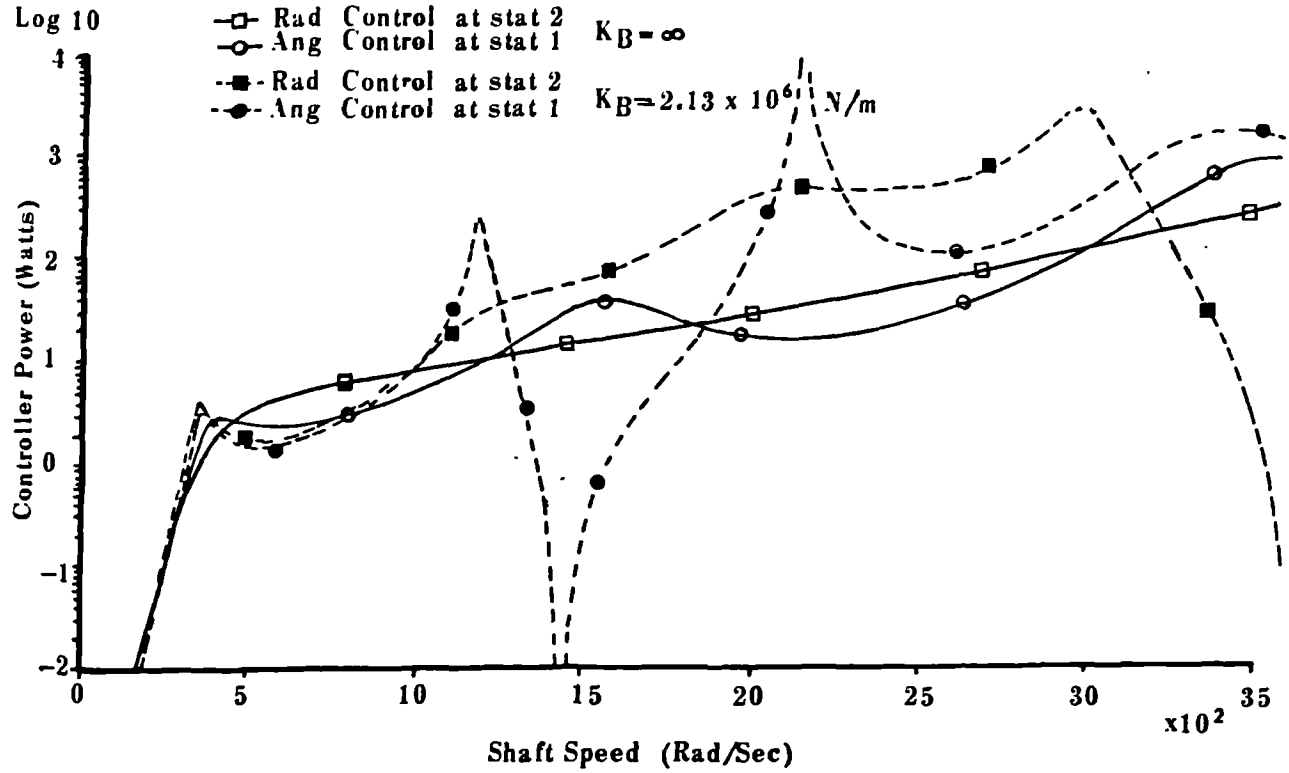

FIG. 5.8 CONTROLLER POWER VERSUS SHAFT SPEED

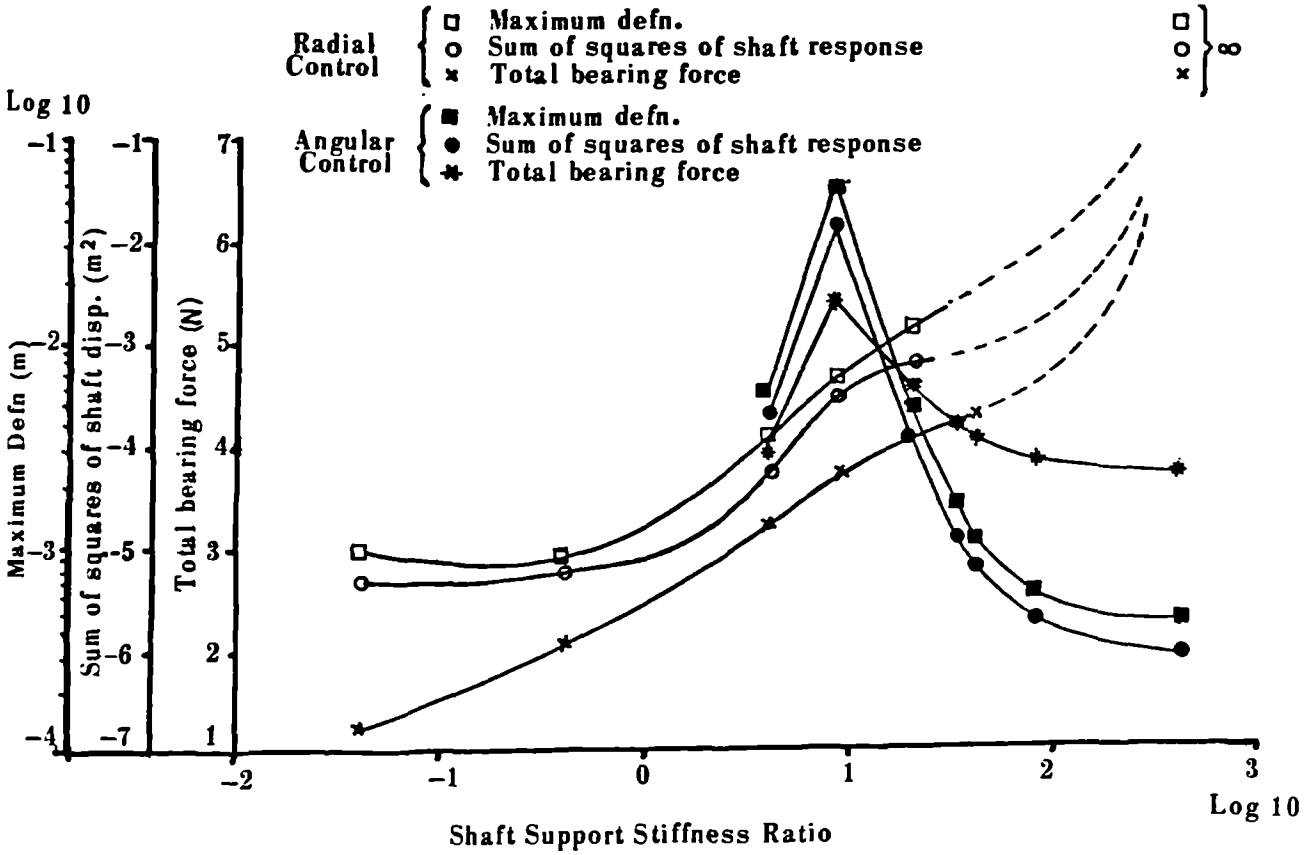

FIG. 5.9a MINIMISED PERFORMANCE INDEX VERSUS SHAFT SUPPORT STIFFNESS RATIO

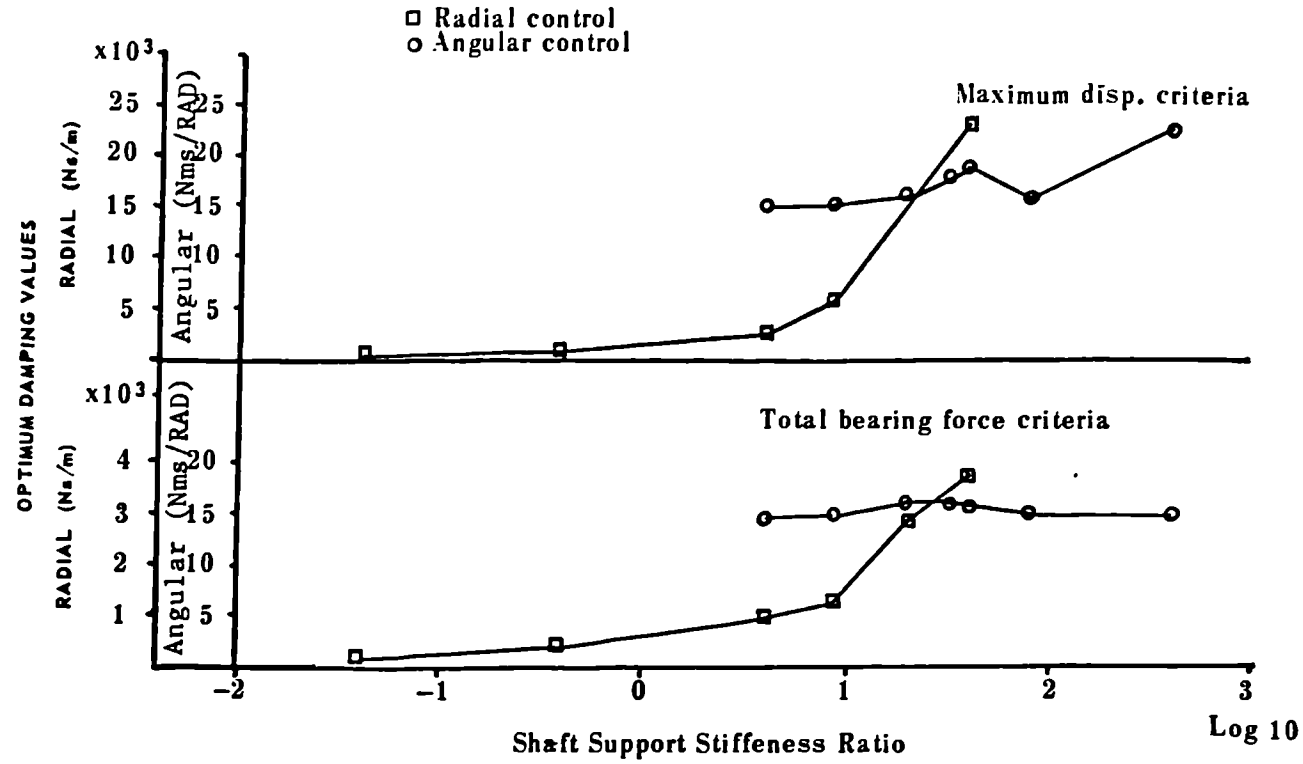

FIG. 5.9b OPTIMUM DAMPING VALUES VERSUS SHAFT SUPPORT STIFFNESS RATIO

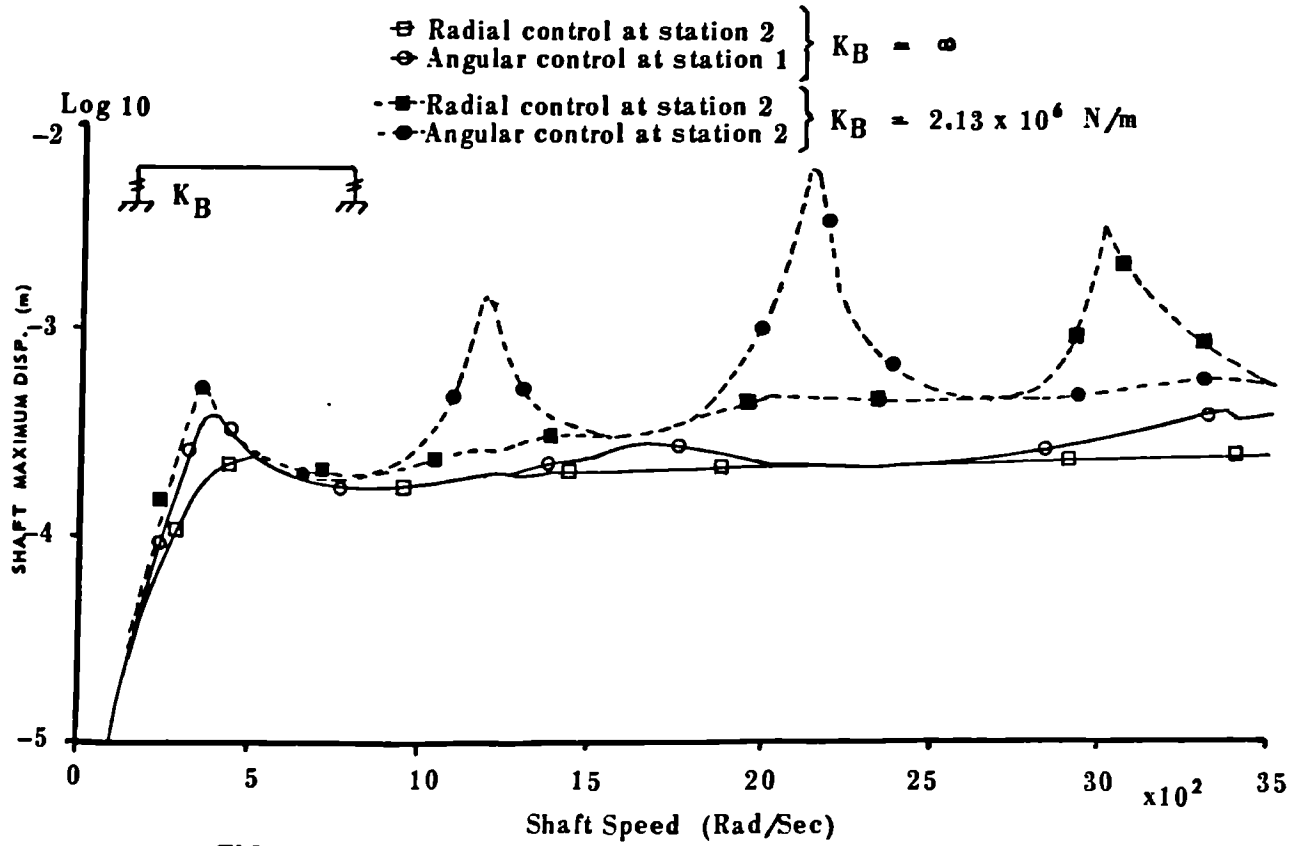

FIG. 5.10a SYSTEM RESPONSE WITH ADAPTIVE CONTROL - CONTROLLERS AT OPTIMUM LOCATIONS

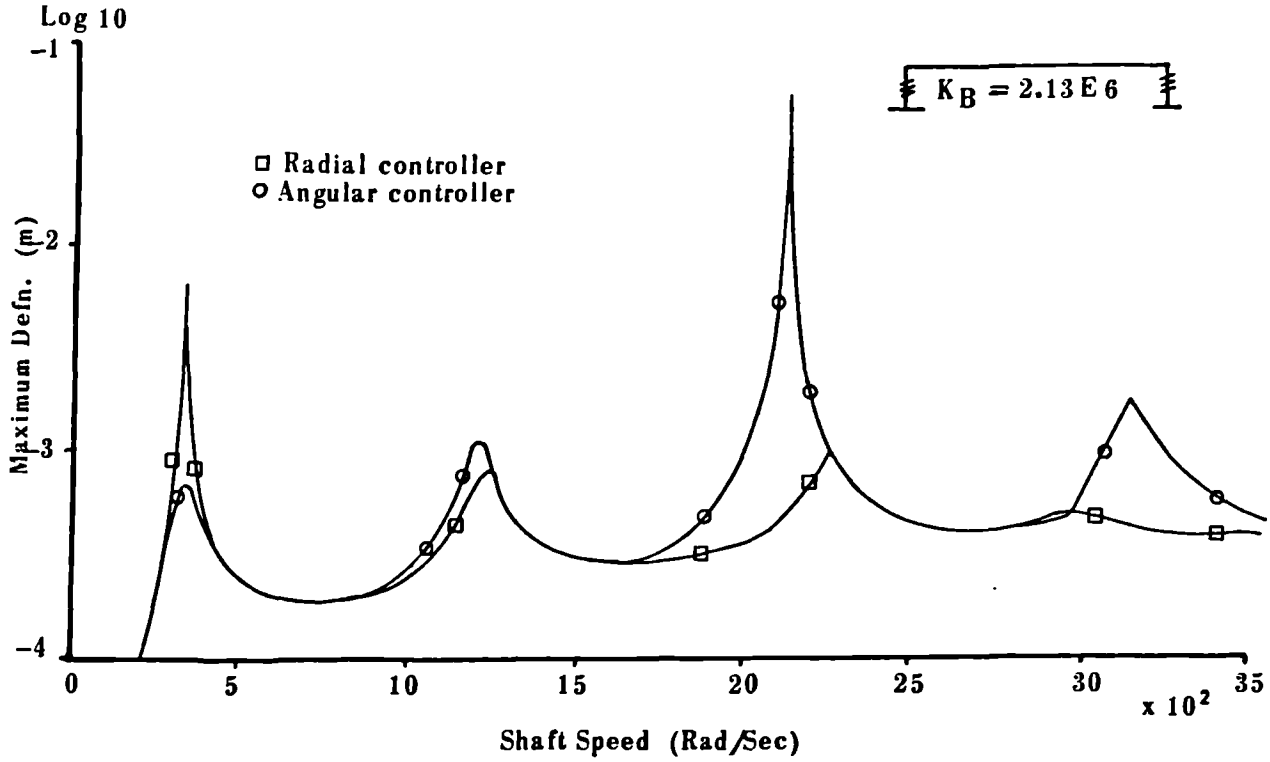

FIG. 5.10b SYSTEM RESPONSE WITH ADAPTIVE CONTROL – CONTROLLERS AT LH SUPPORT

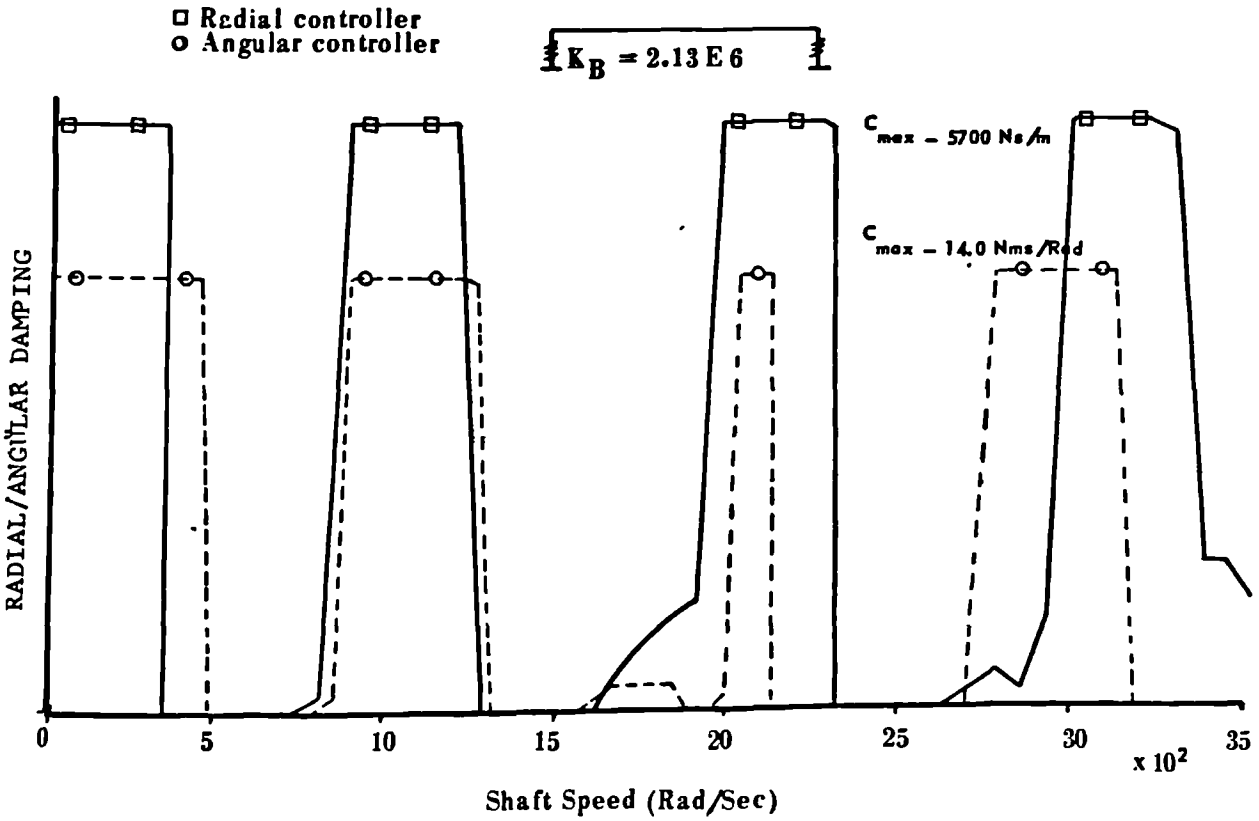

FIG. 5.10c VARIATION OF OPTIMUM DAMPING – ADAPTIVE CONTROL

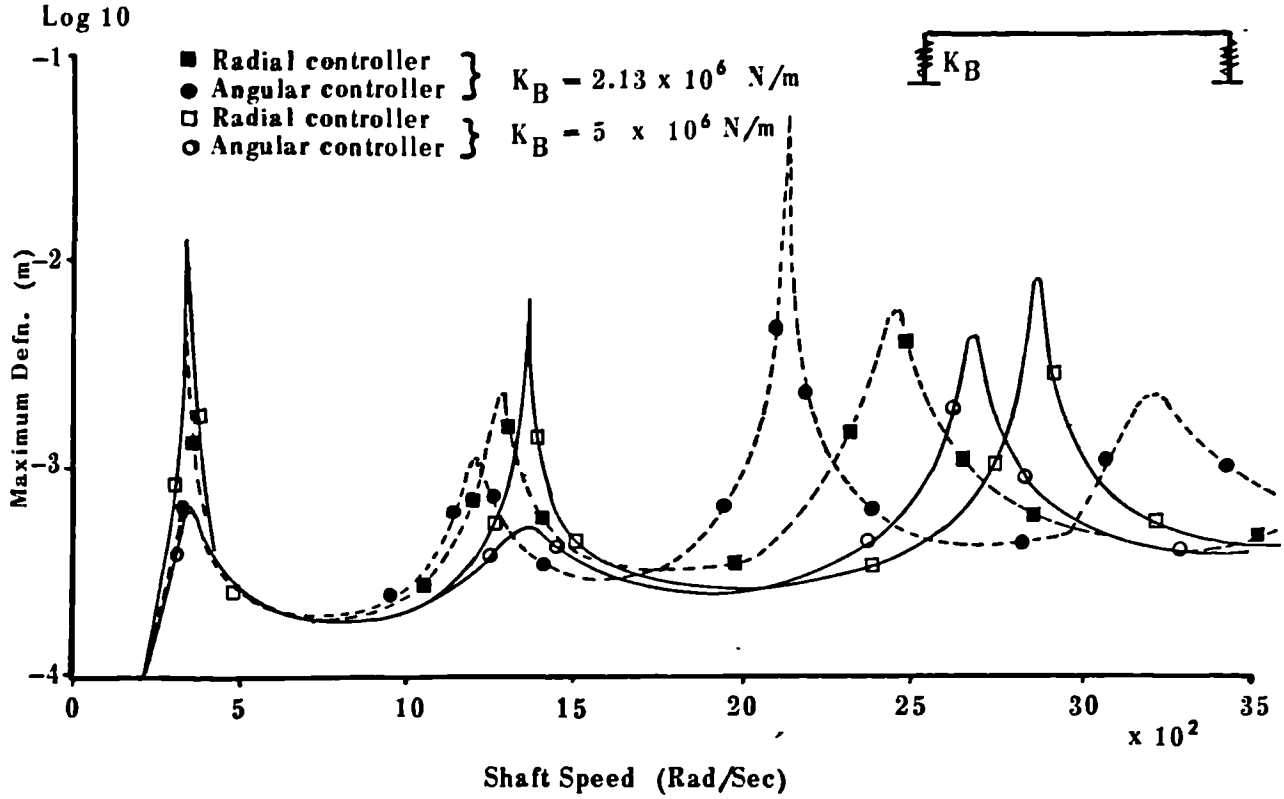

FIG. 5.10d SYSTEM RESPONSE WITH PASSIVE CONTROL
– CONTROLLERS AT LH SUPPORT

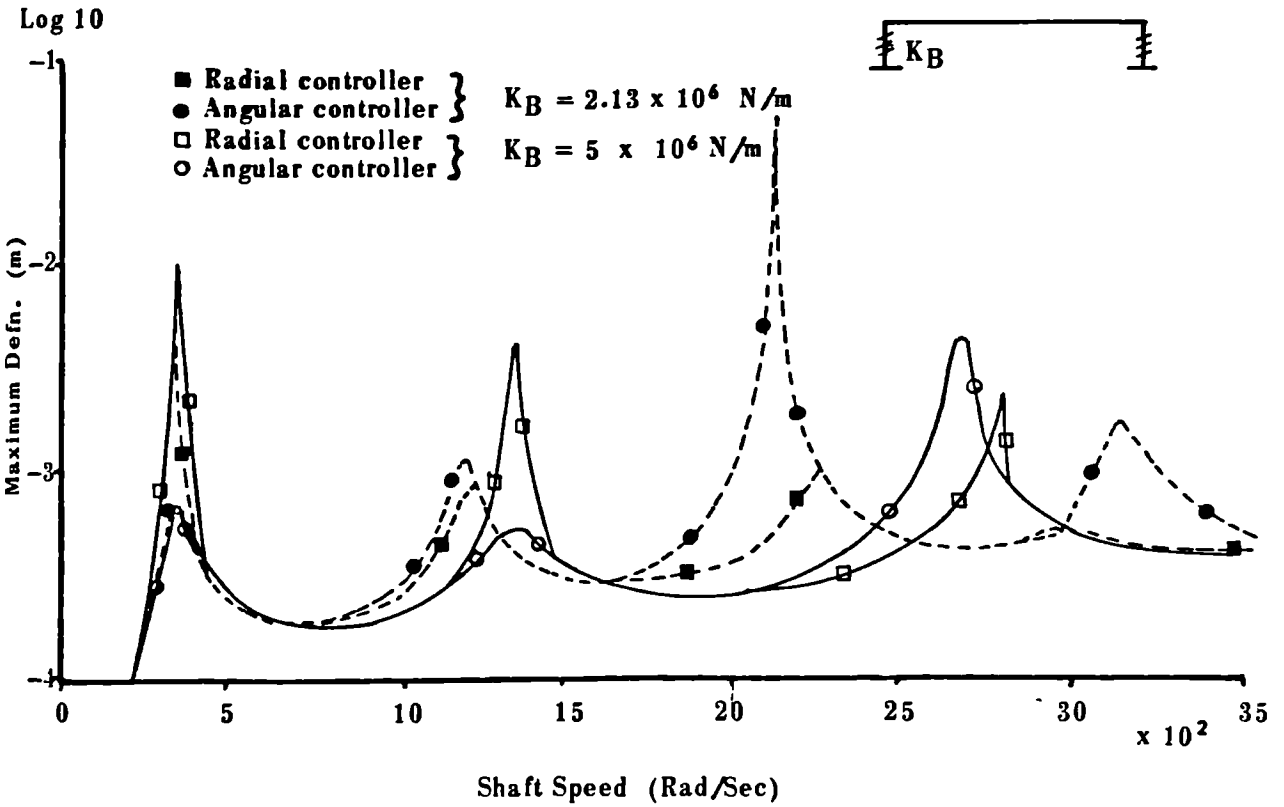

FIG. 5.10e SYSTEM RESPONSE WITH ADAPTIVE CONTROL
– CONTROLLERS AT LH SUPPORT

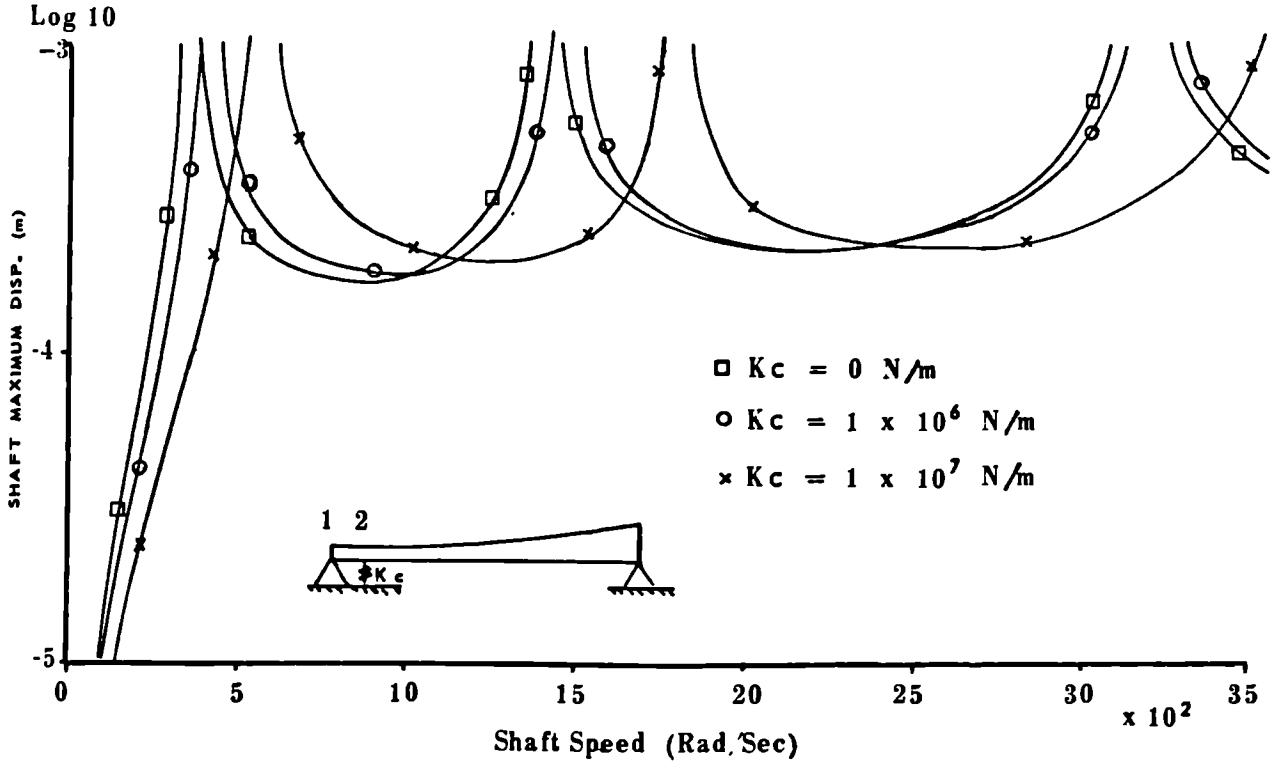

FIG. 5.11a RADIAL PASSIVE STIFFNESS CONTROL

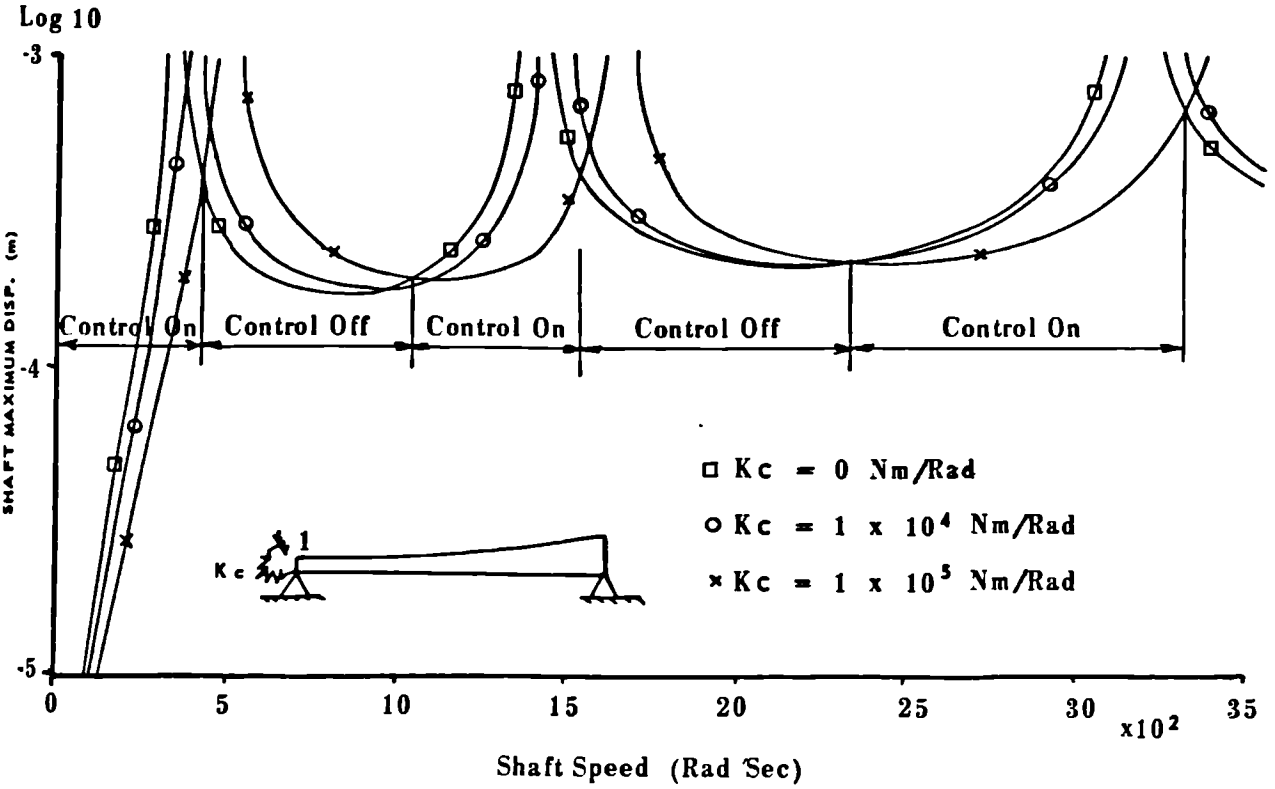

FIG. 5.11b ANGULAR PASSIVE STIFFNESS CONTROL

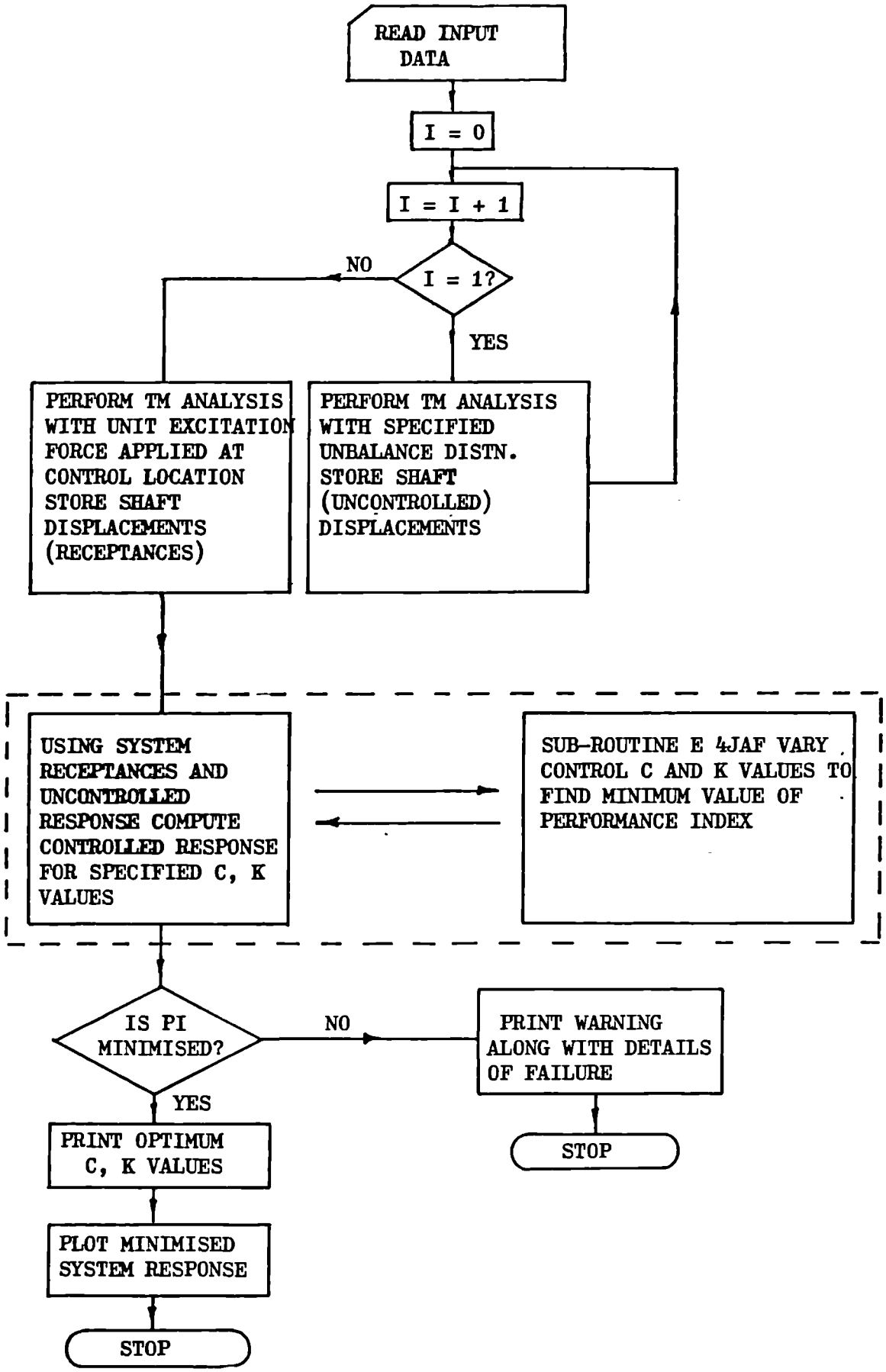

FIG. 5.12 OPTIMISATION PROGRAM FLOW CHART

ALL DIMENSIONS IN MILLIMETRES

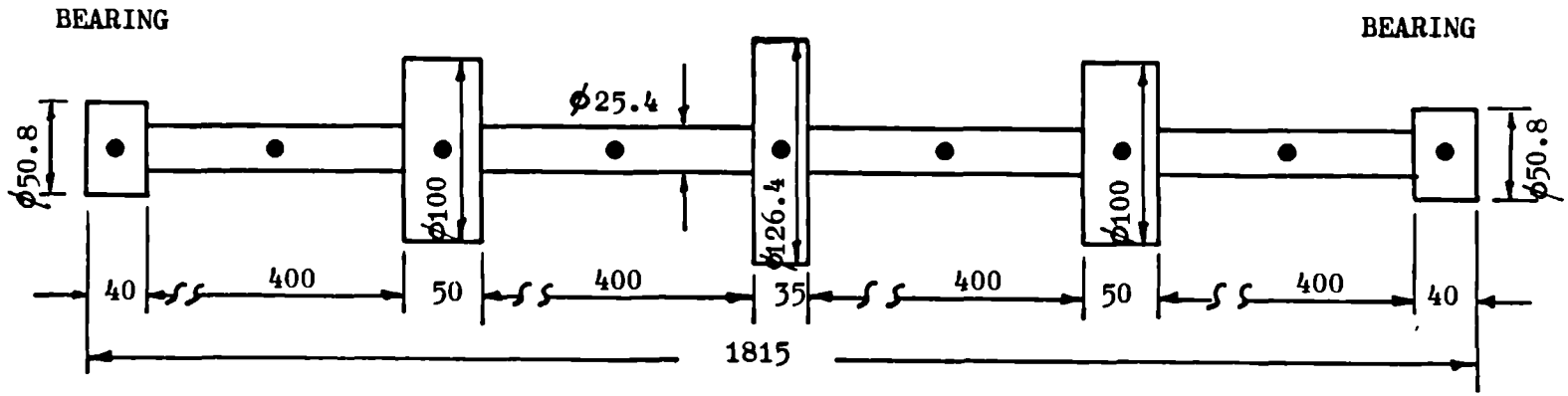

BEARING DETAILS

JOURNAL LENGTH, ℓ = 0.0169 m
JOURNAL RADIUS, R = 0.0254 m
RADIAL CLEARANCE, C = 1.27×10^{-4} m
LUBRICANT VISCOSITY, μ = 0.015 Ns/m^2

FIG. 5.13 ROTOR MODEL (DUE TO BURROWS et al [92]) USED FOR STABILITY ANALYSIS

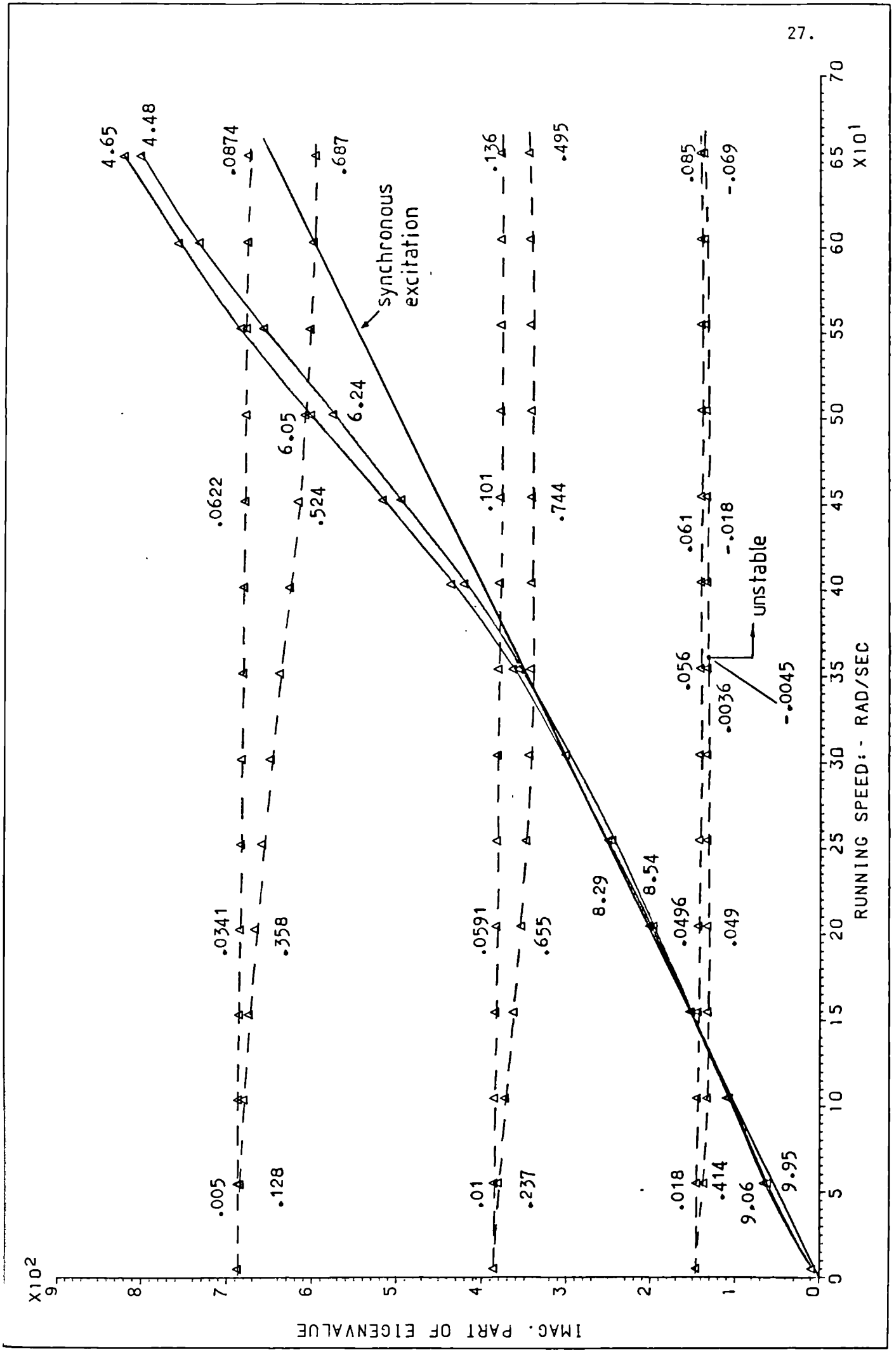

FIG. 5.14a PLOT OF EIGENVALUES VERSUS SPEED (UNCONTROLLED)

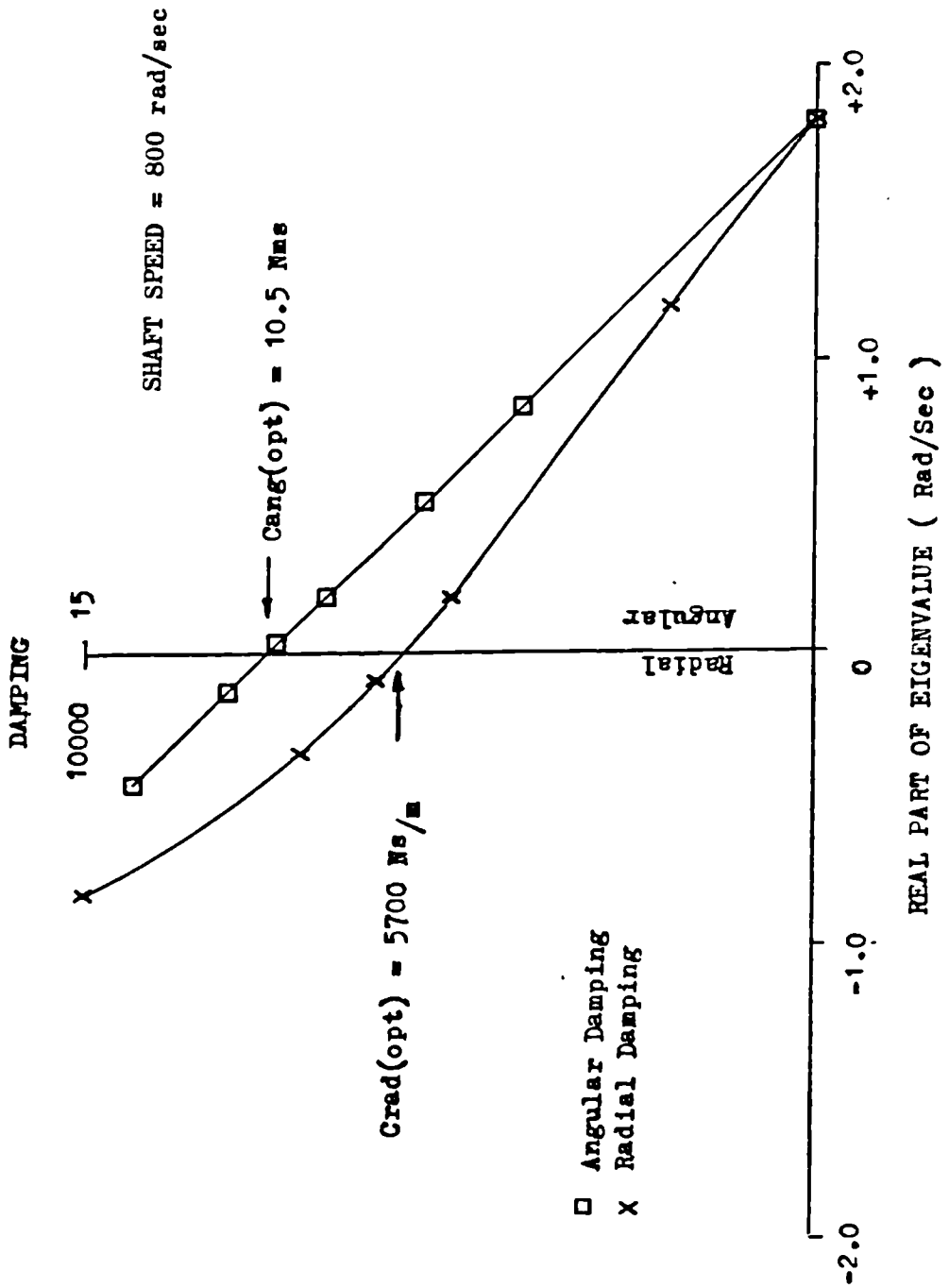

FIG. 5.14b EFFECT OF DAMPING CONTROL ON SYSTEM STABILITY

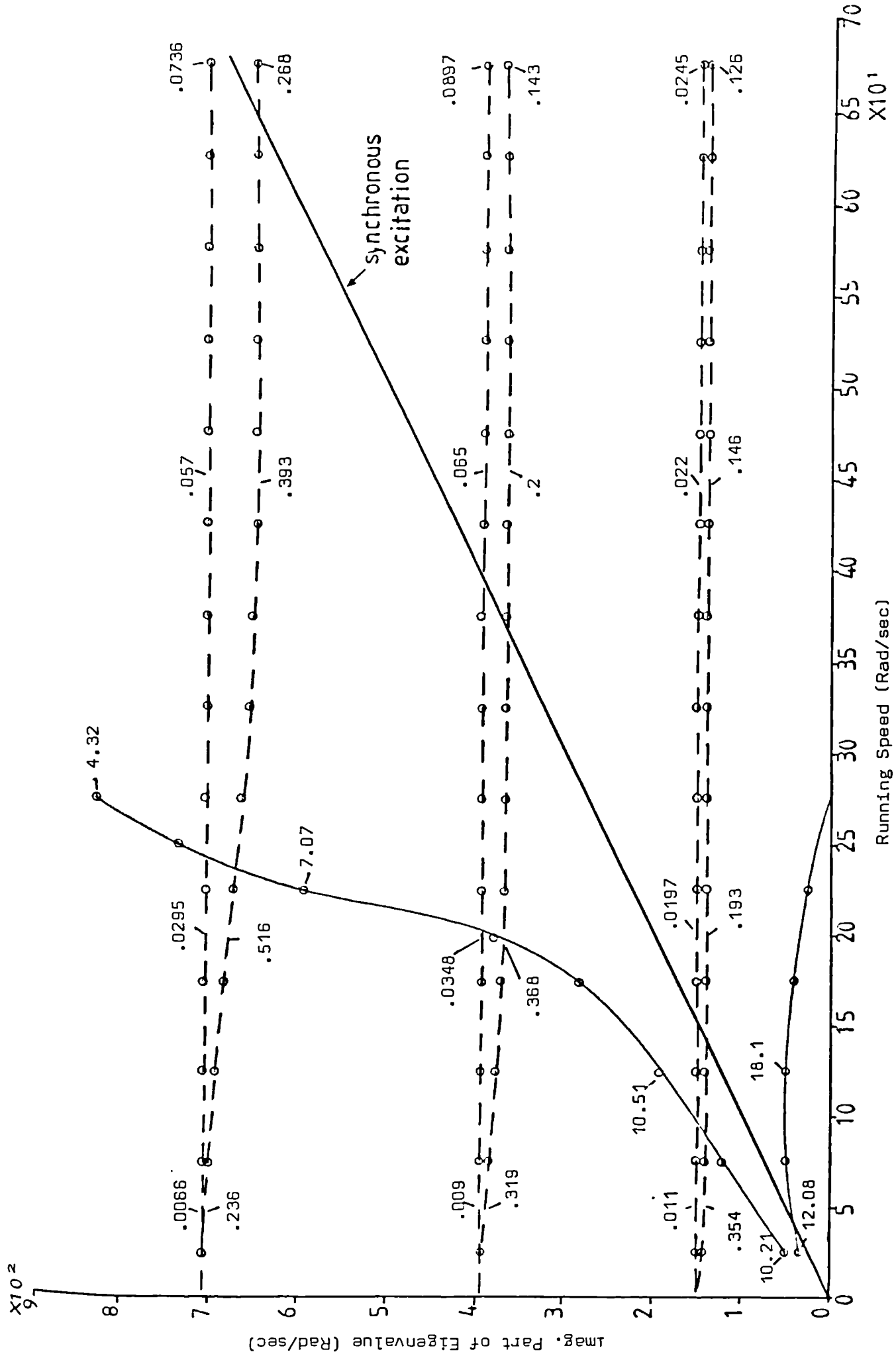

FIG. 5.14c PLOT OF SYSTEM EIGENVALUES (RADIAL DAMPING = 5700 Ns/m)

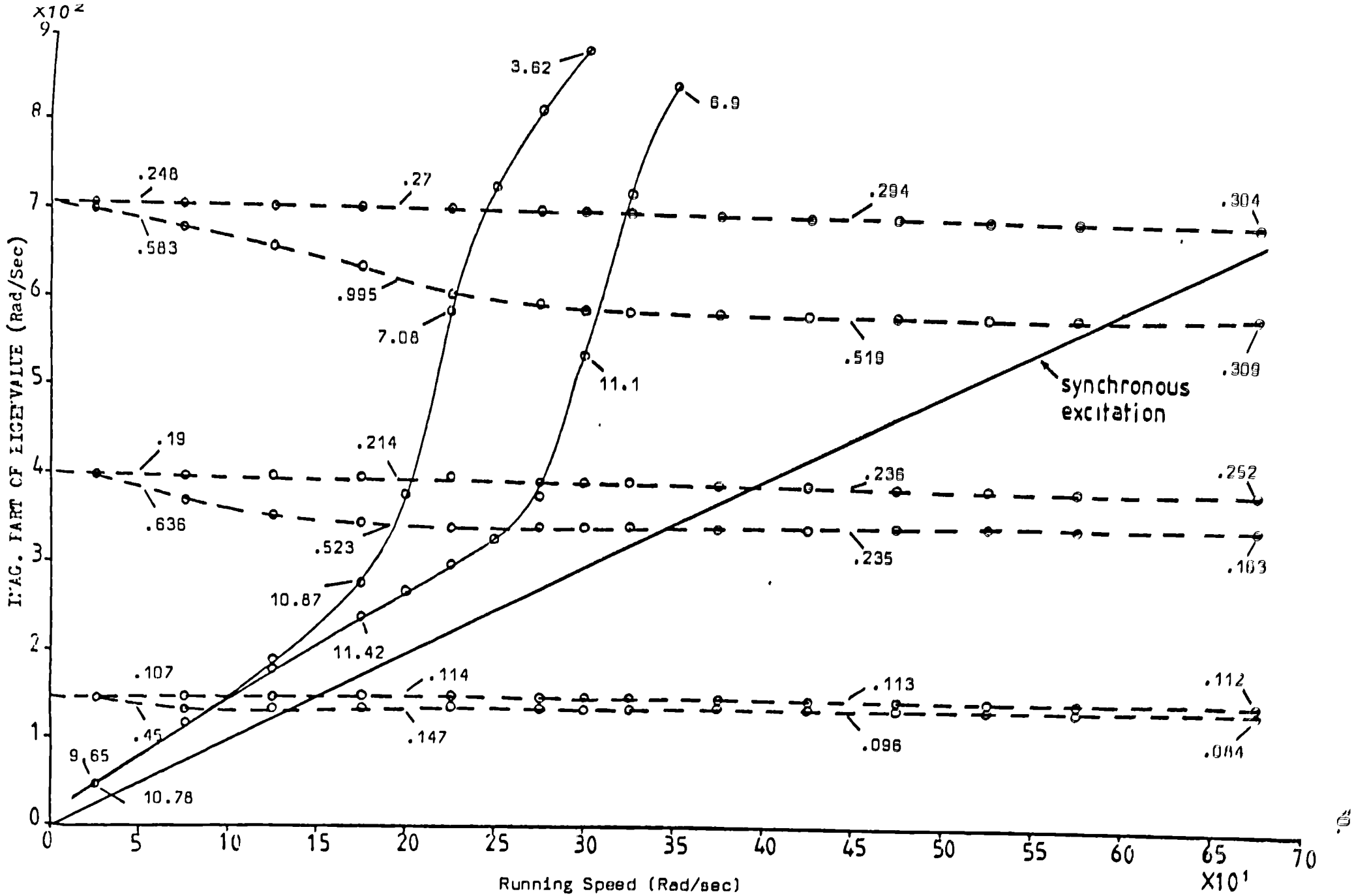

FIG. 5.14d PLOT OF SYSTEM EIGENVALUES (ANGULAR DAMPING = 10.5 Nms/rad)

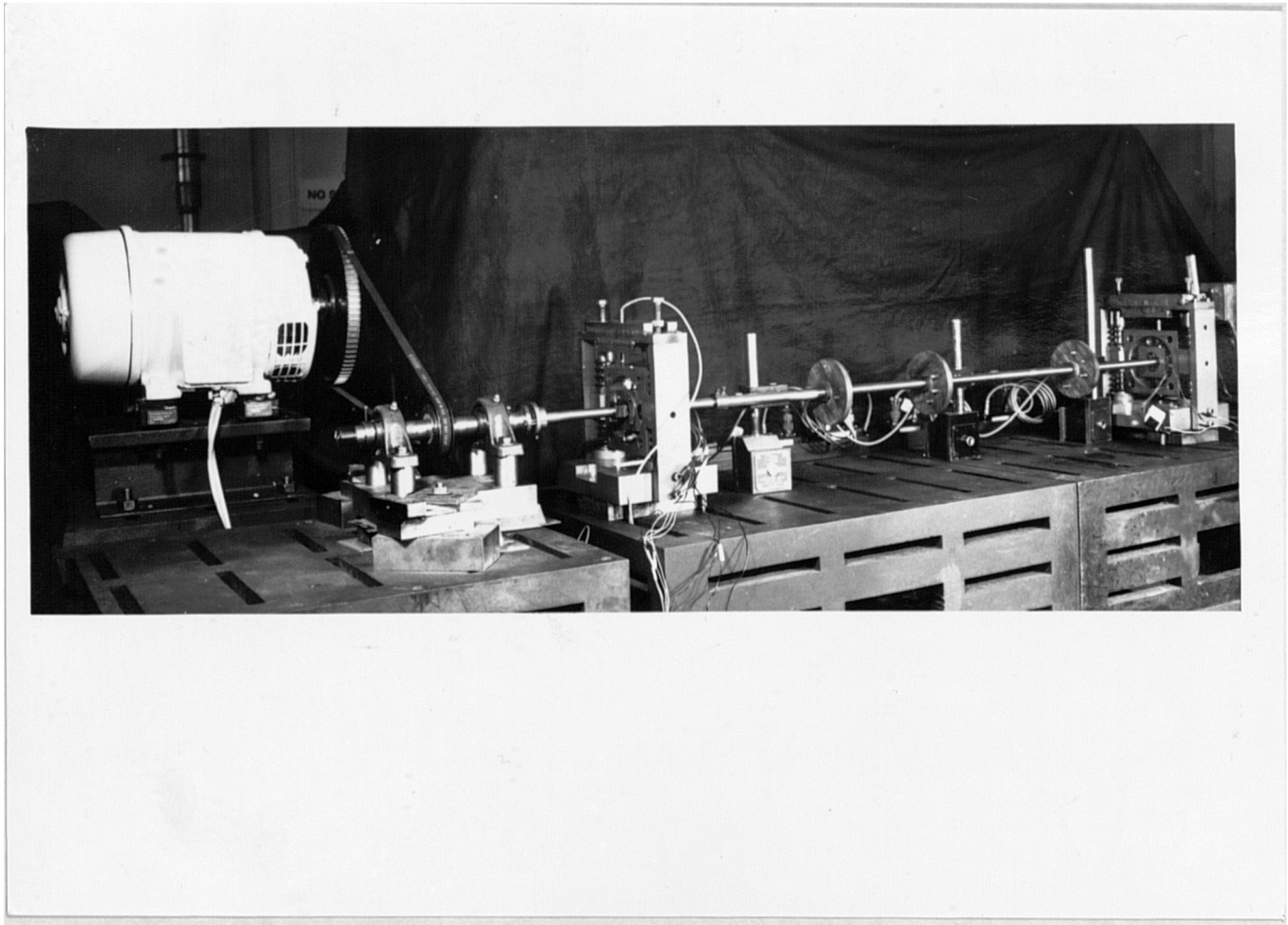

FIG. 6.1a TEST RIG - GENERAL ARRANGEMENT

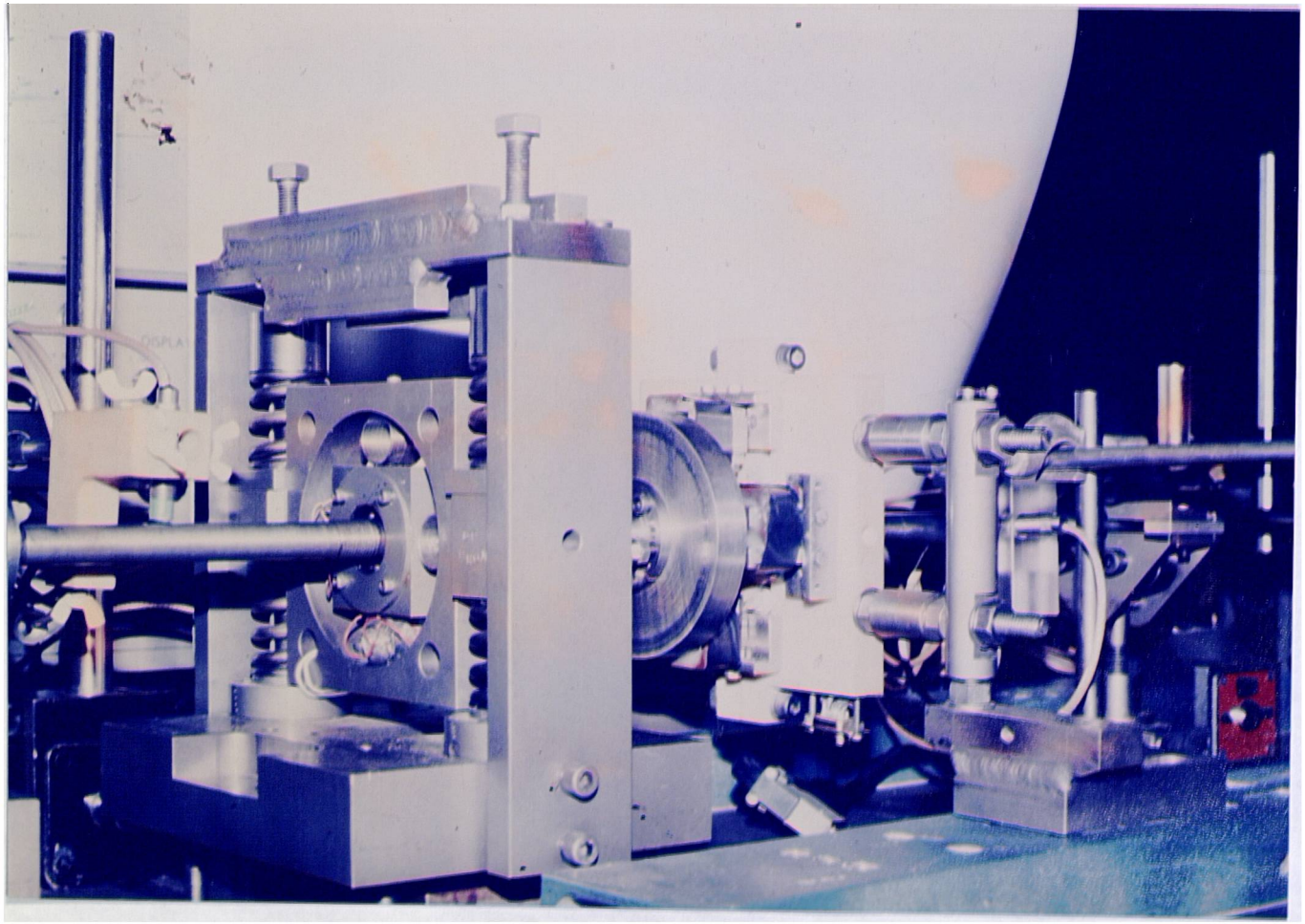

FIG. 6.1b TEST RIG WITH ANGULAR ELECTROMAGNETIC CONTROLLER

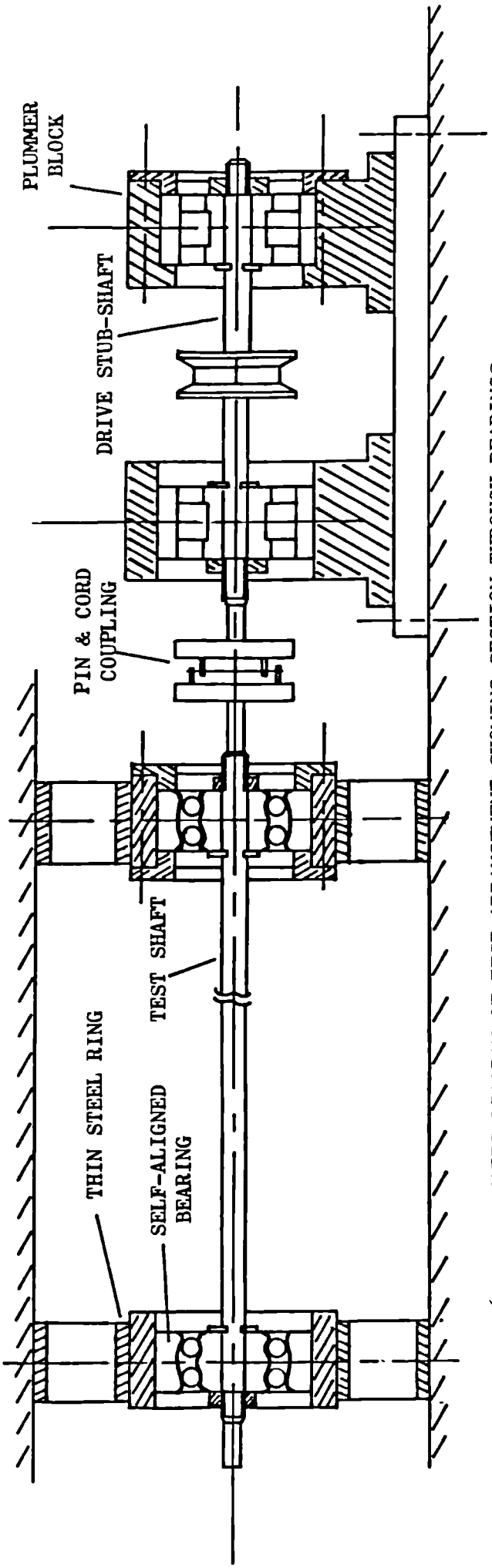

FIG. 6.2 SCHEMATIC DIAGRAM OF TEST ARRANGEMENT SHOWING SECTION THROUGH BEARINGS

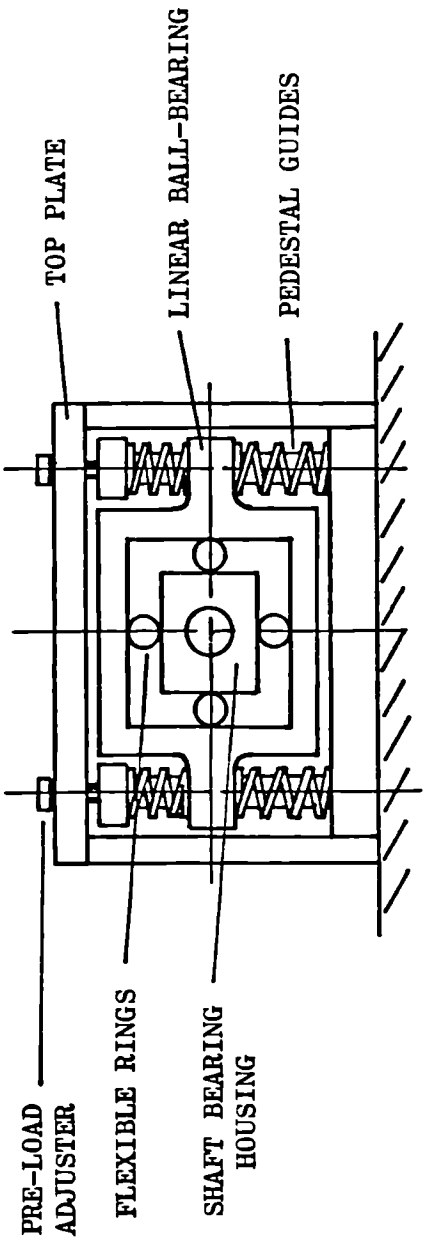

FIG. 6.3 BEARING SUPPORT STRUCTURE

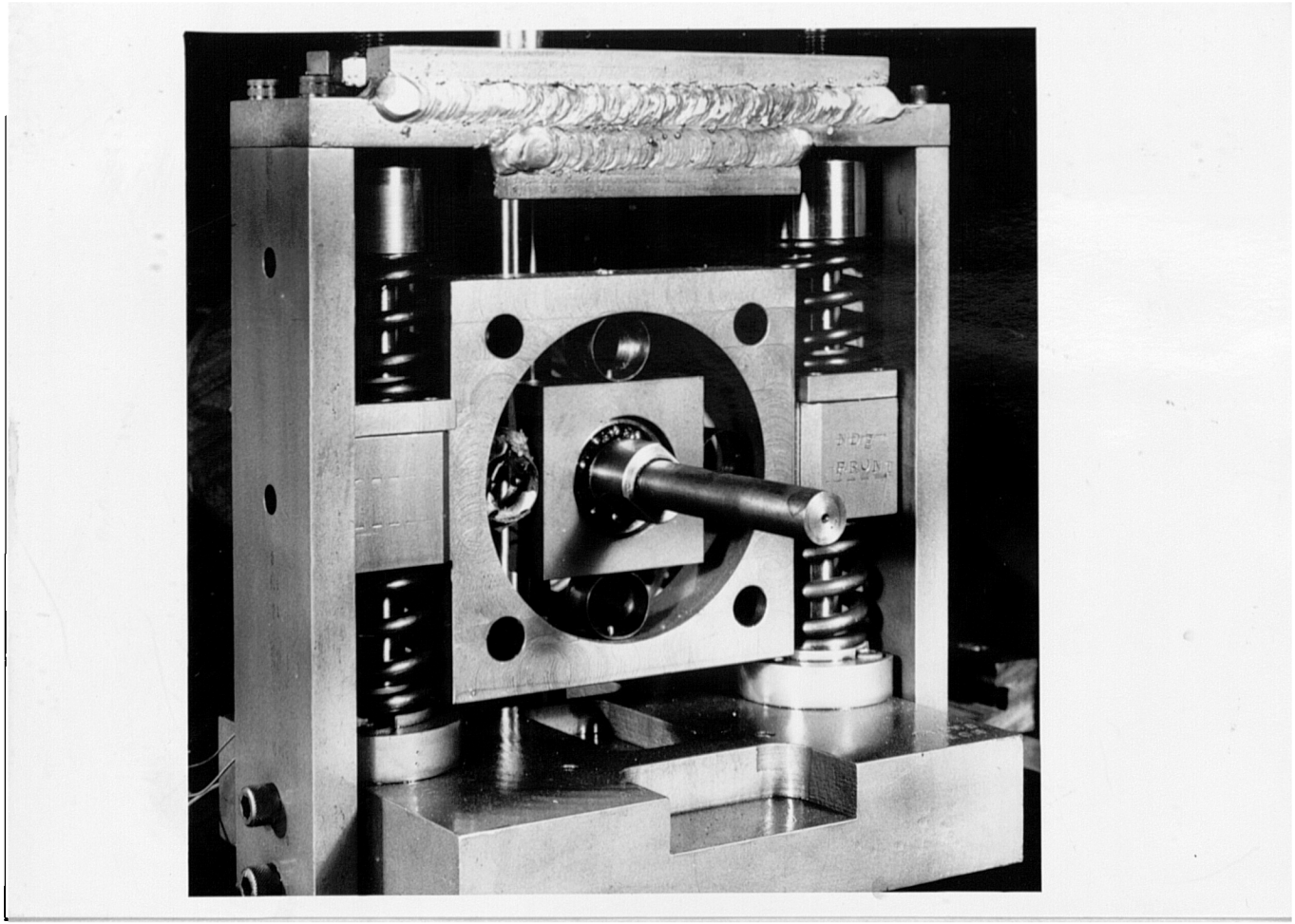

FIG. 6.4 BEARING SUPPORT STRUCTURE

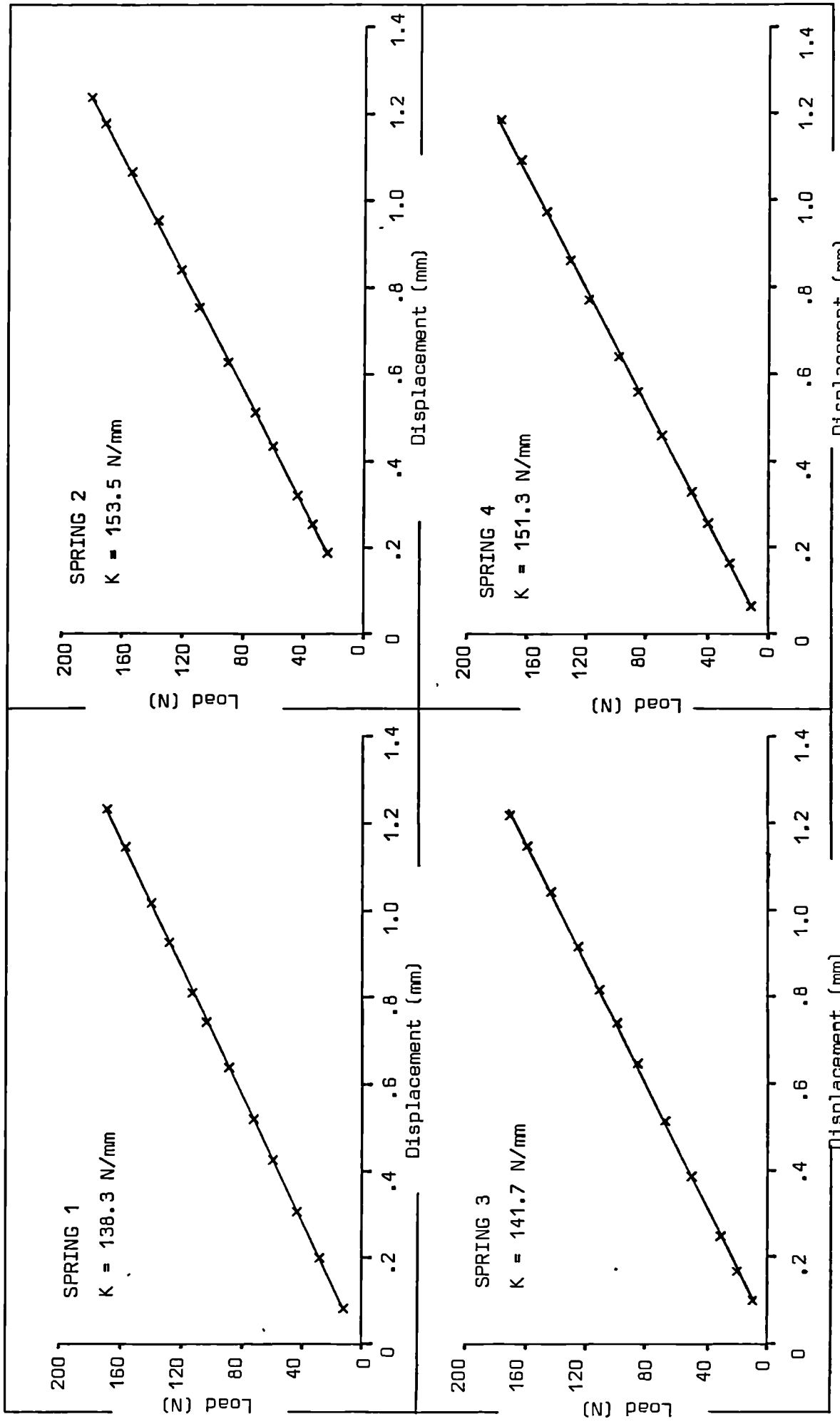

FIG. 6.5 MEASURED BEARING PEDESTAL SPRING STIFFNESS (FIRST FOUR SPRINGS)

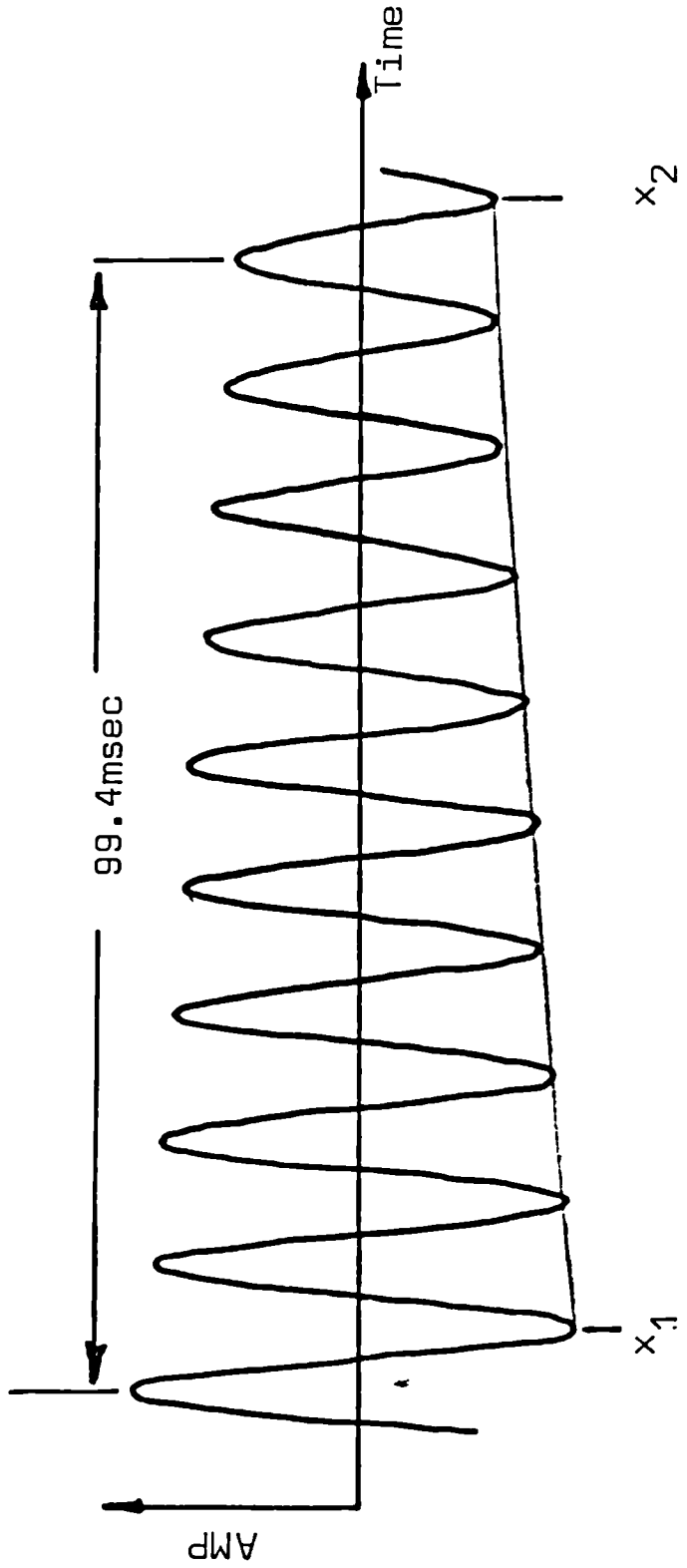

Log Decrement = .0496

Damping Factor = .0079

Frequency = 5435 cyc/min

Fig.6.6 Transient Response of N.D.E. Bearing Pedestal Arrangement

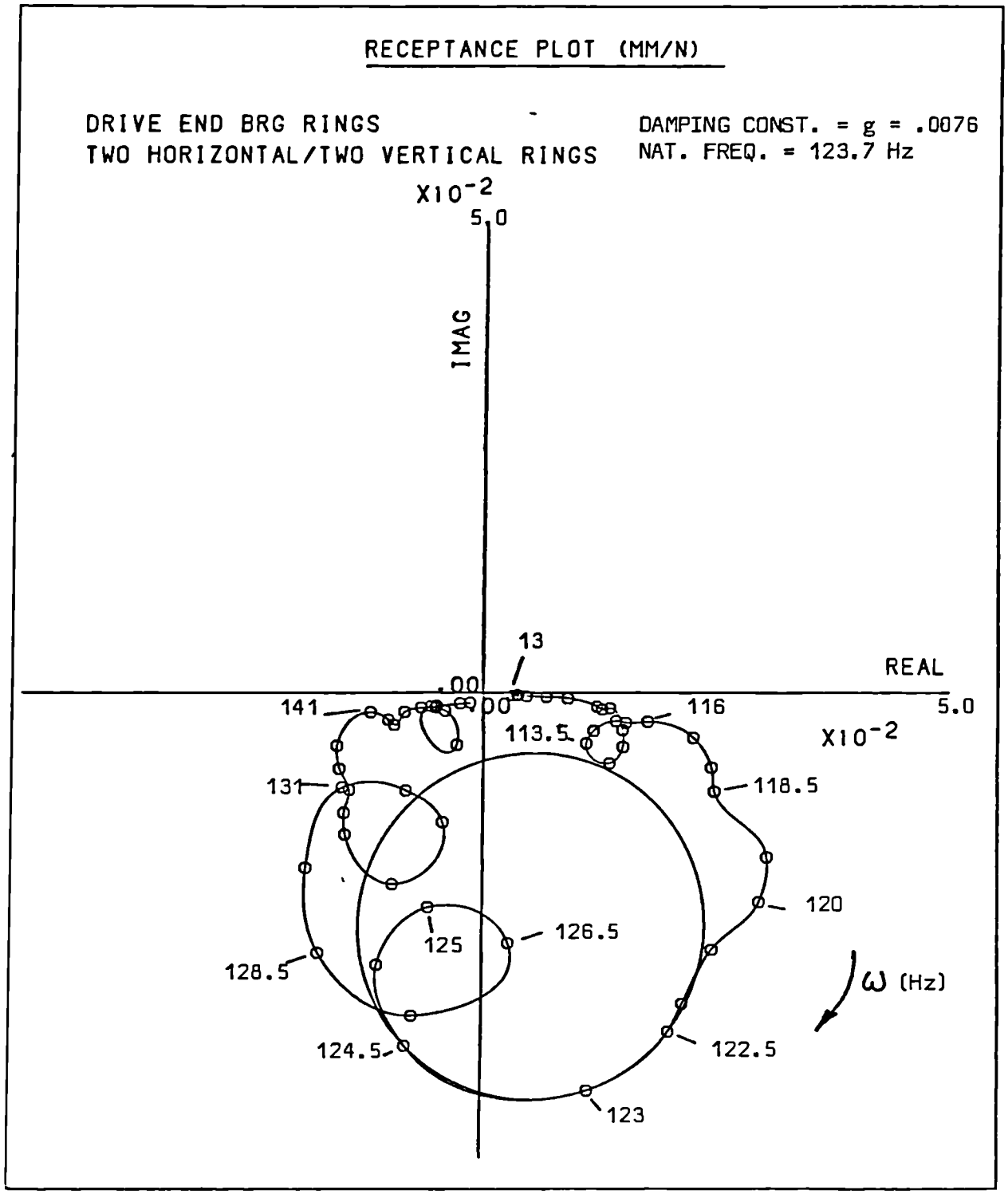

Fig. 6.7 Brg. Hsg. Receptance Details

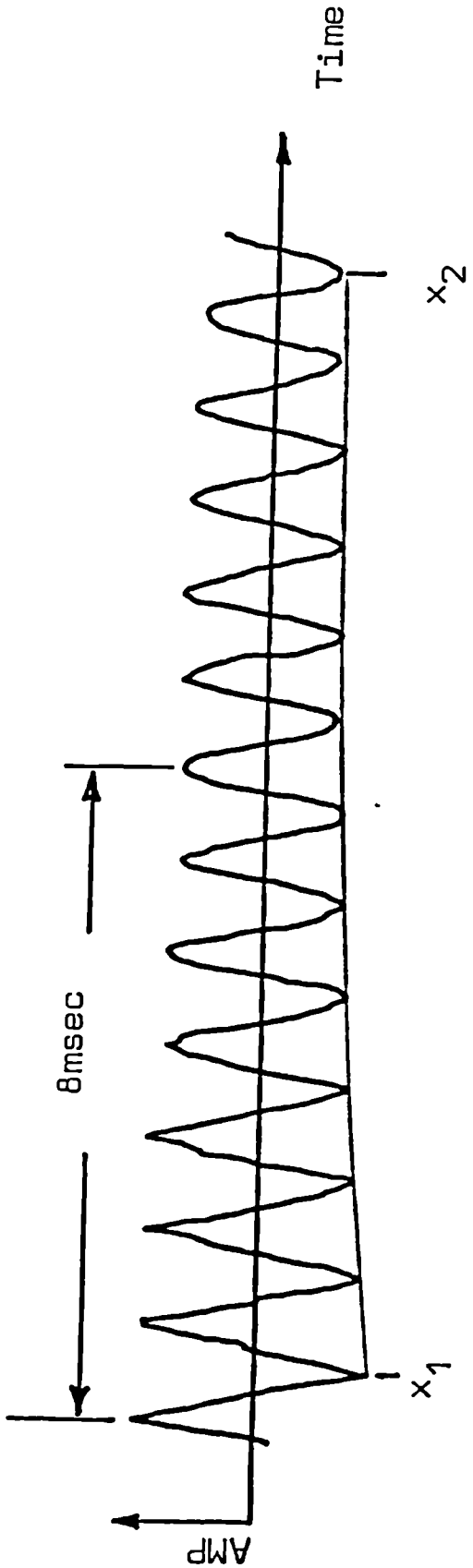

Log Decrement = .0505

Damping Factor .008

Fig. 6.8 Bearing Ring Transient Response

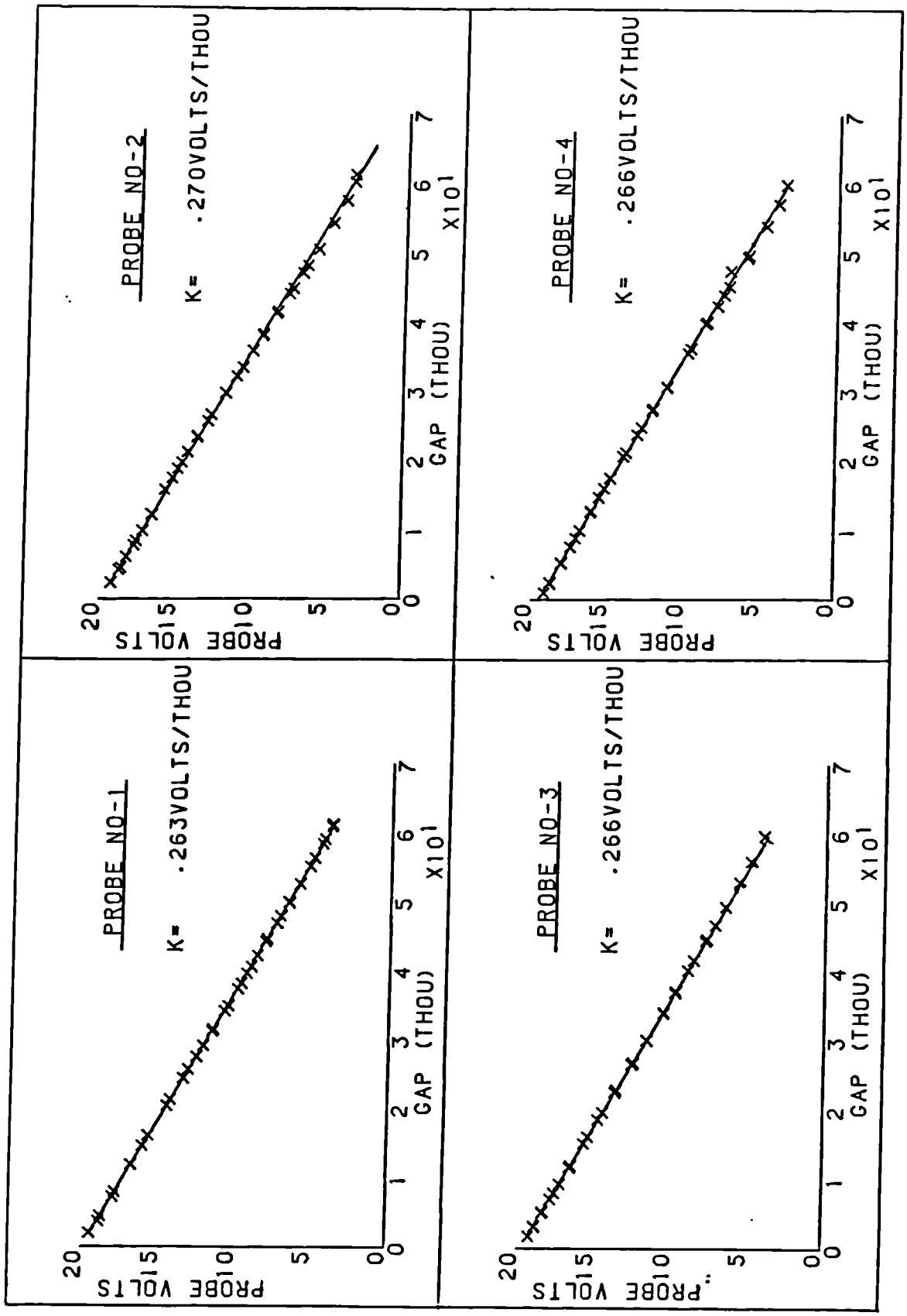

Fig.6.9 DISP. PROBE CALIBRATION DATA

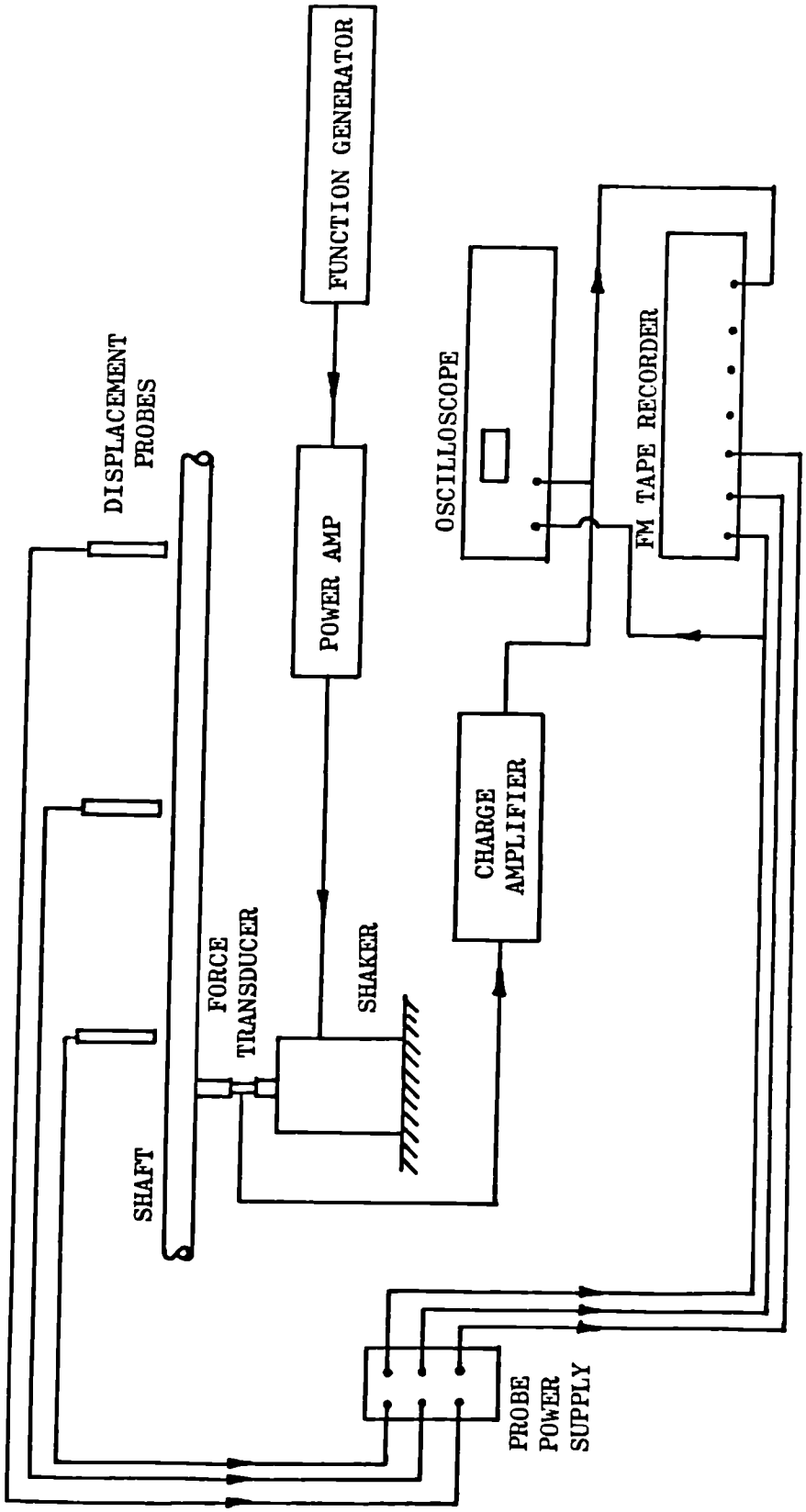

FIG. 6.10 SCHEMATIC OF EXPERIMENTAL SET-UP FOR SHAFT RECEPTANCE MEASUREMENT

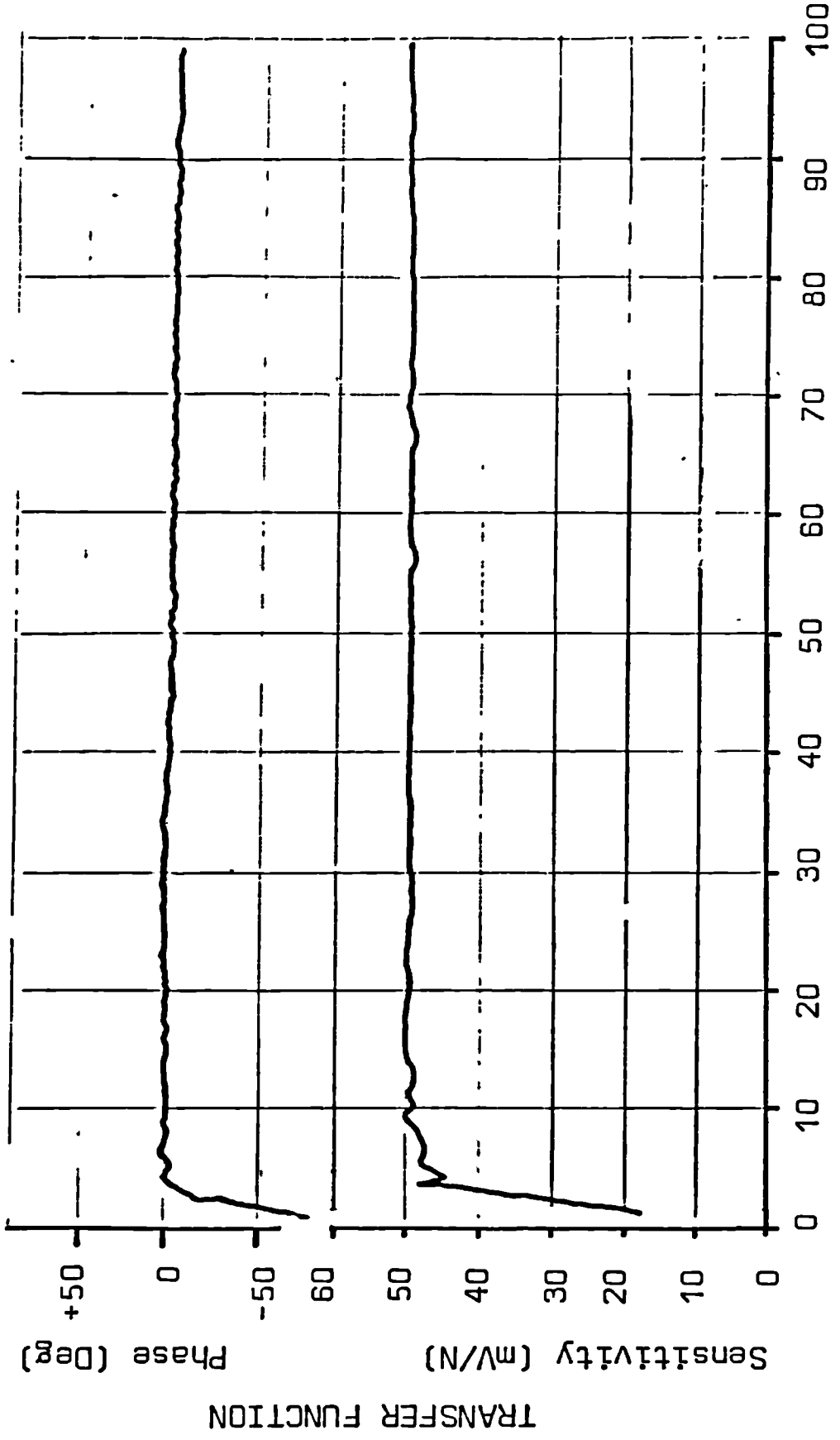

Fig.6.11 Characteristics of Axial Semi-Conductor Strain Gauge Force Transducer/AMP.

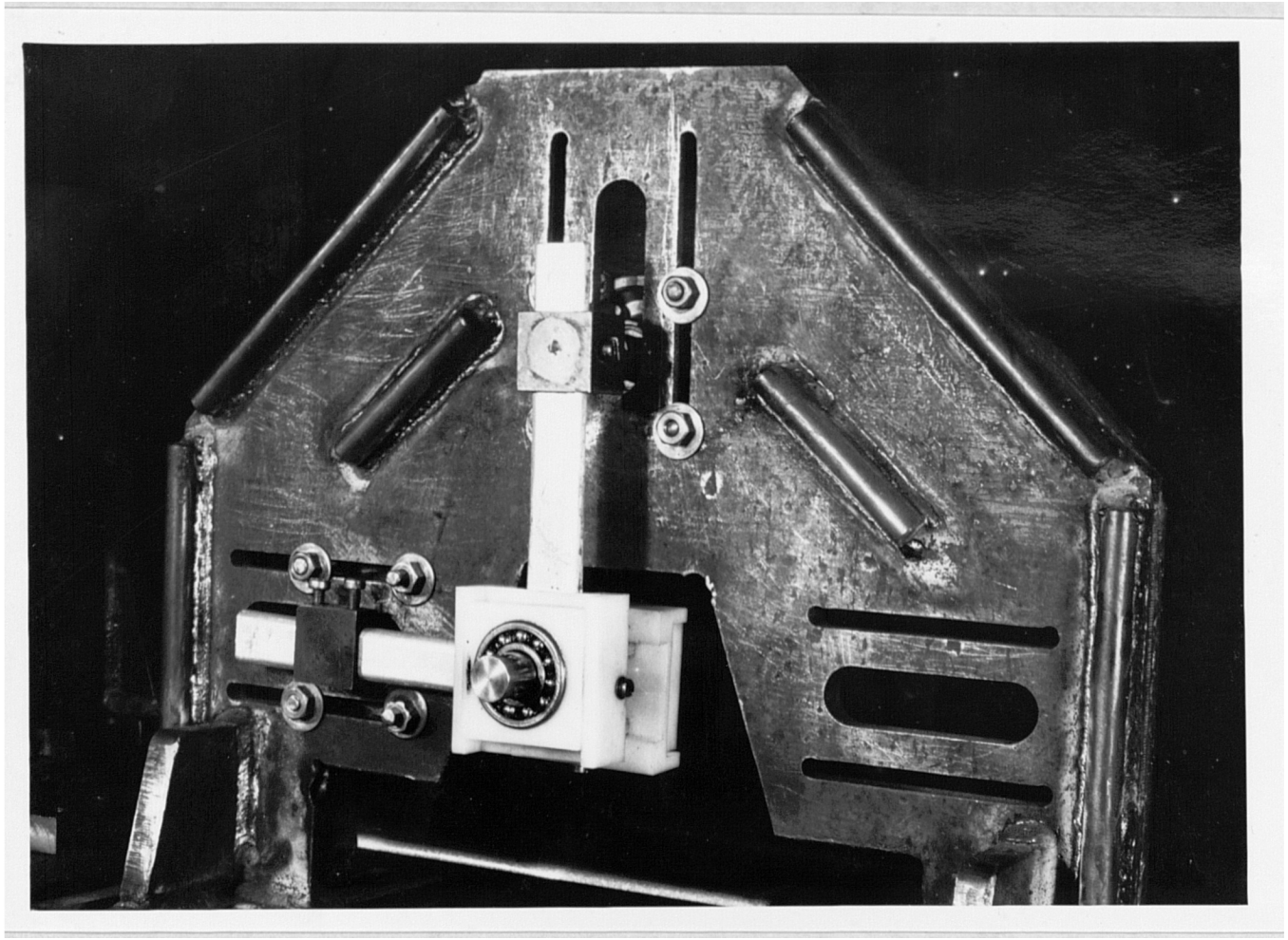

FIG. 6.12 RADIAL MECHANICAL DAMPER ARRANGEMENT

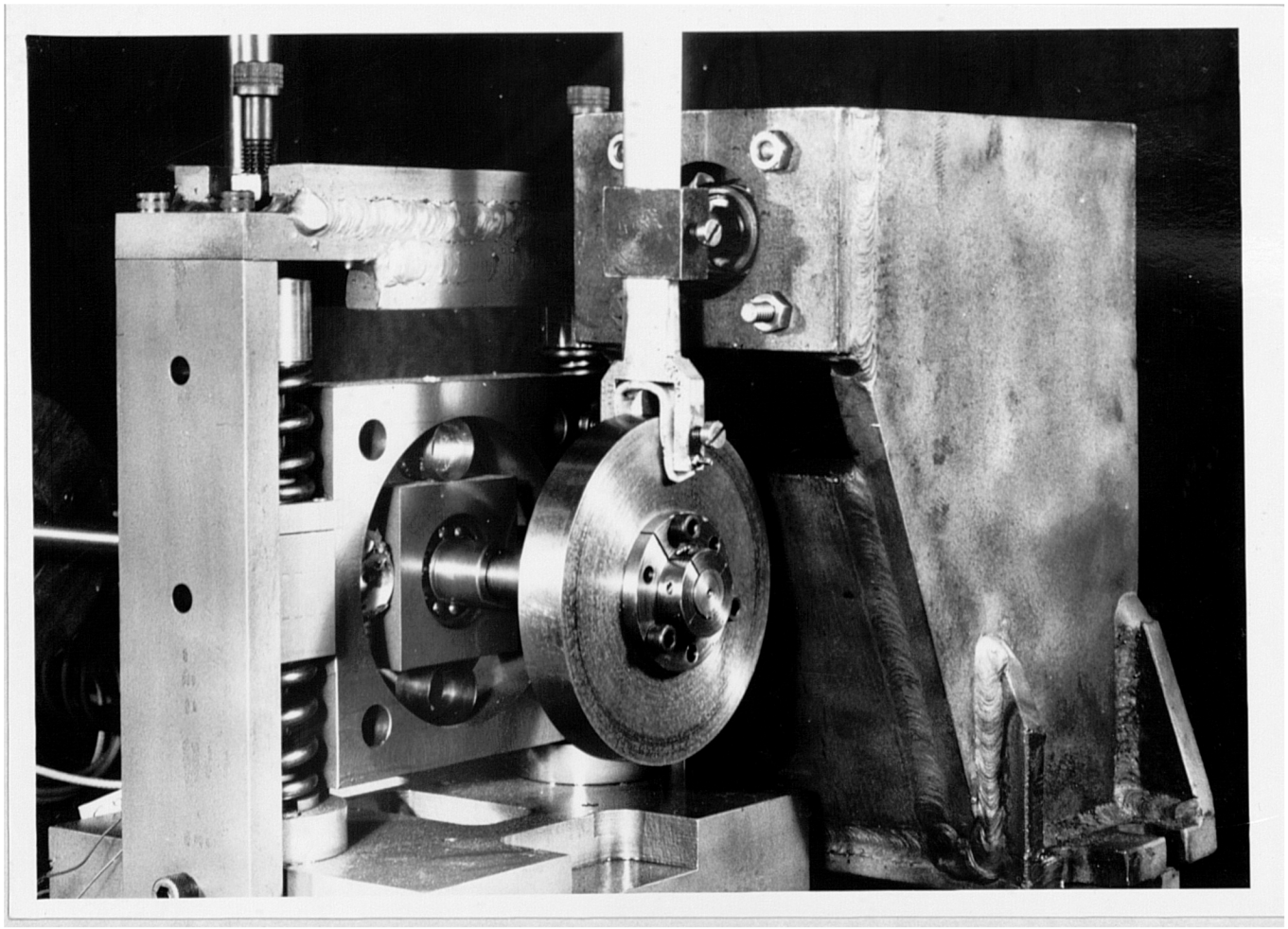

FIG. 6.13 ANGULAR MECHANICAL DAMPING ARRANGEMENT

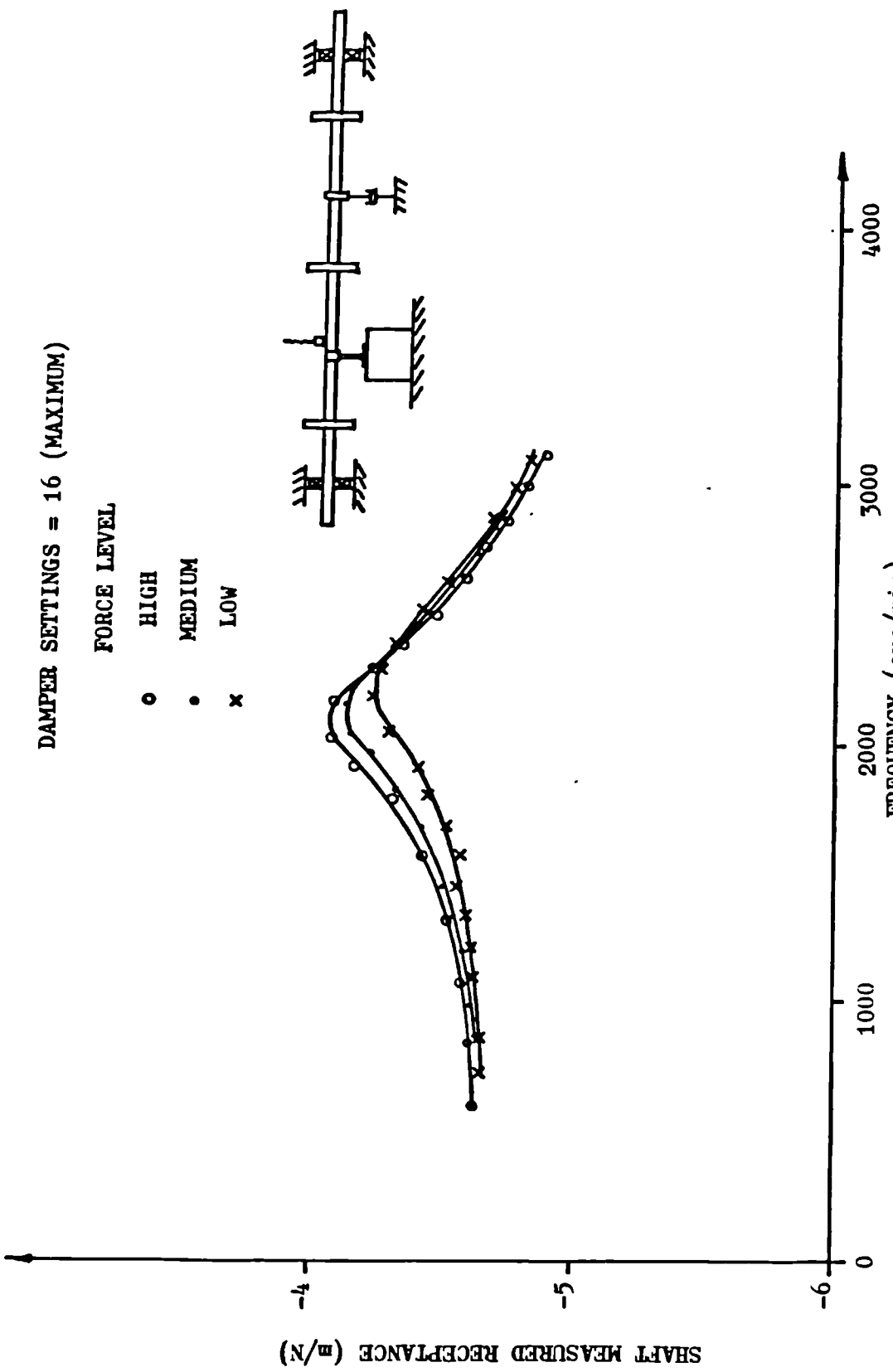

FIG. 6.14 INFLUENCE OF EXCITATION FORCE LEVEL ON THE RESPONSE OF "KINETROL" DAMPERS

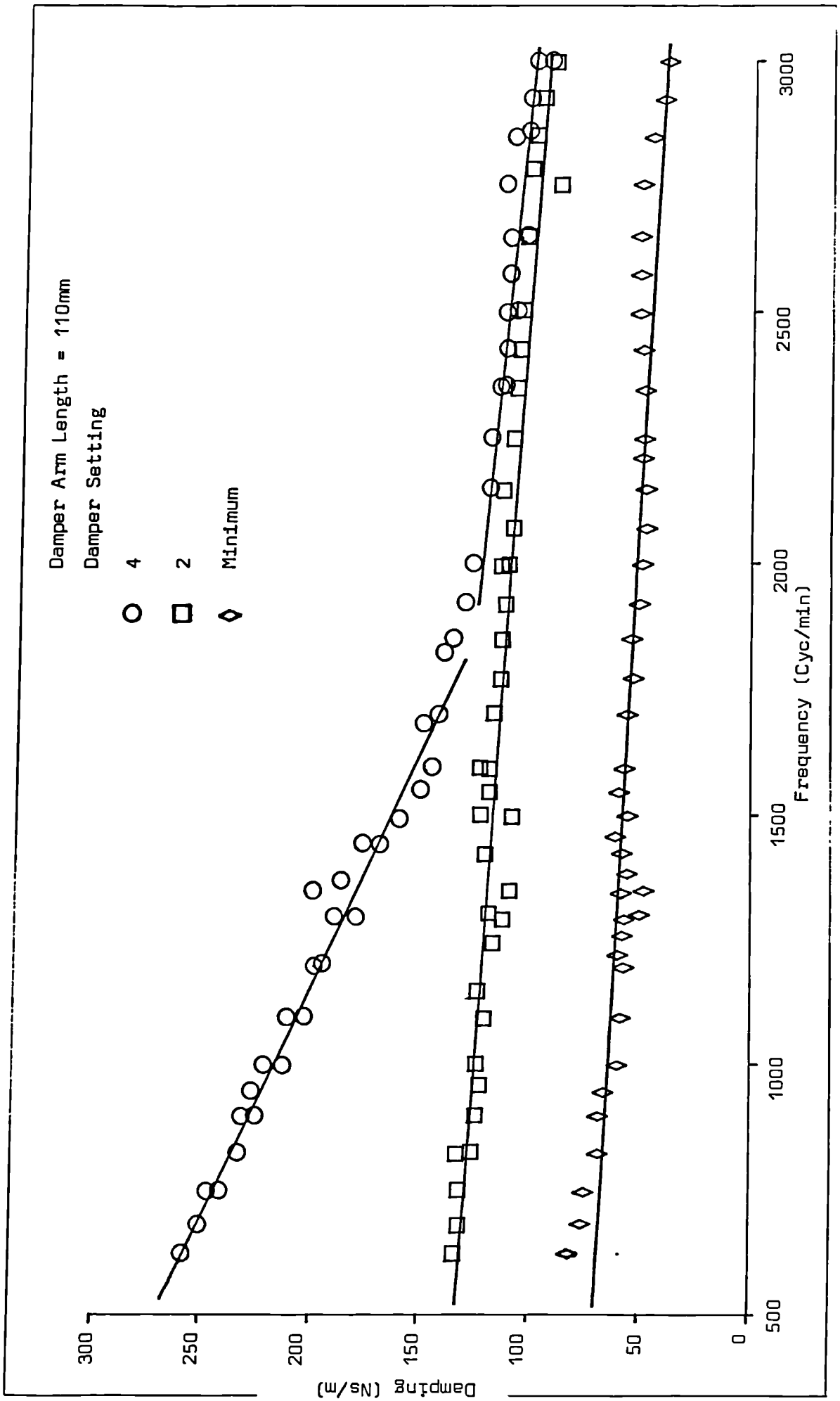

Fig. 6.15 Kinetrol Damper Calibration Data

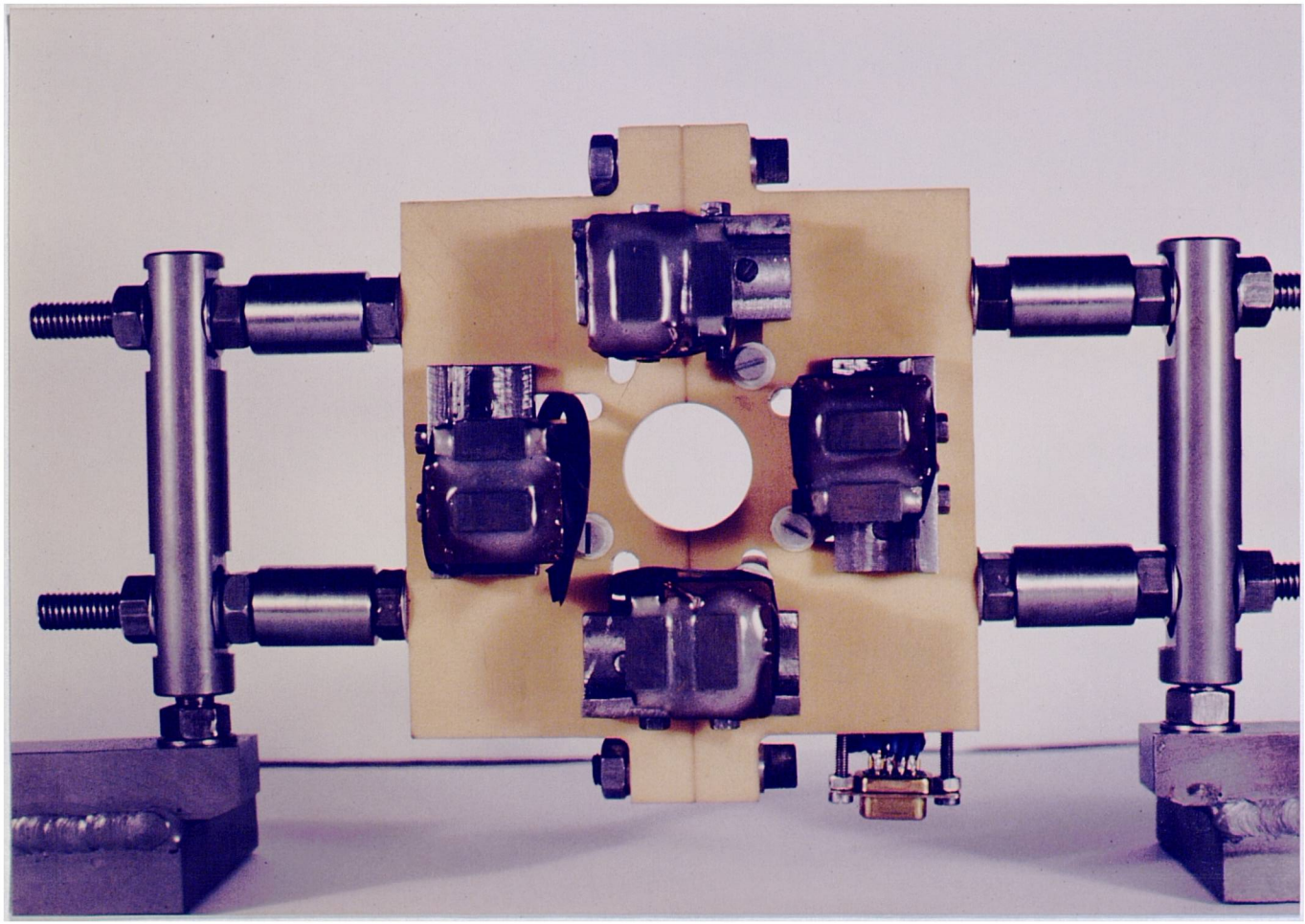

FIG. 6.16 ANGULAR ELECTROMAGNETIC ACTUATOR

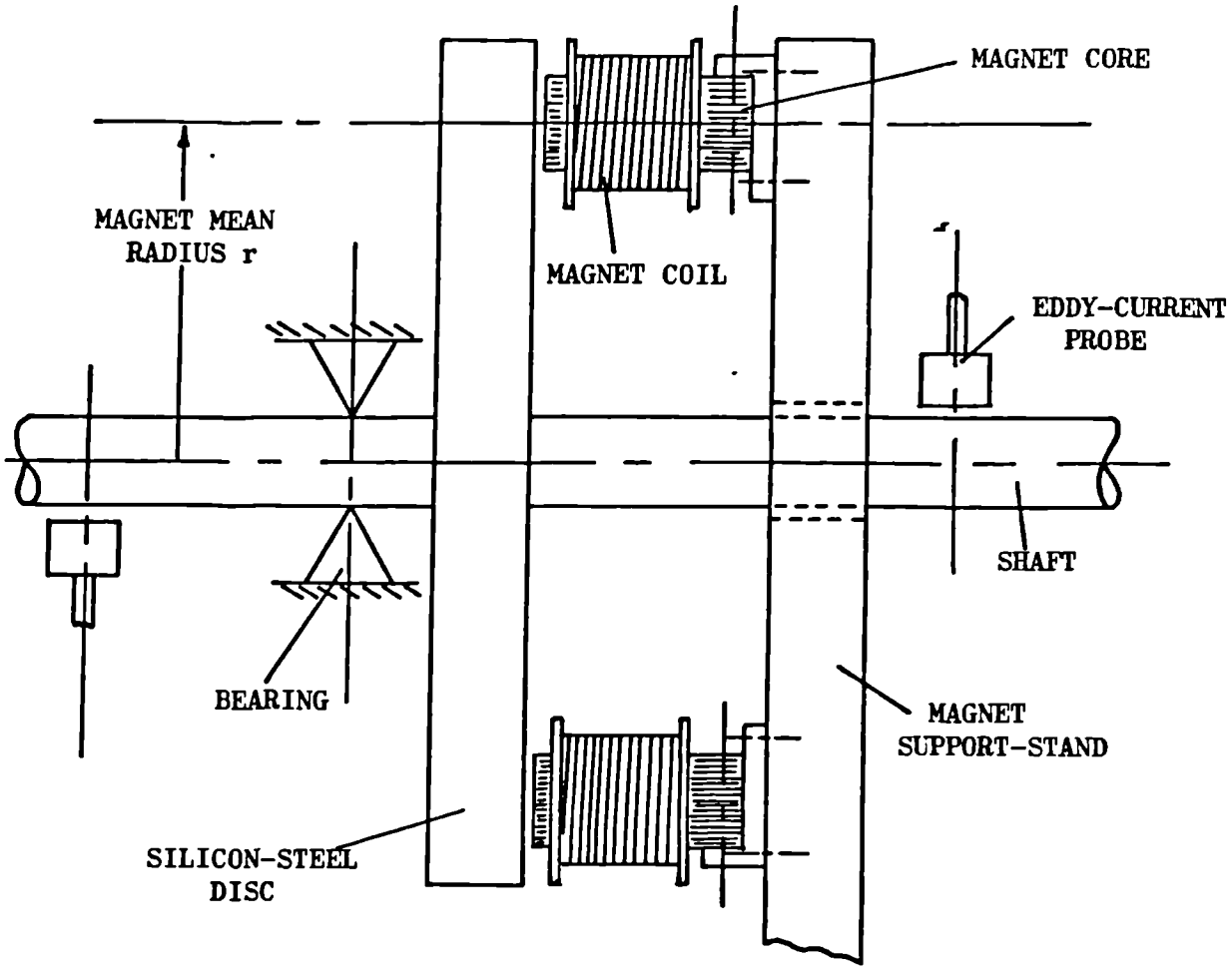

FIG. 6.17 ANGULAR CONTROLLER SET-UP (ONE-PLANE SHOWN)

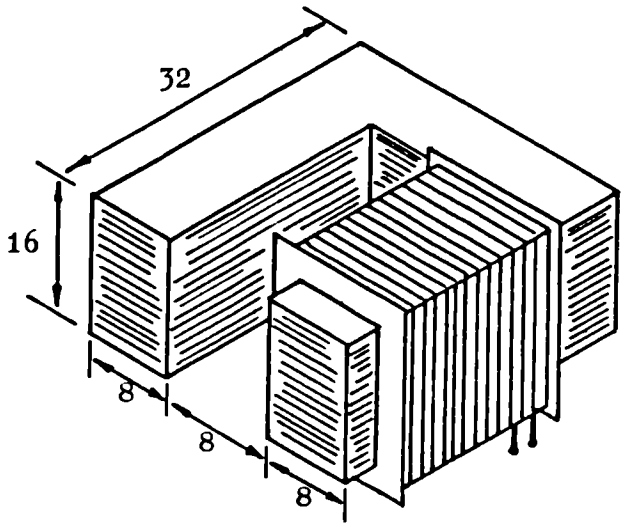

FIG. 6.18 MAGNET DETAILS (DIMENSIONS IN MILLIMETRES)

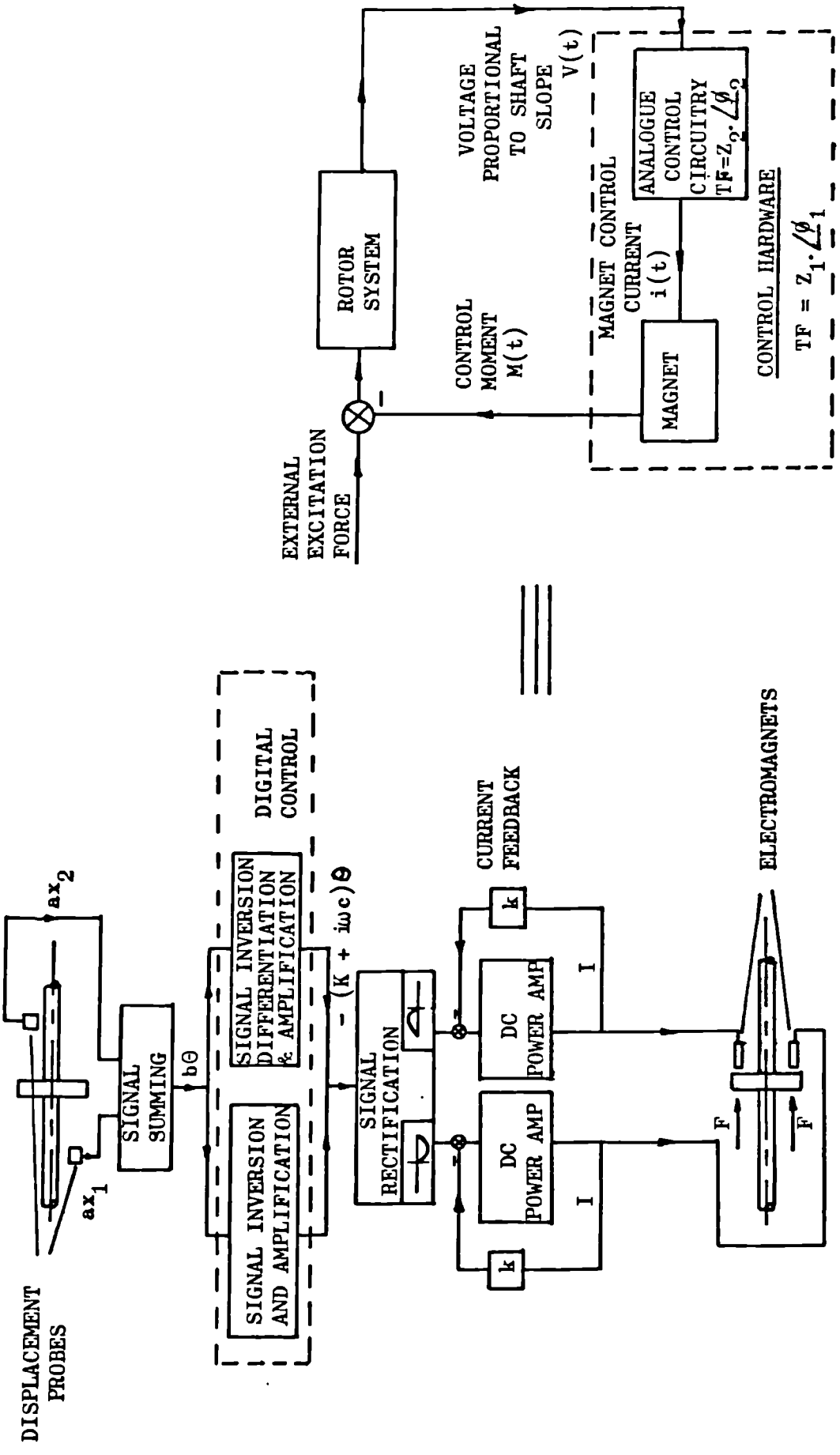

FIG. 6.19a SCHEMATIC OF CONTROL HARDWARE

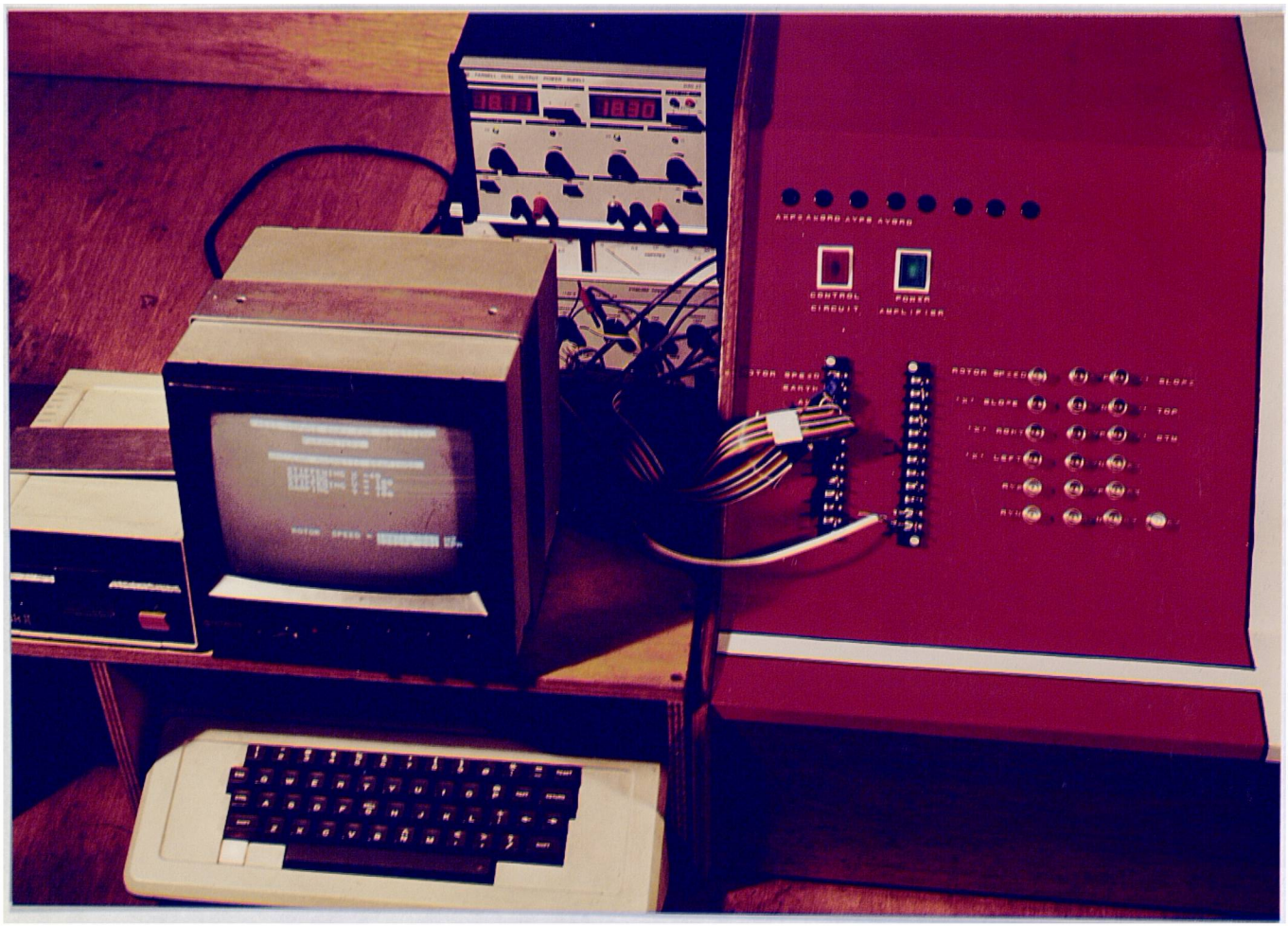

FIG 6.19b ELECTRONIC CONTROL HARDWARE

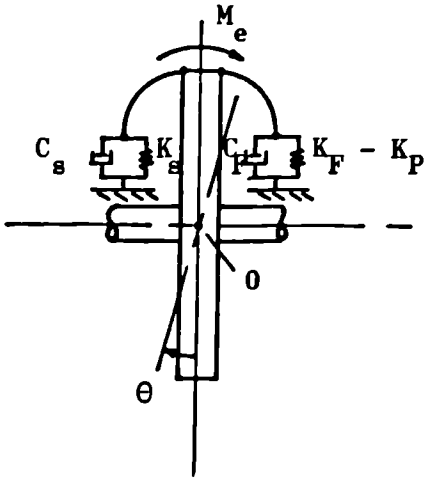

(a) EQUIVALENT SYSTEM

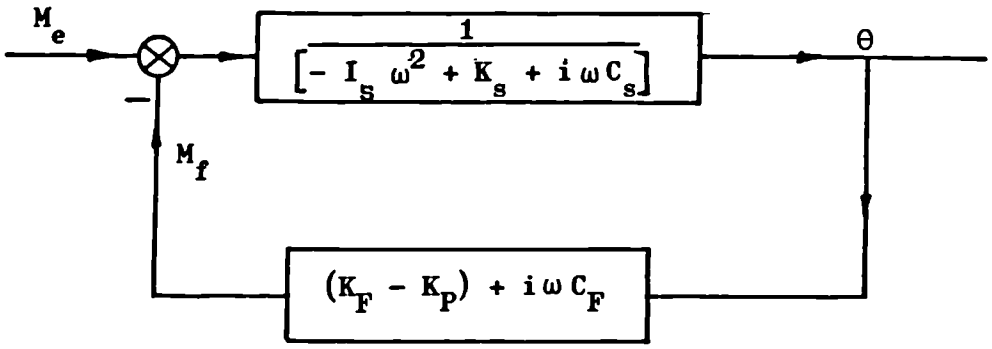

(b) BLOCK DIAGRAM OF CONTROL STRATEGY

FIG. 6.20 MAGNETIC ANGULAR FEEDBACK CONTROL OF A SIMPLE SYSTEM

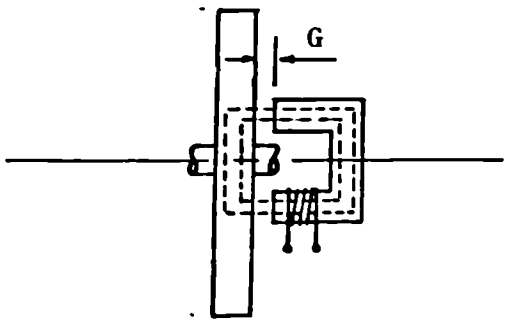

FIG. 6.21 MAGNET FLUX PATH

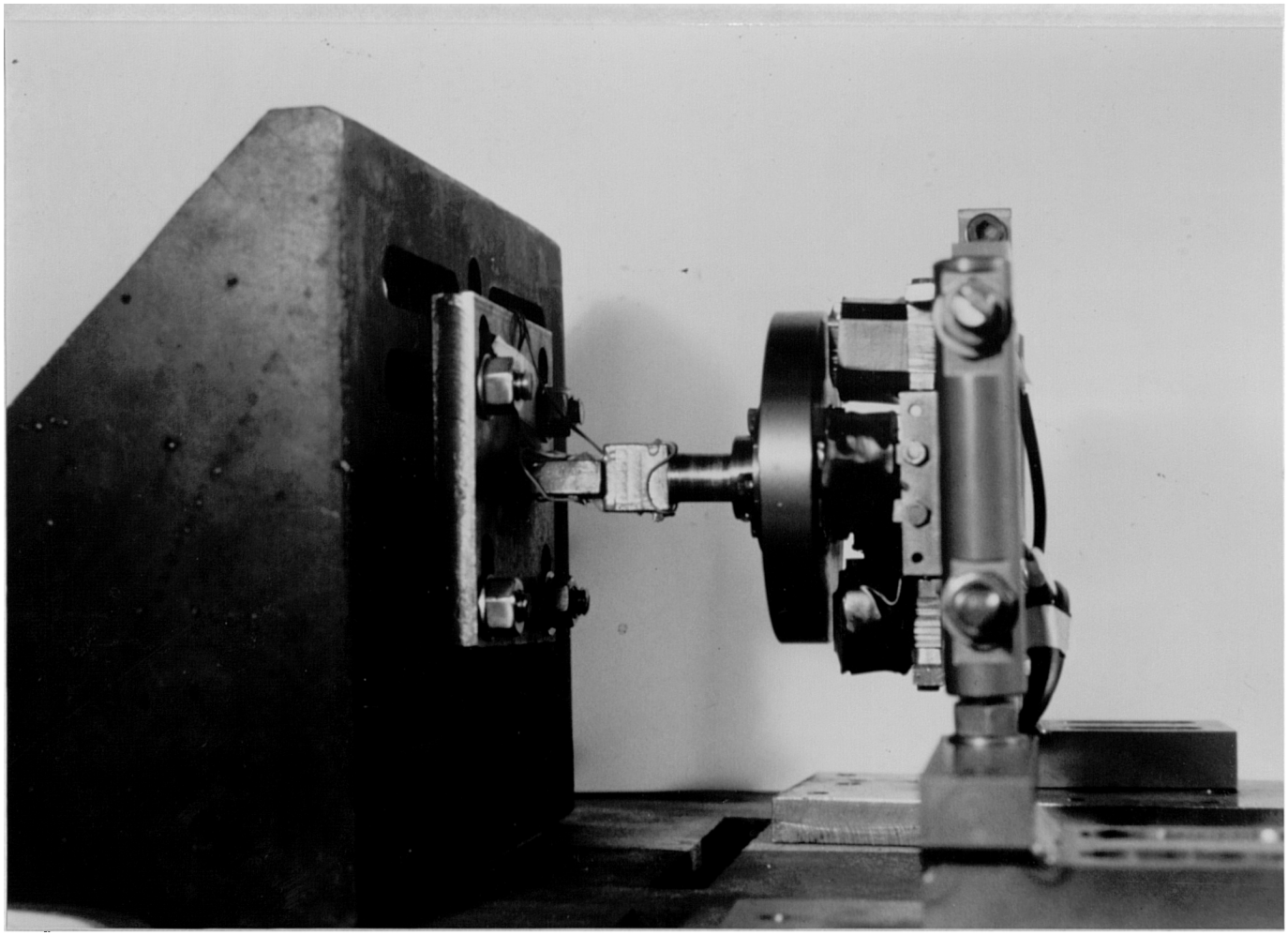

FIG. 6.22 ELECTROMAGNET CALIBRATION RIG

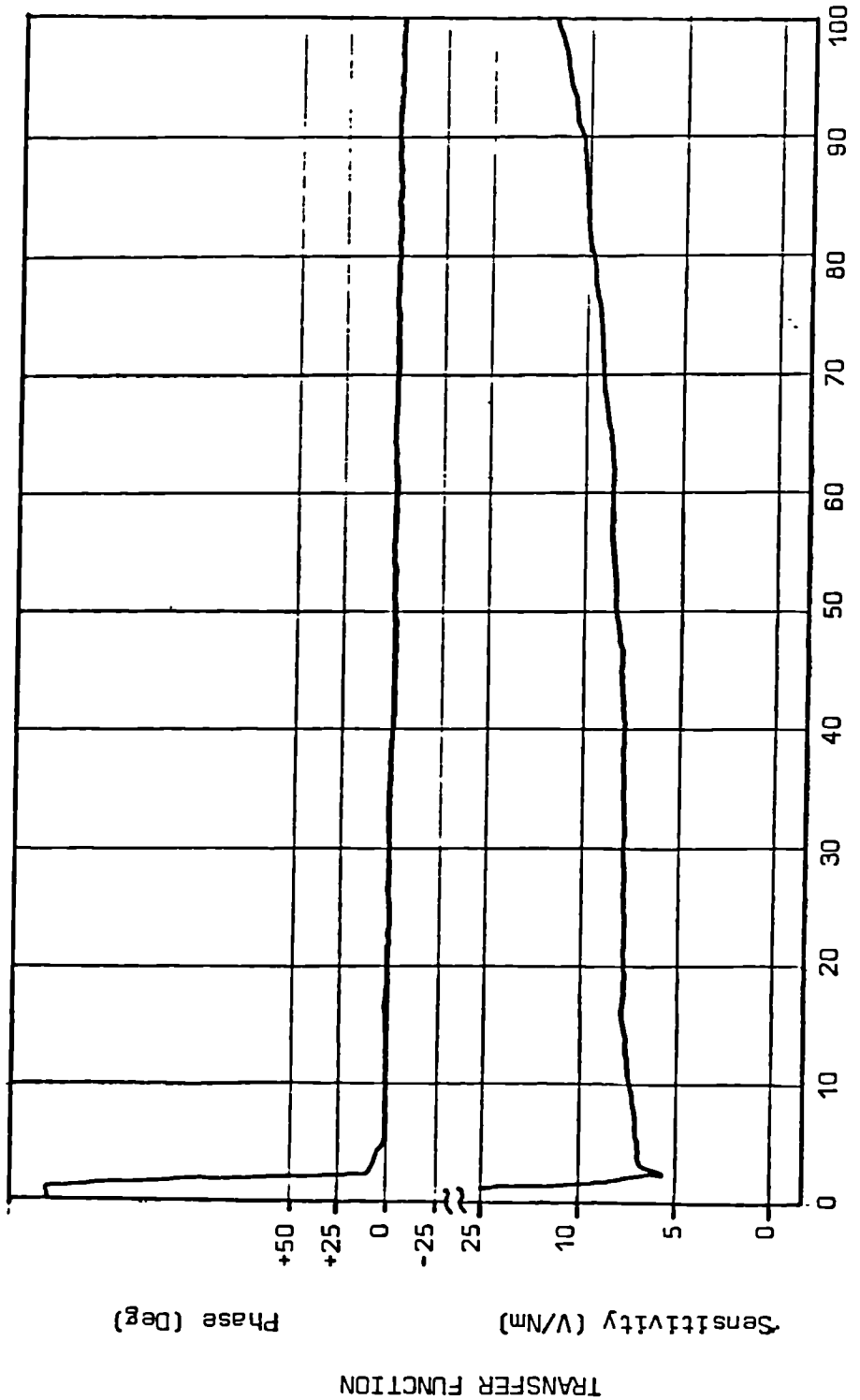

Fig.6.23 Frequency Response of E/Magnet Calibrator/Amp.

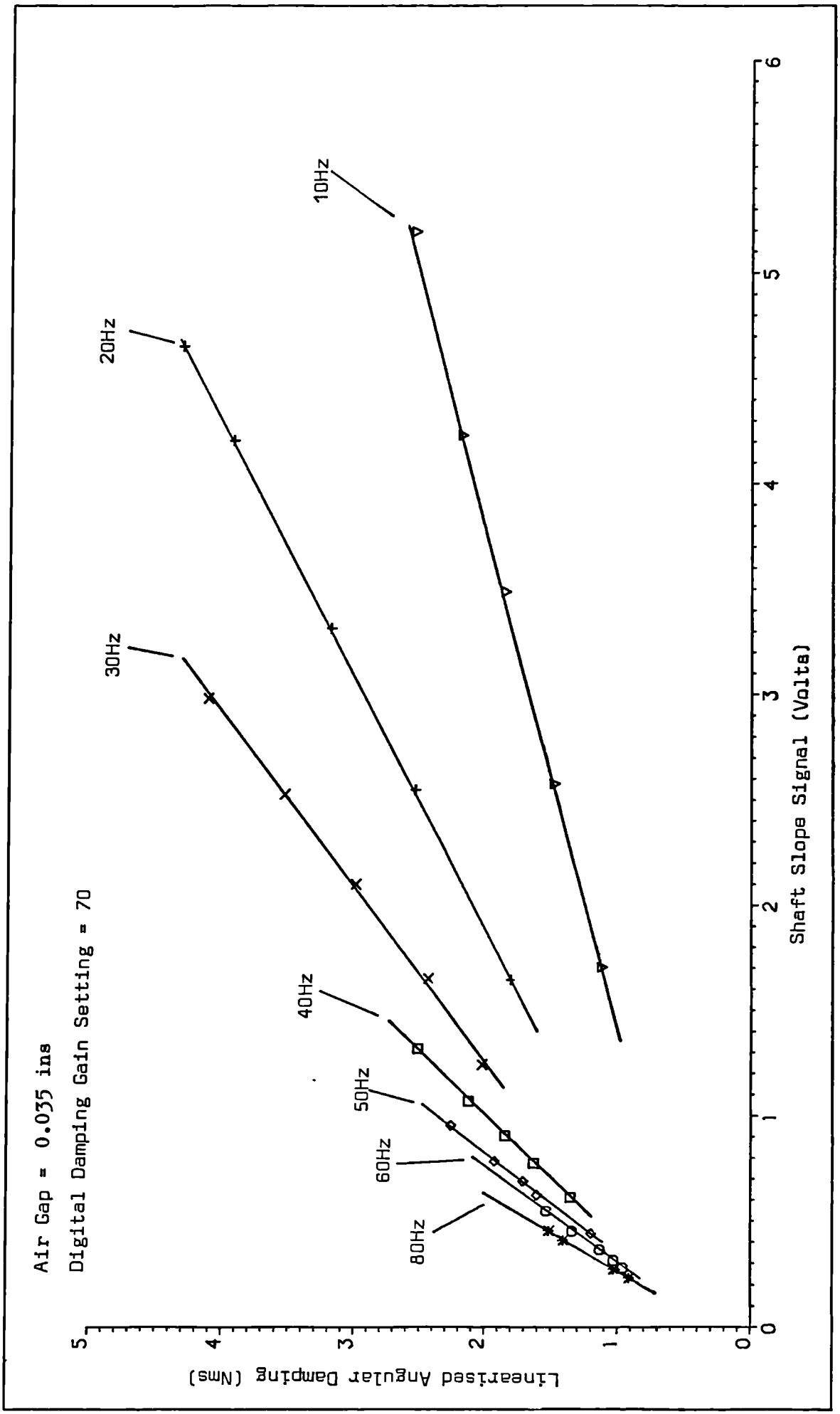

FIG. 6.24a MAGNET CALIBRATION DATA

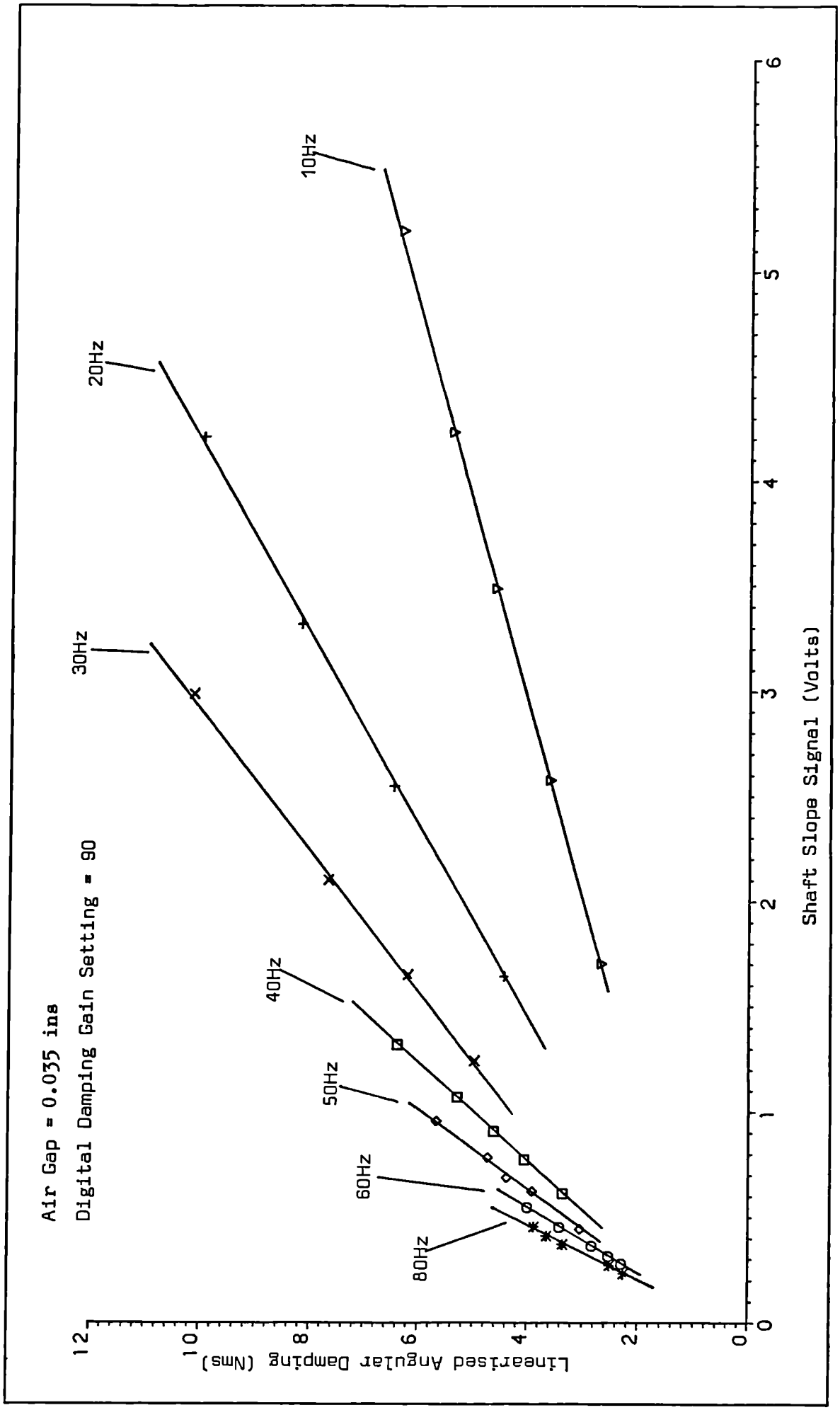

FIG. 6.24b MAGNET CALIBRATION DATA

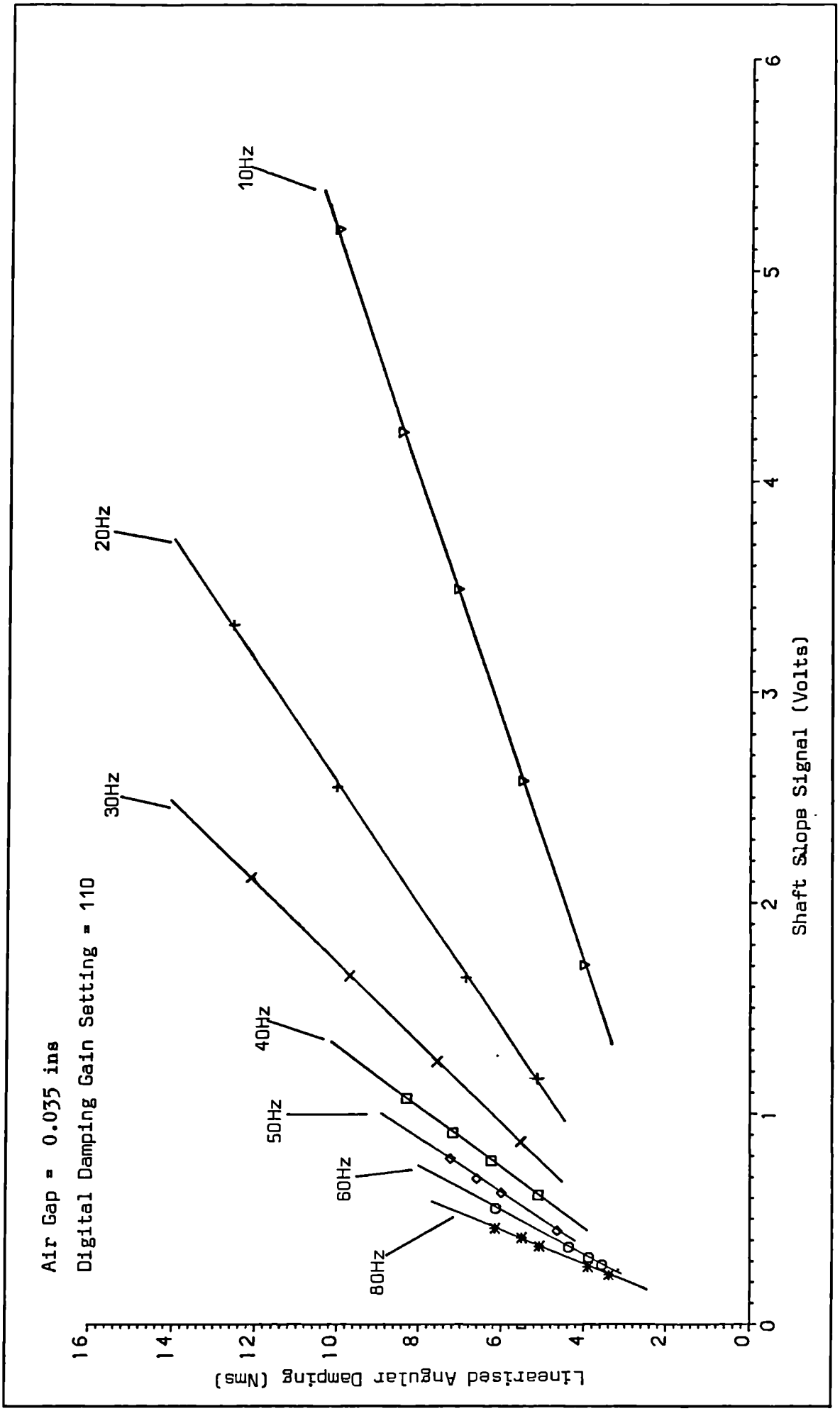

FIG. 6.24c MAGNET CALIBRATION DATA

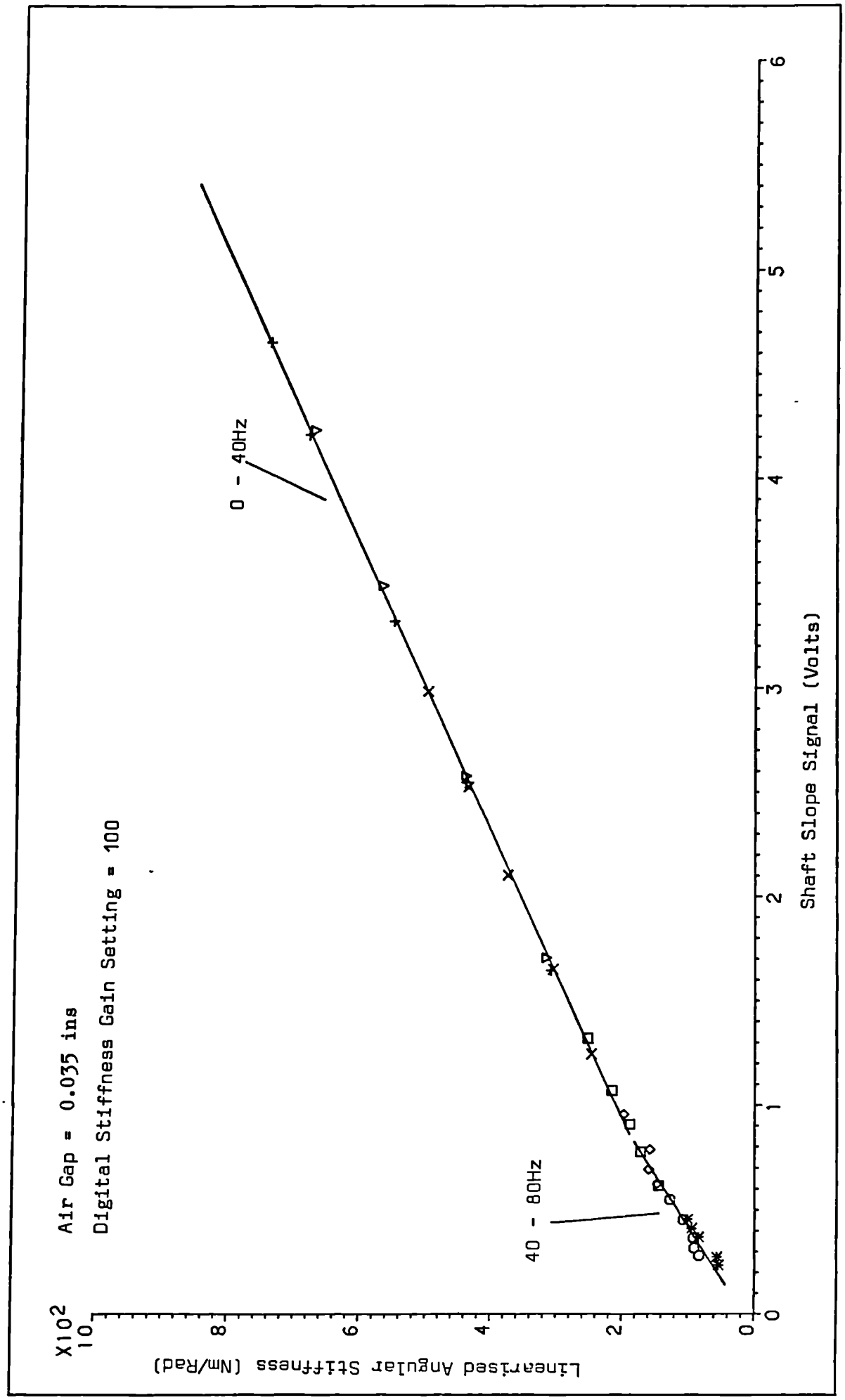

FIG. 6.24d MAGNET CALIBRATION DATA

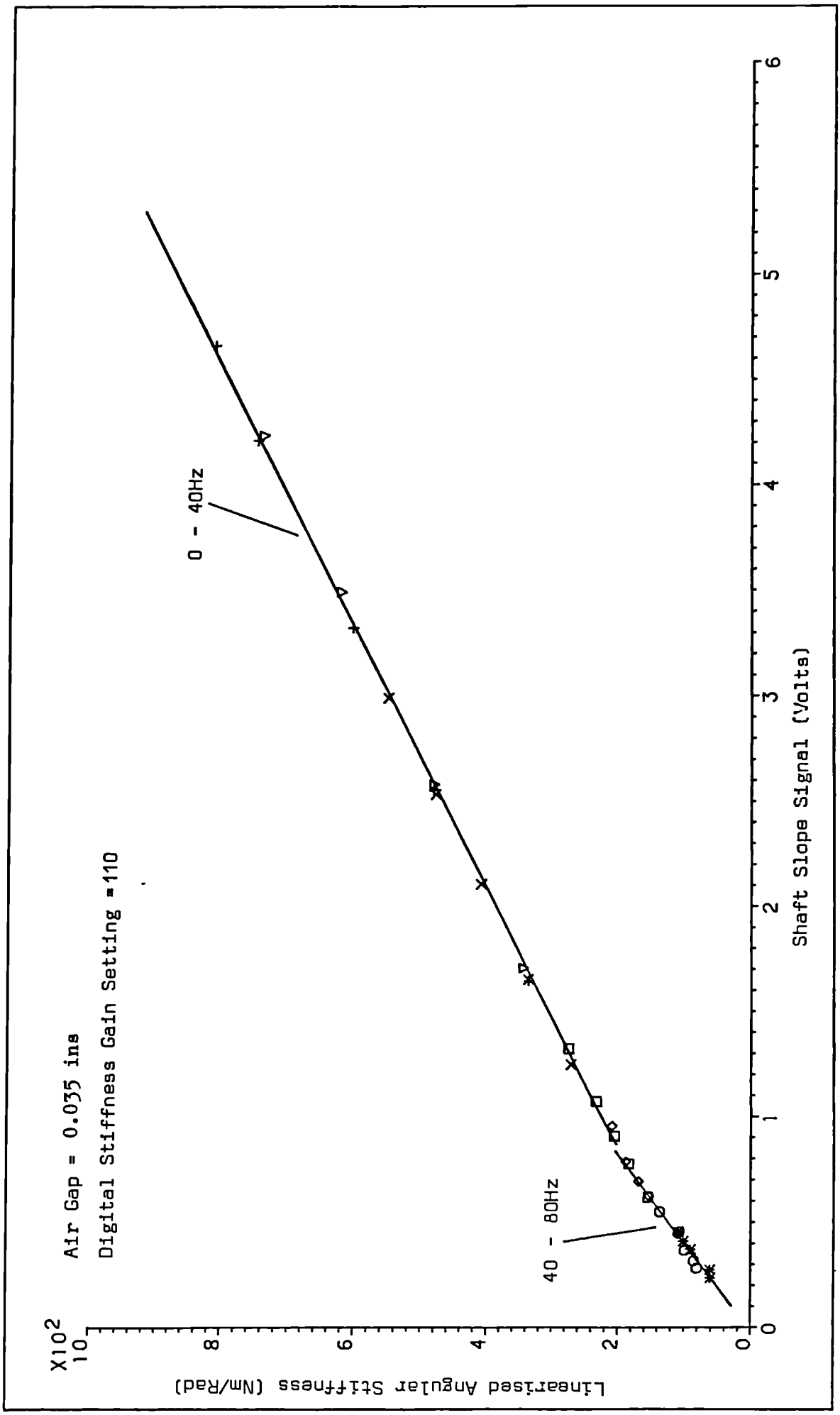

FIG. 6.24e MAGNET CALIBRATION DATA

$$Z_1 \angle p_1 = \frac{M\ (i\omega)}{V} \quad ; \quad Z_2 \angle p_2 = \frac{i\ (i\omega)}{V}$$

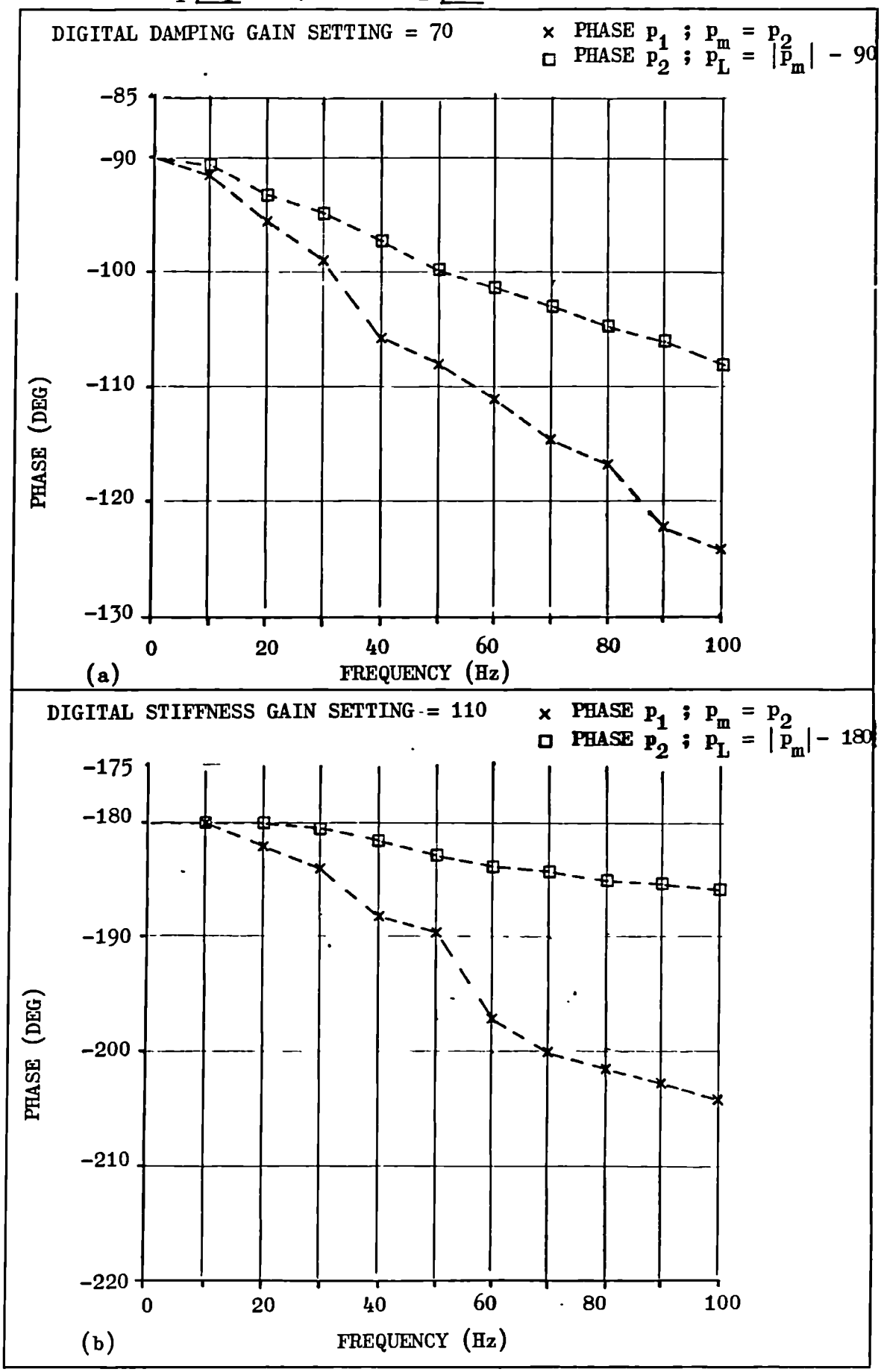

FIG. 6.25 CONTROL CIRCUIT PHASE-FREQUENCY DETAILS

(a) DAMPING CONTROL
(b) STIFFNESS CONTROL

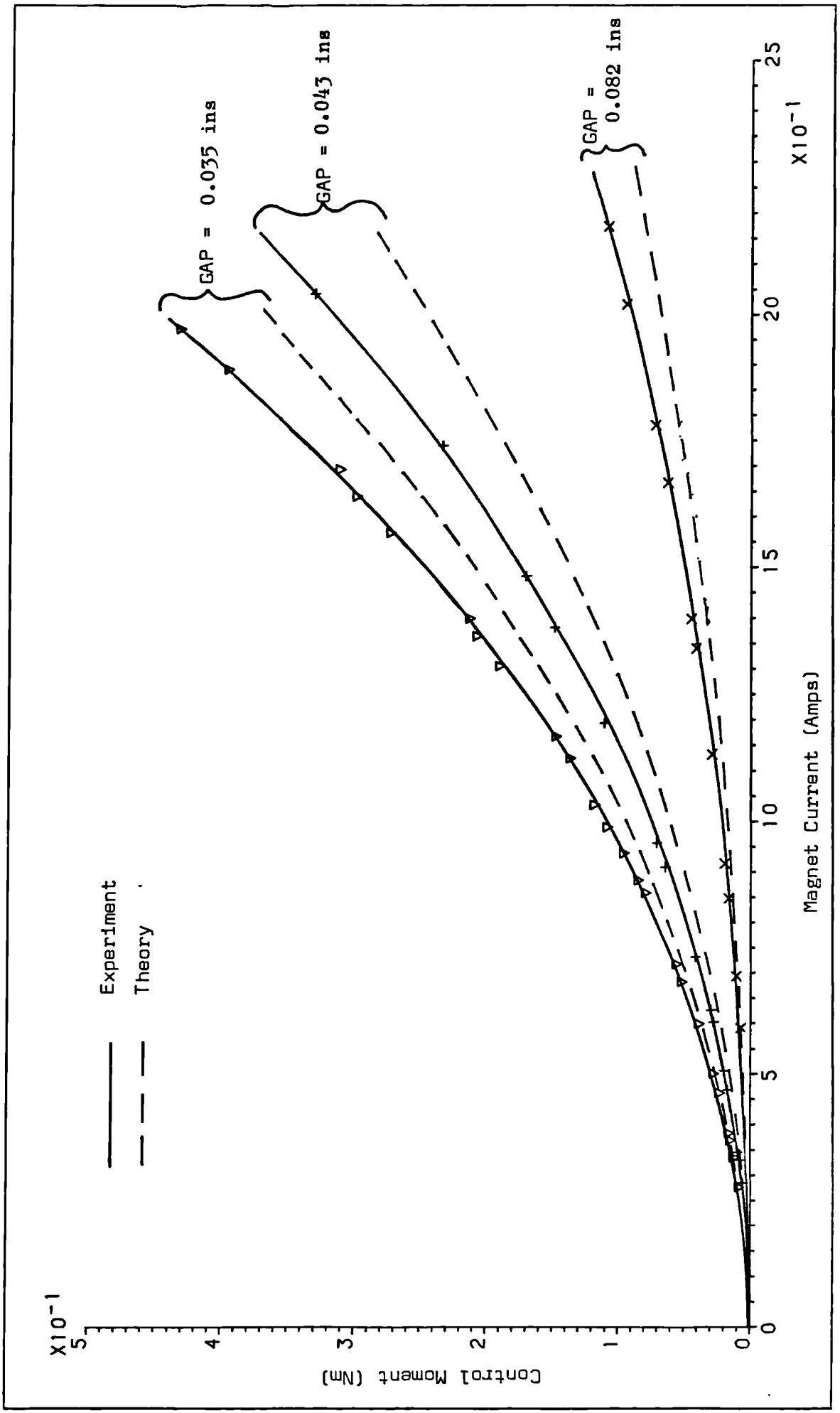

FIG. 6.26 MAGNET BENDING MOMENT VERSUS CONTROL CURRENT

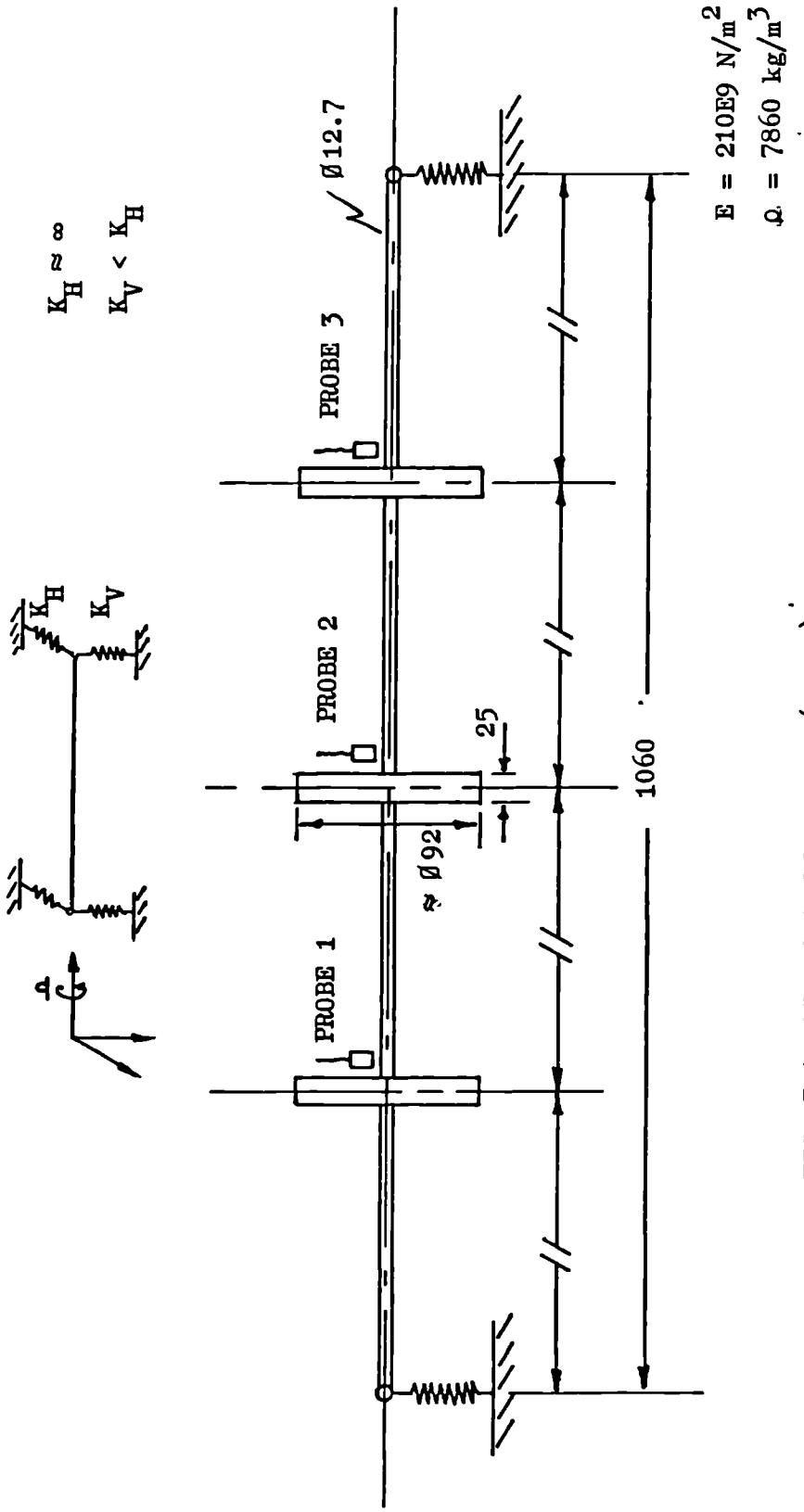

FIG. 7.1 AUXILLIARY TEST RIG (RIG A) DETAILS

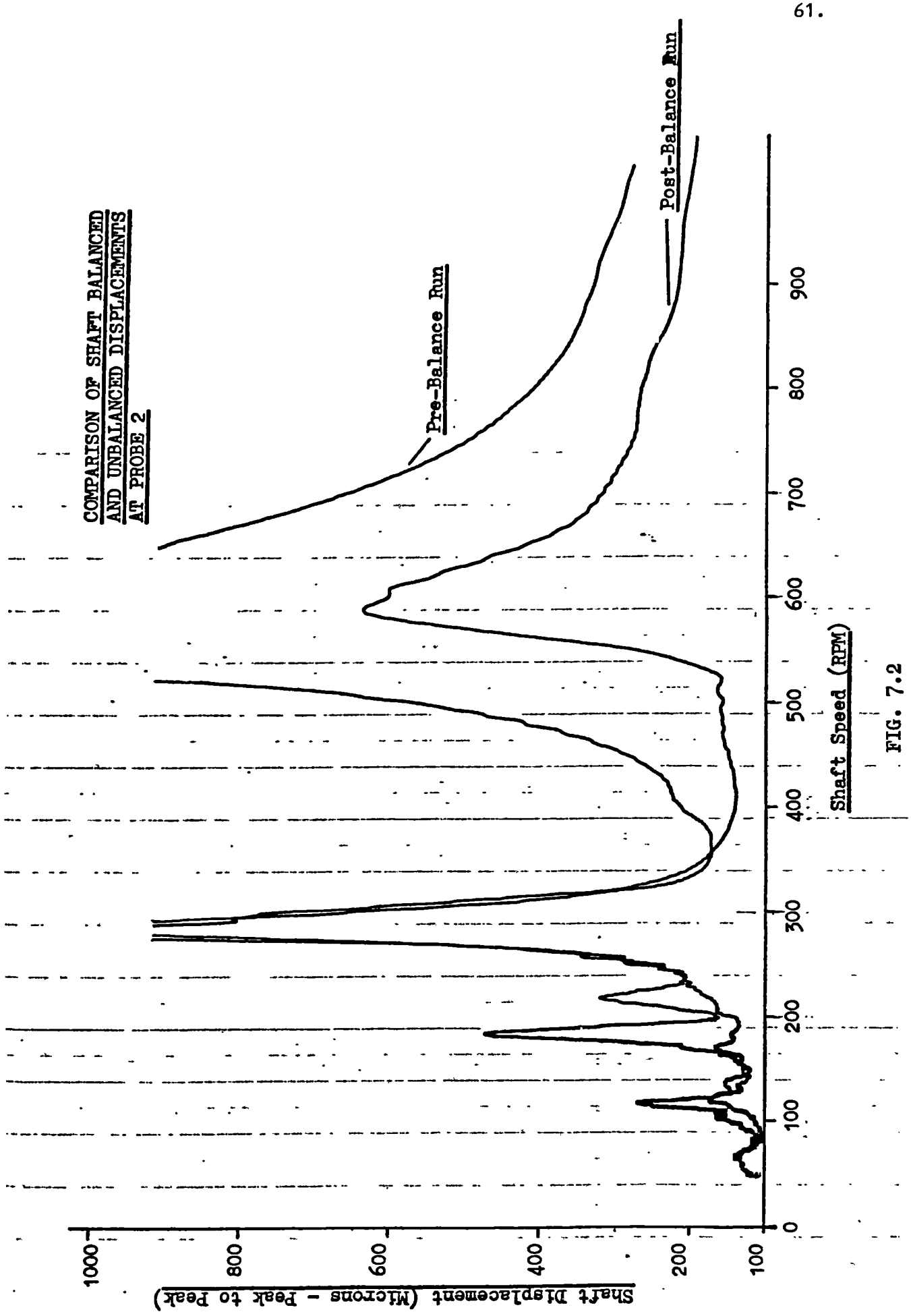
COMPARISON OF SHAFT BALANCED AND UNBALANCED DISPLACEMENTS AT PROBE 2
Pre-Balance Run
Post-Balance Run
Shaft Displacement (Microns - Peak to Peak)
1000
800
600
400
200
100
0
100
200
300
400
500
600
700
800
900
Shaft Speed (RPM)

FIG. 7.2

SHAFT RUNOUT READINGS

(Shaft Speed = 170 rpm)

Measurement	Probe 1	Probe 2	Probe 3
Displacement P-P	25	68	18
Phase	366	314	204

FIG. 7.3a

ZERO-CONDITION SHAFT READINGS

Shaft speed	Measurement	Probe 1	Probe 2	Probe 3
545 rpm	Displacement	680	1130	715
" "	Phase	293	298	284
750 rpm	Displacement	198	210	245
" "	Phase	100	110	113

FIG. 7.3b

TRIAL-MASS DATA

Trial mass of 7.0 grams at 38 mm radius in Plane 1.

Shaft speed	Measurement	Probe 1	Probe2	Probe 3
545 rpm	Displacement	560	930	620
" "	Phase	307	310	298
750 rpm	Displacement	174	169	210
" "	Phase	118	135	135

FIG. 7.3c

Trial mass of 7.0 grams at 38 mm radius in Plane 2.

Shaft speed	Measurement	Probe 1	Probe 2	Probe 3
545 rpm	Displacement	720	1180	770
" "	Phase	275	281	269
750 rpm	Displacement	200	215	200
" "	Phase	87	87	93

FIG. 7.3d

Trial mass of 7.0 grams at 38 mm radius in Plane 3.

Shaft speed	Measurement	Probe 1	Probe 2	Probe 3
545 rpm	Displacement	535	910	550
" "	Phase	284	290	276
750 rpm	Displacement	150	150	180
" "	Phase	96	99	110

FIG. 7.3e

FINAL (BALANCED) SHAFT VIBRATION READINGS

Shaft speed	Measurement	Probe 1	Probe 2	Probe 3
545 rpm	Displacement	80	57	65
" "	Phase	97	93	115
750 rpm	Displacement	14.5	53	25
" "	Phase	37	335	273

FIG. 7.3f

```
*OLD BAL
*FRN
IF BALANCING AT ONE SPEED TYPE 1 IF NOT TYPE 2
=1
CORR MASS(GMS)     PLANE     ANGLE(DEG)

      10.75          1.        40.4

      21.71          2.       268.8

      13.27          3.       128.6

*FRN
IF BALANCING AT ONE SPEED TYPE 1 IF NOT TYPE 2
=2
CORR MASS(GMS)   PLANE   ANGLE(DEG)

      17.10          1.        92.4

      13.08          2.       224.9

       3.64          3.       297.8
RES.VIB.AMP.    RES.VIB.ANGLE   PLANE   SPEED

      48.69        155.9           1.          1.

      25.04        290.7           2.          1.

      18.60         40.9           3.          1.

      31.85        157.6           1.          2.

      11.76         83.1           2.          2.

      42.80        186.7           3.          2.
RMS RESIDUAL

      32.48

*
```

FIG. 7.4a BALANCE PROGRAM - SAMPLE OUTPUT - FIRST BALANCE (SINGLE SPEED AND TWO SPEEDS)

```
*OLD BAL
*FRN
IF BALANCING AT ONE SPEED TYPE 1 IF NOT TYPE 2
=2
CORR MASS(GMS)  PLANE  ANGLE(DEG)

      4.34        1.      230.5

      7.72        2.      302.2

      9.81        3.      137.3
RES.VIB.AMP.   RES.VIB.ANGLE  PLANE  SPEED

     30.52        75.8        1.      1.

     26.29       265.8        2.      1.

     11.29       121.8        3.      1.

     32.94       107.0        1.      2.

      9.99       275.0        2.      2.

     12.64       216.9        3.      2.
RMS RESIDUAL

     22.71

*
```

FIG. 7.4b SAMPLE OUTPUT CONTINUED - SECOND BALANCE (TWO SPEEDS)

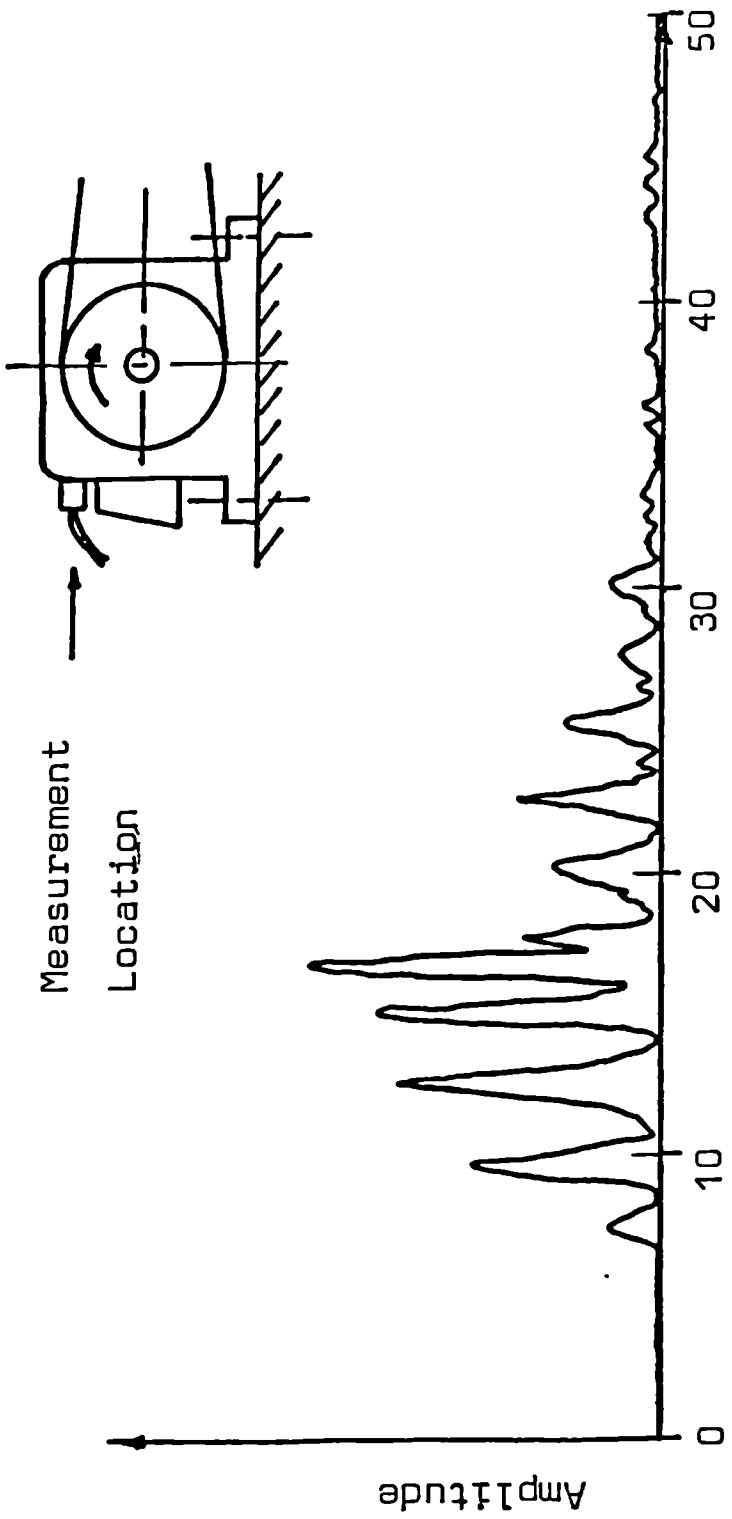

Fig. 7.5 Vibration Response of Drive Arrangement (Equivalent Shaft Speed = 1000rpm.)

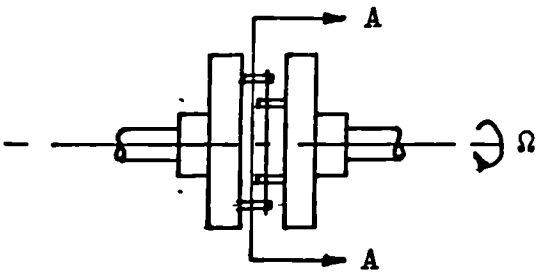

(a) SIDE VIEW

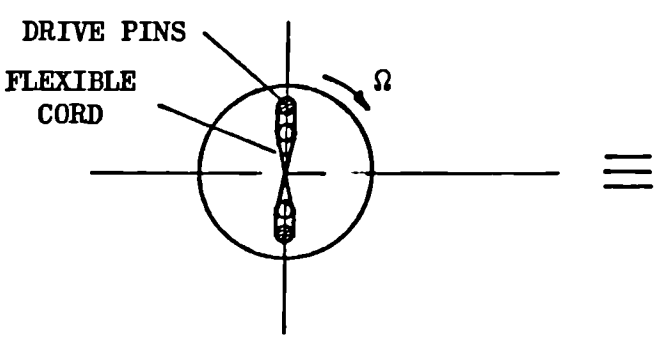

(b) VIEW ON A-A

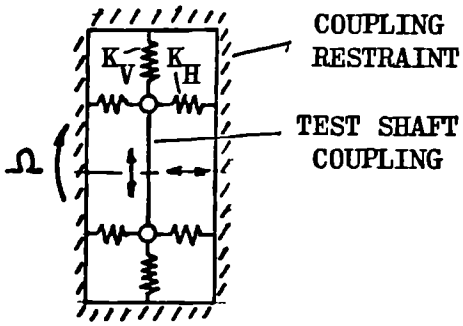

(c) MODEL SHOWING ROTATING STIFFNESS ASYMMETRY ($K_H > 0.5\ K_V$)

FIG. 7.6 TEST SHAFT COUPLING ARRANGEMENT

(b) SHAFT BEND DETAILS

SHAFT LOCATION	1	2	3	4	5	6	7	8	9	10	11
SHAFT BEND AMPLITUDE (mm)	0.059	0	0.036	0.054	0.076	0.105	0.141	0.164	0.115	0	0.143
SHAFT BEND PHASE REF. (DEG)	0	0	164	168	172	167	162	171	180	0	7

EXT MASS (kg) 0.113

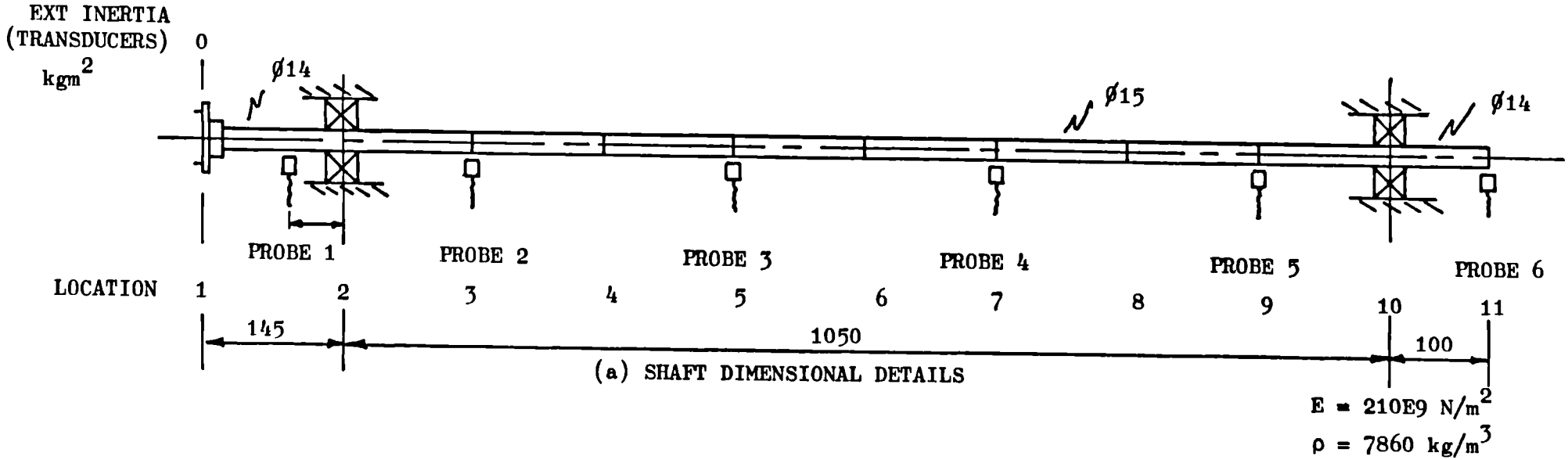

(a) SHAFT DIMENSIONAL DETAILS

FIG. 7.7 SHAFT ARRANGEMENT FOR TEST 1

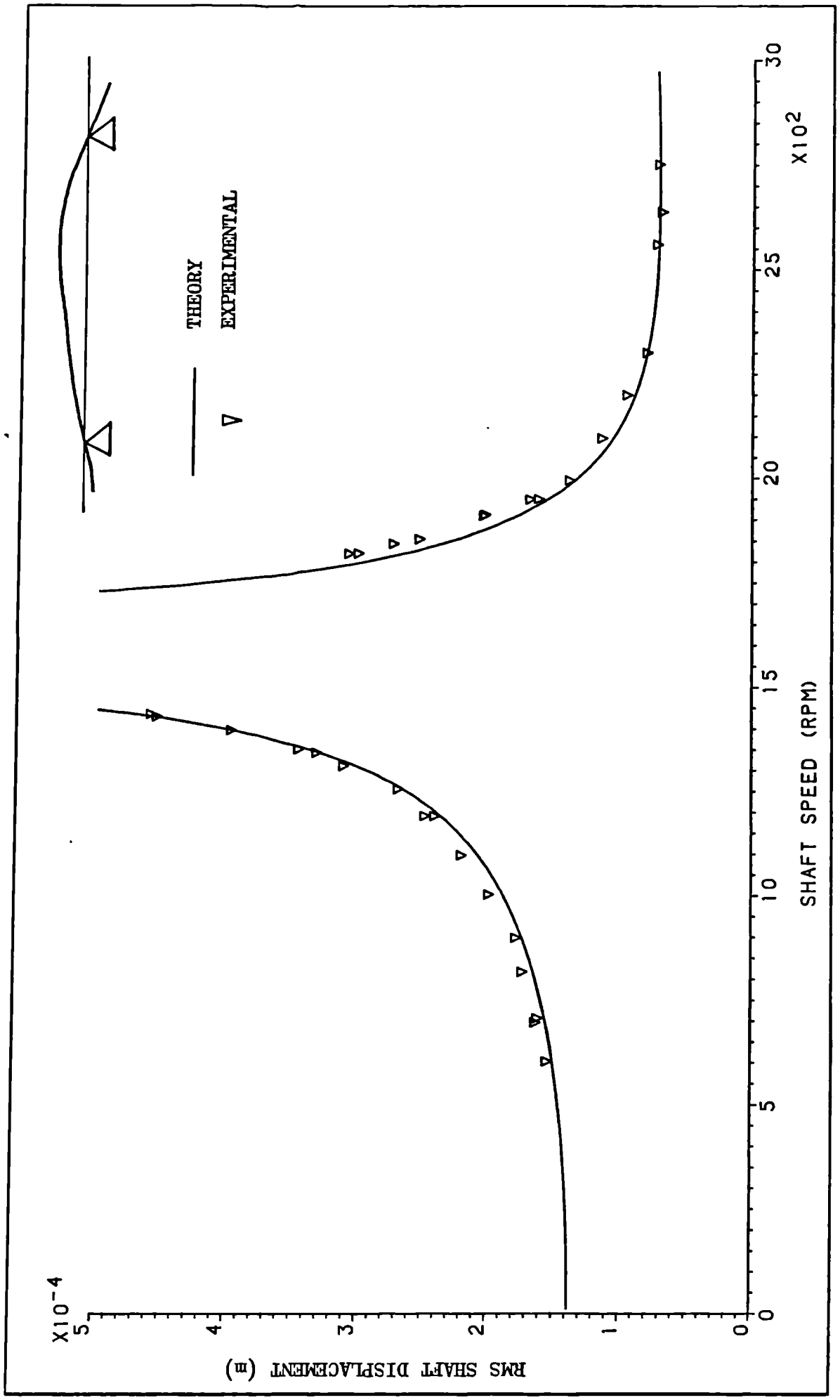

FIG. 7.7c SHAFT RESPONSE DUE TO INITIAL-BEND

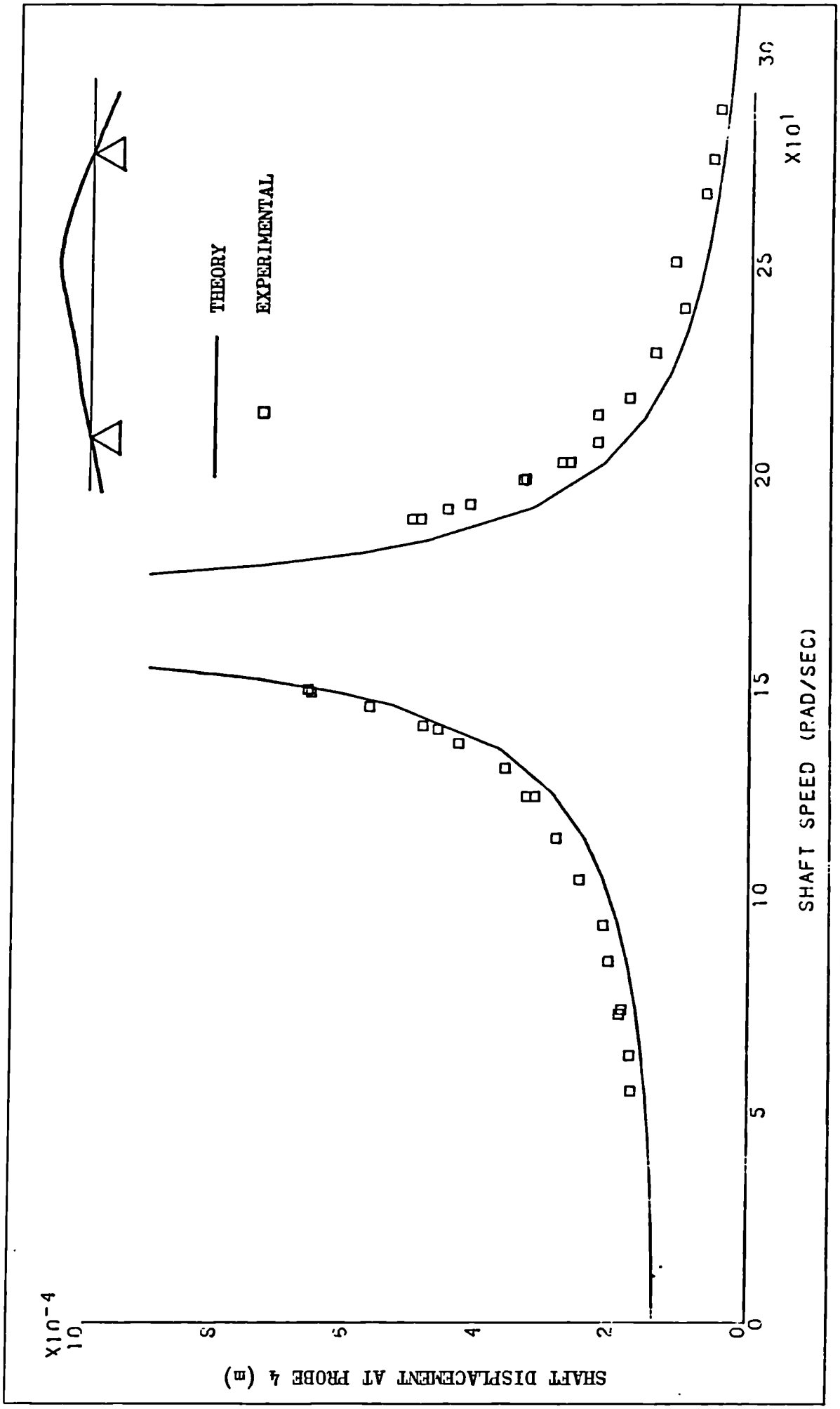

FIG. 7.7d SHAFT RESPONSE DUE TO INITIAL-BEND

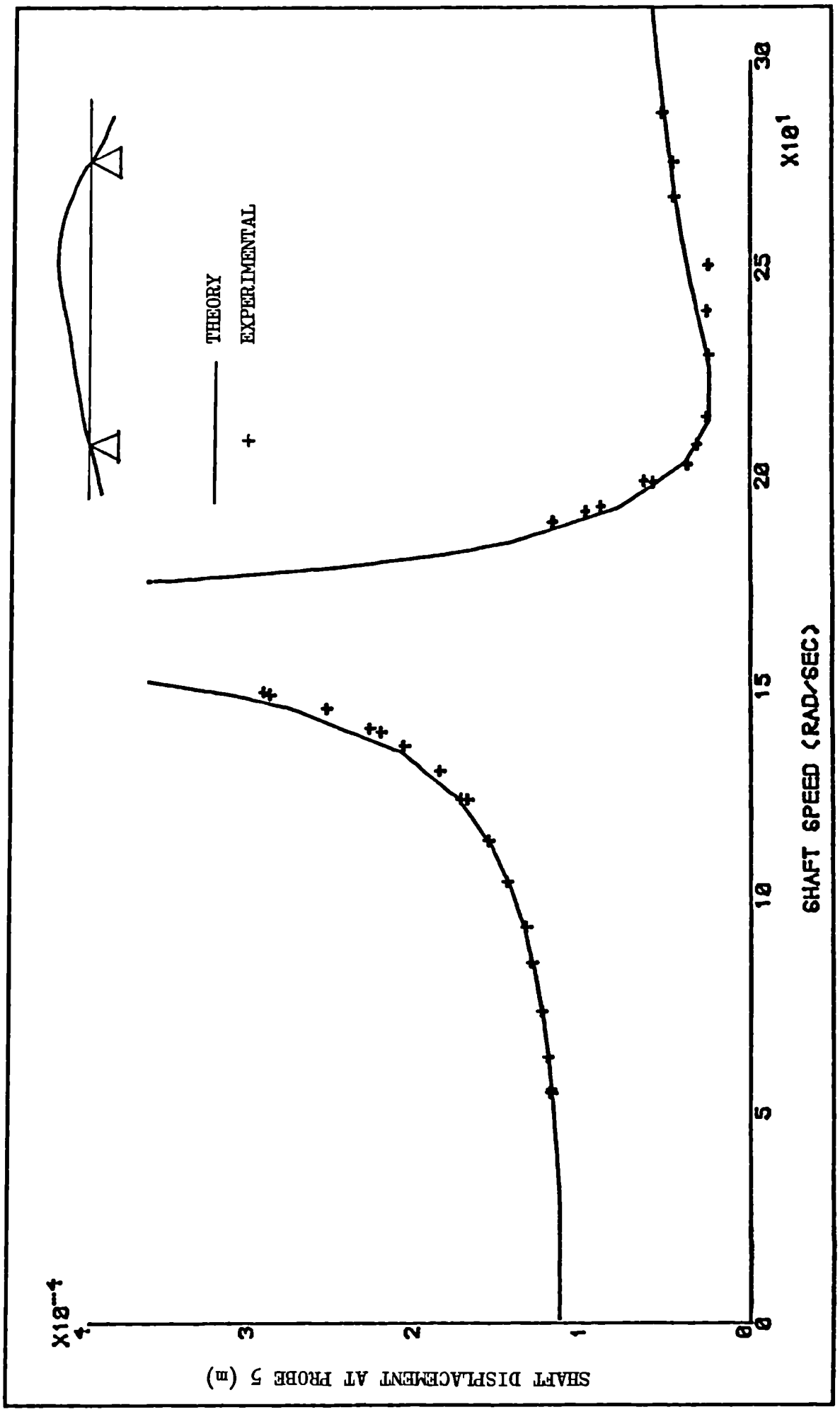

FIG. 7.7e SHAFT RESPONSE DUE TO INITIAL BEND

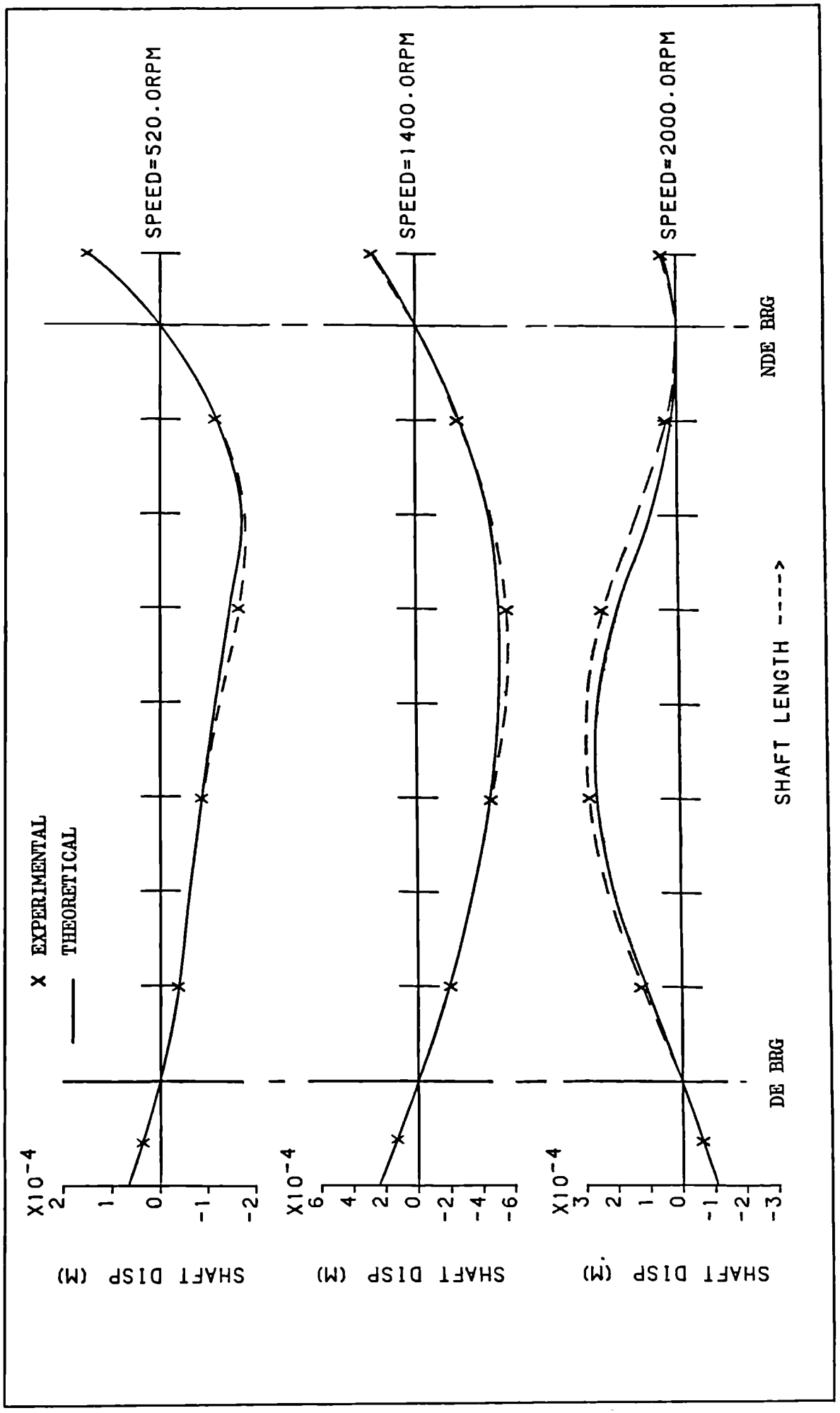

FIG. 7.7f SHAFT DEFLECTED FORMS DUE TO INITIAL-BEND

(b) SHAFT BEND DETAILS

SHAFT LOCATION	1	2	3	4	5	6	7	8	9	10	11
SHAFT BEND AMPLITUDE (mm)	0.069	0	0.026	0.055	0.075	0.091	0.139	0.148	0.107	0	0.105
SHAFT BEND PHASE REF. (DEG)	0	0	166	167	170	172	164	168	175	0	. 6

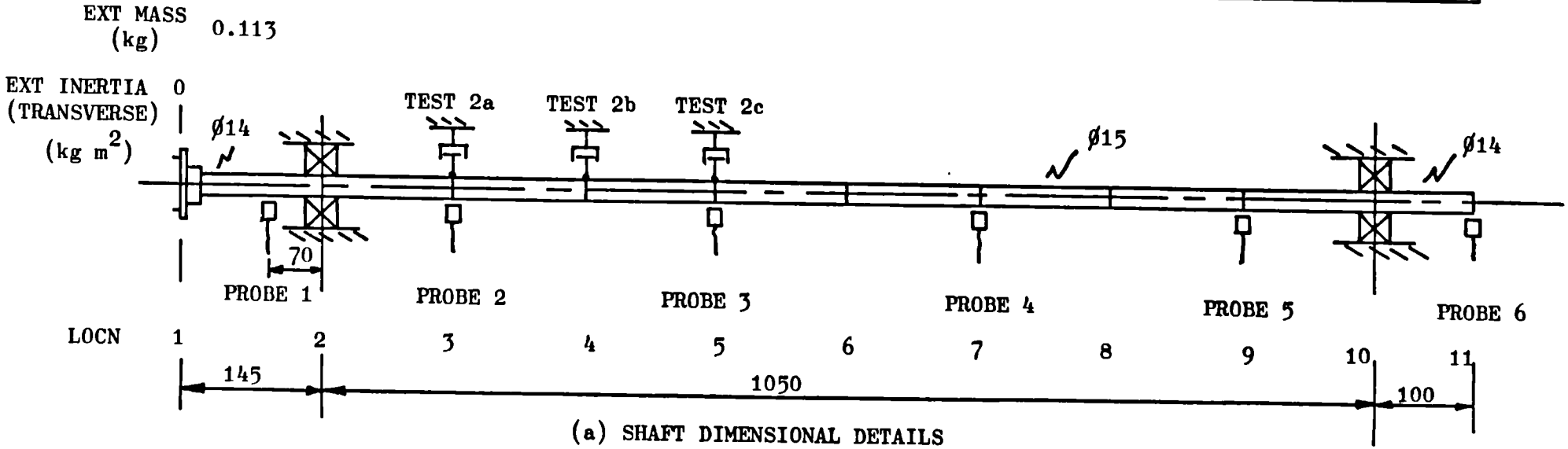

(a) SHAFT DIMENSIONAL DETAILS

$E = 210E9\ N/m^2$

$\rho = 7860\ kg/m^3$

FIG. 7.8 SHAFT ARRANGEMENT FOR TEST 2

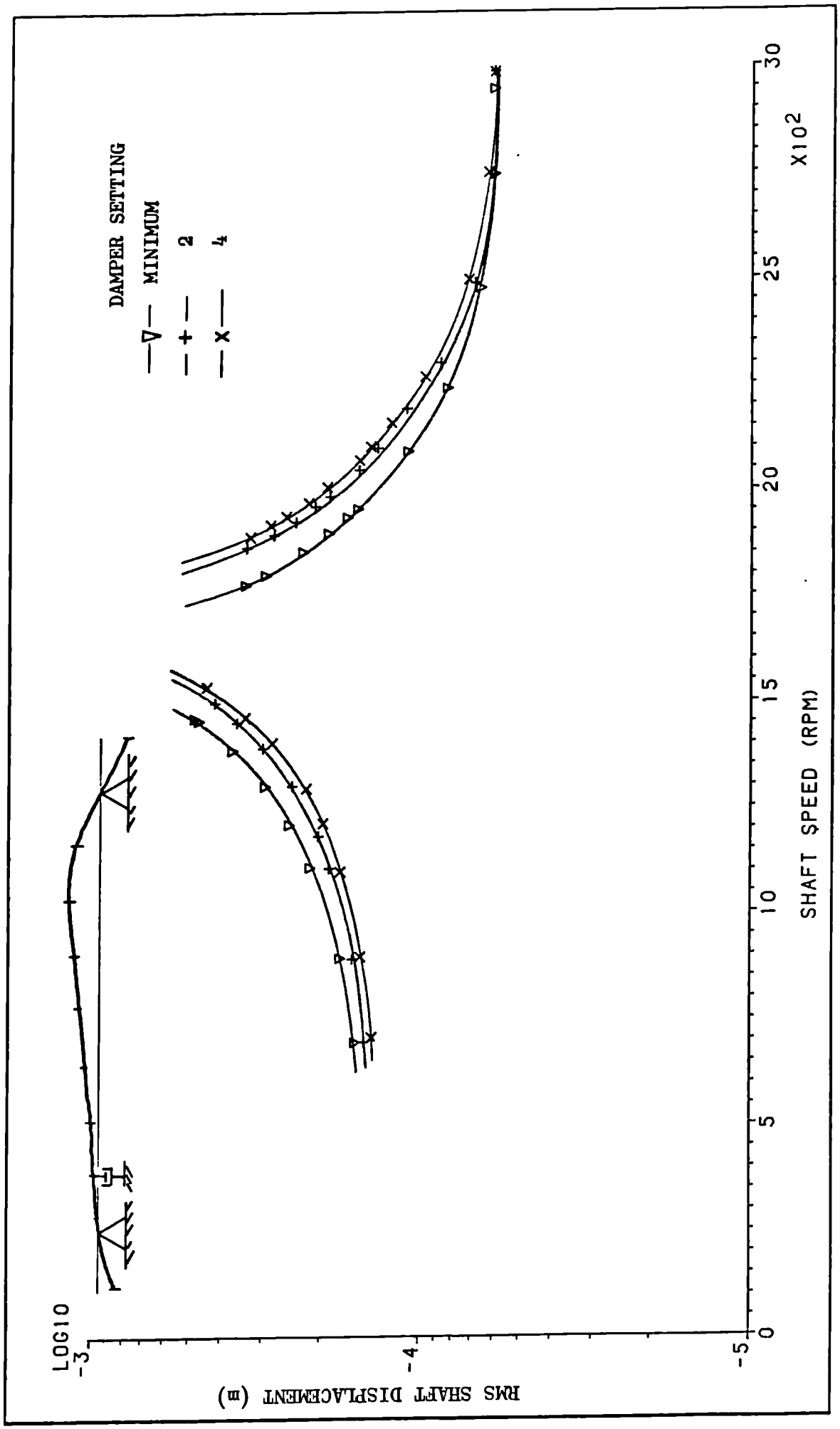

FIG. 7.8c(i) MEASURED SHAFT RESPONSE (TEST 2a)

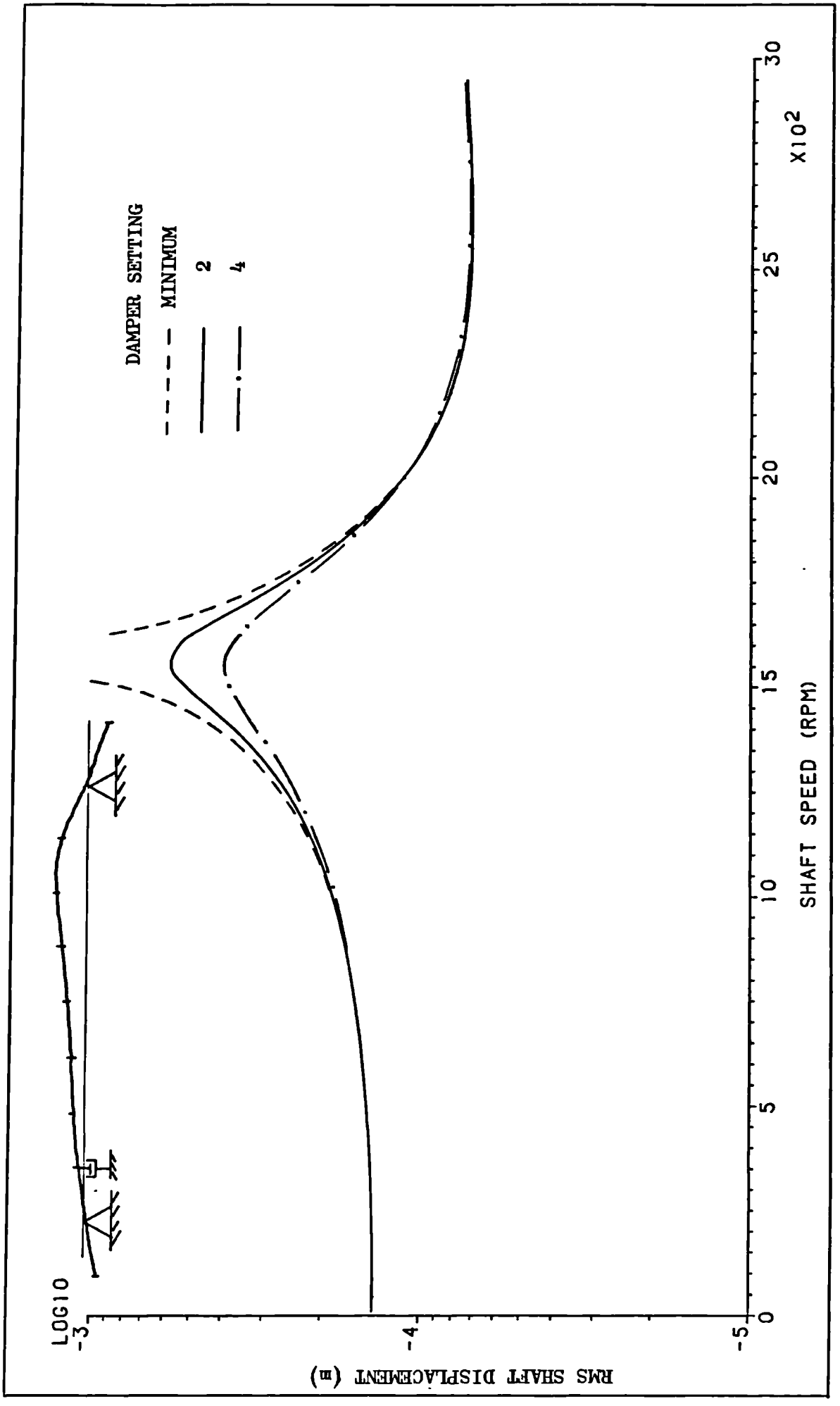

FIG. 7.8c(ii) PREDICTED SHAFT RESPONSE (TEST 2a)

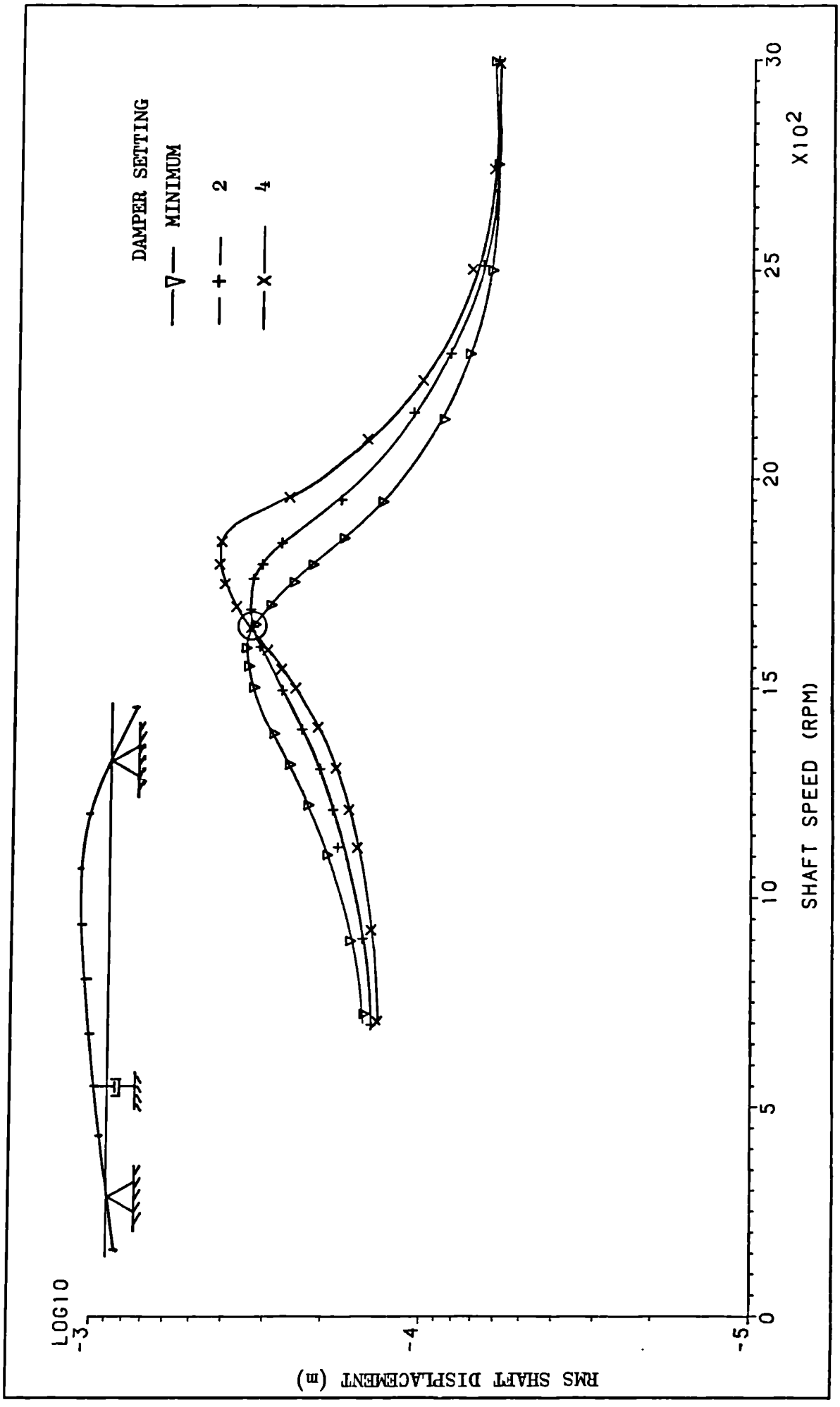

FIG. 7.8d(i) MEASURED SHAFT RESPONSE (TEST 2b)

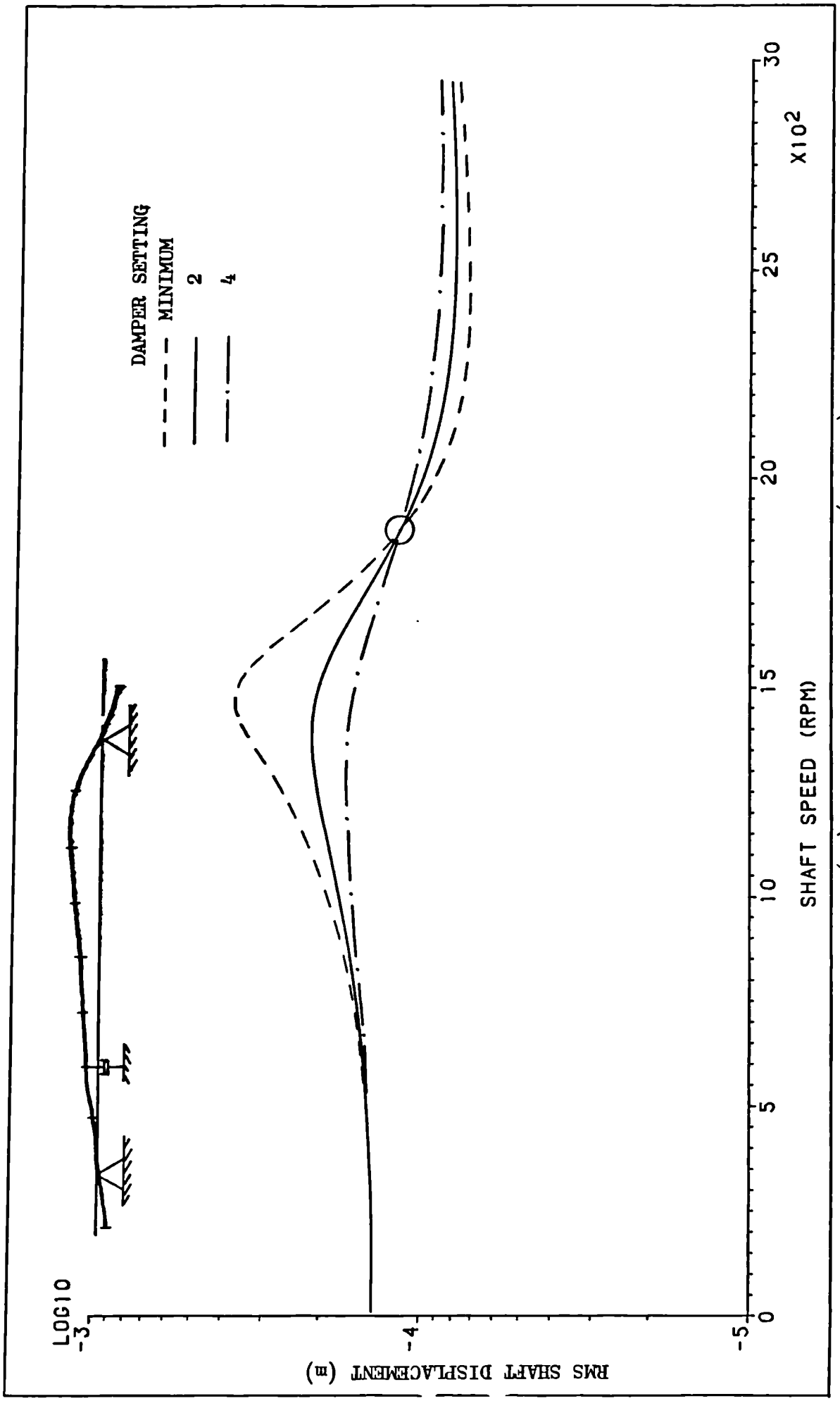

FIG. 7.8d(ii) PREDICTED SHAFT RESPONSE (TEST 2b)

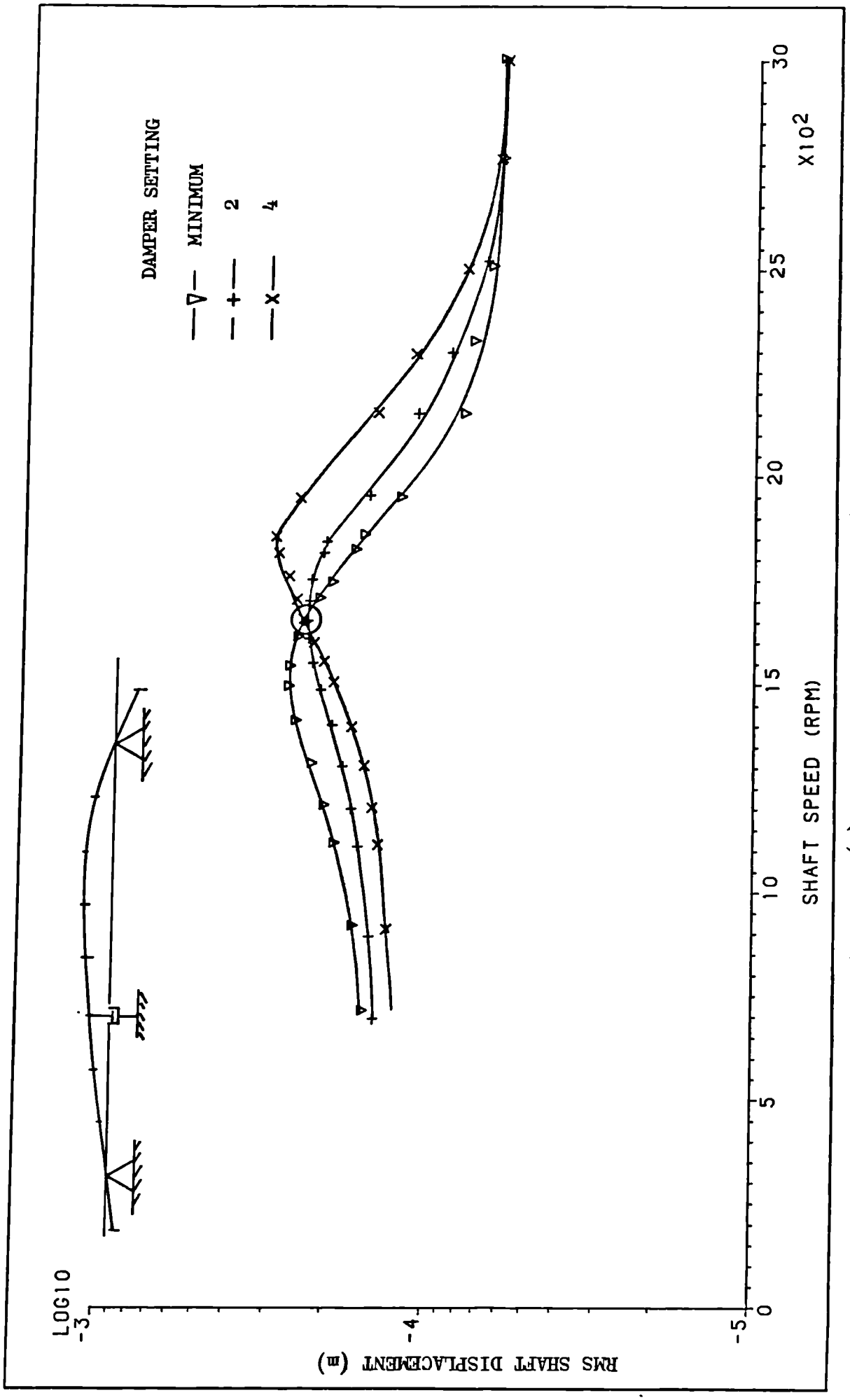

FIG. 7.8e(i) MEASURED SHAFT RESPONSE (TEST 2c)

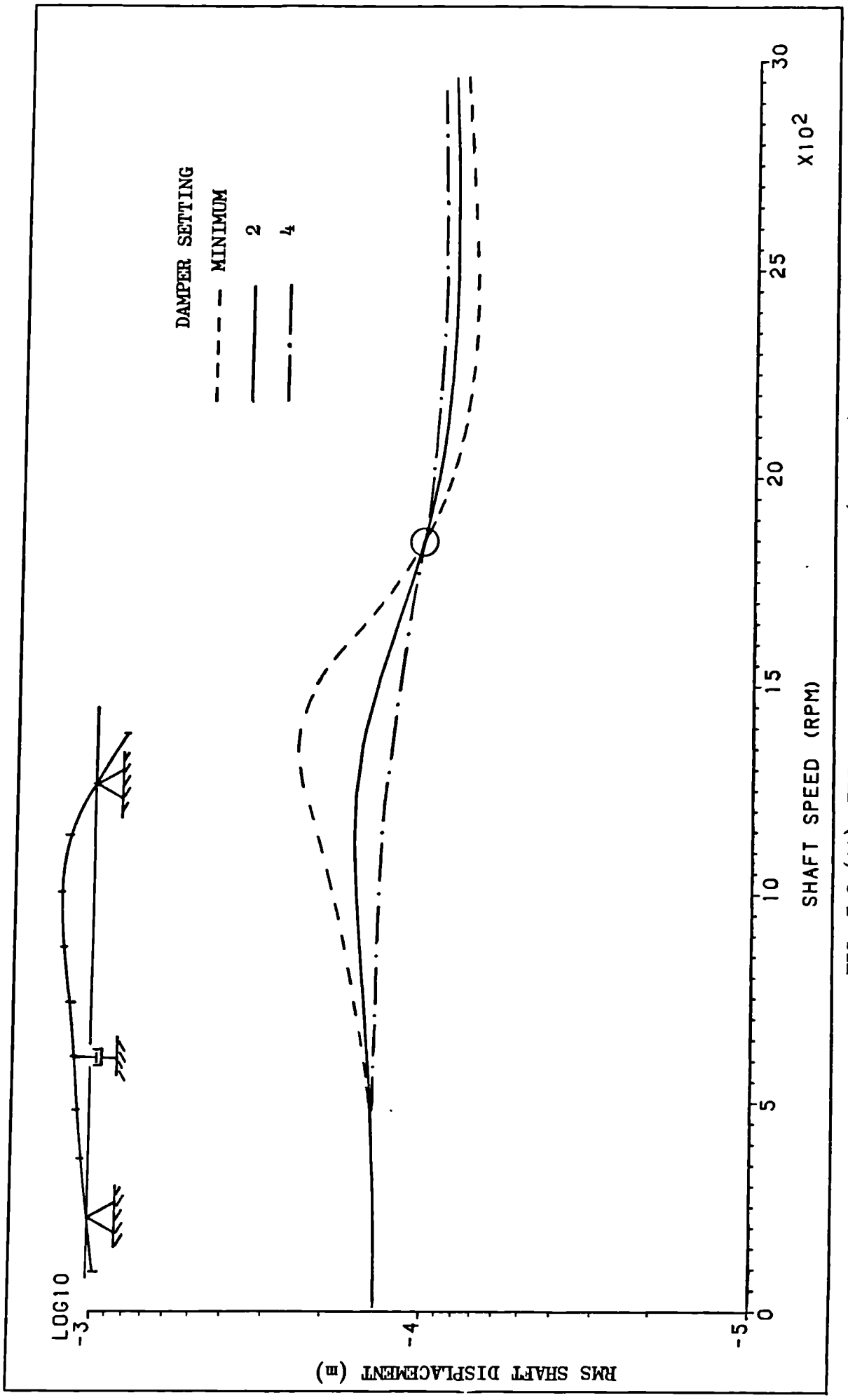

FIG. 7.8e(ii) PREDICTED SHAFT RESPONSE (TEST 2c)

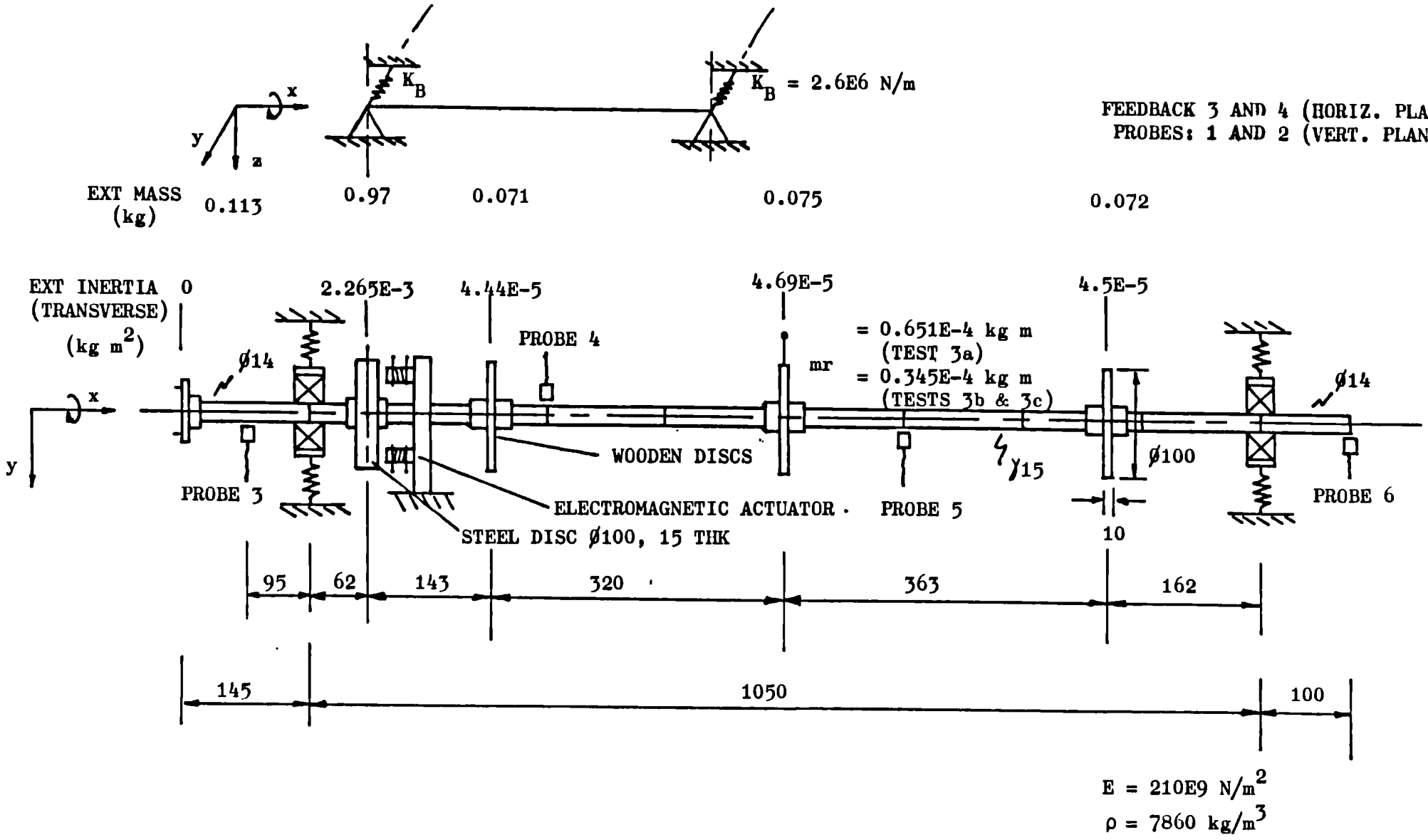

FIG. 7.9a SHAFT ARRANGEMENT FOR TEST 3

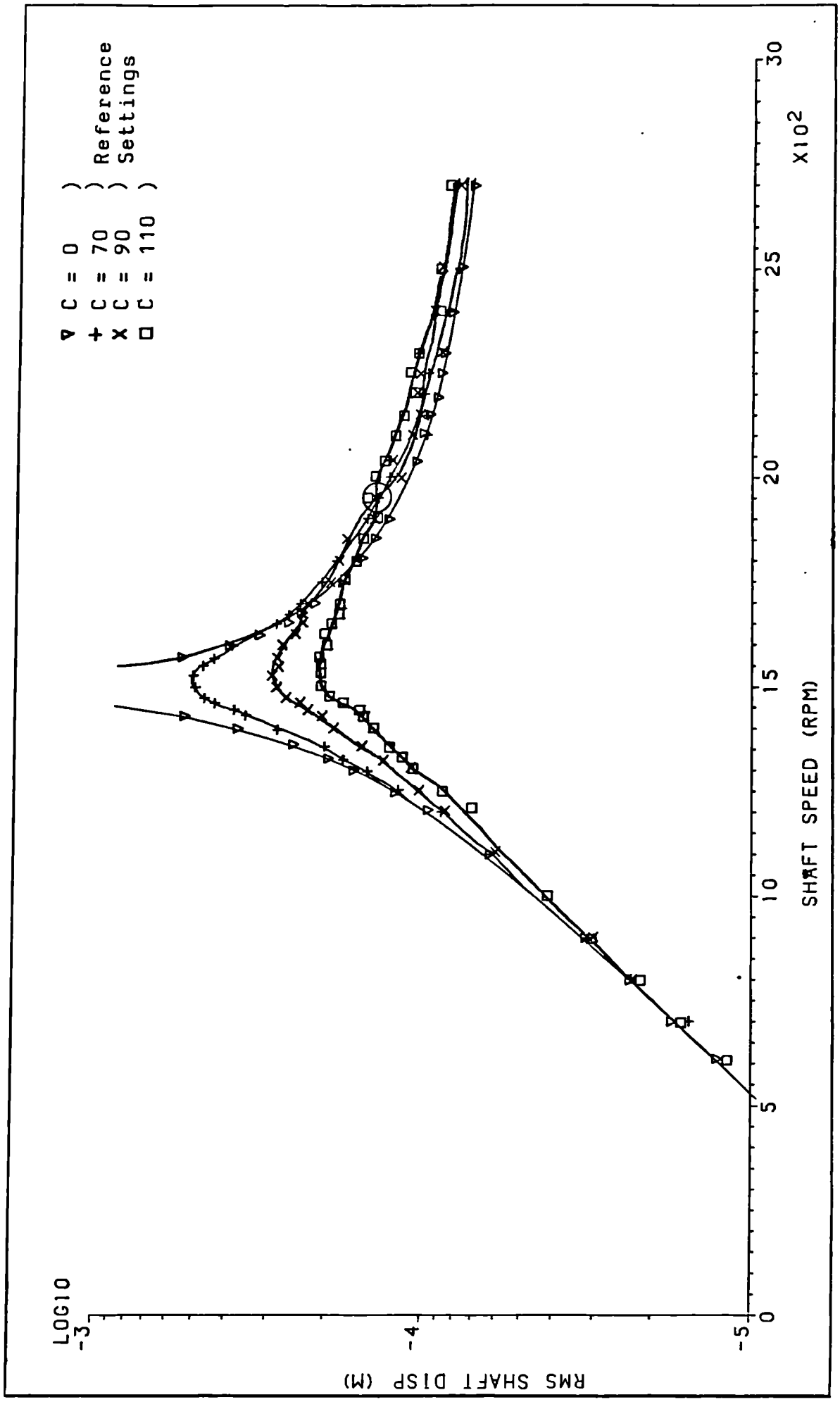

FIG. 7.9b(i) MEASURED SHAFT RESPONSE WITH ELECTROMAGNETIC DAMPING (TEST 3a)

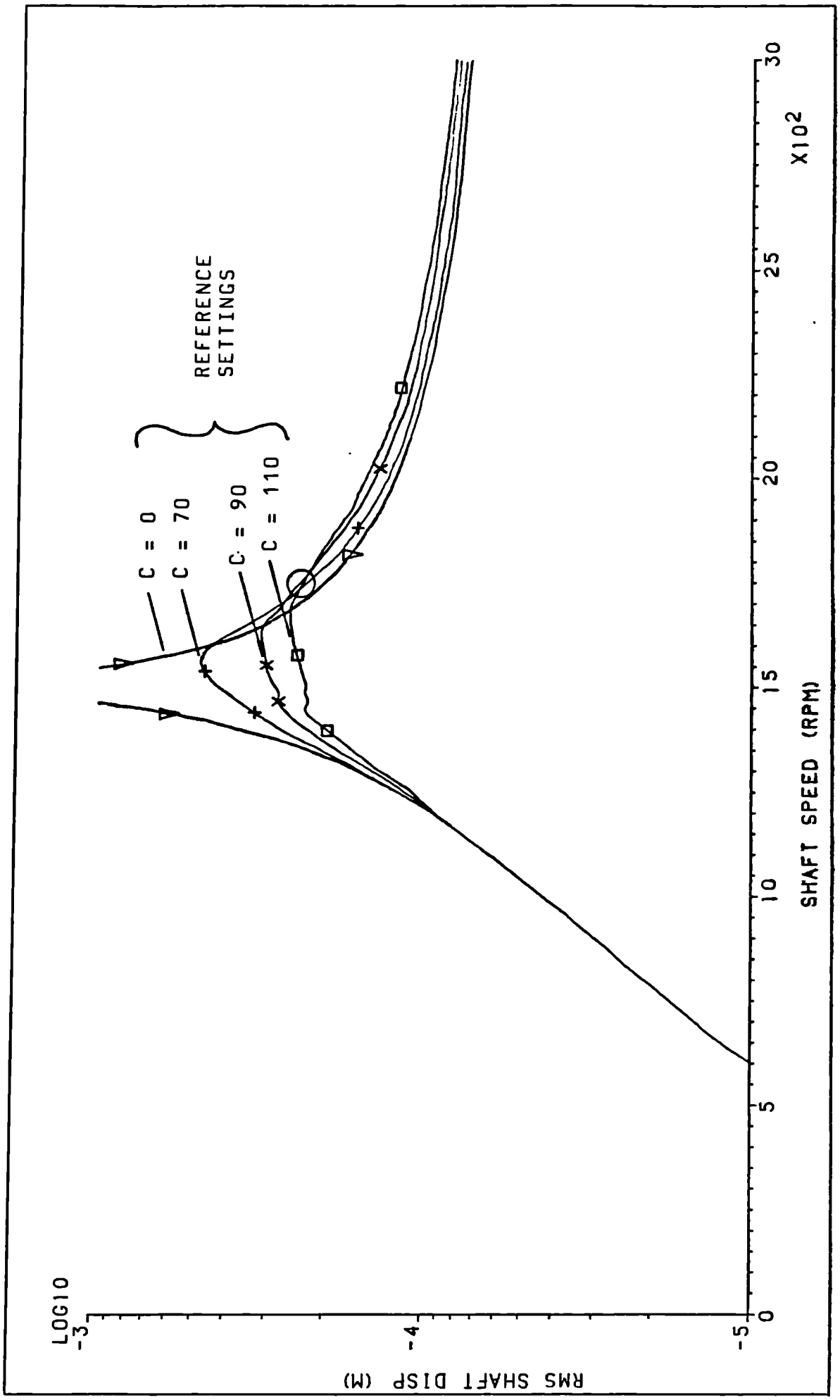

FIG. 7.9b(ii) PREDICTED SHAFT RESPONSE WITH ELECTROMAGNETIC DAMPING (TEST 3a)

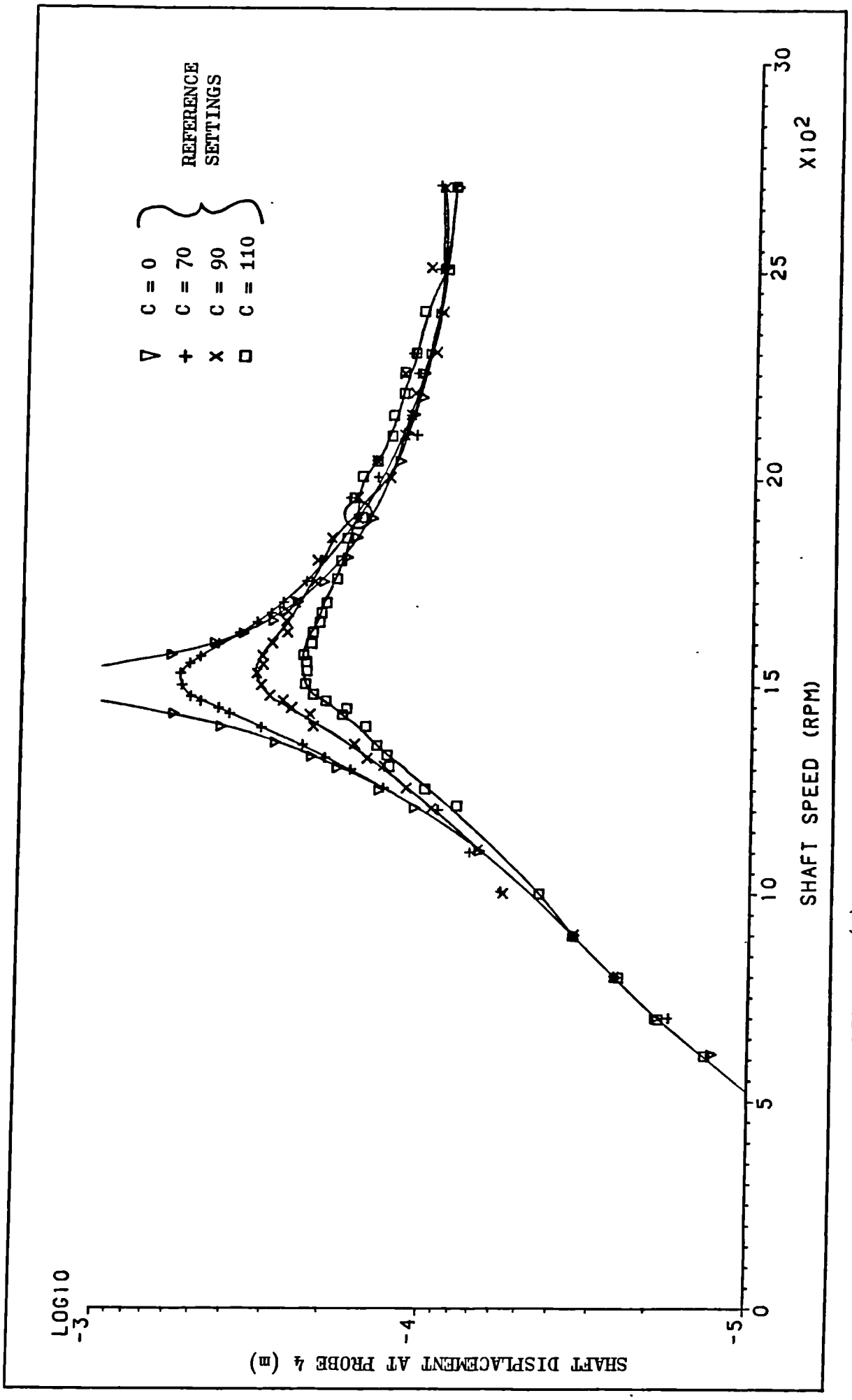

FIG. 7.9c(i) MEASURED SHAFT DISPLACEMENT VERSUS SPEED (TEST 3a)

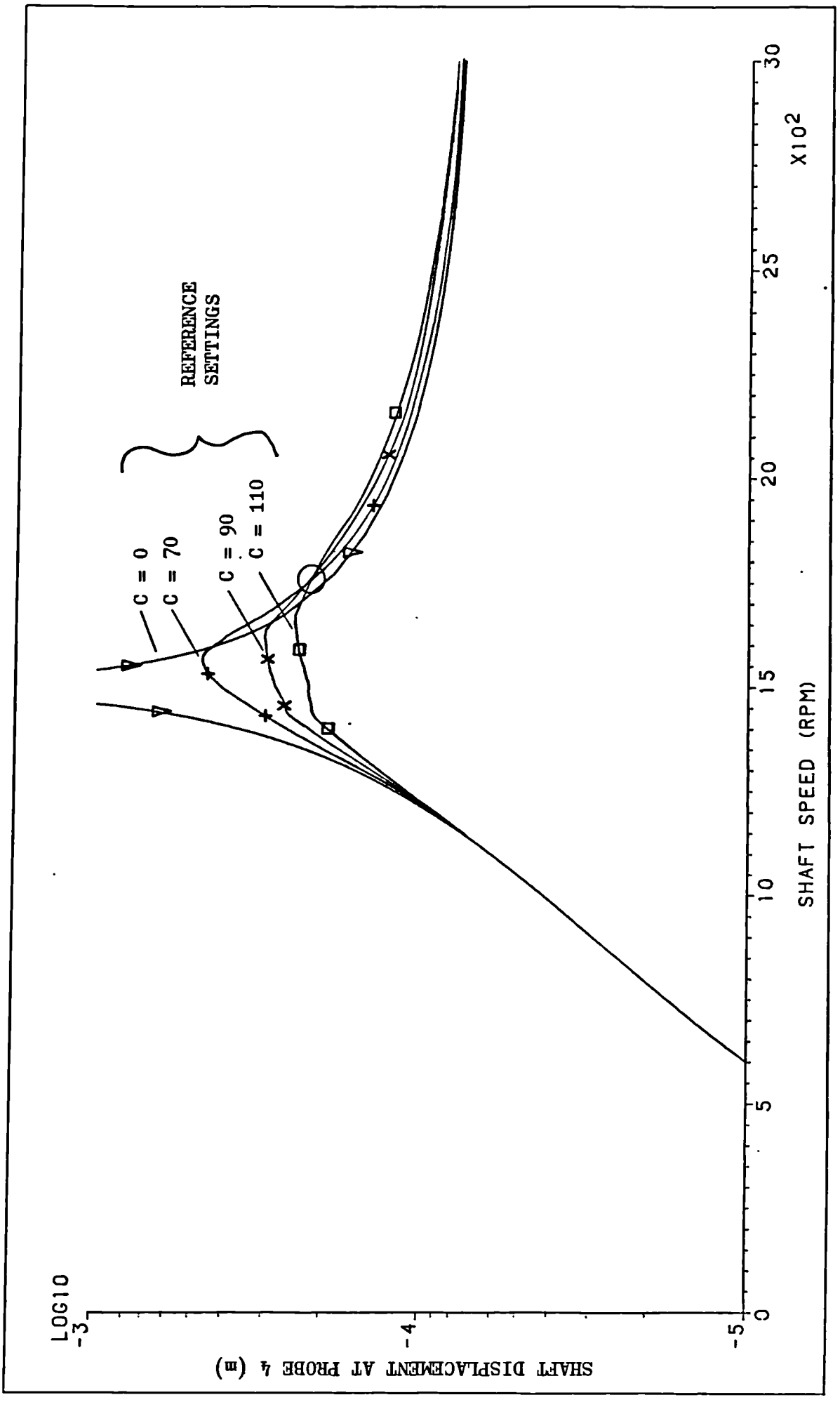

FIG. 7.9c(ii) PREDICTED SHAFT DISPLACEMENT VERSUS SPEED (TEST 3a)

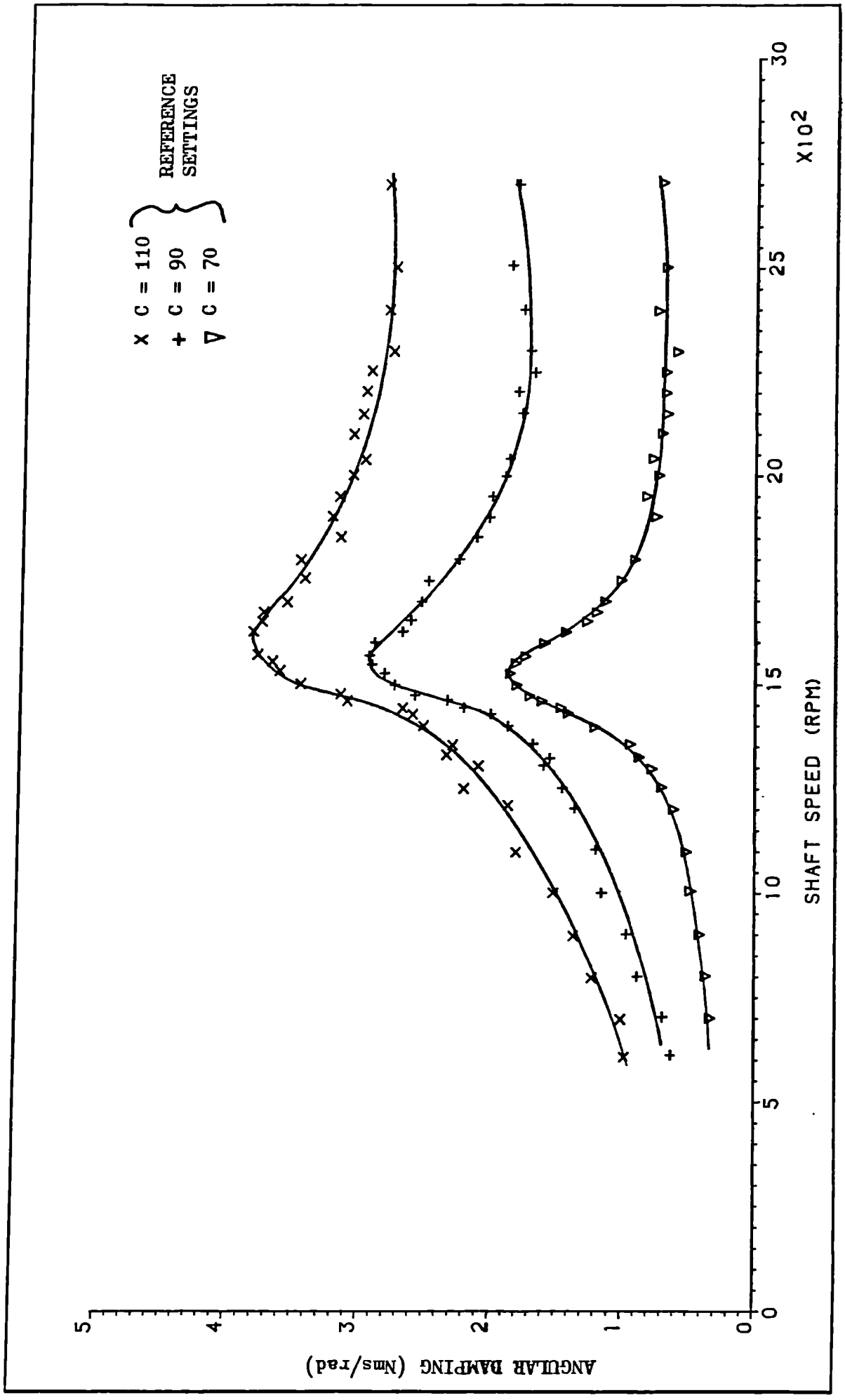

FIG. 7.9d VARIATION OF DAMPING WITH SHAFT SPEED (TEST 3a)

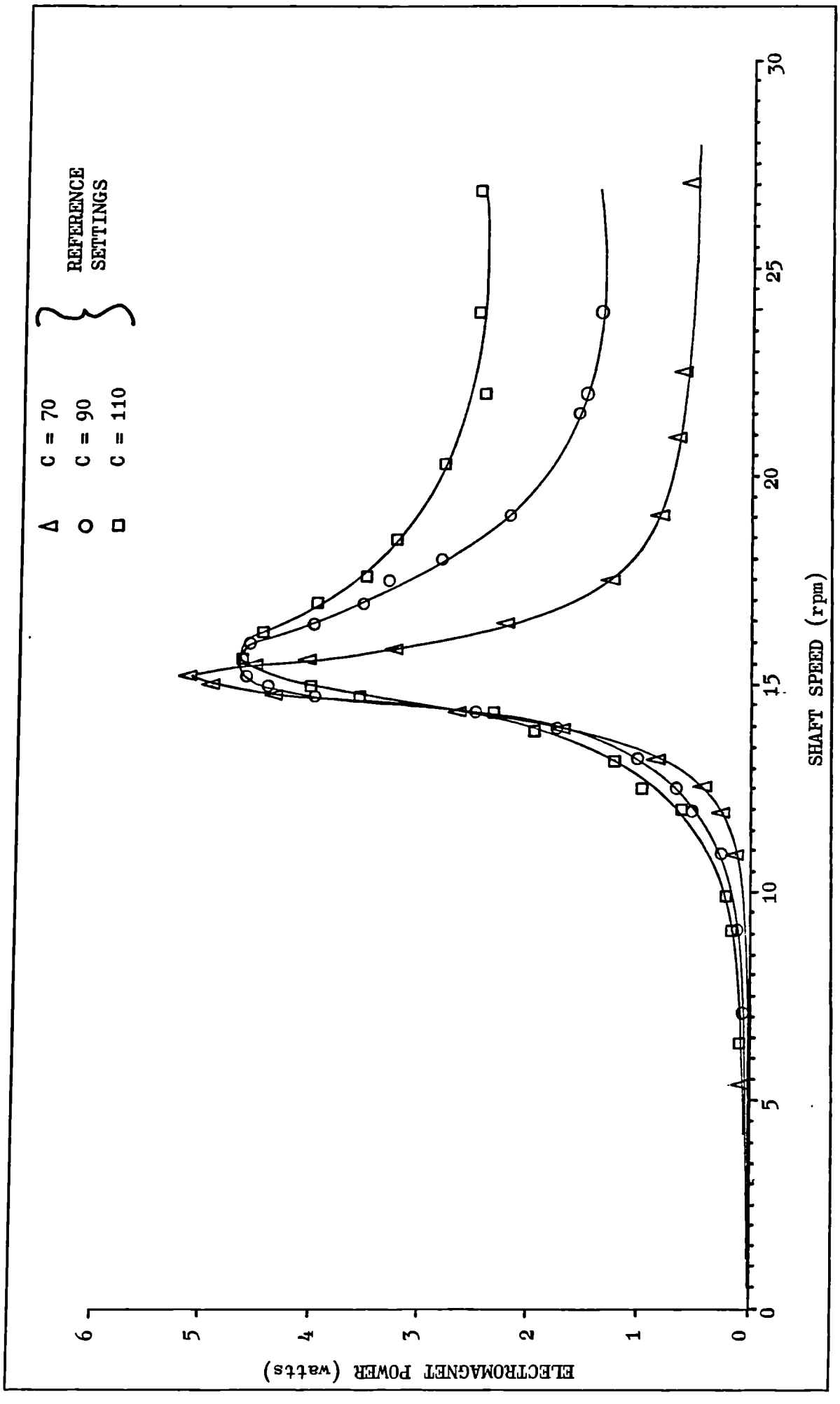

FIG. 7.9e MAGNET POWER FOR A RANGE OF DAMPING SETTINGS

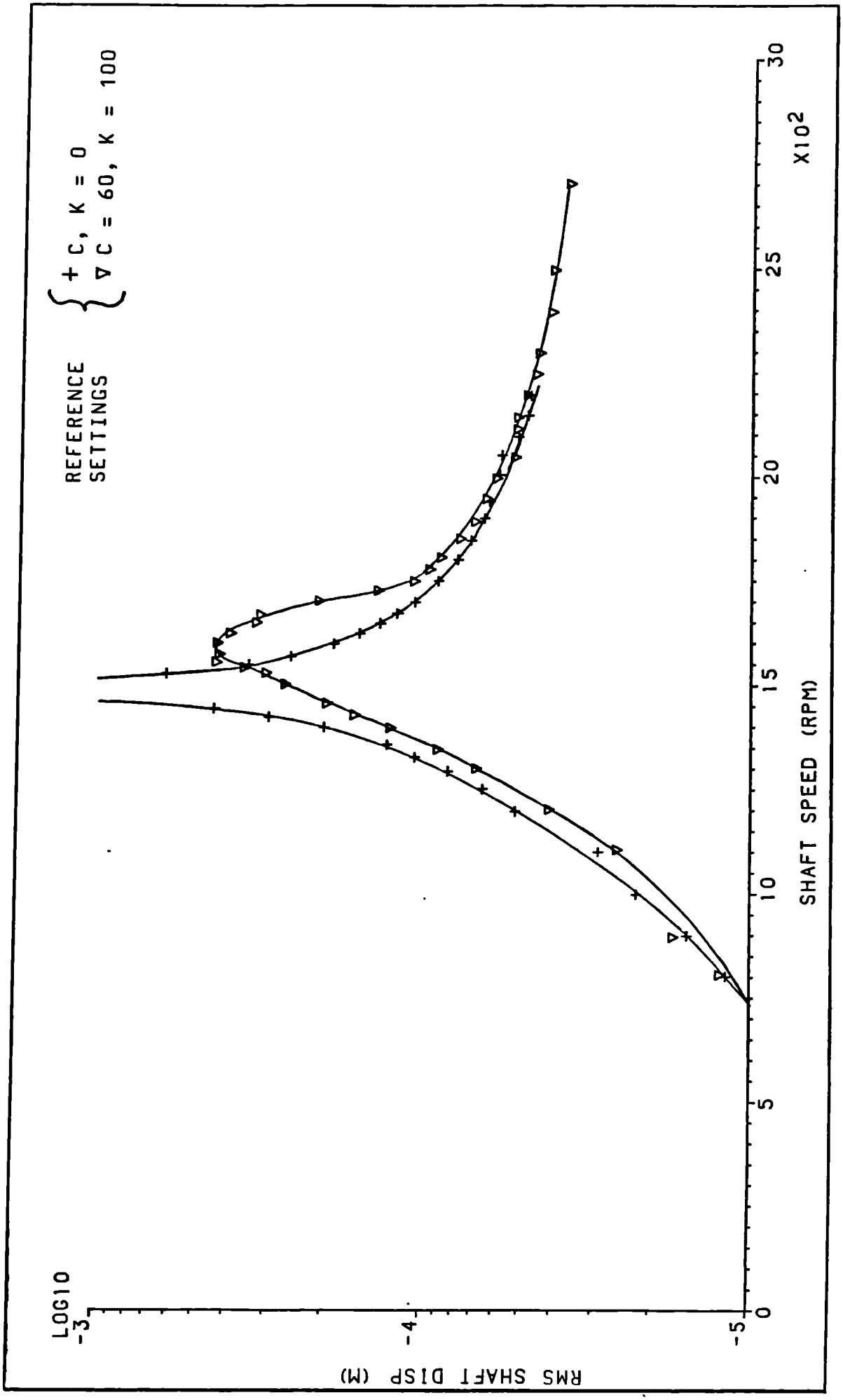

FIG. 7.9f MEASURED SHAFT RESPONSE WITH ELECTROMAGNETIC STIFFNESS/DAMPING (TEST 3b)

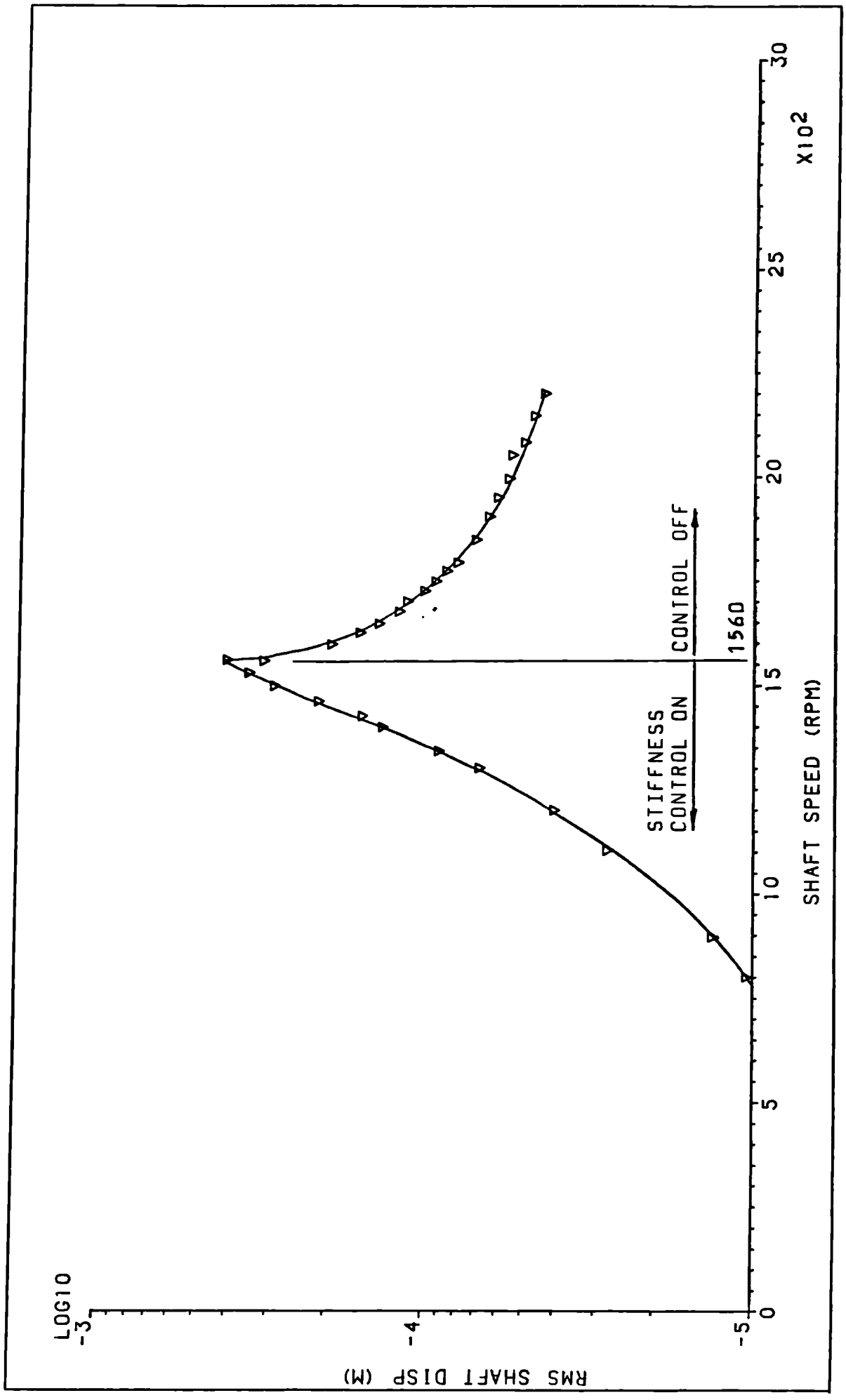

FIG. 7.9g(i) MEASURED SHAFT RESPONSE WITH "ON-OFF" STIFFNESS CONTROL (TEST 3c)

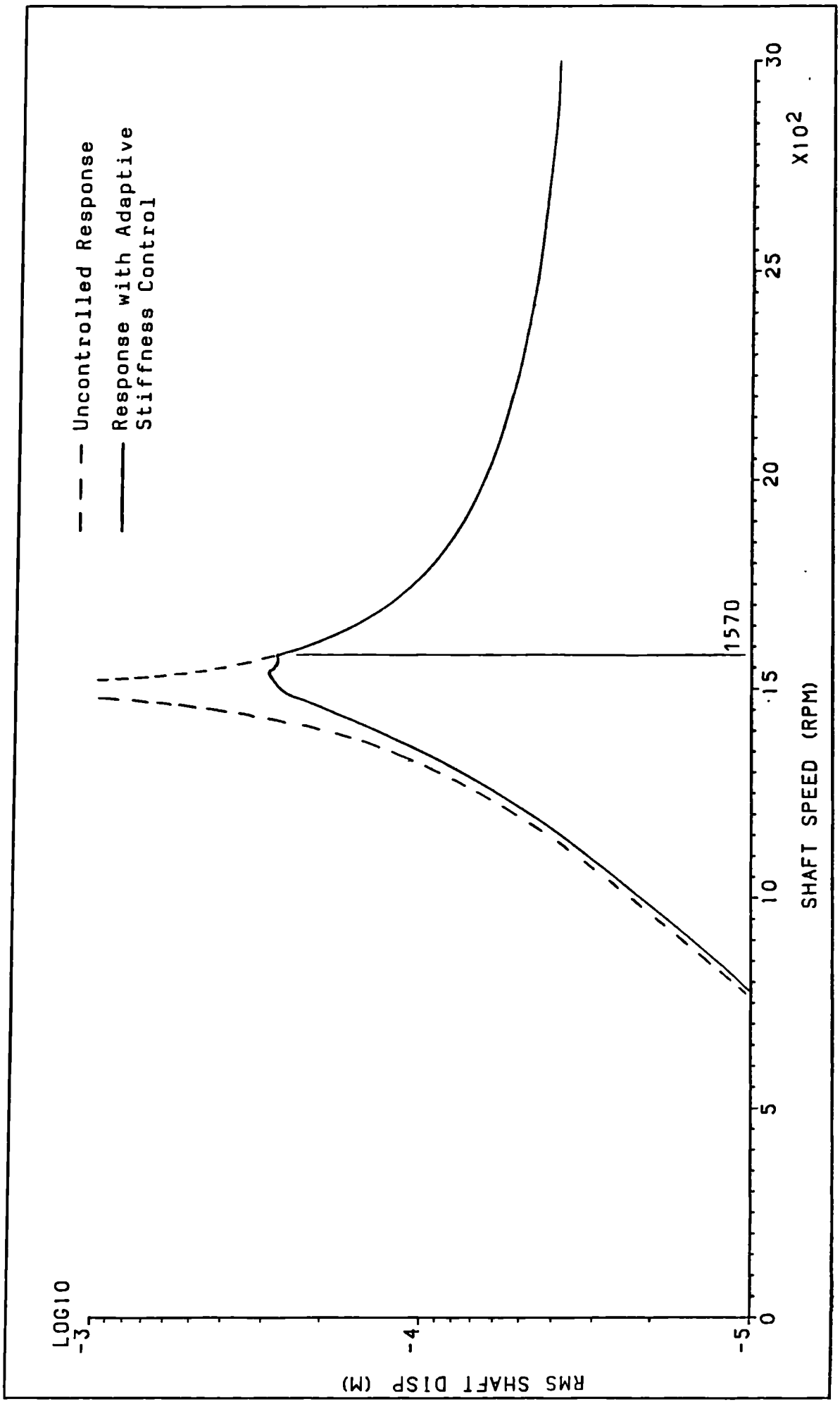

FIG. 7.9g(ii) PREDICTED RESPONSE EMPLOYING "ON-OFF" STIFFNESS CONTROL (TEST 3c)

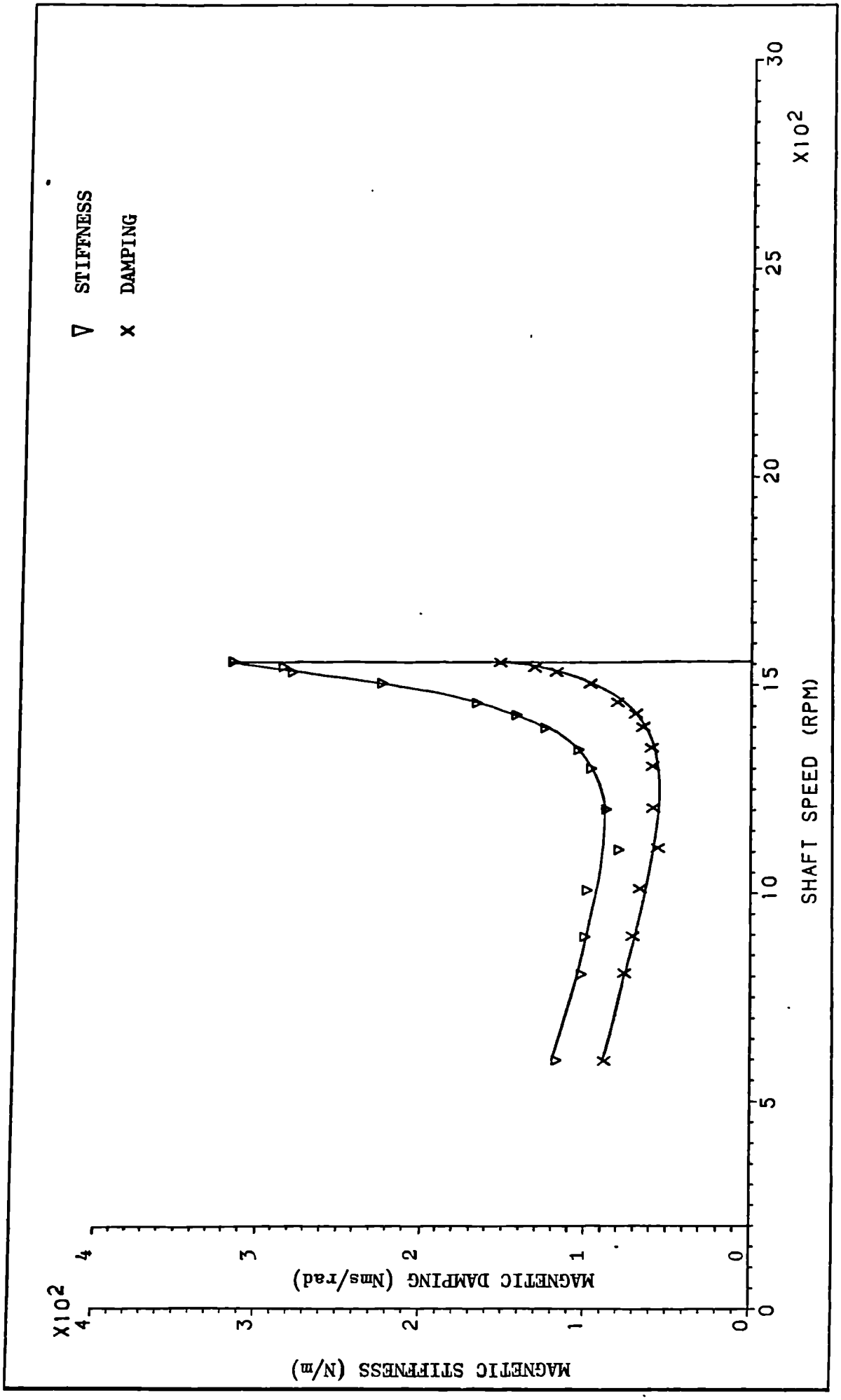

FIG. 7.9b PLOT OF MAGNETIC DAMPING AND STIFFNESS (TEST 3c)

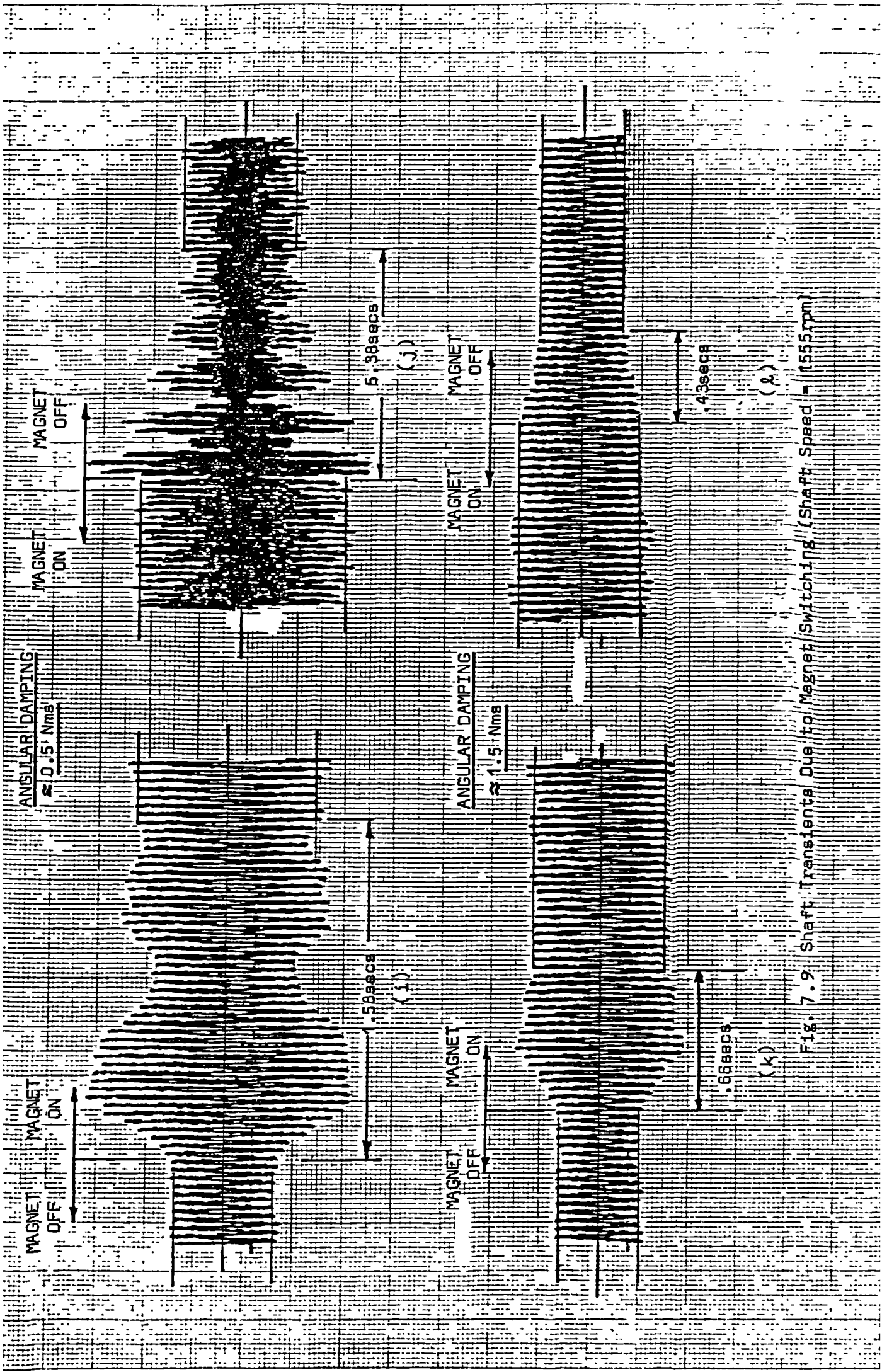

Fig. 7.9 Shaft Transients Due to Magnet Switching (Shaft Speed = 1555rpm)

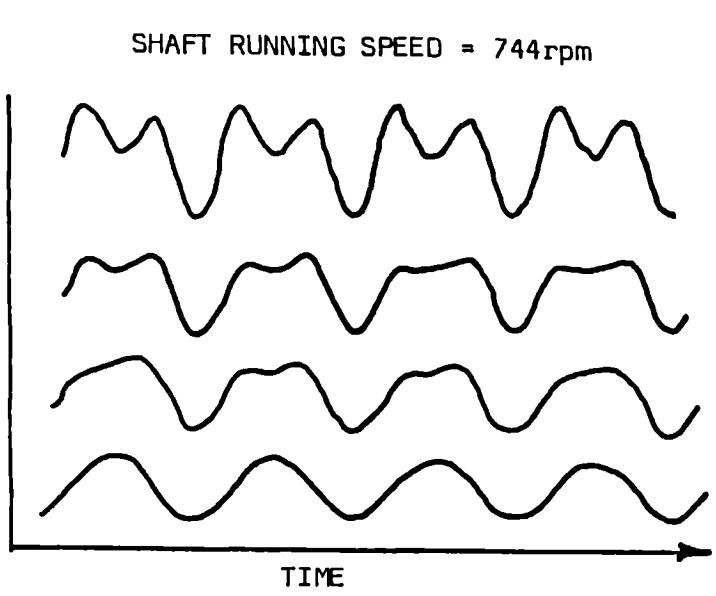

Fig. 7.9(m) Elimination of Non-Synchronous Components

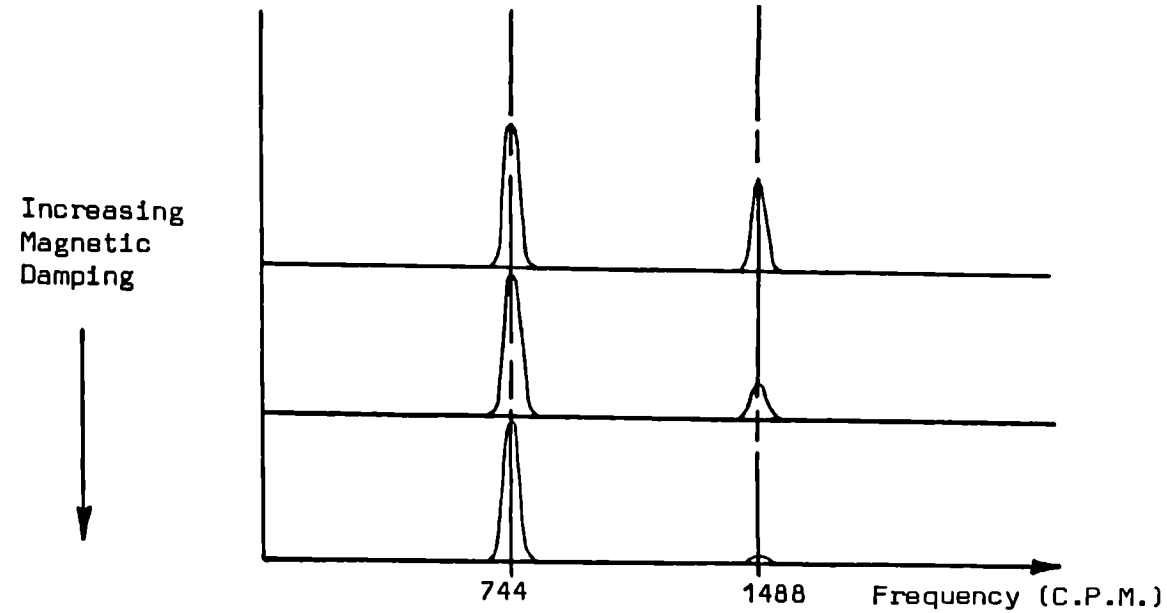

Fig. 7.9 (n)

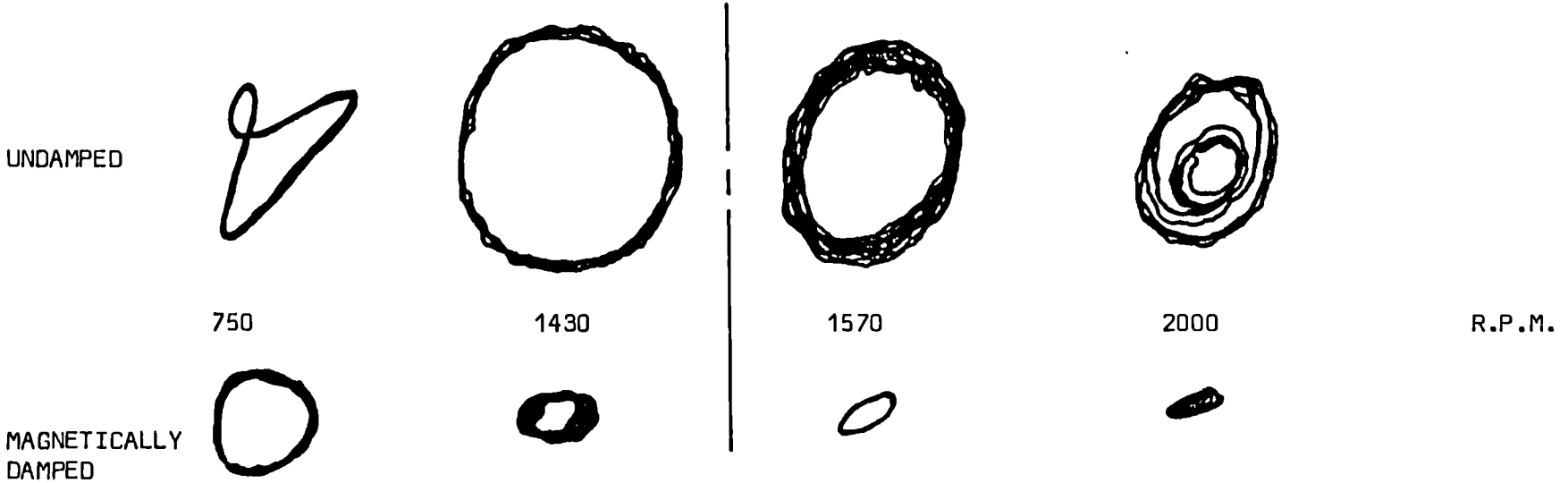

Fig. 7.9(p)Effect of Electromagnetic Damping on Shaft Orbit

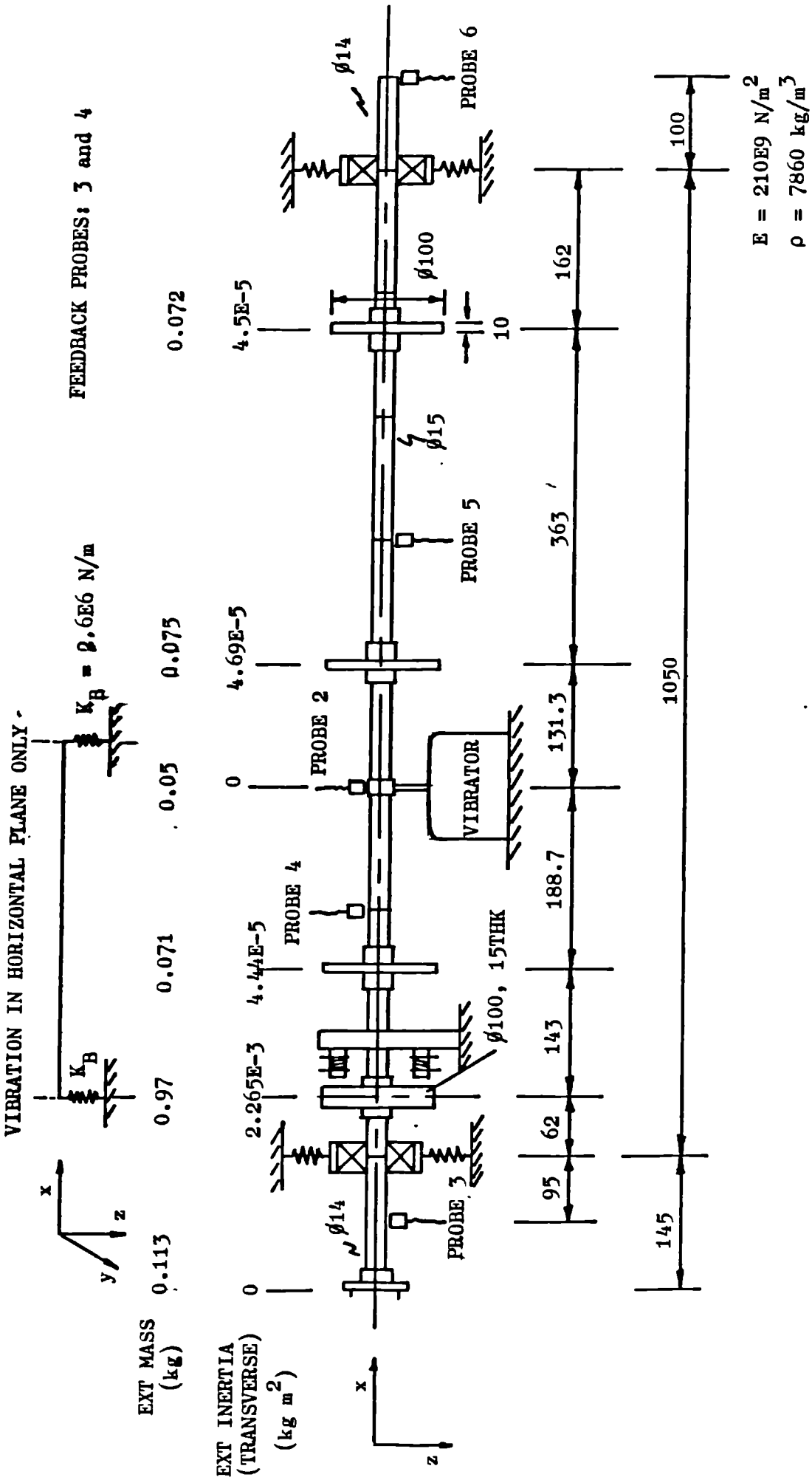

FIG. 7.10a SHAFT ARRANGEMENT FOR TEST 4

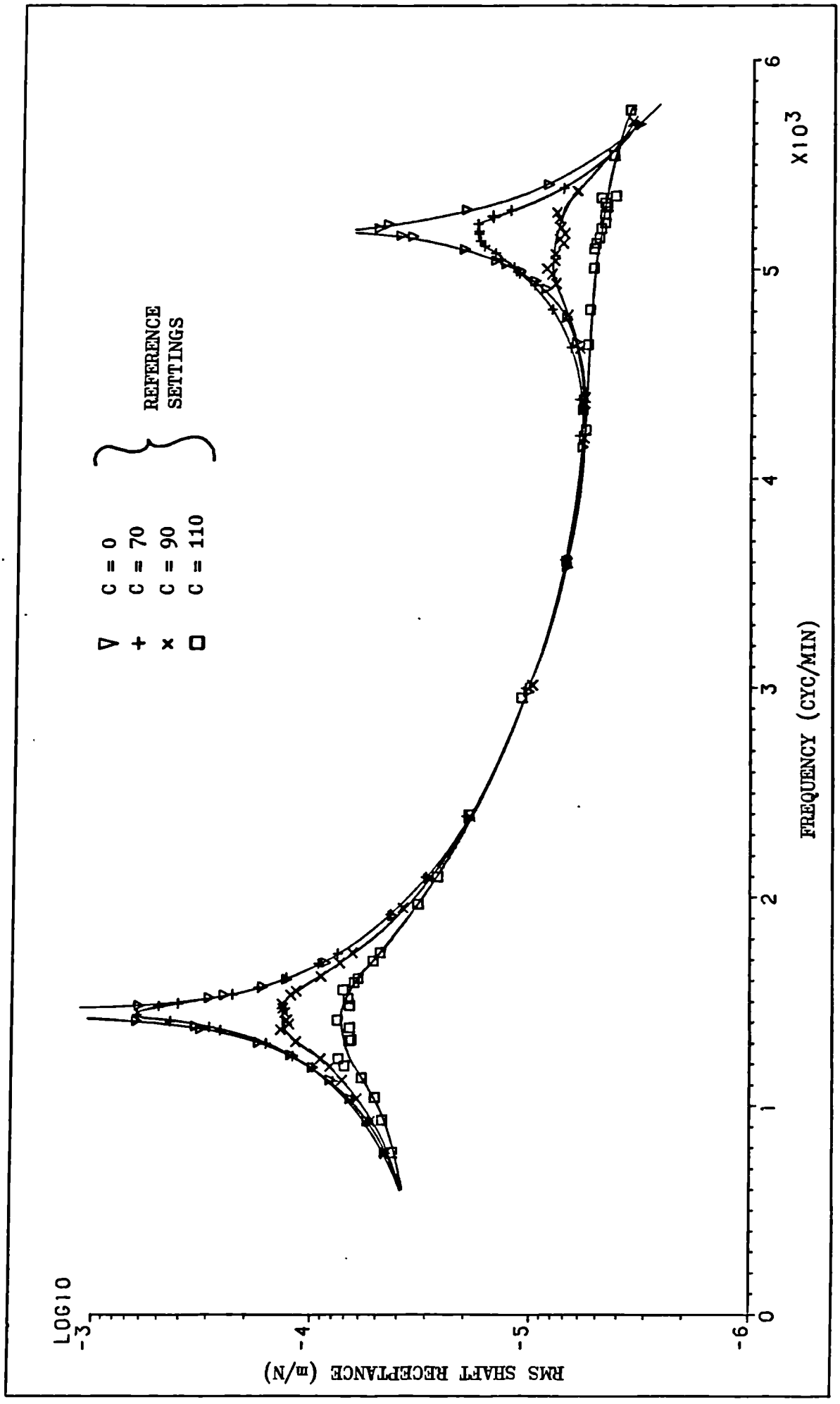

FIG. 7.10b PLOT OF SHAFT RECEPTANCE VERSUS FREQUENCY (TEST 4a) - DAMPING CONTROL

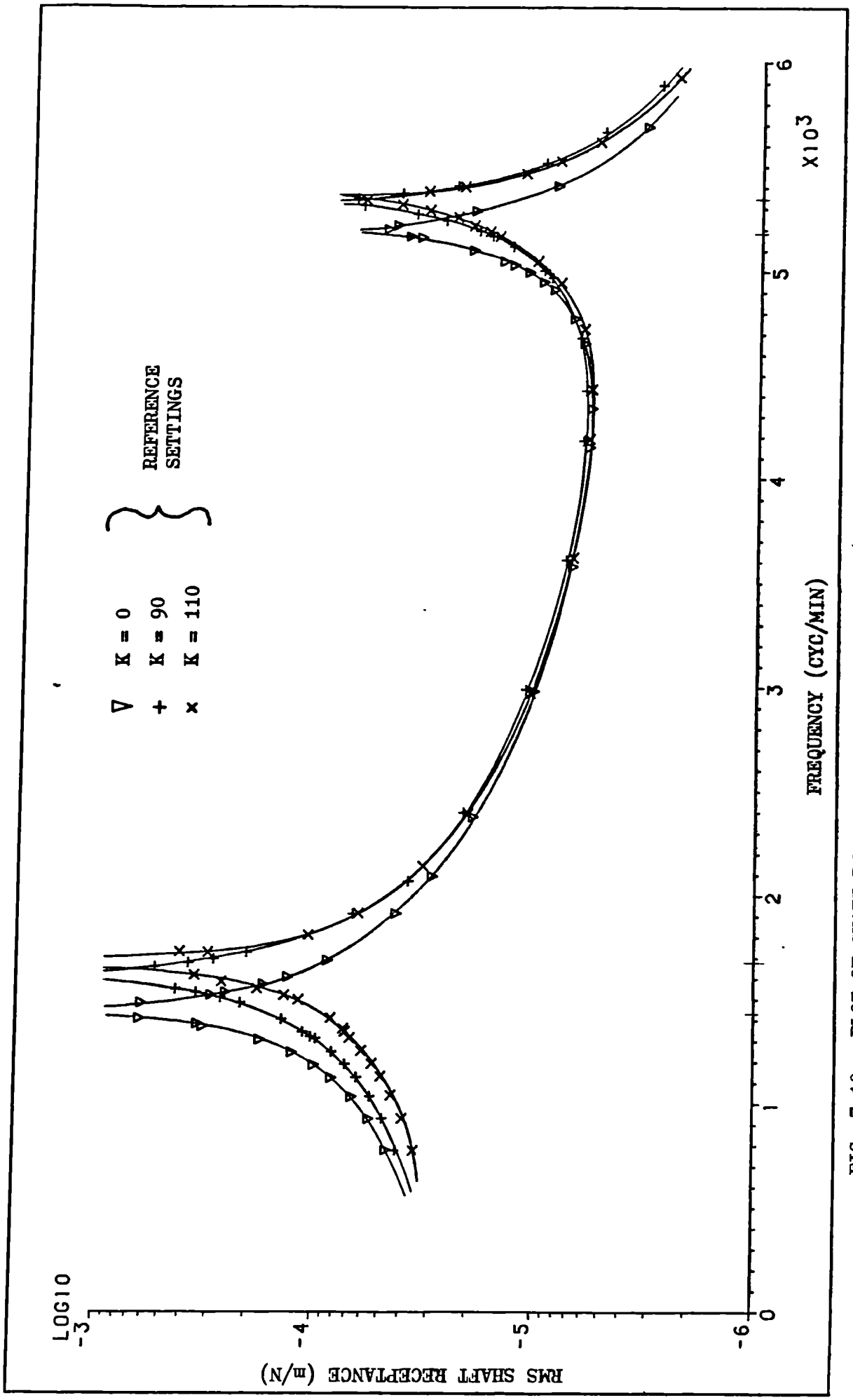

FIG. 7.10c PLOT OF SHAFT RECEPTANCE VERSUS FREQUENCY (TEST 4b) - STIFFNESS CONTROL

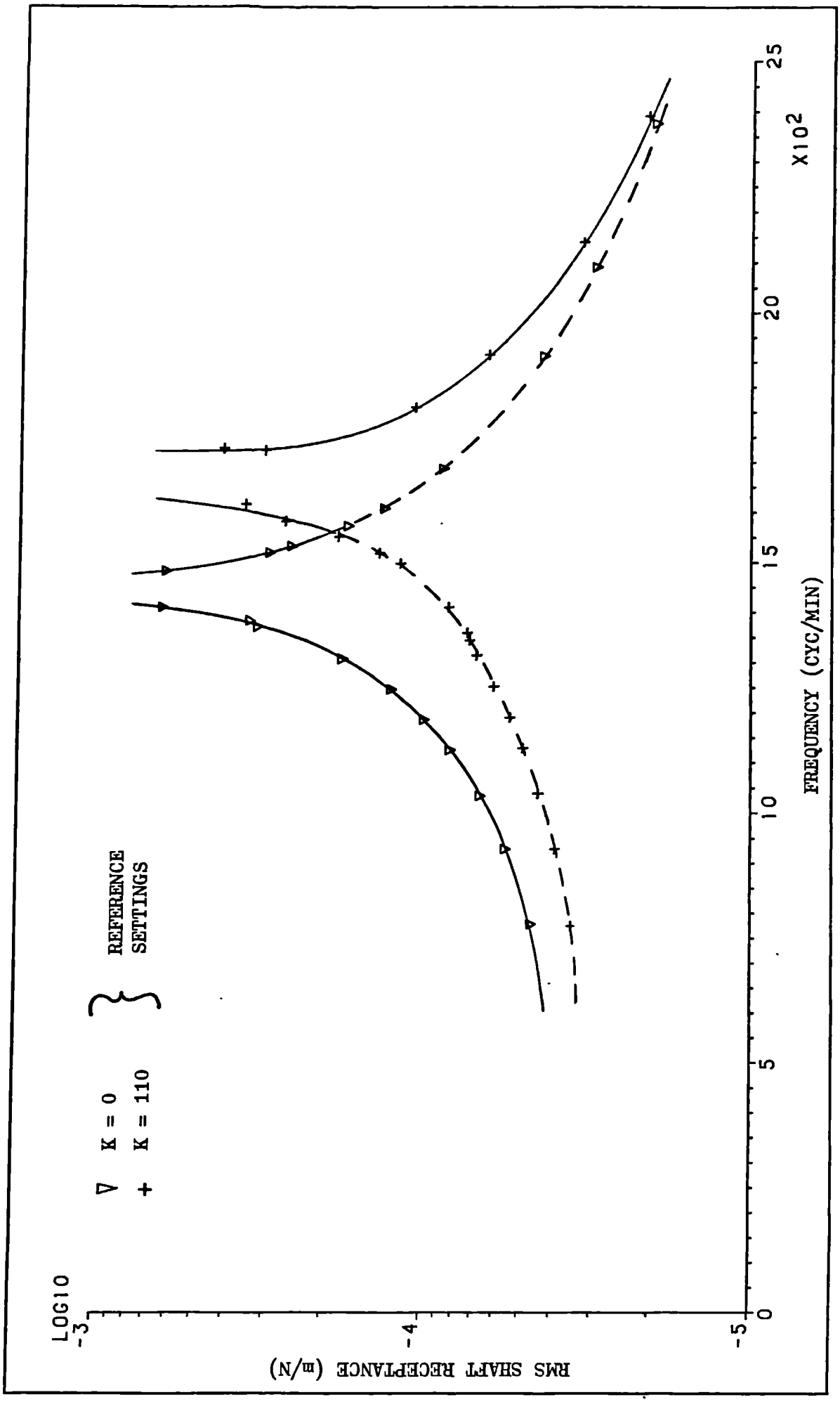

FIG. 7.10d PLOT OF SHAFT RECEPTANCE VERSUS FREQUENCY (TEST 4b) - STIFFNESS CONTROL

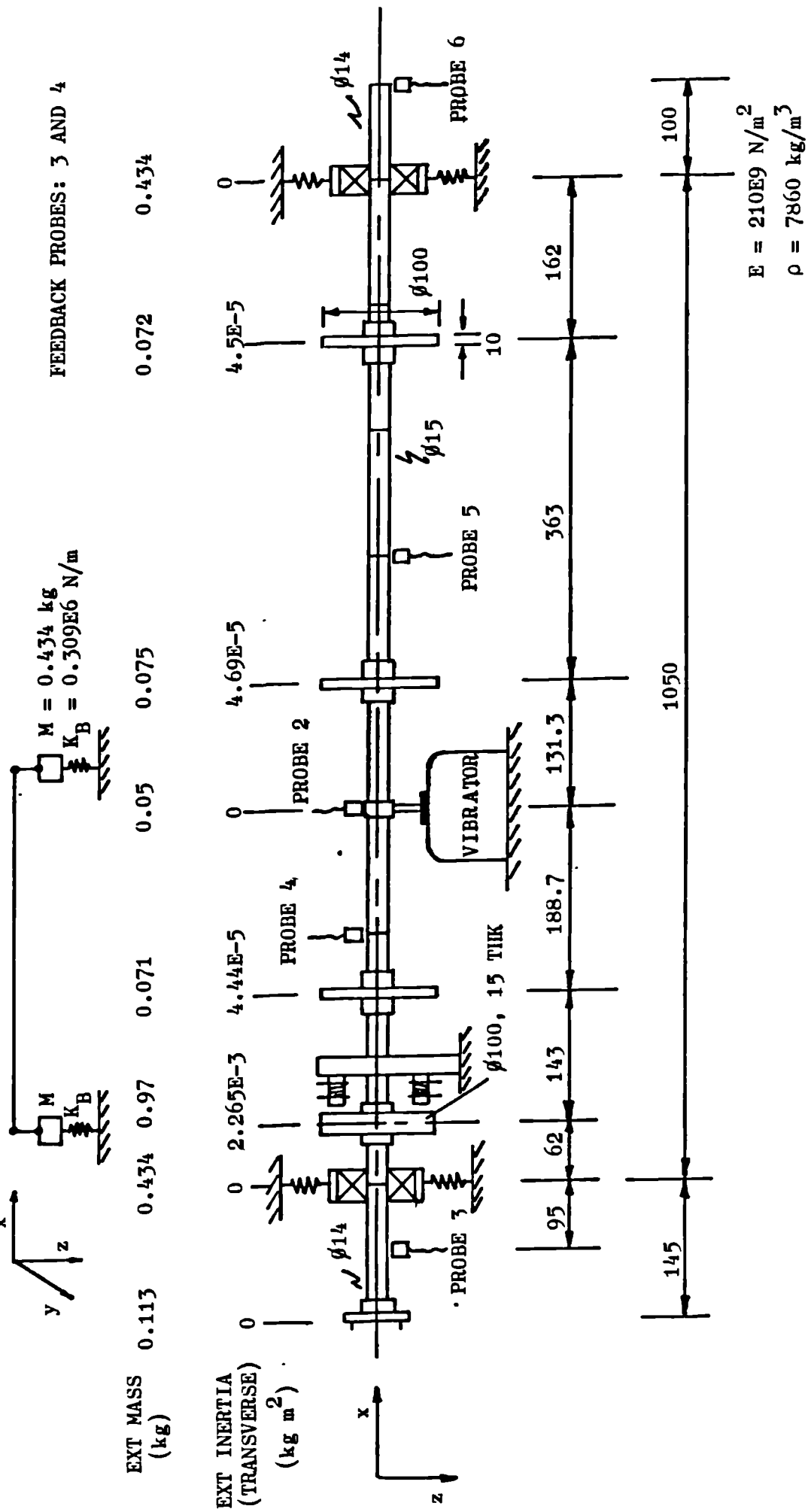

FIG. 7.11a SHAFT ARRANGEMENT FOR TEST 5

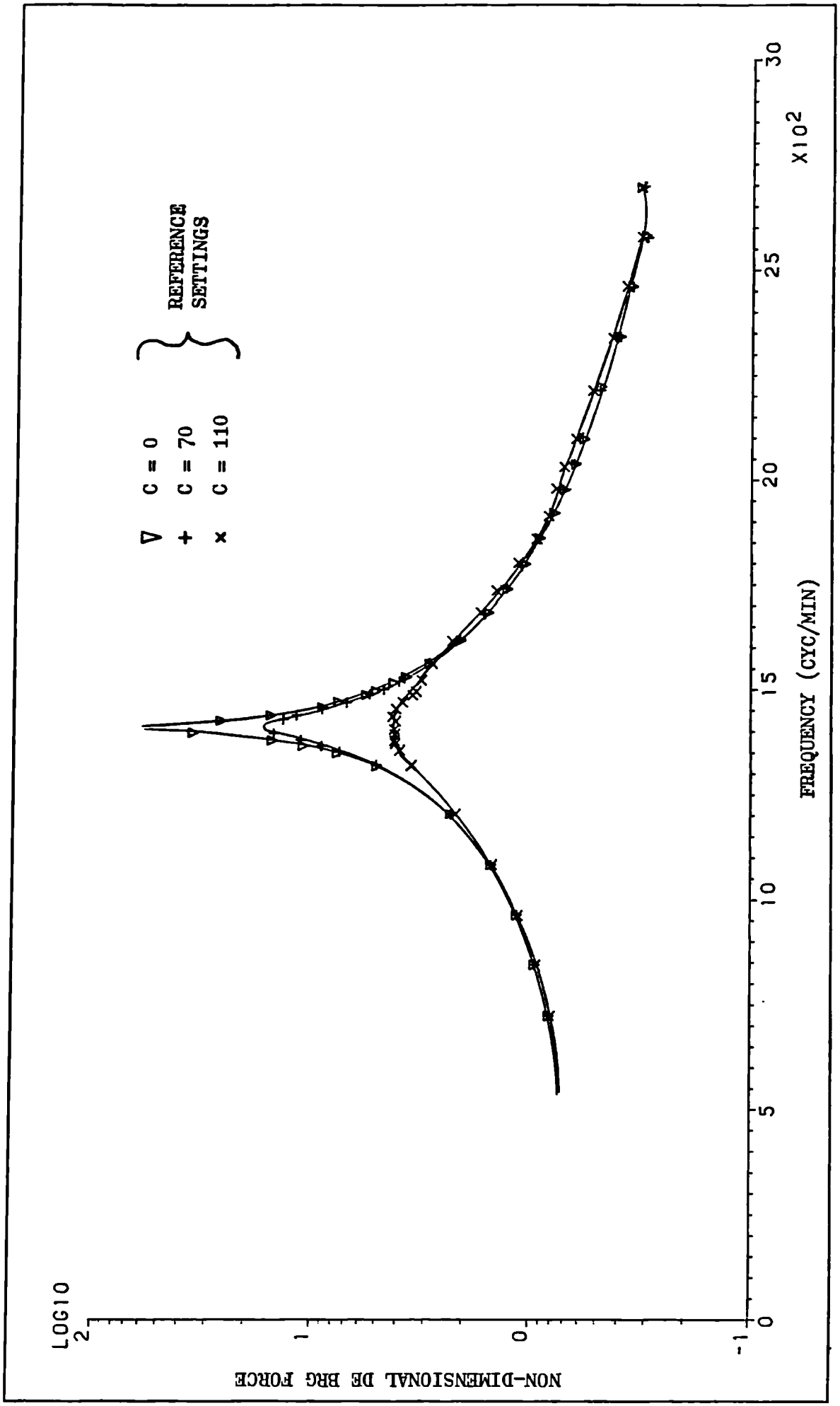

FIG. 7.11b PLOT OF MEASURED DIMENSIONLESS DE BRG FORCE VERSUS FREQUENCY - DAMPING CONTROL

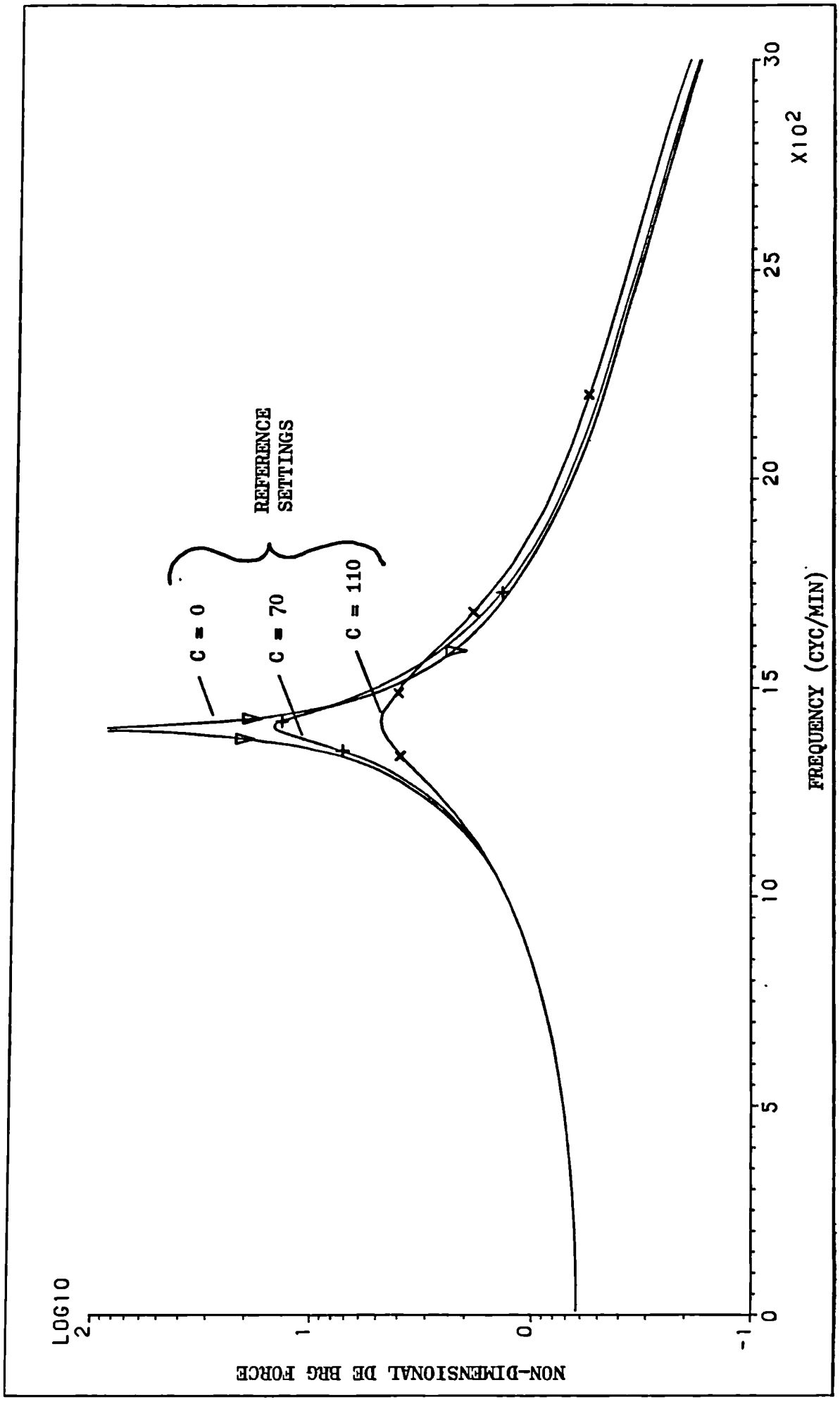

FIG. 7.11c PLOT OF PREDICTED DIMENSIONLESS DE BRG FORCE VERSUS FREQUENCY - DAMPING CONTROL

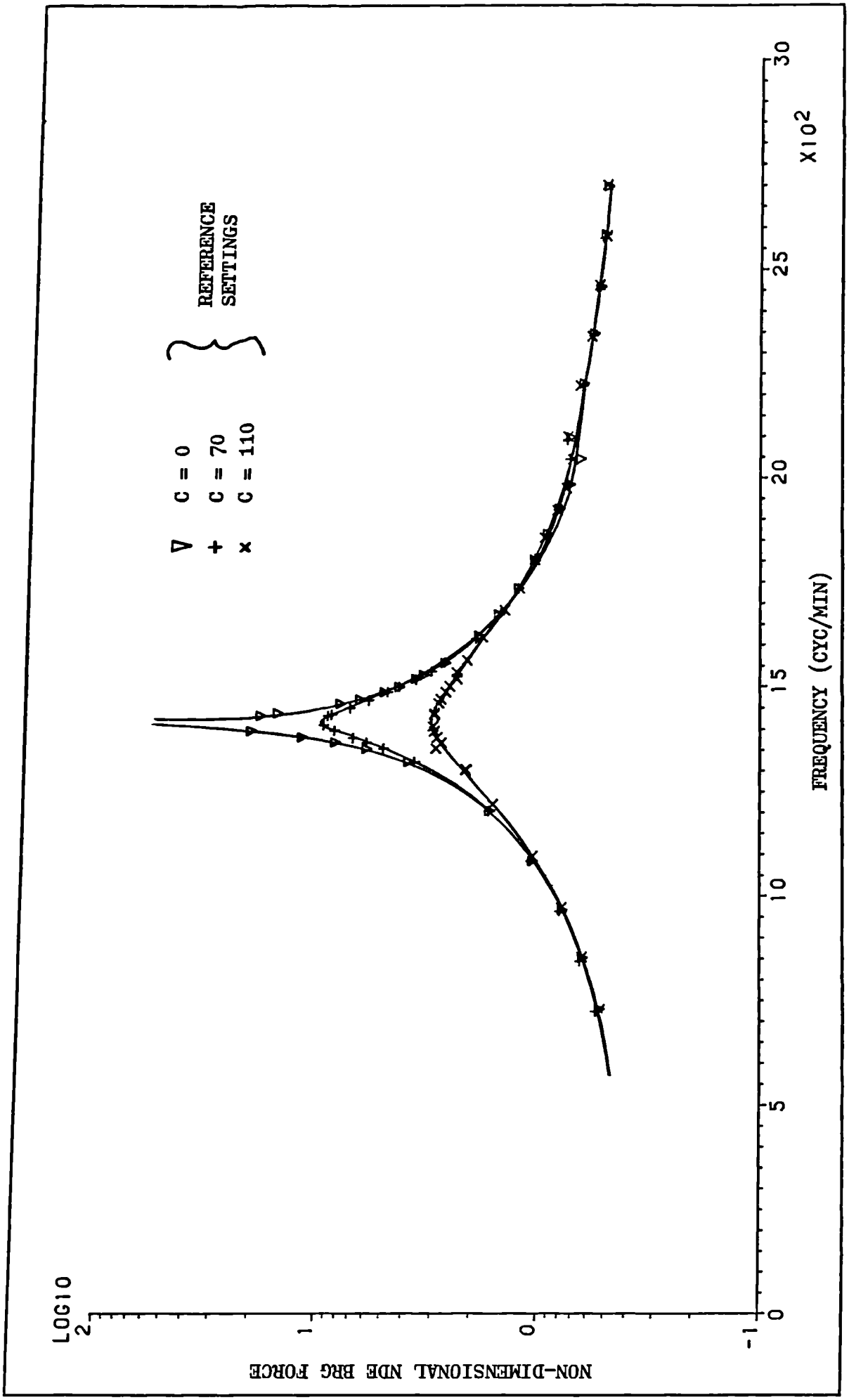

FIG. 7.11d PLOT OF MEASURED DIMENSIONLESS NDE BRG FORCE VERSUS FREQUENCY - DAMPING CONTROL

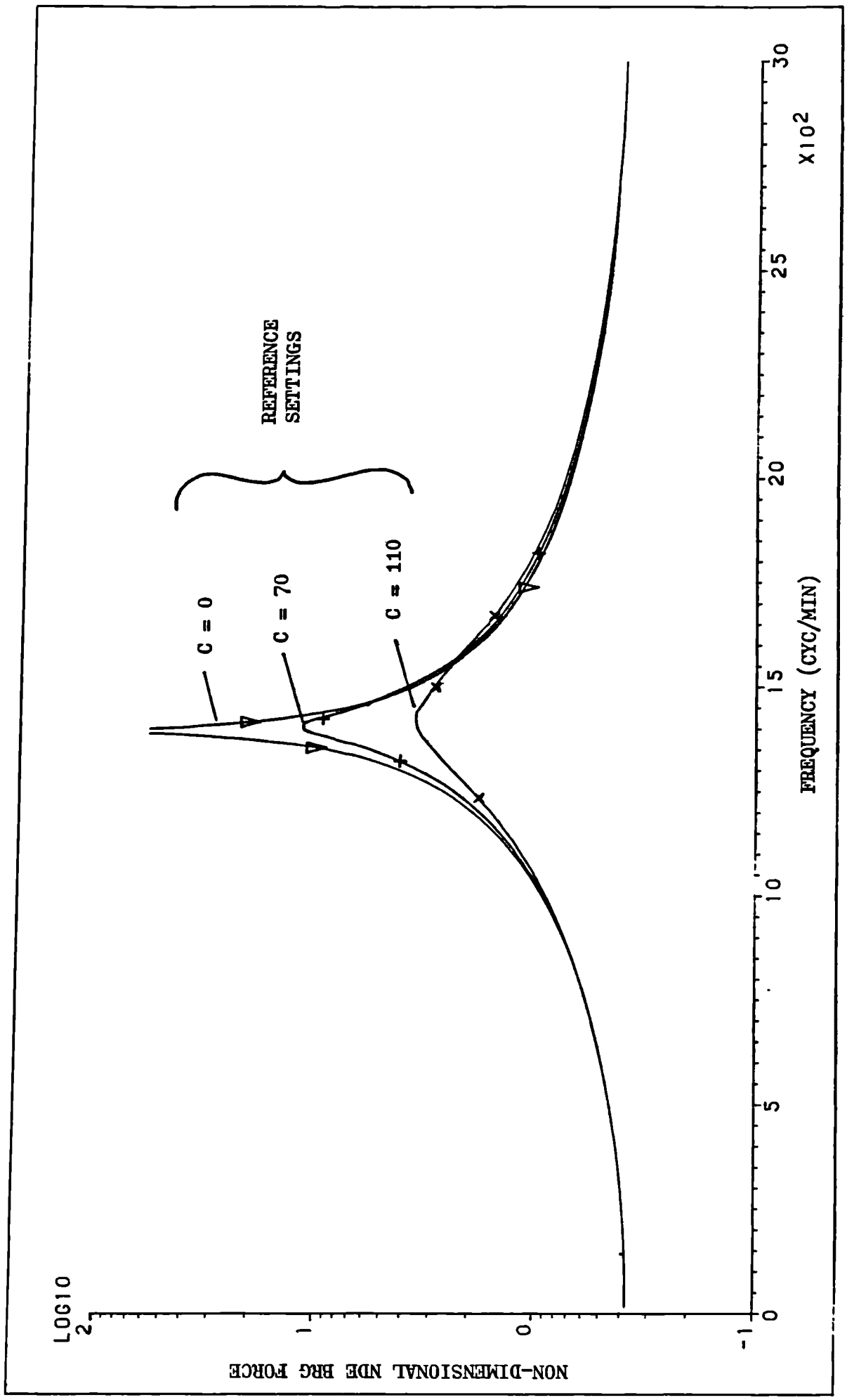

FIG. 7.11e PLOT OF PREDICTED DIMENSIONLESS NDE BRG FORCE VERSUS FREQUENCY - DAMPING CONTROL

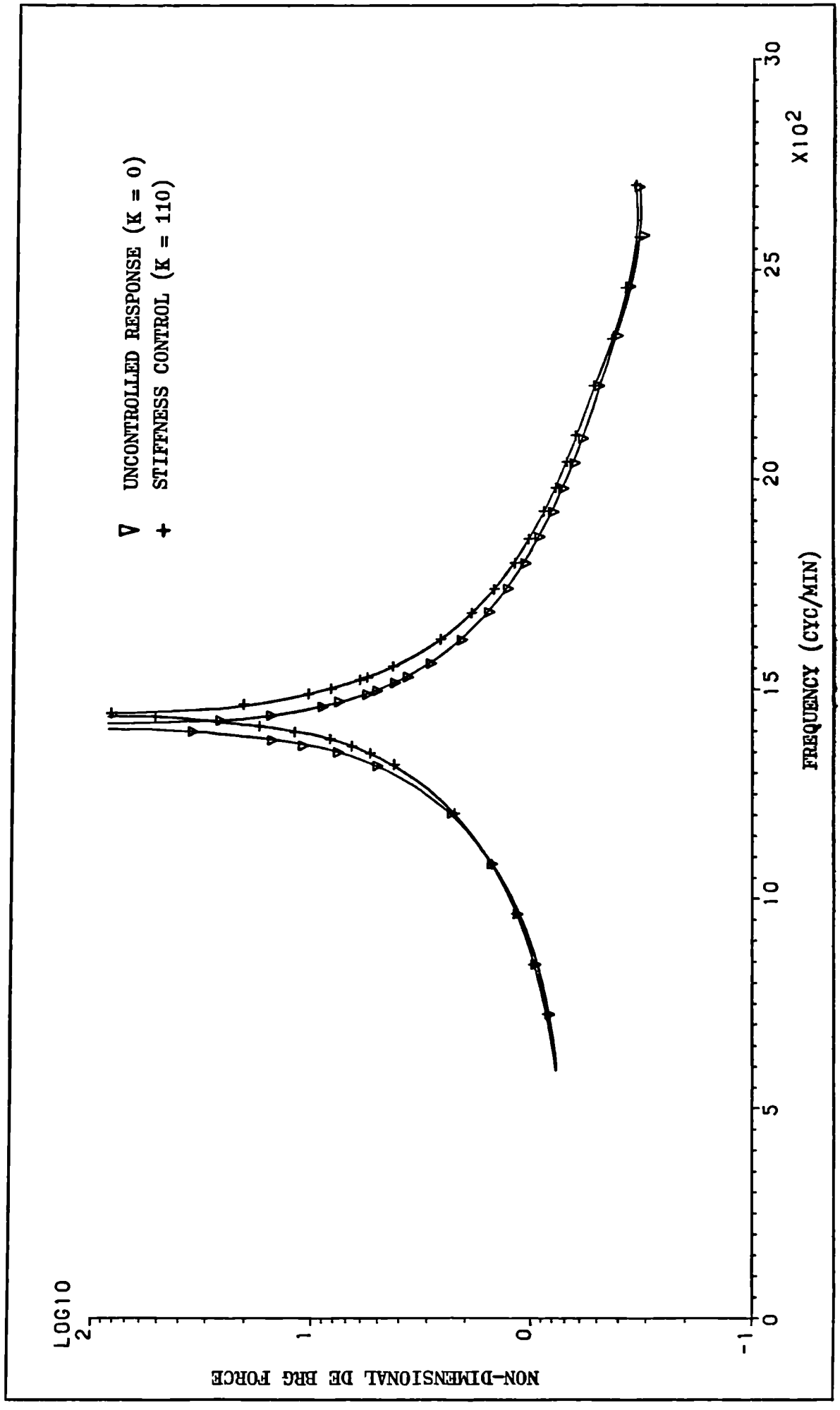

FIG. 7.11f PLOT OF MEASURED DIMENSIONLESS DE BRG FORCE VERSUS FREQUENCY - STIFFNESS CONTROL

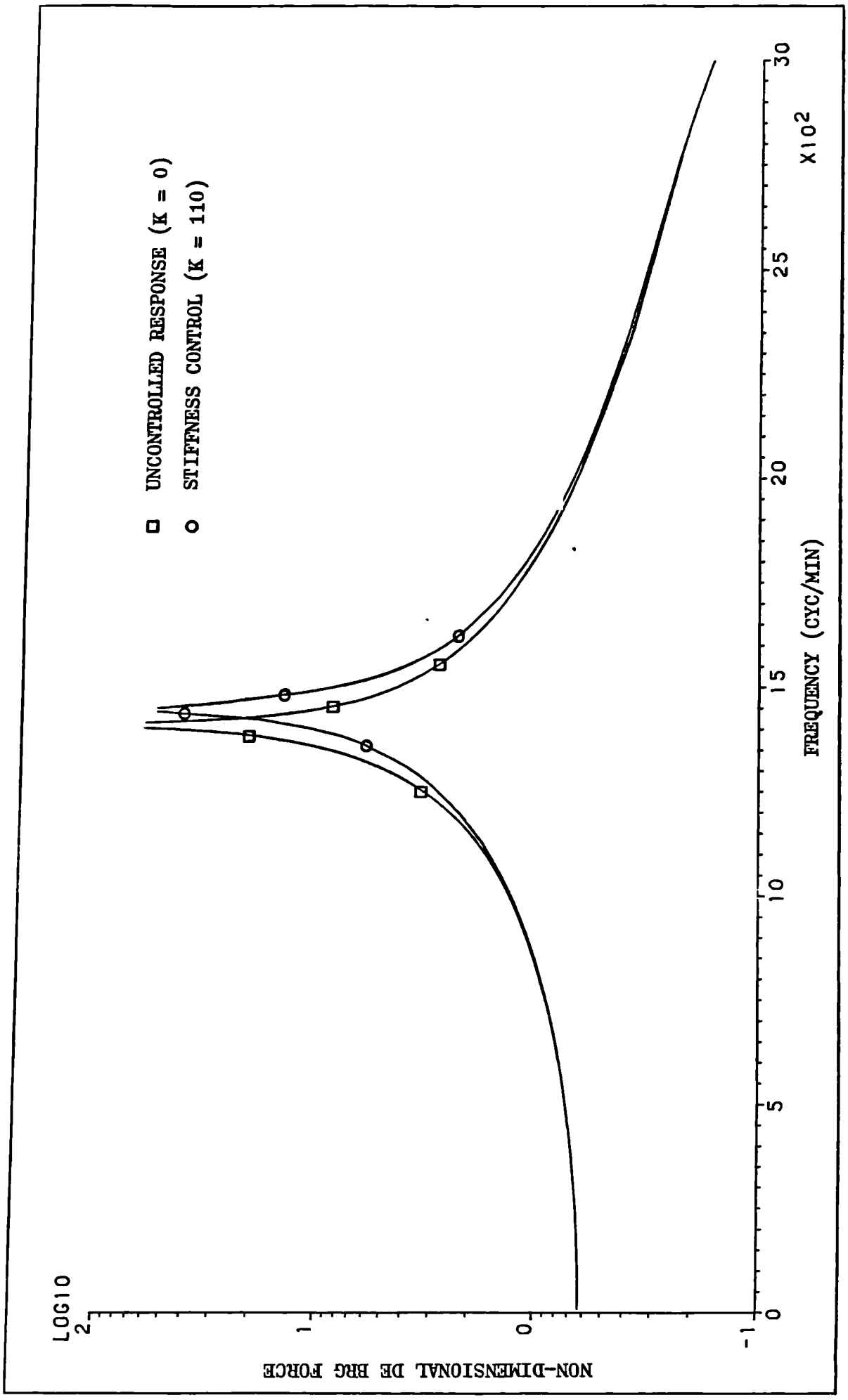

FIG. 7.11g PLOT OF PREDICTED DIMENSIONLESS DE BRG FORCE VERSUS FREQUENCY - STIFFNESS CONTROL

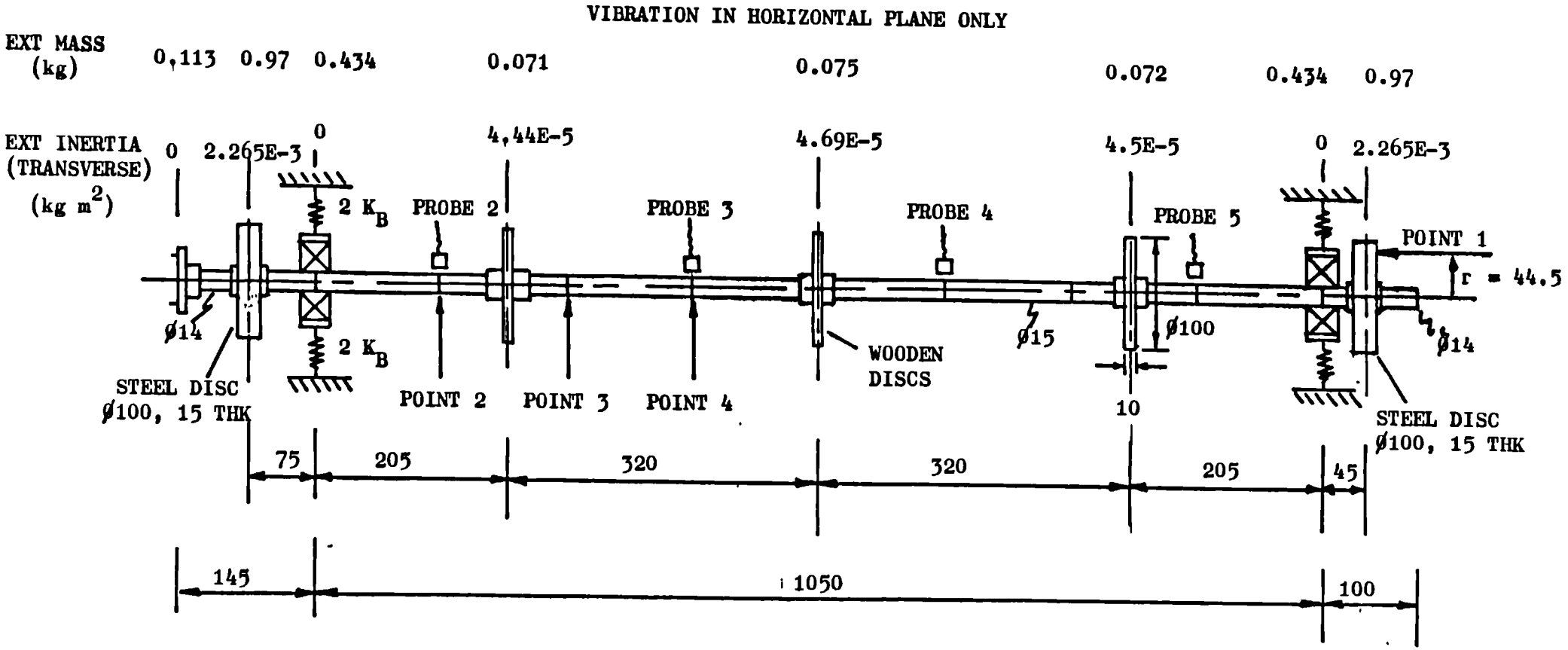

	EXCITATION LOCATION	STIFFNESS, K_B (N/m)
FIG. 7.12a	POINTS 1, 2, 3 AND 4	∞ (RIGID SUPPORTS)
FIG. 7.12b	POINTS 1 AND 2	0.309E6

FIG. 7.12 SHAFT ARRANGEMENT FOR RECEPTANCE TESTS (TEST 6)

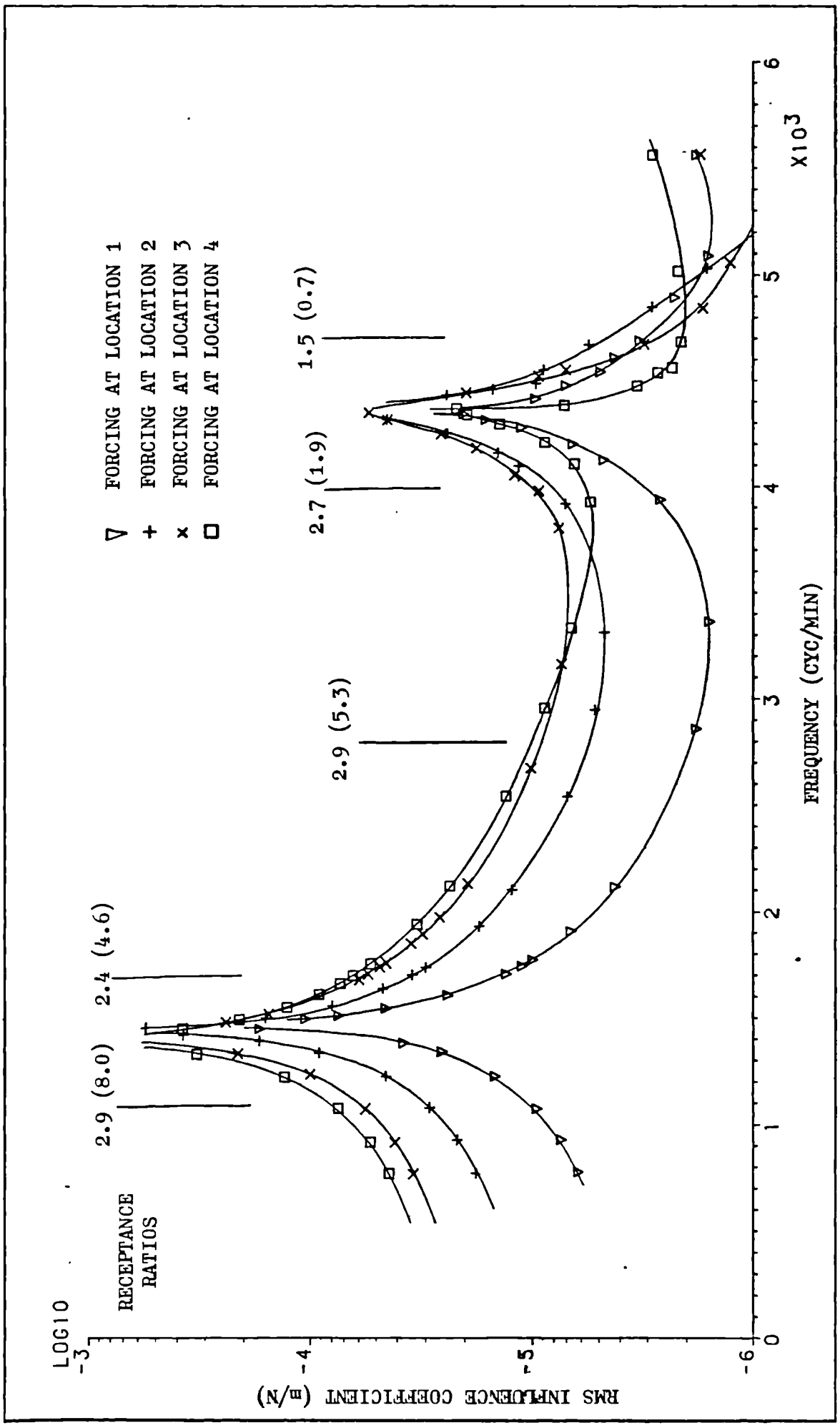

FIG. 7.12c PLOT OF SHAFT MEASURED RMS INFLUENCE COEFFICIENT VERSUS FREQUENCY

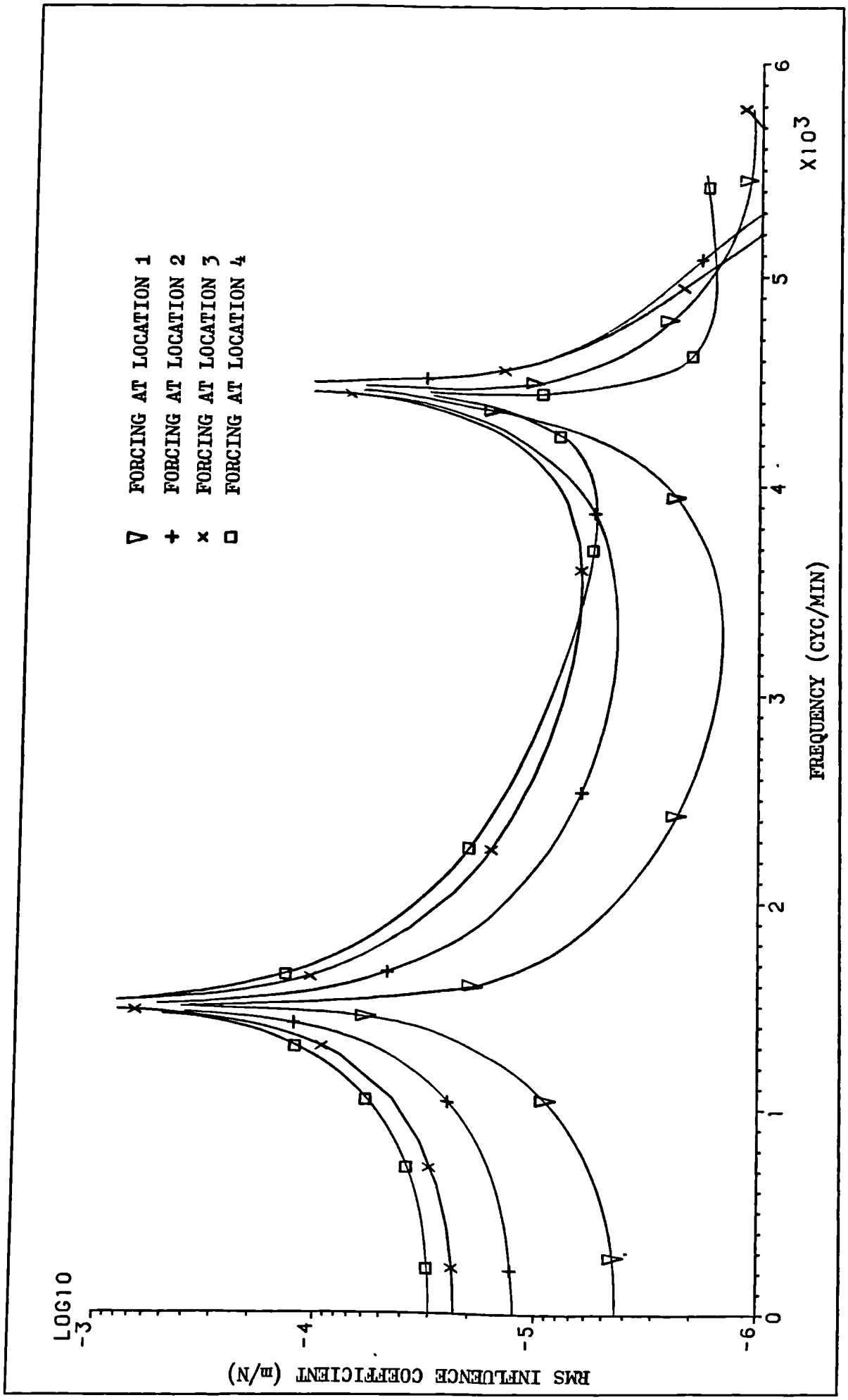

FIG. 7.12d PLOT OF SHAFT PREDICTED RMS INFLUENCE COEFFICIENT VERSUS FREQUENCY

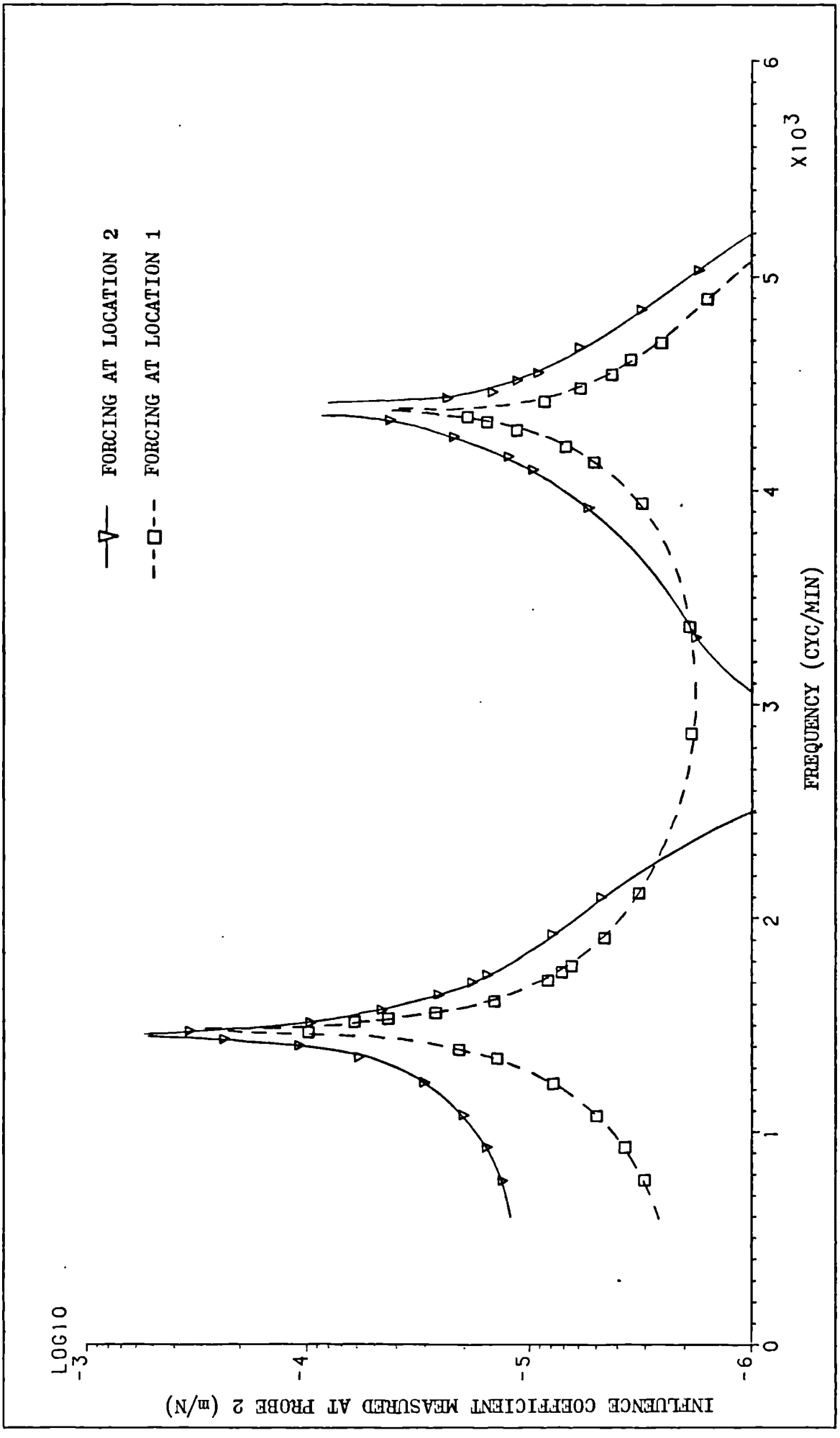

FIG. 7.12e PLOT OF SHAFT MEASURED SINGLE-POINT INFLUENCE COEFFICIENT VERSUS FREQUENCY

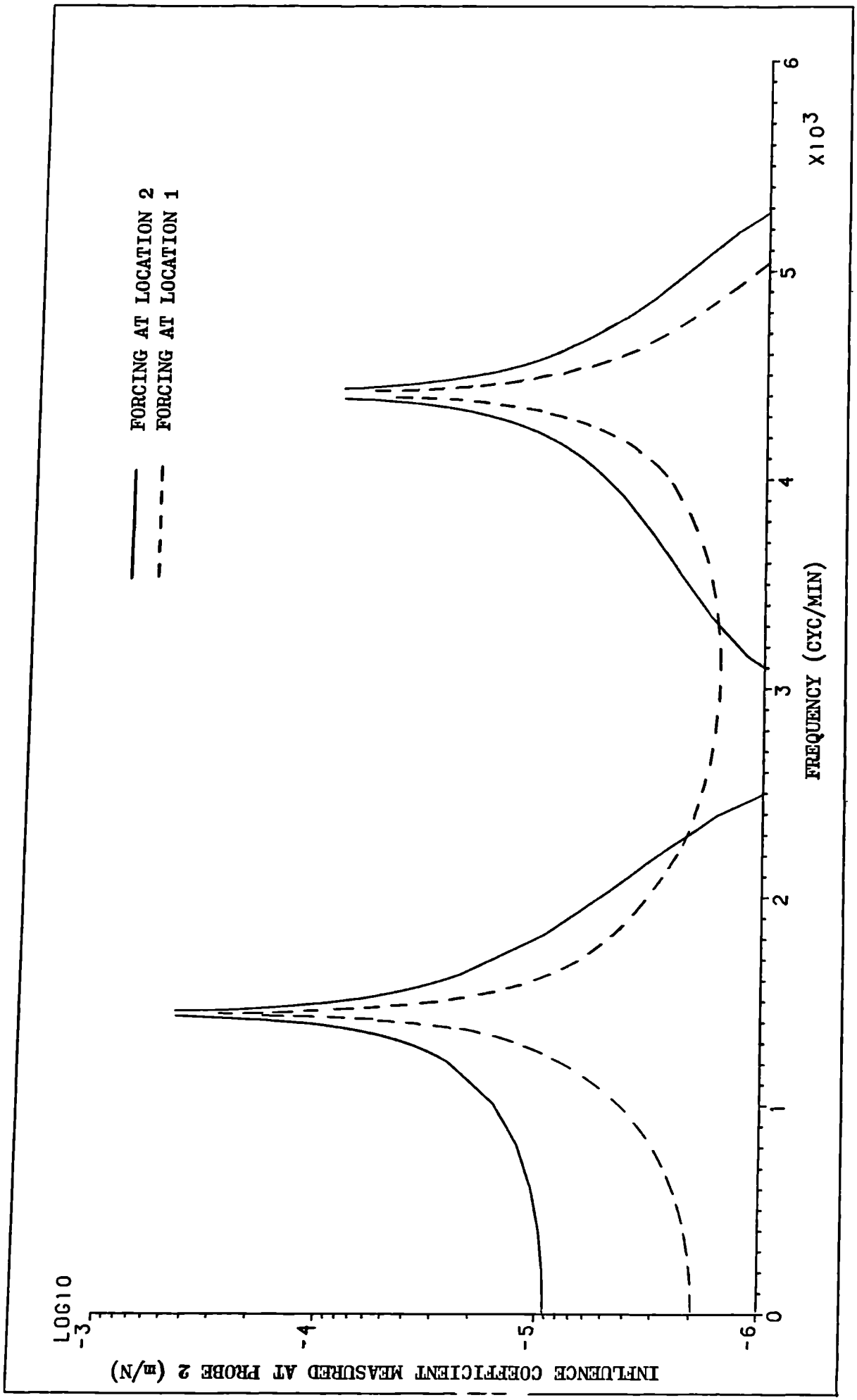

FIG. 7.12f PLOT OF SHAFT PREDICTED SINGLE-POINT INFLUENCE COEFFICIENT VERSUS FREQUENCY

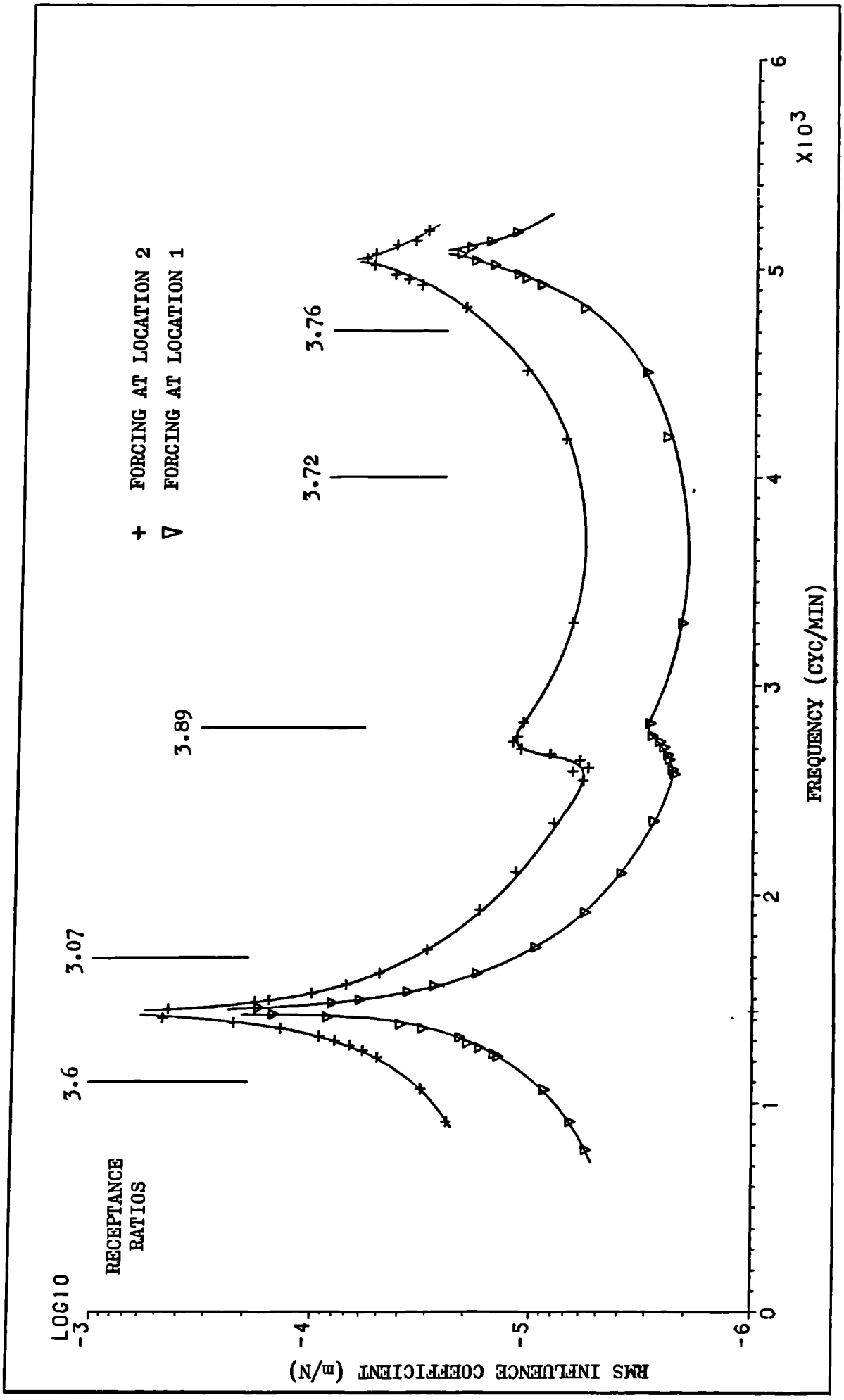

FIG. 7.12g SHAFT MEASURED RMS INFLUENCE COEFFICIENT VERSUS FREQUENCY - FLEXIBLE SUPPORTS

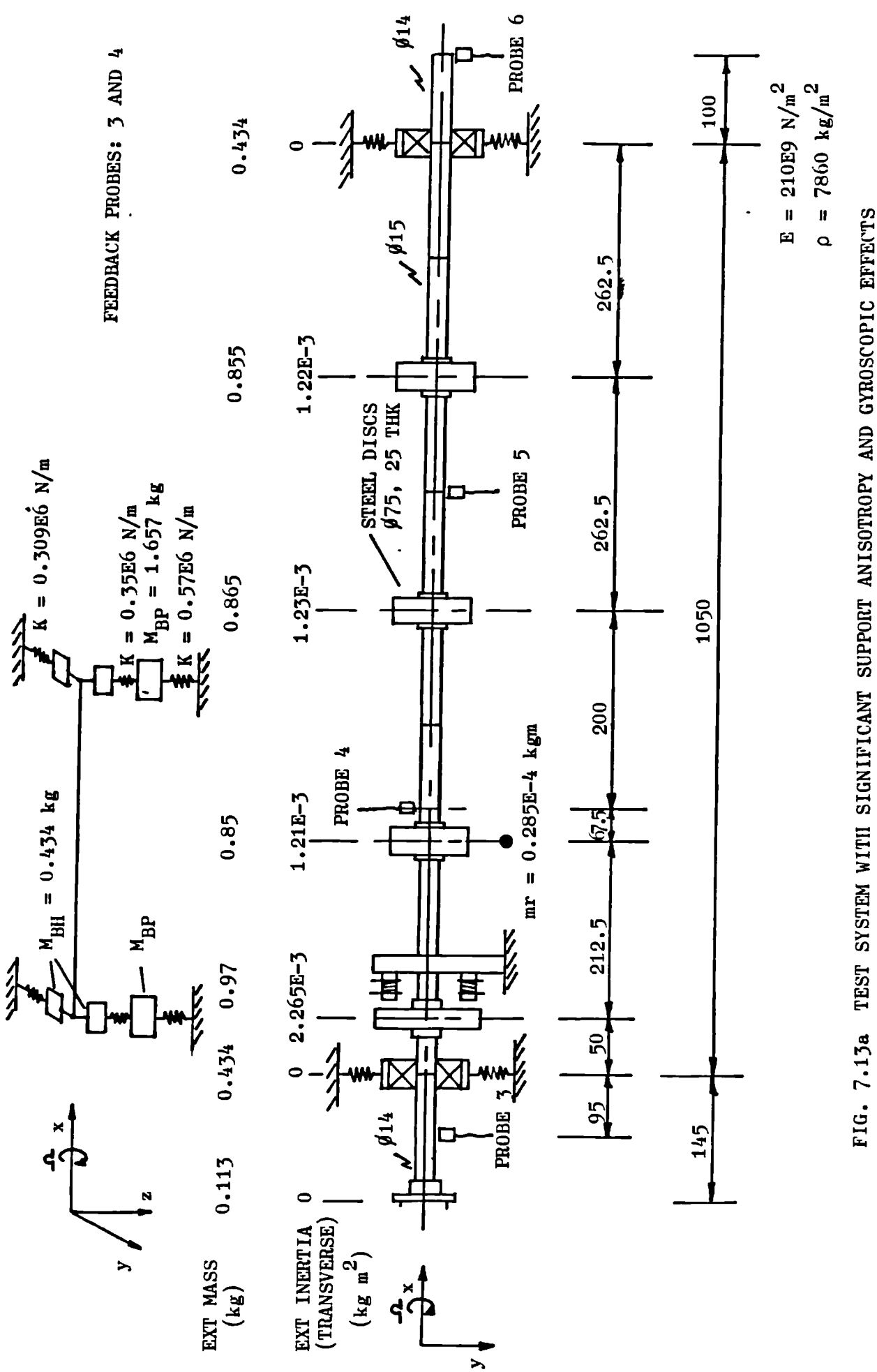

FIG. 7.13a TEST SYSTEM WITH SIGNIFICANT SUPPORT ANISOTROPY AND GYROSCOPIC EFFECTS

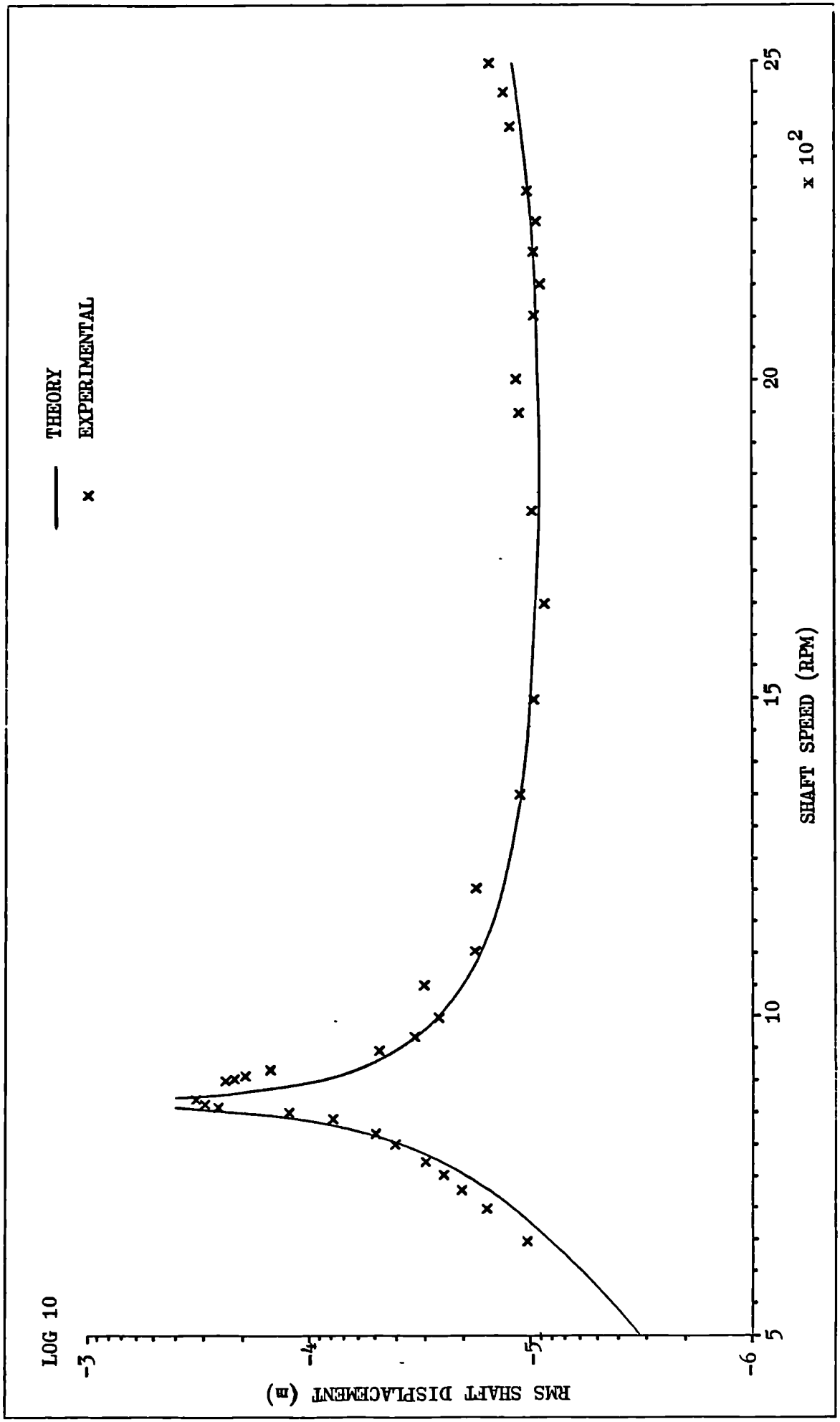

FIG. 7.13b SHAFT UNDAMPED RMS RESPONSE

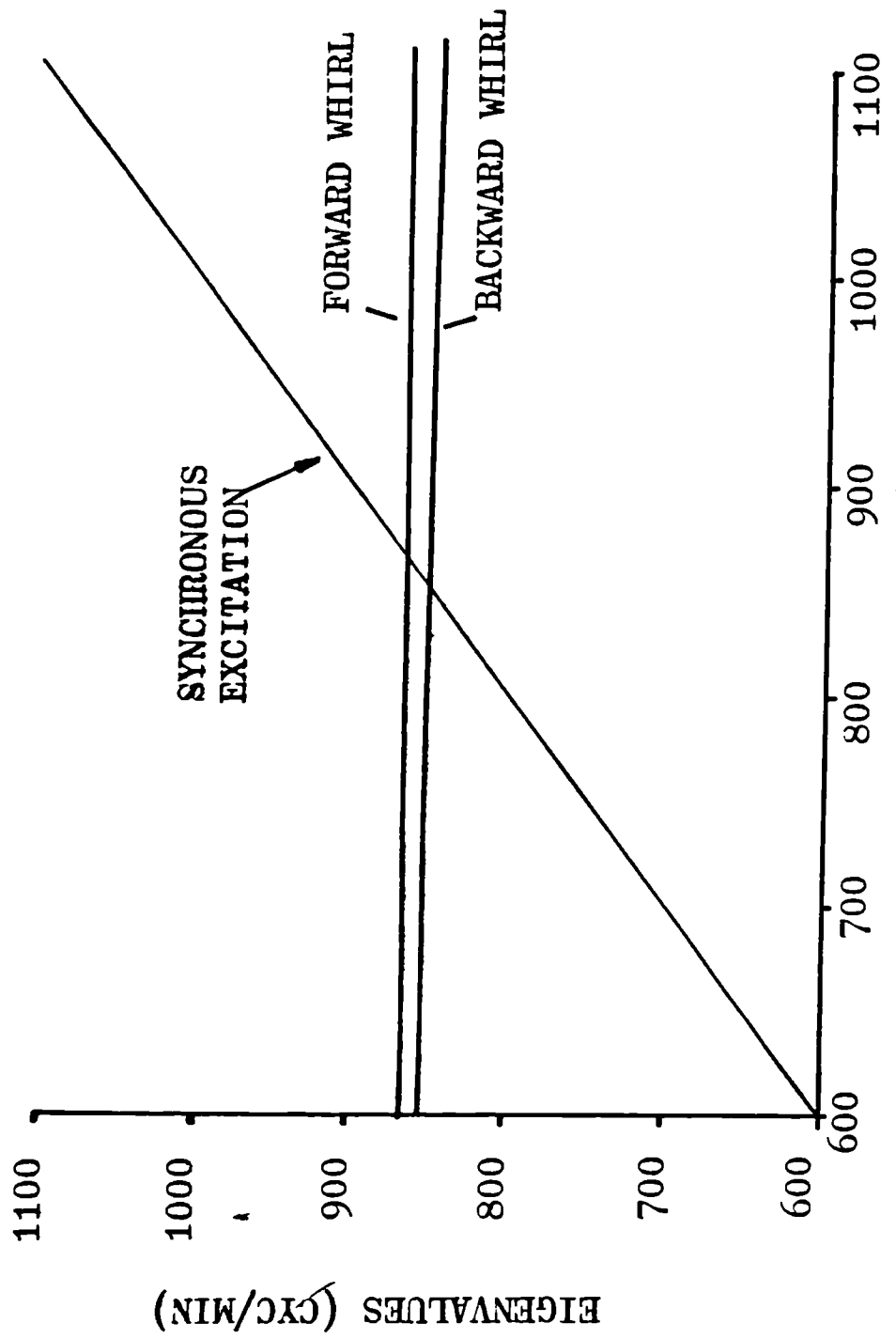

FIG. 7.13c SYSTEM EIGENVALUE PLOT

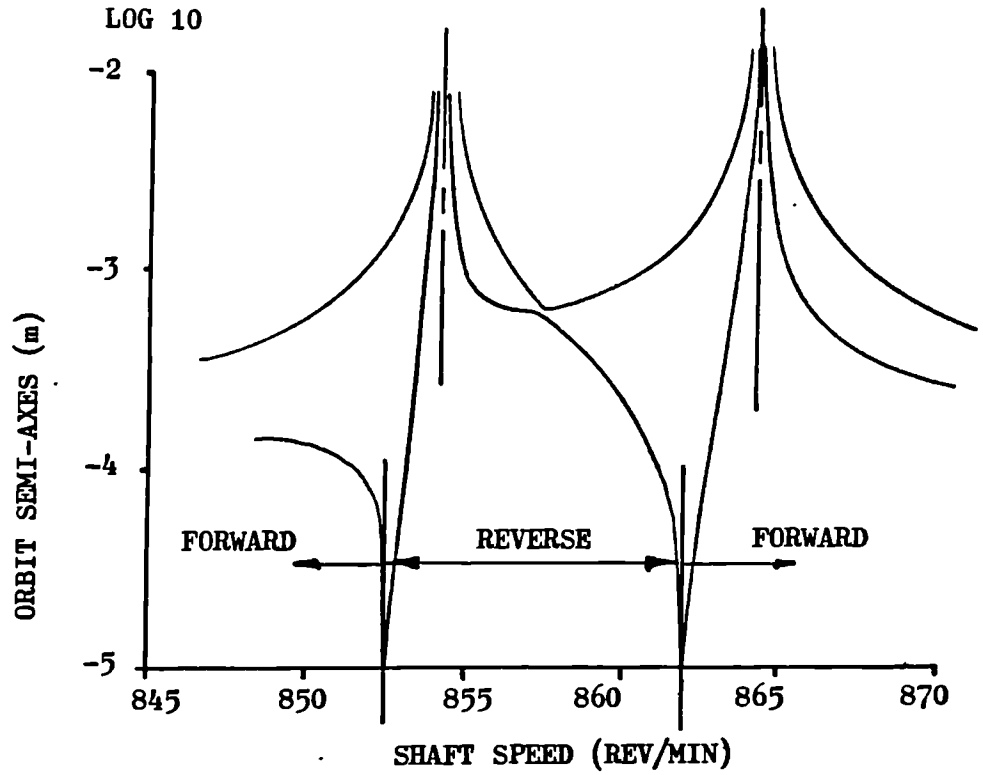

(d) UNDAMPED

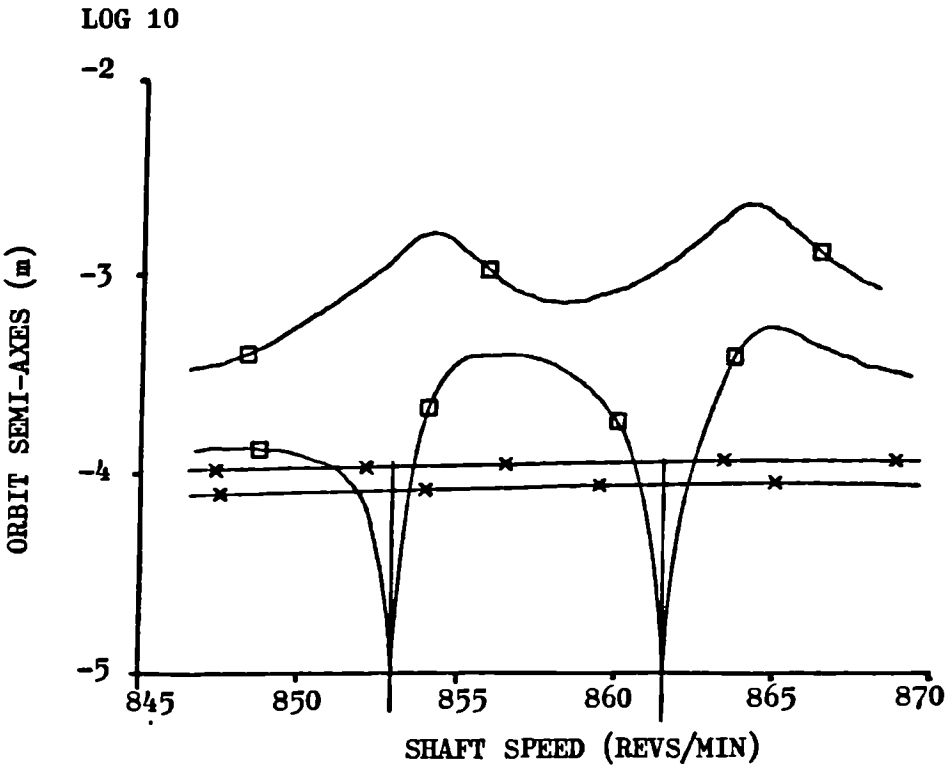

(e) DAMPED: -□- C_{ANG} = 0.1 Nms/rad; -x- C_{ANG} = 2.0 Nms/rad

FIG. 7.13 SHAFT ORBIT DETAILS

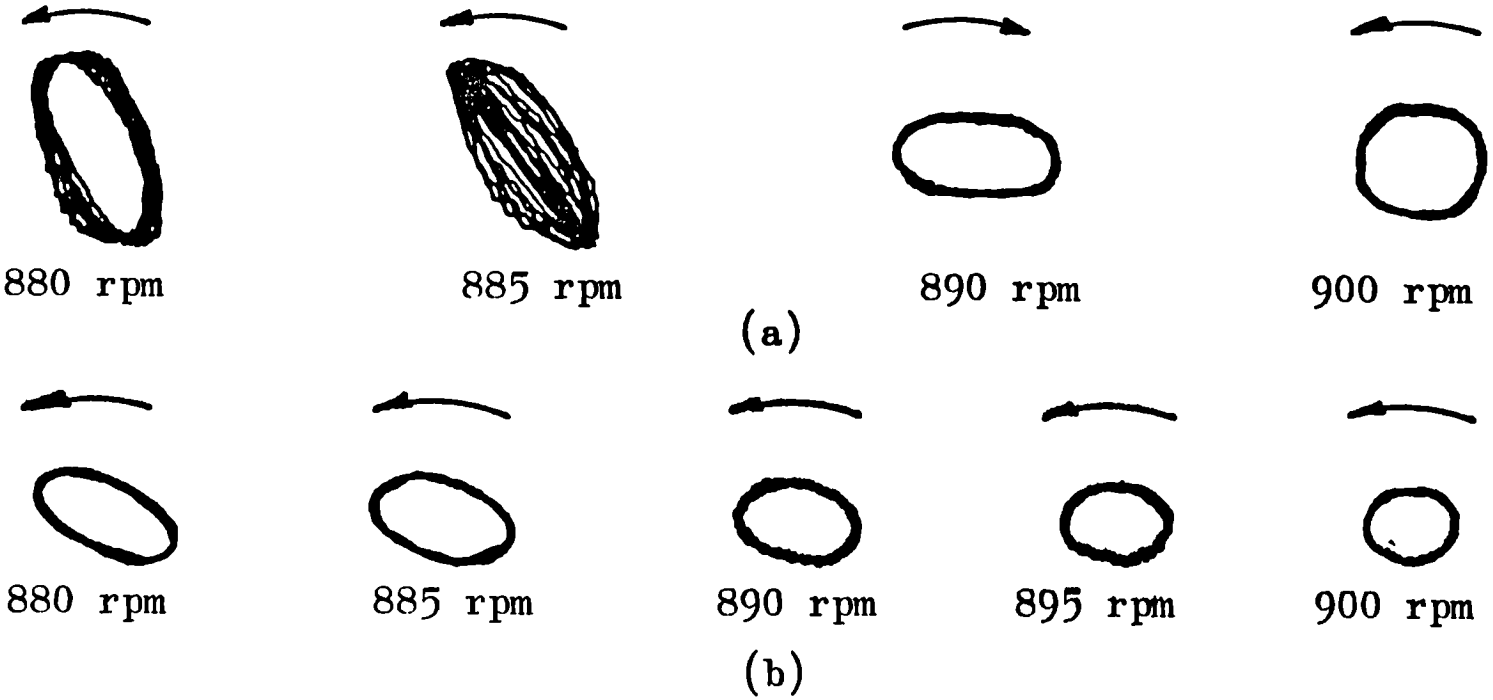

FIG. 7.14 SHAFT ORBITS: (a) UNDAMPED, (b) MAGNETICALLY DAMPED

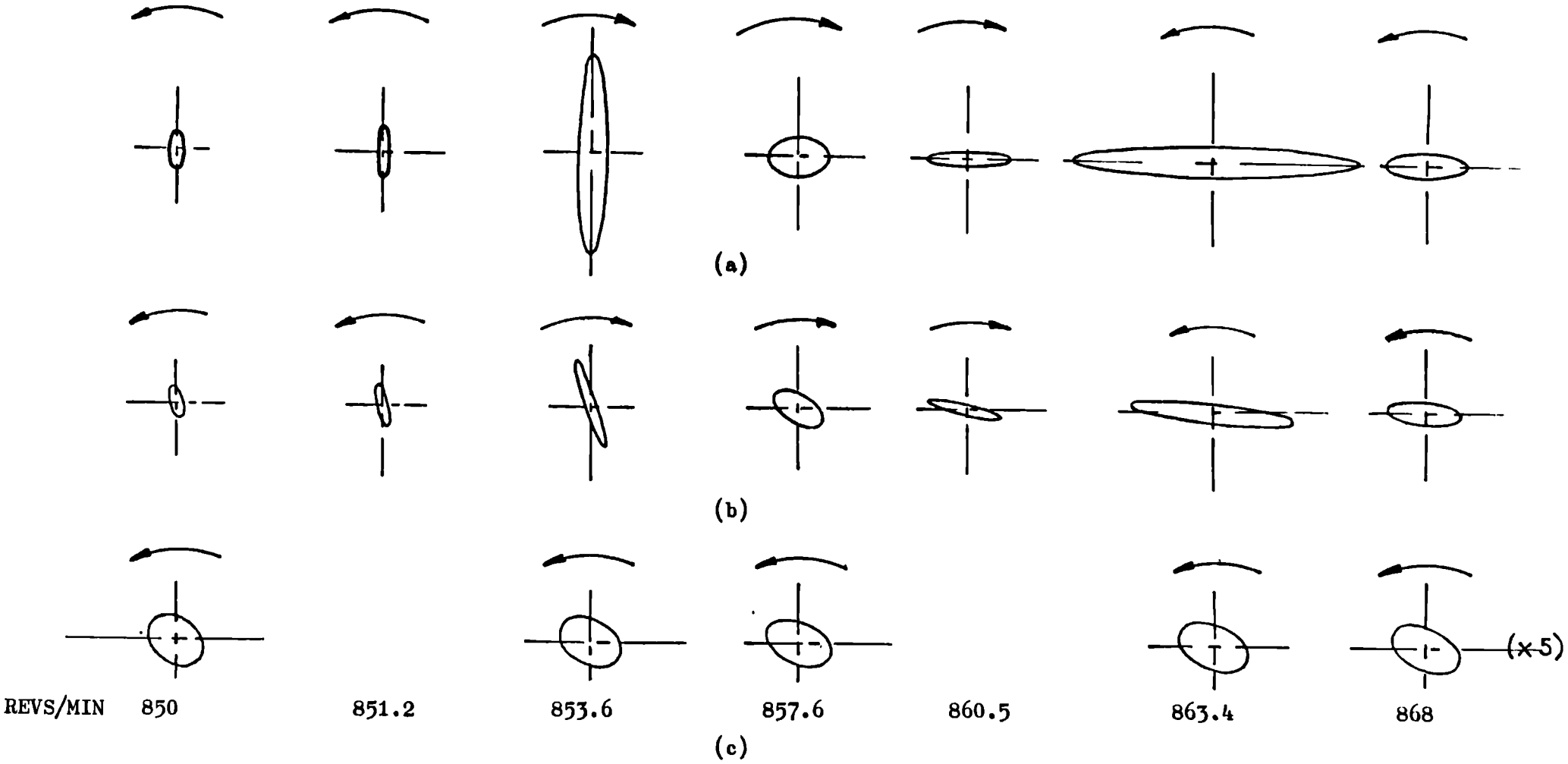

FIG. 7.15 SHAFT ORBITS: (a) UNDAMPED, (b) C_{ANG} = 0.1 Nms/rad, (c) C_{ANG} = 2.0 Nms/rad

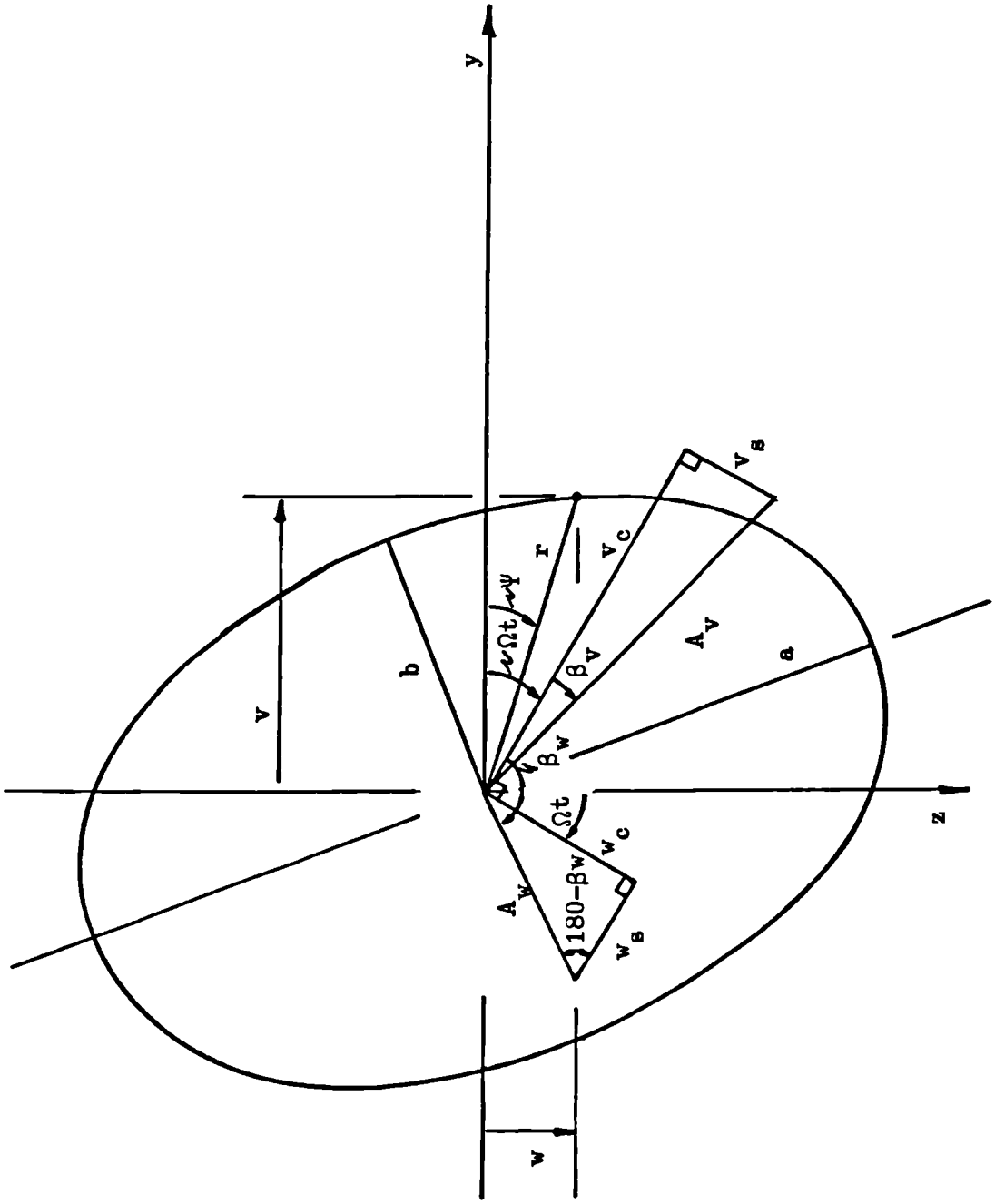

FIG. A.1 SHAFT WHIRL ORBIT DETAILS

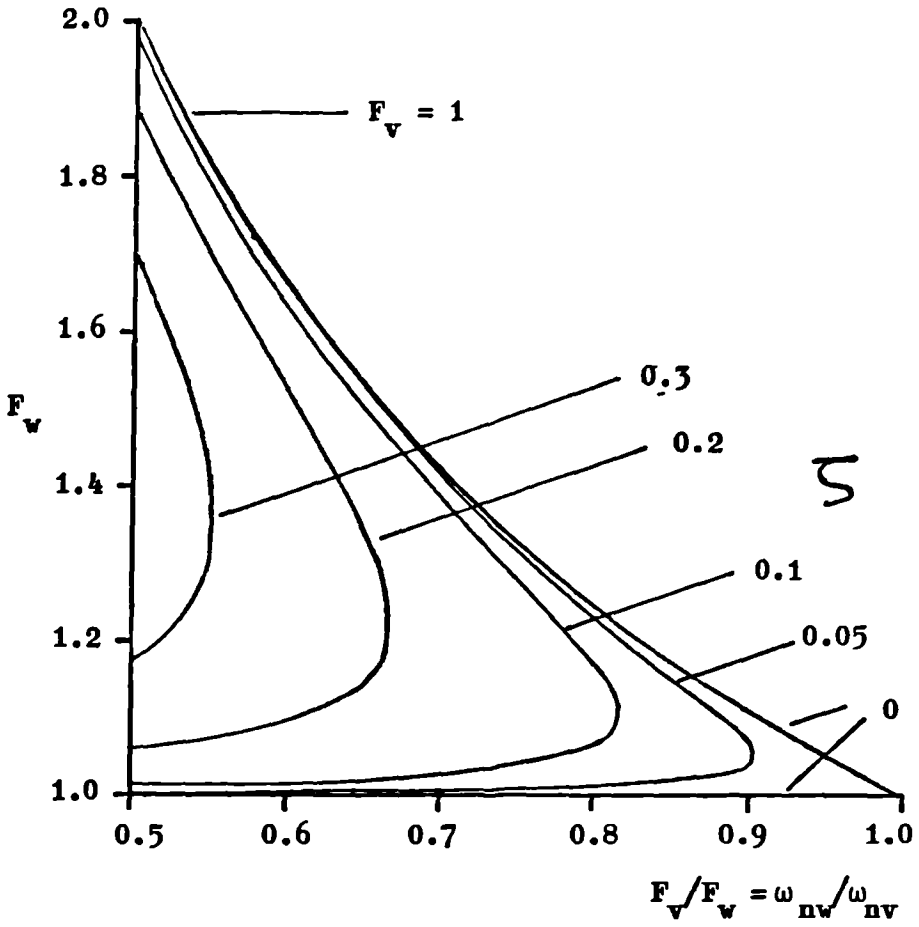

FIG. F.1 EFFECT OF DAMPING ON SHAFT REVERSE WHIRL OF A JEFFCOTT-ROTOR WITH SUPPORT ASYMMETRY